Particle Settling in shear-thinning non-Newtonian drilling fluids

Effect of oscillatory motion

by

P. D. Malitha Maduranga Amaratunga

Thesis submitted in fulfillment of
the requirements for the degree of
PHILOSOPHIAE DOCTOR
(PhD)

Department of Energy and Petroleum Engineering
Faculty of Science and Technology
2020

University of Stavanger
NO-4036 Stavanger
NORWAY
www.uis.no

ISBN: 978-82-7644-944-0
ISSN: 1890-1387
PhD: Thesis UiS No. 537

Preface

This thesis is submitted in partial fulfillment of the requirements for the degree of Philosophiae Doctor (PhD) in the Department of Energy and Petroleum Engineering, at the Faculty of Science and Technology, University of Stavanger (UiS), Norway. The research work is mainly experimental and contains a numerical sub-study as well. All the experiments were carried out in the multiphase flow laboratory at UiS. The research focused on investigating the effect of low-frequency oscillatory motion on the particle settling in shear-thinning non-Newtonian drilling fluids to fill the research gaps and to understand the underlying physics.

The thesis consists of two sections namely; Part I and Part II. To achieve the main aim of the research, a few numbers of studies were performed as separate sub-studies. Some of them employed specific experimental setups for the dedicated sub-study while the others were performed using the single setup. Introductory details of these sub-studies and the main remarks of them are mentioned in Part I, which is presented in six chapters. Chapter one, 'Background of the research' explains the way the afore-mentioned sub-studies are categorized and presented in the thesis. It includes the aims of the research as well. Chapter two, 'Introduction' revises the relevant literature in connection to the sub-studies of the present research. Chapter three describes "Methodology, measurement techniques and data analysis" in detail for different cases. Chapter four, 'Main Remarks' presents the main results produced by the research activities (different sub-studies) while Chapter five, 'Conclusion' presents a concise insight into the research findings. However, the detailed discussion of the results can be found in the scientific publications attached in Part II. Finally, chapter six includes the "Recommendations for future work" according to the author's point of view.

Part II presents the scientific publications of the research and consists of three already published journal articles, one article which is being reviewed by a scientific journal and three other already published conference papers.

The research work was carried out between November 2015 to April 2019. It was funded by the Norwegian Research Council under the project “NFR Improved Model Support in Drilling Automation” and paid through SINTEF, petroleum research, Bergen.

Maduranga Amaratunga
30th April 2020
Stavanger

To my parents,
Austin Amaratunga & Jennet Perera,
and to my family,
Kshanthi, Sanjali, Adithya and Sandesh with Love...

Acknowledgments

First and foremost, I would like to thank God Almighty for giving me the strength, knowledge, ability, and opportunity to undertake this research study and to complete it satisfactorily. I strongly believe that, without his continuous blessings, this achievement would not have been possible.

I would like to express my sincere gratitude to my PhD supervisor, Professor Rune W. Time, for his continuous support and guidance throughout this research. Being in his research team has been a great privilege that I will never forget and I will always be thankful to him for giving me the opportunity to enter the journey of adventure.

My sincere gratitude also goes to my co-supervisor Dr. Eng. A. H. Rabenjafimanantsoa for always been helpful and interested in my work, for valuable discussions, and the helping hand provided during the designing, constructing, and conducting the experiments in the multiphase flow laboratory at UiS.

Special thanks to Roar Nybø, Senior Business Developer and Scientist at SINTEF Petroleum, Bergen for the support and valuable discussions especially at the beginning of the research. The supportive reading materials and the discussions made a good foundation for my PhD study.

I would like to thank Knut Steinar Bjørkevoll, Senior Research Scientist and the Leader at SINTEF Petroleum, Bergen for the valuable advice, financial supports for the experimental facilities, and also for the visit at UiS.

I thank Stein Tore Johansen, Principal Scientist at SINTEF process, Trondheim for the valuable discussions regarding numerical studies related to oscillatory flows.

I appreciate the institute leader of the Department of Energy and Petroleum at UiS, Øystein Arild, for the support throughout this period.

I am grateful to Norbert Puttkamer, the office manager of the TN faculty administration at UiS for the kind supports.

Many thanks to Hilde Carlsen Jonsbråten, the laboratory leader of our department, Senior Engineers Kim Andre Nesse Vorland and Jostein Djuve for the safety concerns, technical and administrative supports during the experiments.

Thanks to the department Engineer, Inger Johanne Munthe-Kaas Olsen for the supports given in ordering the necessary items for the experiments.

Thanks to Jørgen Fandrem from Radipro AS, Stavanger for the quick responses in assessing and approving the laser safety status related to the experimental setups.

I am thankful to Jon Fidjeland and Romuald K. Bernacki from the Department of Computer and Electrical Engineering at UiS for the advice and supports related to electrical devices and instruments.

I appreciate the valuable support provided by the Engineer Jon Arne Evjenth in our department at UiS in preparing the data acquisition system for the experiments.

Thanks to Jan Magne Nygård from the engineering workshop at UiS for the helping hand provided when constructing small parts of my experimental setup.

I gratefully acknowledge the Norwegian Research Council for funding this research project.

Thanks to all my friends in Stavanger who were with me and supported me during this journey in numerous ways.

I remember my family with a lot of love where I always find warmth and comfort. My loving wife Kshanthi is my mentor, my best friend, and the closest colleague for the past fourteen years of my life. Her advice encouraged me a lot and I appreciate her dedication in taking care of our family during the busy times.

I thank my beautiful daughter Sanjali and adorable sons Adithya and Sandesh for their loving company during this whole period and bearing the hard times together.

Finally, I thank my loving parents for all their sacrifices to see me as a doctoral graduate today. Thanks to my two sisters Krishanthi and Kaushalya, who gifted me with countless, beautiful childhood memories, supports, love, and prayers.

I gratefully acknowledge all who offered their kind supports in numerous ways and apologies if I have missed someone.

------ * * * ------

Abstract

When drilling fluids circulate through the well and during the solids control operations, they are exposed to vibrations and oscillations of different frequencies and amplitudes. The secondary flow structures in oscillatory motion influence the liquid shear rate and rheological characterization of drilling fluids. Hence, oscillations understandably influence the cuttings carrying capacity of the drilling fluids and the solids separation efficiency as well.

The majority of pipe flow investigations available in the scientific literature are related to the steady flow. However, more attention should be paid to unsteady flows, since there are many industrial and biological applications in the fields of applied fluid mechanics. As an example, even local geometrical variations and gas kicks in oil-well drilling operations might cause flow instabilities and fluctuations along the pipe trajectory. The problem of shear rate change in time-periodic flows of viscoelastic fluids is relevant in particular for the oil industry, as acknowledged by the research, and also for physiological flows such as blood flow in veins and arteries and the flow of mucus driven by cilia oscillations; hence the interest of the proposed research.

This thesis presents a collection of six experimental studies and one numerical study which aims to investigate the effect of zero-mean oscillatory flow on particle settling in shear-thinning polymeric non-Newtonian fluids of interest in drilling and maintenance of petroleum wells. In most of the cases, a mixture of water-based polymeric solutions of Polyanionic Cellulose (PAC) and Carboxymethyl Cellulose (CMC) has been employed as the test fluids and in some cases, an individual type of polymer solution has been employed with the viscosifier, Xanthan gum (Xg). The rheological properties of the slightly viscoelastic test fluids have always been characterized in all the sub-studies based on the specific experimental conditions and it is shown that the test fluids

exhibit a shear-thinning viscosity in the linear range of the experimental viscosity data depending on fluid composition.

After conducting a successful prestudy which includes;

- rheological characterization of model drilling fluids,
- an acoustic approach of providing the oscillatory motion to the liquid medium,
- horizontal oscillation of a vertical liquid column and
- a numerical investigation,

a core study was planned, designed and executed successfully. For that, an oscillatory flow in a vertical pipe (1.2 m high, 50 mm inner diameter), driven by a zero-mean oscillatory pressure gradient has been used to mimic the practical scenario takes place within a vertical oil well and to achieve the main aim of the research. Driving frequencies were set constant at values ranging from 0 (stationary) to 0.75 Hz. The oscillation amplitude ratio ($A = a/D$) was set constant at values ranging from 0.3 – 0.5, where a is the displacement amplitude of the piston, and D is the pipe inner diameter. Flow visualization was deployed to compare the velocity distributions in Newtonian (deionized water) and non-Newtonian test fluids using particle image velocimetry (PIV) and high-speed imaging techniques. Care was taken to avoid any relevant entrance effects.

Particle settling in oscillatory systems is a practically important example under dynamic settling since sinusoidal oscillatory fluid motion exhibits a condition of continuously changing acceleration and thus the flow patterns and drag phenomena could be significantly different from those at steady state. Achieving the goal of the research, an experimental investigation was carried out to study the effects of oscillatory motion on the settling of spherical particles in Newtonian and non-Newtonian fluids as the last part of the research study. Three different sphere diameters (1, 2, and 3 mm) were employed in the study and the particles were released at three different locations within the pipe diameter to study the effects

of the shear region on particle settling in non-Newtonian fluids at oscillatory conditions.

The velocity profiles were used to investigate the possible flow nonlinearities caused by shear-thinning behaviour of the non-Newtonian fluids and to determine the shear rate profiles which arguably have a major influence on particle settling. Oscillatory flows of non-Newtonian fluids in wall-bounded large domains, such as the vertical pipe considered in this research, have received continued attention in the literature because they show strikingly different features than their Newtonian counterparts, including resonant behaviour, flow enhancement, and bifurcation to complex flow structures (vortex rings and low Reynolds number turbulence).

The study reveals that the axial velocity amplitude along the pipe centreline increases with increasing frequency and with increasing oscillation amplitude irrespective of the fluid type. The thickness of the shear region close to the wall decreases with increasing frequency. The change of shear rate is maximum near the wall region of the pipe, and that is achieved at the maximum position of the sinusoidal velocity profile, where the axial velocity possesses its highest magnitude.

The settling velocity was smaller if particles were released close to the pipe wall, independently on the rheology of the fluid. The main result of the investigation is the observation of a significant reduction of the settling velocity in the presence of an oscillatory flow when a fluid characterized by shear-thinning viscosity is used. It was found that the liquid oscillations decreased the average settling velocity in Newtonian fluid up to 7% and a reduction of 23% in non-Newtonian fluids. Moreover, when the fluid oscillates, the combination of the shear-layer associated with the particle wake and with the pipe wall does not result in any reduction of the settling velocity. In other words, the effect of the near-wall shear layer, which reduces the viscosity of shear-thinning

fluids, dominates over the other effects that would not keep the particle longer in suspension.

List of scientific publications

I. Maduranga Amaratunga, Milad Khatibi, Nikita Potokin and Rune W. Time, (2018), "*Predicting rheological properties of water-based polymer mixtures from their component properties – Polyanionic Cellulose and Xanthan gum*", Annual Transactions of the Nordic Rheology Society, vol. 26, pp 31 - 39

II. Maduranga Amaratunga, Rune W. Time, (2018), "*Visualization of acoustic streaming using PIV in Newtonian and non-Newtonian liquids*", International Journal of Computational Methods and Experimental Measurements, Volume 6, Issue 4, pp 814 – 826

III. Maduranga Amaratunga, Roar Nybø, Rune W. Time, (2018), "*PIV analysis of dynamic velocity profiles in non-Newtonian drilling fluids exposed to oscillatory motion*", Proceedings of the ASME 2018 - 37th International Conference on Ocean, Offshore and Arctic Engineering. Volume 8: Polar and Arctic Sciences and Technology; Petroleum Technology, held on 17th – 22nd June 2018, Madrid, Spain

IV. Maduranga Amaratunga, H. A. Rabenjafimanantsoa, Rune W. Time, (2019), "*CFD Analysis of low-frequency oscillations in Newtonian and non-Newtonian fluids in a vertical pipe*". WIT Transactions on Engineering Sciences, 125, pp 37-48.

V. Maduranga Amaratunga, H. A. Rabenjafimanantsoa, Rune W. Time, (2019), "*Comparison of oscillatory flow conditions in Newtonian and non-Newtonian fluids using PIV and high-speed image analysis*". Flow Measurement and Instrumentation, 70: 101628.

VI. Maduranga Amaratunga, H. A. Rabenjafimanantsoa, Rune W. Time, (2020), "*Estimation of shear rate change in vertically*

oscillating non-Newtonian fluids: Predictions on particle settling", Journal of Non-Newtonian Fluid Mechanics 277: 104236

VII. Maduranga Amaratunga, H. A. Rabenjafimanantsoa, Rune W. Time, (2020), "*Influence of low-frequency oscillatory motion on particle settling in Newtonian and shear-thinning non-Newtonian fluids*", Accepted by the Journal of Petroleum Science and Engineering. Manuscript is in press.

Table of Contents

List of Figures

List of Tables

Notations

CMC	Carboxymethyl Cellulose
CFD	Computational Fluid Dynamics
CLAHE	Contrast limited adaptive histogram equalization
CW	Continuous Wave
CY	Carreau-Yasuda
DCC	Discrete cross-correlation
DPIV	Digital particle image velocimetry
FFT	Fast Fourier Transformation
HV	High viscous
LVE	Linear viscoelastic range
MV	Medium viscous
NNF	Non-Newtonian fluid
PAC	Polyanionic Cellulose
PIV	Particle Image Velocimetry
PSP	Polyamide seeding particles
PTV	Particle Tracking Velocimetry
ROI	Region of interest
SAOS	Small amplitude oscillation shear
UDF	User-defined function
VOF	Volume of fluid method
Xg	Xanthan gum
a	Displacement amplitude of the piston
a'	Displacement amplitude of the liquid medium
a_p	Particle amplitude within the oscillating liquid medium
A	Amplitude ratio based on the displacement amplitude of the piston
$B(t)$	Basset term
C_D	Drag coefficient at oscillatory conditions
C_{D0}	Drag coefficient at stationary conditions

$C_{D0-correlation}$	Drag coefficient of particles at stationary conditions based on the correlation presented in literature
C_{PAC}	PAC concentration in w/w%
C_{Xg}	Xg concentration in w/w%
d	Diameter of the spherical particle
D	Diameter of the pipe
D_t	Diameter of the acoustic transducer
De	Deborah number
f	Frequency of oscillation, Hz; $\omega/2\pi$
g	Gravitational acceleration
G'	Elastic (or storage) modulus
G''	Viscous (or loss) modulus
H_t	Thickness of the acoustic transducer
K	Consistency index of the non-Newtonian fluid
K'	Generalized consistency index of any blended polymer solution
L_x	Location of particle release (x = 1, 2 and 3)
M	Factor as a function of C_{PAC}
n	Behaviour index for the non-Newtonian fluid
r	Radial position
R	Radius of the pipe
Stk	Stokes number
t	Time
t_v	Viscous time scale
U	Horizontal velocity component of the liquid medium
$\boldsymbol{U}$	Velocity vector in the CFD model
T	Oscillation period (characteristic time)
v_p	Instantaneous velocity of the particle (taken as positive downwards)
v_{p0}	Terminal settling velocity of the particle at stationary conditions
v_f	Instantaneous velocity of the fluid medium (taken as positive downwards)
$V(t)$	Linear velocity of the liquid medium in the axial direction at the centreline
$\|V\|$	Velocity amplitude of the liquid medium in the axial direction, $\|V\| = \|a'\|\omega$

$\|V_P\|$	Velocity amplitude of the piston
V_{pk}	Peak velocity of the liquid medium due to acoustic propagation
V_{ave}	Cross-sectional average velocity
R^2	R-squared value of the linear curve fitting
Re_p	Particle Reynolds number in oscillatory conditions
Re'_p	Particle Reynolds number in oscillatory conditions (using particle amplitude)
Re_{p0}	Particle Reynolds number in stationary conditions
Re_D	Reynolds number for the general pipe flow
Re_δ	Oscillatory Reynolds number based on Stokes layer thickness
Re_f	Oscillatory Reynolds number based on the oscillating frequency
Re_ω	Pulsating Reynolds number
Wi	Weissenberg number
Wo	Womersley number
$y(t)$	Vertical displacement of the liquid medium

Greek Letters

α	Frequency parameter or non-dimensional frequency
β	Particle settling velocity ratio; v_p/v_{p0}
β'	Liquid velocity amplitude ratio; $\|V\|/\|V_P\|$
γ	Strain
γ_L	Limiting value of shear strain
$\dot{\gamma}$	Shear rate of the liquid
$\dot{\gamma}_p$	Shear rate of the particle
δ	Oscillating boundary layer (Stokes layer)
δ_{ve}	Viscous penetration depth for a viscoelastic fluid
ϑ	Phase angle
ω	Angular frequency; $2\pi f$
ν	Kinematic viscosity of the fluid
λ	Relaxation time of the (slightly) viscoelastic non-Newtonian fluid
μ_f	Dynamic viscosity of the fluid medium
μ_{PL}	Viscosity predicted by the power-law model
$\|\mu^*\|$	Complex dynamic viscosity

ρ_p	Density of the particle
ρ_f	Density of the oscillating fluid (continuous phase)
χ	Added mass coefficient
Λ	Stokes parameter
Λ_{ve}	Viscoelastic Stokes parameter
ψ	Viscous to relaxation time ratio

Part I

1 Background of Research

Drilling fluids perform many tasks while being circulated through the well. From the very basic function of transporting the drilled cuttings back to the ground, it helps in controlling the formation pressure, cooling and cleaning the drill bit, reducing friction and avoiding the loss of fluids to the formation, etc. [1-3]. Furthermore, it is essential to remove drilled cuttings from drilling fluid coming out of the well to obtain better drilling conditions where it is mostly achieved by the use of shale shakers and vacuum devices [4]. When the drilling fluids circulate through the well and during these primary solids control operations, they are exposed to vibrations and oscillations of different frequencies and amplitudes.

It is important to know these oscillatory effects at different frequencies, since they influence the formation of particle structures within the drilling fluid [5] and hence the rheological characterization of it. Newtonian liquids are not noticeably affected by vibrations at low amplitudes ("linear thermo-hydrodynamics") [6]. However, any material with a yield value or showing non-Newtonian behaviour is affected rheologically when subjected to vibrations [7]. Therefore, to investigate the influence of oscillatory motion on the particle settling in non-Newtonian drilling fluids, this research has been carried out in two main approaches namely; pre-study and core study. Under the pre-study, a few numbers of investigations were conducted to collect the background information and to check the feasibility of performing quality and reliable research (core study). Since this particular research is regarding shear-thinning non-Newtonian drilling fluids under oscillatory conditions, a rheological investigation was carried out as the first step to study the capabilities of designing a model drilling fluid with some desired rheological characteristics (**Paper I**). With that knowledge, the possibilities of employing an acoustic pressure field in shear-thinning model drilling fluids were investigated in terms of acoustic streaming (**Paper II**). The overall conclusion using acoustic fields was that

suspended particles were only little impacted and transported. It was therefore decided to go for mechanical oscillations and vibrations to provide higher energies and higher energy transfer from liquid to particles. As a result of that, an investigation was carried out to study the dynamic behaviour of drilling fluids in the presence of a horizontal oscillatory motion in a low-frequency range (**Paper III**). However, it was found that horizontal oscillatory motion impacted in a complex way on the particle settling. Therefore it was decided to develop a new experimental setup to investigate the vertical oscillatory motion of Newtonian and non-Newtonian fluids and its effect on settling of particles. The studies carried out in this new experimental setup were considered under the core study of the research (**Paper V, VI** and **VII**). A numerical approach using computational fluid dynamics (CFD) was also taken to study the dynamics of oscillatory motion in vertical Newtonian and non-Newtonian fluids as the last part of the pre-study during the designing stage of the new experimental setup (**Paper IV**). The following chapter provides an introduction to those different sub-studies under pre-study and core study together with a brief literature review.

2 Introduction

2.1 Pre-study

2.1.1 Rheological approach to study the possibilities of designing a model drilling fluid with desired rheological characteristics

The drilled cuttings are usually transported up to the ground with drilling fluids ("drilling muds"). In addition to the transportation of drilled cuttings, drilling fluids play an important role in different ways [1, 2, 8, 9]. To fulfill the intended tasks, drilling fluids need to be designed; so that they perform efficiently. Water-based drilling muds are the most widely used drilling fluid type in the oil industry due to many reasons, including fewer environmental issues [1, 9]. They are usually non-Newtonian, exhibiting both viscous and elastic properties under deformation; referred to as viscoelasticity, which helps in suspending proppants within the well. Rheology of the drilling fluid is a governing factor in consideration of proppant settling as well as achieving the aforementioned tasks.

Rheological models such as the power-law model, Bingham Plastic model, Casson model, Carreau model, Herschel-Bulkley model, etc. generally characterize drilling fluids. The parameters of any particular drilling fluid can then be derived from the appropriate rheological model. The complexity of the water-based drilling mud is mainly due to the different additives such as viscosifiers, shale inhibitors, weighting material, etc. Today, there are many types of polymers and viscosifiers, which are added to the drilling mud to enhance the capacity of colloidal and rheological properties of drilling fluids [1]. That means the interaction between different polymers has been considered to achieve different properties of drilling fluids. Polyanionic Cellulose (PAC) and Xanthan gum (Xg) are two such types of polymers, which in some cases

are used as viscosifiers too. In the literature, many scientific articles have been addressed the rheological properties of individual polymers [8, 10-12]. However, the studies that have addressed the combined effect of the polymers mentioned above are very limited.

Nowadays, researchers [13, 14] have paid attention to investigate whether the shear viscosity of the fluid or its elasticity is more dominant in controlling the suspended solids when viscoelastic drilling fluids are used. In such a situation, accurate measurement of rheological properties is vital in understanding the non-Newtonian fluid behaviour of drilling fluids together with its physics and structure [15]. Viscoelastic properties of the drilling fluids strongly influence the gel strength, solids controlling, solids transportation, filtration loss characteristics, etc. [16]. Therefore, the study of elasticity and the relative importance of shear viscosity together with elasticity of the drilling fluid has become very important where the possibility of predicting the rheological properties of polymer mixtures would make the decision easier. Refer to **Paper I** for more details.

2.1.2 *Effect of low-frequency acoustics on the rheology of Newtonian and non-Newtonian liquids*

An acoustic wave is pressure oscillation in a medium, propagation with the sound velocity. For small amplitude waves, there is no net measurable mass transport since there is no net molecular motion, only a net transport of energy and momentum. However, when a sufficiently strong acoustic pressure field is applied into a viscous liquid, non-linear effects set in. In such cases, the liquid can start to flow in the same direction as the propagation of acoustic waves. This fact is explained as momentum transfer from the wave to the fluid by viscous attenuation of a sound (pressure). Due to spatial variation in pressure amplitude around the acoustic beam and the degree of sound attenuation, shear induced

eddies and circulation currents can be generated. The liquid motion or the steady bulk flow within any fluid medium under these influences of acoustic waves is called acoustic streaming [17-19].

Out of the six different mechanisms of acoustic interaction with colloidal systems that are explained by Dukhin and Goetz [20], the viscous mechanism is hydrodynamic in nature. It is associated with the shear waves generated by the particles oscillating in the acoustic pressure field. A shear wave is a non-stationary sliding motion of the liquid near the particles. Furthermore, he explains that the shear waves appear as a result of the density difference of the particle and the liquid medium. Because of the density contrast, the particles tend to move with respect to the fluid medium and then the liquid layers in the vicinity of the particles slide relative to each other. This viscous mechanism causes losses in acoustic energy due to shear friction.

Studies of acoustic streaming within non-Newtonian liquids are very limited except in the medical field with regarding to the biological applications. The background for this preliminary acoustic experiment at low-frequency (lower part of the acoustic range) is to investigate whether they can make any considerable influence on the rheology of drilling fluids and subsequently on the particle settling within non-Newtonian drilling fluids. It is obvious that scaling up of such acoustic processes has shown to be difficult due to the interactions between the sound field and the subsequently generated flow. For that, better analytical and numerical studies of this type of low-frequency acoustic streaming are important and valuable. It was not intended to test acoustic standing waves in the ultrasound range (high kHz to MHz) since that could lead to some undesired states of cavitation/agitation. Such phenomena could result in differences in temperature and pressure within the fluid medium which leads to the changes in viscosity and density of the fluid medium. Refer to **Paper II** for more details.

2.1.3 Application of PIV technique to quantify the effect of horizontal vibration on shear-thinning non-Newtonian polymers

There are several studies on the effect of vibration and oscillatory motion on the rheological properties of fresh cement pastes or concretes in literature [21, 22]. However, there is sparse information in the open literature about the influence of vibration on the rheological characterization of drilling fluids. Fard et al. [5] have used some water-based drilling fluids and one oil-based drilling fluid to measure the in-situ shear stress of the fluids in the presence of a vibrational field. They have investigated that vibrations influence the particle system structures and gel structures within the fluids and claim that oscillations do not affect the viscosity profiles of purely polymeric liquids.

Solids separation is one of the key intentions of applying oscillatory motion to the particle carrying liquids. The effect of vibration or oscillation on particle settling is also of practical importance since many applications are found with non-homogenous fluid mixtures containing solid particles. Drilling fluids also undergo a series of vibrations when they are at the stage of returned cuttings separation. The correct use of primary solids control devices such as shale shakers in the drilling industry is crucial to avoid the generation of unnecessary waste streams with drilling fluid additives following the drilled cuttings [4]. According to the studies performed by Saasen et al. [4, 23], the primary function of oscillatory motion on solids controlling equipment is to reduce the low shear rate viscosity and yield stress of the solids carrying liquid. Most of the drilling fluids are shear-thinning non-Newtonian liquids, where the effective viscosity of these fluids is much lower in high shear rates compared to that of Newtonian fluids. Bird et al. [24] state that, shear-thinning behaviour of the fluid assists the settling of suspended particles in a vibration-induced environment. Therefore, it is of great importance to discuss the impact of oscillatory motion on the rheological characteristics of fluids and settling rates of conveyed particles.

One of the key points in this particular study was the use of particle image velocimetry (PIV) technique applied to flows in oscillating systems. Out of many available publications on PIV, almost all of them are reported about the measurement of velocity profiles in non-moving experimental facilities where the boundaries are fixed compared to the image frame. Refer to **Paper III** for more details. However, the experimental setup designed for this sub-study (described in section 3.3.3) and the provision of the horizontal oscillatory motion were quite complex and it was decided to design a new experimental setup with the possibilities of studying vertical liquid oscillations in more detail.

2.1.4 Computational study on the vertical liquid vibrations in Newtonian and non-Newtonian fluids

The shear-thinning behaviour of typical water-based drilling fluids contributes to a reduction in flow friction against the drill pipe walls. The apparent viscosity of such fluids decreases with the shear rate, which will eventually alter the dynamical behaviour of the drilling fluids. That is the main reason why the oscillatory motion should be considered so important when shear-thinning non-Newtonian drilling fluids are circulating through the well. Since the shear rate and shear stress of drilling fluids may vary substantially over time under such scenarios, it is vital to design them accordingly to achieve desired solids carrying capacities and solids separation capacities.

Understanding of dynamic velocity variation and thus the change of the rate of shear within a vertically oscillating liquid body is hard due to complex rheology of the non-Newtonian fluid and its behaviour at different oscillating conditions. CFD modelling is an advanced tool to study the various aspects of dynamic velocity variations within such complex systems. In literature, studies can be found related to oscillatory non-Newtonian fluid flow in pipelines or simply in tubes [25-29].

However, almost all of them have investigated the flow enhancement or retardation when the liquid containing pipe is oscillated by different means and confirms that the pulsatile flow of shear-thinning non-Newtonian fluids enhances the flow within pipelines [25]. The experimental and numerical study performed by Mena et al. [27] to examine the flow enhancement of viscoelastic fluids through pipes vibrated longitudinally reveals that the maximum enhancement achieved at maximum frequency and amplitude. However, the dominating factor in the oscillating flow of viscoelastic liquids in pipes is the shear dependent viscosity. According to the studies performed by Torralba et al. [30], it has been identified that the remarkable enhancement in the dynamic response of the viscoelastic behaviour in the presence of a pulsating environment could be attributed to a resonant effect due to the elastic behaviour of the fluid and the geometry of the container as well.

However, numerical (or computational) studies that address the effect of oscillatory motion on the rheology of non-Newtonian fluids are limited. The concept of applying vertical liquid vibrations in the newly designed experimental setup for the core study has been utilized as the basis for these numerical simulations. See **Paper IV** for more details.

2.2 Core study

2.2.1 Dynamics in oscillating fluids

The majority of pipe flow investigations available in the scientific literature are related to the steady flow. However, more attention should be paid to unsteady flows, since there are many industrial and biological applications in the fields of applied fluid mechanics such as blood flow in the large arteries [31], respiratory flow in the trachea [32], oil pressure engineering, reciprocating compressors, gas kicks and pressure oscillations in oil well drilling [15], food transportation [33], etc.

According to literature, there are two major types of unsteady flows: namely, pulsating (or pulsatile) flow and pure oscillating flow [32, 34, 35]. The pulsatile flow is an oscillating flow superimposed on a steady flow with a non-zero mean velocity, whereas the pure oscillating flow has zero mean velocity. Harmonic oscillating flow is the simplest unsteady flow [36]. This research focuses on the pure oscillating flow, close to being harmonic.

The kinematic structure of the flow is noticeably altered by oscillatory motion within a pipe. It can significantly deform the velocity profile [37-40] or can influence the turbulent characteristics [32], by leading to a change of integral flow parameters such as hydraulic resistance and heat transfer [41]. Further, it can produce a boundary layer on the bottom of a channel by the progressive liquid waves and cause liquid hammer [42] too, which can be detrimental to the durability of the pipeline. Furthermore, if the fluid in the oscillatory environment which is at least close to turbulent, the process becomes even more complicated from a rheological point of view.

2.2.2 Past work regarding the oscillatory flow in Newtonian and non-Newtonian fluids

Some theoretical, numerical and experimental approaches to investigate this oscillatory motion within pipes were found in the literature where many researchers have investigated them in horizontal ducts and pipes. However, the majority of those studies are hydrodynamic flow regime testing experiments for Newtonian fluids [32, 34, 38, 42-48], where they mostly talk about the transition from laminar to turbulent flow regime. some of them have studied different geometries such as rectangular ducts [49-51] also.

Significant contributions have been given from researchers who have employed different non-Newtonian fluids in their studies regarding oscillatory laminar flow. Such studies could be either between infinitely

large parallel plates [52] or in a rigid tube of infinite length and circular cross-section [53]. The non-Newtonian fluids used in such studies have different rheological characteristics such as highly viscous and shear-thinning, constant viscosity but elastic (Boger fluids), viscoelastic, etc. See the introduction section in **Paper V** and **VI** for detailed examples.

2.2.3 Significance of oscillatory motion on non-Newtonian fluids

The oscillatory flow of a non-Newtonian fluid is remarkably different from that of a Newtonian fluid, even at low driving frequencies. Particularly, viscoelastic fluids could exhibit both viscous dissipative behaviour of simple fluids and also the elastic response characteristic of solids which originates from the reorientation and stretching of the fluid molecules. When subjected to oscillatory motion highly viscoelastic non-Newtonian fluids could display resonance behaviour [54, 55] and also with vortex ring formation [56]. Substantial differences in the dynamic response of non-Newtonian fluids compared with Newtonian fluid are reported [30, 57-59].

Furthermore, oscillatory motion naturally leads shear-thinning non-Newtonian fluids to experience shear rate related changes in rheological parameters such as shear viscosity, gel formation and extensional viscosity [60], etc. Most of the water-based drilling fluids usually have a strong gel structure since they possess a high extensional viscosity. According to Saasen and Hodne [4, 23], such drilling fluids having high extensional viscosity are generally not that much affected by vibrations/oscillations. The reduction of viscosity of non-Newtonian polymeric liquid under vibrations/oscillations could be explained using the structural units that contain within the polymeric non-Newtonian fluids [61]. These structural units are local agglomerations of particles and polymers that govern the viscosity of the fluid. The agglomerations are usually stabilized by the interaction of surface charges of the different

particles and when any vibrational field is applied to the fluid, these structural units are partially destroyed and the viscosity is altered.

2.2.4 Governing non-dimensional parameters for an oscillatory flow

The most relevant dimensionless parameters that characterize the oscillatory flow at a given driving frequency and amplitude are revisited here.

If the sinusoidal oscillatory movement is imposed in the transversal y-direction parallel to the flow as shown in Fig. 2-1, the vertical displacement, $y(t)$ of any particular liquid point along the centreline of the pipe can be written as;

$$y(t) = |a'| \sin(\omega t) \tag{2-1}$$

where, a' is the displacement amplitude of the liquid medium, t is the time and $\omega = 2\pi f$, where f is the frequency of oscillation.

The vertical linear velocity of the bulk liquid medium at the centreline of the pipe $V(t)$ due to the oscillation is, therefore,

$$V(t) = \frac{dy}{dt} = |V| \cos(\omega t) \tag{2-2}$$

where $|V| = |a'|\omega$ is the amplitude of the centreline velocity in the axial direction.

2.2.4.1 Oscillating Reynolds number (Re_δ)

According to the general approach for a steady flow, the Reynolds number for a circular pipe flow (Re_D) is given for example by Clamen and Minton [62];

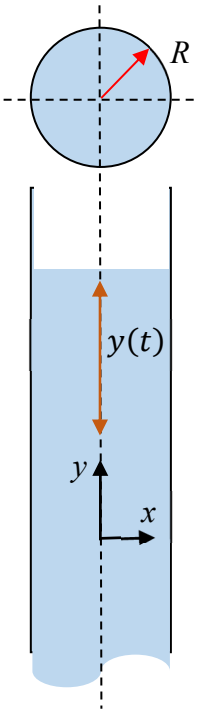

Figure 2-1: Sinusoidal oscillatory motion imposed on the fluid in a vertical pipe

$$Re_D = \frac{|V|D}{\nu} \tag{2-3}$$

where D is the pipe diameter and ν is the kinematic viscosity of the fluid concerning within the circular pipe. However, since the oscillatory flow is of the main focus in this study, it is important to introduce the Reynolds number associated with the oscillatory flow. The Reynolds number measures the ratio of inertial forces to viscous forces where the oscillating Reynolds number (Re_δ) based on the Stokes boundary layer thickness (δ) is [32, 40, 63, 64];

$$Re_{\delta} = \frac{|V|\delta}{\nu} \tag{2-4}$$

This Stokes boundary layer or the viscous penetration depth is defined as [32];

$$\delta = \sqrt{\frac{2\nu}{\omega}} \tag{2-5}$$

It is to be noted that, δ is particularly defined for a Newtonian fluid where transverse oscillations are therefore overdamped (cannot propagate into the fluid). However, since things are different for viscoelastic non-Newtonian fluids, this special notion has been successfully extended to adapt for the simplest viscoelastic fluid (a Maxwell fluid) as described in section 2.2.4.4.

Moreover, since $|V| = |a'|\omega$, Re_D in Eq. (2-3) can be re-written including the oscillatory behaviour [48, 65] as;

$$Re_D = \frac{(|a'|\omega)D}{\nu} \tag{2-6}$$

which is by definition higher in value than Re_{δ} expressed in Eq. (2-4) (since $D \gg \delta$). Some researchers have used the expression in Eq. (2-4) as the oscillating Reynolds number since the term $|a'|\omega$ represents the maximum velocity amplitude of the liquid medium.

Other researchers have presented the oscillating Reynolds number with some slight changes to the expression presented in Eq. (2-4). For instance, Khabakhpasheva et al. [66] introduced the pulsating/oscillating Reynolds number (Re_f) as the ratio of time scale for the diffusion of

momentum to the time scale of oscillation. Notation-wise, Re_f can be written as;

$$Re_f = \frac{R^2/\nu}{1/f} = \frac{R^2 f}{\nu} \tag{2-7}$$

Zhao and Cheng [67] defined the pulsating Reynolds number (Re_ω) as;

$$Re_\omega = \frac{\omega D^2}{\nu} \tag{2-8}$$

Both Eqs. (2-7) and (2-8) result in a very large value compared to that of Re_δ. After considering different values reported in the literature, it was concluded that, Re_δ = 500 (based on viscoelastic Stokes boundary layer which will be defined later in this thesis) is to be considered as the critical Reynolds number for this research on oscillatory flow in a vertical pipe. Refer to **Paper V** and **VI** for a detailed evaluation of the critical Re_δ.

2.2.4.2 Womersley number (Wo)

It is a measure of the ratio of the pipe radius to the distance through which vorticity diffuses away from the wall in one period of oscillation [68]. It was introduced by Womersley [69] and considered as the basic parameter of oscillatory flow. In some instances, it is referred to as the "non-dimensional frequency" [34, 38, 43, 68] or the "frequency parameter" (α) [62] and can be expressed as [70];

$$Wo = \alpha = \frac{D/2}{\sqrt{\nu/\omega}} \tag{2-9}$$

Fishler and Brodkey [32] state the physical interpretation of α as the ratio of the time of a cycle ($1/\omega$) to the time necessary for the amplification

of disturbances (R^2/ν). They claim that increasing α should lead to a stable state of the flow if Re_D is held constant.

2.2.4.3 Stokes parameter (Λ)

The Stokes parameter measures the ratio of the pipe radius ($R = D/2$) to the viscous penetration depth (δ) for oscillatory viscous flow in a pipe. Thus, Λ can be expressed as [34, 42];

$$\Lambda = \frac{D/2}{\delta} = \frac{D}{2}\sqrt{\frac{\omega}{2\nu}} \tag{2-10}$$

where the relation between Re_D and Re_δ can be written as;

$$Re_D = 2\Lambda\, Re_\delta \tag{2-11}$$

Here, Λ is defined based on δ for a Newtonian fluid and relevant adaptations for a non-Newtonian fluid are explained in section 2.2.4.4.

2.2.4.4 Deborah number (De)

This is one of the main dimensionless parameters to describe the flow of any non-Newtonian viscoelastic fluid. For a simple viscoelastic fluid (a Maxwell fluid), since the stress relaxation can be described by a single time constant which we call the relaxation time (λ) of the fluid, it has been employed in defining the non-dimensional parameters related to non-Newtonian oscillatory flows. De is the measure of the relative importance of the relaxation time (λ) of any viscoelastic fluid to the scale of the flow which is the same as the characteristic time or the oscillation period ($T = 2\pi/\omega$) for the deformation process [71]. De can be expressed as;

$$De = \frac{2\pi\lambda}{T} = \lambda\omega \tag{2-12}$$

As explained in section 2.2.1, since the behaviour of non-Newtonian fluids are different from that of simple dissipative Newtonian fluids, the viscous penetration depth for a viscoelastic fluid (δ_{ve}) is expressed as [72];

$$\delta_{ve} = \delta(De + \sqrt{1 + De^2}) \tag{2-13}$$

It is clear that the difference between Eqs. (2-5) and (2-13) is imposed by the elasticity of the fluid ($De > 0$), so that the transverse oscillations can effectively propagate before they are attenuated.

Furthermore, the viscoelastic Stokes parameter (Λ_{ve}) can be expressed as [72];

$$\Lambda_{ve} = \frac{R}{\delta} \tag{2-14}$$

In analogy to Λ, the parameter Λ_{ve} is the ratio of the radius to the extension of the shear waves generated by the pipe walls. In the theoretical analysis performed on the laminar oscillatory flow of Maxwell and Oldroyd-B fluids, Casanellas and Ortin [72] characterize the non-Newtonian oscillatory systems into two main categories as; (1) 'narrow' systems for $\Lambda_{ve} < 1$, when viscoelastic shear waves extend through the whole system and (2) 'wide' systems for $\Lambda_{ve} > 1$, when an inviscid core is present at the centre of the pipe.

2.2.4.5 Viscous to relaxation time ratio (ψ)

This is another important non-dimensional parameter that characterizes the flow of any non-Newtonian viscoelastic fluid. The viscous time scale (t_v) to relaxation time ratio is expressed as;

$$\psi = \frac{t_v}{\lambda} = \frac{R^2/\nu}{\lambda} \tag{2-15}$$

Following a similar characterization method, Casanellas and Ortin [72] state that, at $\psi \ll 1$ (where highly viscoelastic fluids are oscillated in narrow tubes) the resonant behaviour could occur. At $\psi = 1$ the velocity magnitude at the centre is strongly decreased and for $\psi \gg 1$ the resonances could completely disappear.

2.2.4.6 Weissenberg number (Wi)

The ratio of the relaxation time of the fluid to the characteristic inverse shear rate is defined as the Weissenberg number. Wi is expressed as [71];

$$Wi = \lambda\dot{\gamma} \tag{2-16}$$

Here, $\dot{\gamma}$ is the shear rate and can be calculated as is the relative velocity of two fluid layers moving with respect to each other [73, 74] and is expressed as;

$$\dot{\gamma} = \frac{dv_f}{dr} \tag{2-17}$$

where r denotes the radial distance. A value of higher Wi indicates the elastic stresses become large and the onset of elastic instabilities.

2.2.5 Particle settling in oscillating liquid mediums

After the first introduction of Stokes law for the creeping flow regime by George Stokes in 1851, many researchers have worked a lot on the settling of particles in Newtonian fluids even in higher Reynolds numbers [75-81]. Even the works related to the settling of particles in shear-thinning non-Newtonian fluids are also omnipresent in literature [82-89]. However, all the above-mentioned studies are related to the settling of particles in stationary fluids while dynamic settling [90-93]

has become an interesting topic with respect to its practicality and the importance in industrial applications.

Particle settling in oscillatory systems is a practically important example under dynamic settling. Sinusoidal oscillatory fluid motion exhibits a condition of continuously changing acceleration and thus the flow patterns and drag phenomena could be significantly different from those at steady state. Therefore, the contribution of the lift and drag forces to the dynamics of the particles becomes much more significant [94-96] as a result of the changes in the flow patterns around the particle. Those will eventually have a considerable impact on both the instantaneous relative velocity of the particle to the fluid and also on the mean transport velocity of the particle [97].

2.2.6 Past work related to particle settling in oscillatory flow

Interest in the geophysical as well as in the industrial problems has spawned many theoretical and experimental studies on particle settling in oscillatory Newtonian fluids in the past. Such studies reveal that the drag forces in unsteady systems tend to exceed the average forces that might be expected from the laws of drag under steady conditions [98].

In a fascinating series of papers [99-101], Houghton describes deeply the velocity profile around a particle in a sinusoidal field and introduces a hydrodynamic model based on the non-linear Langevin equation (See Eq. (2-18)) to predict the directional motion of particles by applying a sinusoidal velocity to the continuous phase in which the particles are suspended.

$$(\rho_p + \chi\rho_f)\frac{\pi d^3}{6}\frac{dv_p}{dt} = (\rho_p - \rho_f)g\frac{\pi d^3}{6} - \frac{1}{2}\rho_f C_D \frac{\pi d^2}{4}(v_p - v_f)|v_p - v_f|\#$$

$$+ \rho_f(1+\chi)\frac{\pi d^3}{6}\frac{dv_f}{dt} + B(t) \qquad (2\text{-}18)$$

where, ρ_p is the density of the particle, ρ_f is the density of the oscillating fluid (continuous phase), d is the diameter of the spherical particle, v_p is the instantaneous velocity of the particle taken as positive downwards, v_f is the velocity of the fluid taken as positive downwards, g is the gravitational acceleration, C_D is the drag coefficient, t is the time, χ is the added mass coefficient and $B(t)$ is the Basset term. As expressed in Eq. (2-2), it is assumed that the continuous phase experiences a uniform velocity (v_f), which is sinusoidal with an angular frequency of ω in the direction of particle motion. The term on the left-hand side of Eq. (2-18) represents the inertial forces on the particle. The added mass coefficient (χ) is required to account for the virtual mass that is slightly larger than the ordinary mass of the particle by a fraction of χ of displaced fluid. The first term on the right-hand side of the Eq. (2-18) gives the buoyancy forces on the particle while the second term represents the frictional (drag) forces on the particle. The third term on the right-hand side of the Eq. (2-18) corresponds to the effects of the pressure gradient in the accelerating fluid phase combined with the virtual mass of the fluid displaced by the particle. According to Houghton [99], the simple form of this term arises from the assumption that there are no velocity gradients in the fluid perpendicular to the direction of motion. The Basset term $B(t)$ has been introduced to allow the effects of deviations of the flow pattern around the particle from that at steady state. If the particle diameter is small and the fluid density is small compared with that of the particle, then $B(t)$ becomes insignificant.

Herringe and Flint [97] have studied the free fall of particles through a vertically oscillated Newtonian fluid both theoretically and experimentally and state that the motion of the particle is most accurately predicted when the 'history' and 'added mass' terms are preceded by empirical coefficients which are functions of the instantaneous acceleration number. Many researchers have utilized this non-linear Langevin equation to prove that the settling velocity of particles is caused by the nonlinearity of the fluid drag and the particles exhibit

retardation in oscillatory environments. According to the study performed by Hwang [102], the three major factors that govern the variation of effective fall velocity of particles in oscillating flows are the terminal velocity Reynolds number (Reynolds number of the settling sphere in still fluid), the velocity amplitudes of the flow and particle oscillations and the phase lag. Refer to Paper VII for more details.

The terminal velocity Reynolds number of the particle ($Re_{p0} = \rho_f v_p d/\mu_f$) is not the same as the instantaneous particle Reynolds number (Re_p) in oscillatory conditions which can be explained as [103, 104];

$$Re_p = \frac{\rho_f (v_p - v_f) d}{\mu_f} \tag{2-19}$$

where, μ_f is the dynamic viscosity of the fluid medium. Following the same pattern mentioned in Eq.(2-6), Re_p can be written in another form using the particle amplitude within the oscillating liquid medium (a_p) as [105-108],

$$Re'_p = \frac{\rho_f (a_p \omega) d}{\mu_f} \# \tag{2-20}$$

2.2.7 Significance of particle settling in oscillating non-Newtonian fluids

When a relatively dense particle settles through a sheared flow in a non-Newtonian fluid, the shear rate of the background flow varies and thus the settling velocity of that particle may vary spatially and temporally due to the non-linear rheology of the fluid. Significant measures need to be taken into account with this regard, such as the distance that those

particles can be transported before settling out, the time they take to do so and the geometry of the deposit, etc.

Van den Brule and Gheissary [92] state that the settling velocity of spherical particles at stationary conditions is reduced by the elastic effects of the non-Newtonian fluid medium due to the presence of normal stress differences and high elongational viscosity and mention a reduction of the average settling velocity in viscoelastic fluids in the presence of an orthogonal shear-flow field. In a later study [109], the same authors extend their experiments claiming that an increment in the settling velocity could be observed with an increasing shear rate of the main flow of non-Newtonian fluids. This is related to the non-linear rheology of the fluids and thus the reduced viscosity with increased shear rate. The same conclusion has been confirmed by Talmon and Huisman [110] with their experimental study on particle settling in viscoplastic fluids under shear flow conditions where the settling velocities increase with increasing shear rate.

In the oil industry, most fracturing/drilling fluids exhibit highly shear-thinning, non-Newtonian fluid characteristics. They are used to suspend drilled cuttings where they expose to different oscillatory conditions while they are circulating through the well or during the solids control operations. They possess completely different properties under shear than when it is at rest. Even though most of the particle settling studies are undertaken in stationary fluids, in the actual drilling process the cuttings are settling while the fluid is moving and mostly oscillating within the fracture. Generally, the properties of the cuttings being settled, rheology and density of the drilling fluid and the retardation effect of the confining fracture walls determine the settling rate of cuttings [84]. However, this research shows that the settling of cuttings is governed by the properties of oscillatory motion as well, and illustrates the importance of studying the settling of particles in non-Newtonian fluids under oscillatory conditions since it is not desirable to have deposition of particles in pipes and boreholes.

2.3 Aim and scope of the research

The overall aim of this research is to investigate the effect of oscillatory motion in shear-thinning, non-Newtonian fluids and its influence on particle settling. However, the scope of the study which is partly motivated by challenges associated with operational procedures during drilling and maintenance of petroleum wells extends from pre-study to core study to fulfill the main aim and the whole research focuses on several aspects that involve;

- A rheological study to provide a comprehensive description of shear rate dependent viscosity together with viscoelasticity of model drilling fluids when an additional viscosifier is added. Both steady state and dynamic state experimental procedures have been followed to identify the shear-thinning non-Newtonian and viscoelastic properties of the combined polymer. The authors have investigated the relationship between polymer concentration and the behaviour of the combined polymer. The results of this study provide quantitative information about the dynamic properties of the concerned biopolymers.

- An application of low-frequency (lower part of the acoustic range) acoustic pressure field in both Newtonian and non-Newtonian liquids to investigate whether they can influence the rheology of drilling fluids and subsequently the particle settling within non-Newtonian drilling fluids. The study describes how the streaming velocity is affected in both qualitative and quantitative manner when the frequency, input power as well as the fluid rheology is changed.

- An application of the PIV technique to present the dynamic velocity profiles within the bulk liquid medium, which is corrected by the velocity magnitude of the reference frame. This paper applies a rheological approach to quantify the effect of horizontal vibration on

shear-thinning non-Newtonian polymers, which can be used as model drilling fluids.

- A numerical study to investigate the effect of oscillation frequency and velocity amplitude on the dynamic velocity field within the liquid medium and to interpret its consequences on non-Newtonian rheology and settling of particles within shear-thinning non-Newtonian drilling fluids.

- An investigation of the dynamic velocity profiles in both Newtonian and non-Newtonian fluids oscillated vertically with a zero-mean velocity within a rigid, straight cylindrical geometry. The time-resolved PIV system is employed to obtain a full-field non-intrusive analysis of the fluid system to study the fluid dynamics of unsteady flows in a local scale to mimic the dynamics that take place within a vertical oil well. The study describes how the shear-thinning non-Newtonian drilling fluid rheological properties alter when they are exposed to oscillatory motion within a vertical pipeline and predict the consequences of particle settling.

- An investigation of single particle behaviour in a vertically oscillating Newtonian and non-Newtonian fluid to bring out valuable conclusions concerning the influence of Newtonian and non-Newtonian liquid oscillations upon the average settling velocity of single particles. The aim was to provide information on engineering significance in the design of engineering applications experiencing vibration/oscillation and also to understand the mechanics of particle suspension and dislodgement in wall-bounded oscillatory flows.

3 Methodology, measurement techniques and data analysis

As explained in Chapter 1, this research consists of two main studies named; pre-study and the core study. Therefore, the methodology described in this chapter includes different experimental setups employed in different sub-studies under pre-study and core study. All the experiments were performed in the multi-phase flow laboratory at the University of Stavanger (UiS), Norway.

3.1 Materials and sample preparation

3.1.1 Test fluids

All the sub-studies under pre-study and core study employ shear-thinning non-Newtonian fluids and require preparation of water-based polymeric test fluids for the experiments and investigating the rheological characterization of them. The details of the different polymers used to prepare the test fluids are summarized in Table 3-1.

Table 3-1: Different polymers used to prepare the test fluids

Type of polymer	Supplier	Appearance	Viscosity at 25°C
Poly-anionic Cellulose (PAC) - PolyPAC-R	MI-Swaco	White/off-white colour granular powder	800 - 1200 mPa.s (1% H_2O)
Xanthan Gum (Xg)	MI-Swaco	White/off-white colour granular powder	20 – 700 mPa.s (0.2% H_2O)
Medium viscous Carboxymethyl Cellulose (MV-CMC)	Sigma-Aldrich	White/off-white colour granular powder	400 – 1000 mPa.s (2% H_2O)

High viscous Carboxymethyl Cellulose (HV-CMC)	Sigma-Aldrich	White/off-white colour granular powder	1500 – 3000 mPa.s (1% H_2O)

Every time, the non-Newtonian test fluids were prepared by mixing with deionized water. For the core study, a mixture of PAC, MV-CMC and HV-CMC was used as the non-Newtonian test fluids as described in Table 3-2 and referred them as 'Fluid 1', 'Fluid 2' and 'Fluid 3'. However, for the pre-study, an individual type of polymer solution has been employed as the test fluid and in some cases, the Xg was employed as a viscosifier.

Table 3-2: Composition of non-Newtonian test fluids

Polymer type	Used weight [g] to dissolve in 5 L of deionized water		
	Fluid 1	Fluid 2	Fluid 3
PolyPAC	0.5	7.5	22.5
MV-CMC	5	5	5
HV-CMC	4.5	7.5	2.5

The water-polymer solutions were mixed using the Silverson L4RT-A mixer at low shear conditions for 15 - 20 minutes to minimize shear-induced degradation. The prepared non-Newtonian test fluids were always kept still for 48 hrs, for complete hydration and the eventual release of any trapped air bubbles. Both deionized water and non-Newtonian fluids were assumed to be incompressible.

3.1.2 Particles

Three different sizes of glass beads were employed in the experiment series to study the settling rate under oscillatory conditions. Accurate particle diameters were measured using an Olympus SZX16 stereo

microscope and an average particle diameter was used in the calculations. The weight of the particles was measured using an analytical balance with a digital precision scale and the specific details of the particles used are mentioned in Table 3-3.

Table 3-3: Specific details of the particles (approx. 50 glass beads)

Particle name	Average diameter [mm]	Average Weight [mg]	Density [kg/m^3]
1 mm	1.128 $\pm$ 0.003	1.89 $\pm$ 0.4	2514.9
2 mm	1.986 $\pm$ 0.002	11.11$\pm$ 0.3	2708.8
3 mm	2.960 $\pm$ 0.001	36.69 $\pm$ 0.2	2701.9

However, the particles will be called with their general sizes (as 1 mm, 2 mm and 3 mm) for clarity. Different particles of the same size have been used for each test to cancel out possible effects associated with imperfections of the particle surface.

3.2 Measurement Techniques

3.2.1 Rheological measurements

For every sub-study, the non-Newtonian test fluids were tested for steady-state and dynamic-state rheological properties using an Anton Paar MCR 302 apparatus at ambient pressure. The geometry with concentric cylinder mode (CC27 – bob radius 13.327 mm and cup radius 14.455 mm) was employed to have a high measuring accuracy and low liquid evaporation. The solutions were gently stirred for a few minutes before loading into the cylinder cup to achieve a uniform sample for the experiments. After pouring the required amount of sample to the measuring cup, the bob was lowered at a very slow speed to prevent the disruption of the solution structure. It was assumed that the samples had sufficient adhesion to the measuring bob and the cylinder cup without any wall-slip effects and the samples are deformed homogeneously

throughout the entire shear gap to achieve accurate rheological parameters. All the test runs were carried out four times to check the repeatability and reproducibility.

3.2.1.1 Analysis of the rheological measurements

All sub-cases required characterization of the rheological properties of the test fluids employed for each experiment. This section presents the results of the rheological characterization for the first part of the core study as a general approach used throughout the whole research (in both pre-study and core study). Fig. 3-1 shows the dynamic viscosity (μ_f) curves for the all the three fluids used in the experiment, together with their corresponding power-law parameters. The power-law rheological model as shown in Eq. (3-1) was used in all the sub-studies to model the viscous and the shear-thinning behaviour of the test fluids and in some cases, Carreau-Yasuda (CY) model was also used.

$$\mu_{PL} = K\dot{\gamma}^{n-1} \tag{3-1}$$

Here, μ_{PL} is the viscosity predicted by the power-law model, K is the consistency index, n is the behavioral index and $\dot{\gamma}$ is the shear rate. The parameters for the model are mentioned in Fig. 3-1.

The shear-thinning behaviour of the test fluids can be easily distinguished from the viscosity curves in Fig. 3-1 where Fluid 3 is the most shear-thinning fluid with the lowest n value. It is to be noted that, the power-law model has been applied only for the linear region of the experimental viscosity data and that does not cover the constant viscosity plateau observed in the low values of shear rate.

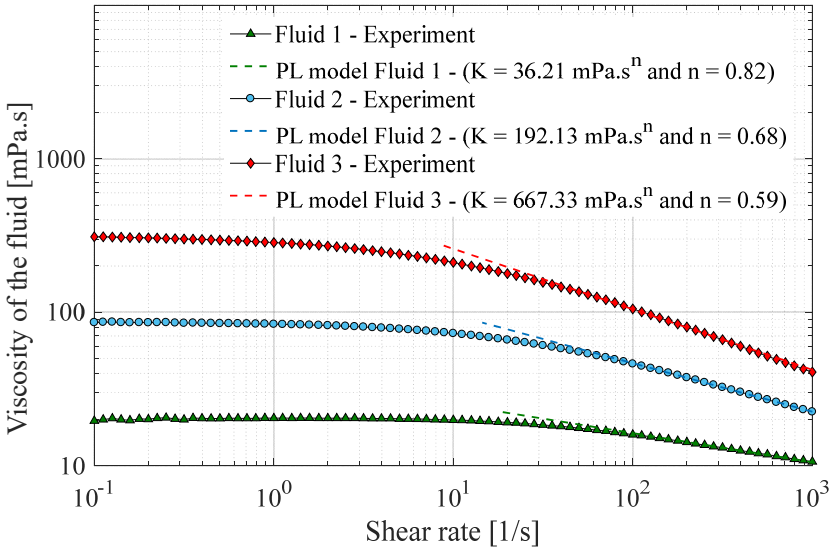

Figure 3-1: Viscosity curves for the test fluids at 21 °C

However, it is important to mention, that for the latter part of the core study where the settling particles were incorporated, the power-law model is fitted to the viscosity data in the range of shear rates encountered by the particles within all the experimental cases. The shear rate used is the maximum particle shear rate defined as [111];

$$\dot{\gamma}_p = \frac{3v_p}{d} \tag{3-2}$$

The viscoelastic properties of the test fluids were also measured in small amplitude oscillation shear (SAOS). To determine the linear viscoelastic (LVE) region at low strain amplitudes, and also to investigate the viscoelastic behaviour of the samples, strain amplitude sweeps and frequency sweeps were conducted. Fig. 3-2 shows the results of the amplitude sweep test only for Fluid 3, over a given strain (γ) range. It was ramped up logarithmically from 1 to 1000%, at a constant angular frequency of ω = 10 rad/s.

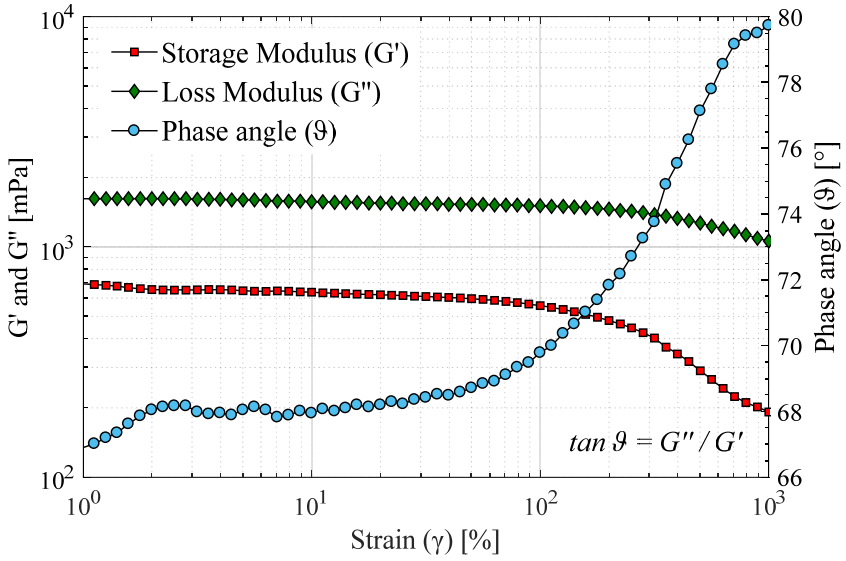

Figure 3-2: Amplitude sweep test for Fluid 3 at a constant angular frequency of ω = 10 rad/s

It can be observed that the viscous (loss) modulus (G'') of Fluid 3 is larger than its elastic (storage) modulus (G'), and the calculated phase angle (ϑ) is varying from approximately 65° to 80°. The variation of moduli curves for the two other test fluids also shows a similar trend, where there is no crossover point between the moduli curves. Therefore, it could be concluded that all three test fluids are slightly viscoelastic at the corresponding low shear region. The G' curve for Fluid 3 starts to lose its plateau value at around 10% of shear strain which corresponds to a shear rate value of $\dot{\gamma}$ = 1 1/s. That is identified as the limiting value of the shear strain (γ_L) for Fluid 3 which defines the LVE range. Other test fluids have shorter LVE ranges than Fluid 3 where Fluid 1 has the shortest with its G' starts to decrease at much lower strain around ($\gamma <$ 2%).

The viscoelastic property of a polymer solution in its LVE range is reflected in the frequency sweep data, which can be used to investigate the time-dependent deformation behaviour. It is a direct measure of

elasticity [112]. Fig. 3-3 shows the results of the frequency sweep test for Fluid 3 over a given angular frequency (ω) range (ramped down logarithmically from 100 to 1 rad/s) at a constant strain 1%.

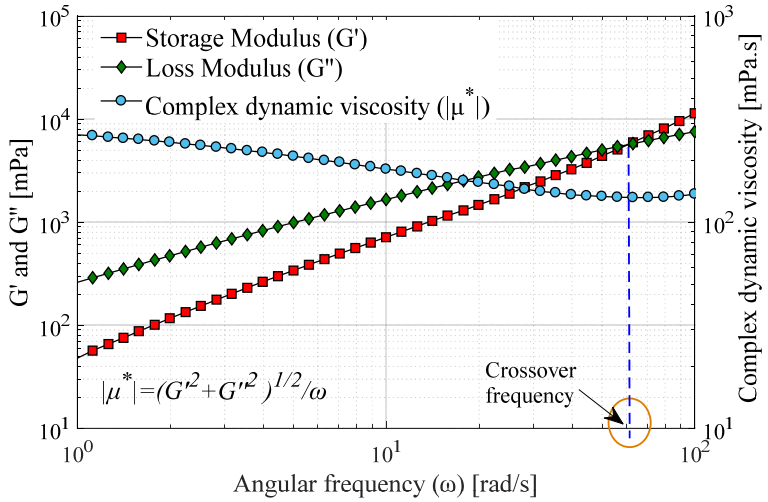

Figure 3-3: Frequency sweep test for Fluid 3 at a constant strain at γ = 1%

It can be seen from Fig. 3-3, that both the elastic and the viscous moduli increase with increasing frequency. However, the elastic modulus (G') increases at a higher rate than the viscous modulus (G'') and the solid-like behavior of the fluid becomes dominant after the crossover frequency as illustrated in Fig. 3-3. The inverse of this crossover frequency represents the longest characteristic relaxation time (λ) of the polymer solution [85] and the corresponding λ values for the three fluids are 0.037 for Fluid 1, 0.021 for Fluid 2 and 0.016 for Fluid 3. That means Fluid 1 has the highest relaxation time of the test fluids and therefore has the highest elasticity. Since the λ values are very small, it could be concluded that the test fluids are only slightly viscoelastic. All the aforementioned rheological properties were measured just after the corresponding experimental run.

3.2.2 The PIV system

Particle Image Velocimetry (PIV) is the main measurement technique employed in this research throughout the various sub-studies under pre-study and also in the core study. The measurement area by the PIV system was set specifically to the experimental setup based on each experiment to avoid/minimize the end-effects as much as possible and described in respective sections within this thesis. A Basler camera (Model: acA800-510um USB 3.0 camera with the ON Semiconductor) was used for image acquisition. Their maximum frame rate is 500 fps at a full resolution of 800 x 600 pixels^2. A Nikon AF Nikkor 50 mm – f/1.4D lens was used in some experiments and Basler C125-0818-5M F1.8 f/8 mm lens was used in some experiments. The acquisition rate and the region of interest (ROI) were set based on the local dynamic conditions for each experiment. The measurement area of the PIV system was illuminated with a Photop LDC-2500S continuous wave (CW) laser (class 3B) at wavelength 532 nm (green light spectrum) and variable output up to 200 mW. The thickness of the laser beam was set to approximately 1 mm using a lens and the collimator system in all the test cases. The laser sheet was aligned such that it illuminates the required plane through the centre of the pipe or the liquid container (see respective sketches of the experimental setups). To illuminate the fluid motion, Polyamide seeding particles were used (Model: PSP50, Dantec Dynamics), with mean particle diameter = 50 µm and specific density = 1.03 g/m^3 as the tracer particles. The Stokes number (Stk) for the seeding particles was approximately $5.5\times10^{-4} \ll 0.1$ and the settling speed of the seeding particles are very small, typically less than 10^{-7} m/s. The change of rheology of the test fluids due to the addition of seeding is negligible.

3.2.2.1 Analysis of PIV images

The PIV analysis was performed using PIVlab – version 2.01 [113], which is a digital particle image velocimetry (DPIV) tool developed in

MATLAB. As shown in Fig. 3-4, the region of interest (ROI) was limited to the conditions of the specific experimental conditions rather than the entire image captured. The size of the smallest interrogation area was selected based on the guidelines provided by Jensen [114].

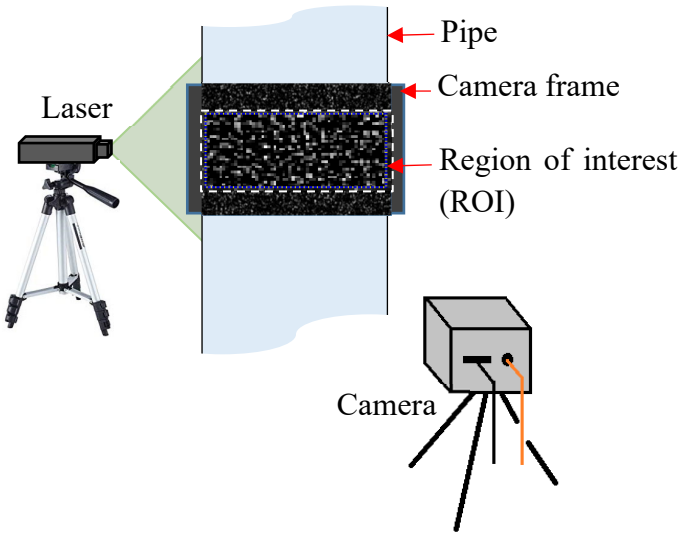

Figure 3-4: Setting up the ROI for the PIV measurements

As explained by Adrian [115] and Westerweel [116], the most probable displacement of the tracer particles which is homogeneously seeded in a small interrogation area can be inferred from the cross-correlation of two successive captures of the flow field. It is a statistical pattern matching technique that tries to find the particle pattern from the interrogation area A (at $t = t_0$) back in the interrogation area B (at $t = t_0 + \Delta t$). In PIVlab, it is accomplished with the discrete cross-correlation (DCC) function [117] and the location of the intensity peak in the resulting correlation matrix gives the most probable displacement of the particles from A to B [113].

All the images were pre-processed using contrast limited adaptive histogram equalization (CLAHE) method [113] and some of the background noise was removed using a high pass filter. For the PIV settings, an FFT window deformation was adopted. The horizontal or vertical velocity components were determined from PIV analysis for further processing based on the specific requirements and aims of the experiments.

3.2.3 High-speed imaging

The test cases under the core study mainly used high-speed imaging in addition to the PIV measurements. The specific measurement area captured by the high-speed images and the acquisition rate for each case is described under the respective experimental setup. Basler lens of model: C125-0818-5M F1.8 f/8mm was used together with a similar type of camera used for PIV measurements. The measurement areas were sufficiently illuminated using a LED lamp without disturbing the PIV system. When two or more cameras are employed, they were synchronized using a LabView program and triggered by a separate control switch. Every time, the results were acquired after allowing the system to achieve a stable periodic motion. The data treatment for the high-speed imaging system was specific to the particular sub-study and is described under each sub-section.

3.2.4 Level measurements by the motion sensor

The motion sensor of model PS-2103A from PASCO scientific instruments was used in 1st sub-study under the core study (see Fig. 3-8). A set of flow measurements with zero oscillation was always recorded initially for calibration and reference with a sampling frequency of 200 Hz. The motion sensor uses an ultrasonic electrostatic transducer (directed along the axis of the pipe) as both an emitter and receiver. For each measured distance (or liquid height), the transducer transmits a burst of 16 ultrasonic pulses with a frequency of about 49 kHz, which

are reflected off the air-liquid interface and returned to the sensor. Time-of-flight between the trigger-rising edge and the echo-rising edge is measured, and the distance to the interface calculated based on the present speed of sound.

The motion sensor was connected to the PC through the PASCO control unit (PS-850) and provided a good indication to get an initial observation on stability (well-developed) of the oscillatory flow before starting image acquisition. The measurements from the motion sensor confirmed the oscillation frequency provided by the piston to the fluid system.

3.2.5 Acceleration measurements using the accelerometer

Instantaneous acceleration measurements provided by a PASCO 3-axis accelerometer PS-2136A were used to set the driving frequency of the shaking table described in the 3rd sub-study (see section 3.3.3 and Fig. 3-6). It contains one acceleration sensor which measures the acceleration in all three dimensions, as well as changes in altitude with a maximum sampling frequency up to 500 Hz. Dynamic variable over-sampling automatically reduces the measurement noise at slower sampling rates.

3.3 Experimental procedures and data treatment methods within pre-study

3.3.1 Rheological study on the combined biopolymer

According to the sample preparation procedure described in section 3.1.1, the individual concentrations of PAC were prepared as 0.2 and 0.4 w/w% while the individual concentrations for Xg were prepared from 0.05 to 0.4 w/w%. After a sequence of calculations and dilutions, nine different samples were prepared to be used in the experiments and kept still for 24 hrs more to enable relaxation of the sample and to reduce

possible still existing pre-stresses deriving from the preparation of the sample. Based on the hysteresis analysis described in **Paper I**, PAC 0.4 w/w% was selected as the base fluid to be mixed with different Xg concentrations. The combined polymer concentrations used for the experiments are mentioned below in Table 3-4.

Table 3-4: Test samples with their components for the rheological study under prestudy

Sample number	PAC concentration	Xg concentration
1	0.4 w/w%	0
2	0.4 w/w%	0.05 w/w%
3	0.4 w/w%	0.10 w/w%
4	0.4 w/w%	0.15 w/w%
5	0.4 w/w%	0.20 w/w%
6	0.4 w/w%	0.25 w/w%
7	0.4 w/w%	0.30 w/w%
8	0.4 w/w%	0.35 w/w%
9	0.4 w/w%	0.40 w/w%

The nine samples shown in Table 3-4 were tested for steady-state and dynamic-state rheological properties. Full details of the experiment and the rheological characterization are mentioned in **Paper I** and some main remarks are highlighted in Chapter 4.1.1.

3.3.2 Study on the suitability of low-frequency acoustic field

In this work acoustic streaming was studied with acoustic waves generated from a low-frequency underwater acoustic transducer in an open liquid container. The experimental setup is shown in Fig. 3-5.

This rectangular channel is made of glass with the dimensions of 0.97 m x 0.13 m x 0.28 m. Deionized water and 1 g/l PAC were used as the Newtonian and non-Newtonian fluids respectively. A volume of 20 L

liquid was used for all the test runs. After performing the test runs with deionized water, 1g/L PAC solution was introduced gradually to the same liquid channel in small quantities to identify the PAC concentration that does not show any streaming or any induced flow. A low-frequency underwater acoustic transducer (circular where D_txH_t = 60x40 mm) with an output frequency ranging from 600 Hz to 15 kHz was utilized.

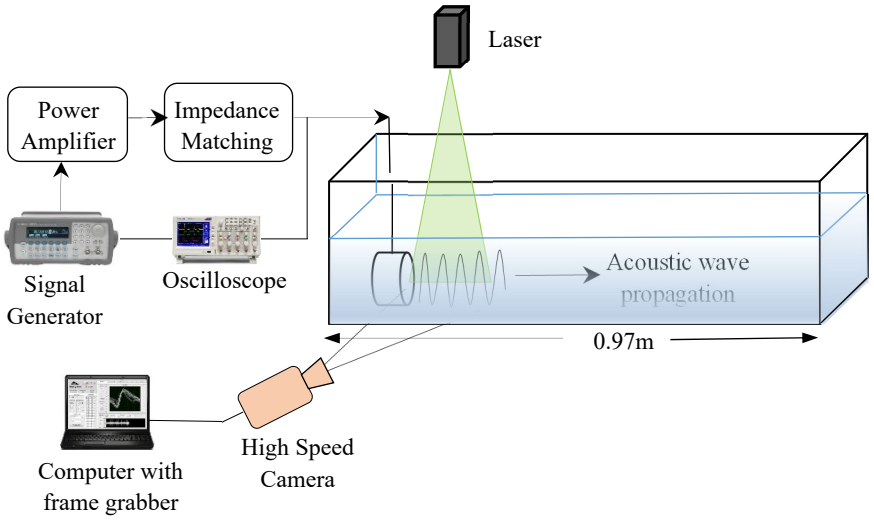

Figure 3-5: Sketch of the experimental set up for the acoustic study

Sonication was provided as continuous sinusoidal waves in a range of frequencies and amplitudes as mentioned in Table 3-5.

The transducer was positioned at the centre of the liquid body 12 cm away from the left wall of the open channel as shown in Fig. 3-5. The two inside ends of the rectangular channel were covered using sponge type sound absorbing material to avoid any sound reflection from the end walls. A function generator model 33220A from Agilent Technologies was used to generate sinusoidal waves of different frequencies and amplitudes with an accuracy of 1 μHz and 0.1 mV. A linear power amplifier with a maximum power output of 200 W at +48 VDC amplified the signal from the function generator. The amplified signal was fed to

an impedance matching unit to match the high acoustic impedance of the transducer.

Table 3-5: Test matrix used for the acoustic experiment

Effect of frequency		
Frequency (Hz)	Amplitude in terms of the supply voltage (mV)	Input power to the acoustic transducer after amplification (W_{RMS})
4	500	11.5
5	500	13.4
6	500	16.6
Effect of power input		
Frequency (Hz)	Amplitude in terms of the supply voltage (mV)	Input power to the acoustic transducer after amplification (W_{RMS})
6	400	10.8
6	500	16.6
6	600	20.3
6	700	25.1
6	800	27.1

Voltage and the current of the amplified signal just upstream of the transducer was read from an oscilloscope where the input power to the transducer was also computed. The effect of input electrical power and frequency of an acoustic wave on the streaming velocity in a Newtonian fluid was studied in axial and radial directions. The effect of the fluid rheology on acoustic streaming was studied by gradually adding some small quantities of 1g/L PAC solution to the deionized water at a constant frequency of 6 kHz and an amplitude of 700 mV. All experiments were conducted at room temperature at 21 °C. The rheological measurements were taken from Anton Paar MCR 302 viscometer at constant temperature and pressure as described in section 3.2.1.

The two-dimensional velocity fields inside the channel were measured using the PIV technique and analyzed using PIVlab as described in section 3.2.2. All the images for the test series were captured at 100 fps with a resolution of 688 x 400 pixels^2 and the measurements were made in a plane parallel to the channel length. Full details of the experiment and the data treatment method are mentioned in **Paper II** and some main remarks are highlighted in Chapter 4.1.2.

3.3.3 Study of horizontal oscillatory motion on non-Newtonian fluid rheology

For this study, a square cross-sectional liquid column made of acrylic with the base dimension of 0.15 m x 0.15 m was used as the container as shown in Fig. 3-6. Deionized water was used as the Newtonian liquid, and two mixtures with 1 g/L and 2 g/L PAC were used to model drilling fluid systems. A volume of 5 L liquid was used for all the test runs. The oscillation driver consisted of an AC motor with a custom made frequency controller. At the time of the experiment, the frequency of the motor and hence, the oscillation frequency for the shaking table was set manually based on the instantaneous acceleration measurements provided by a PASCO 3-axis accelerometer PS-2136A.

The afore-mentioned Basler camera and the lens were used in this experiment. All the images were captured at 300 fps with a resolution of 592 x 400 pixels^2. Capturing images of the oscillating system were challenging since the system was moving constantly and therefore, obtaining fixed reference image frames was not possible. The camera was set so that the image contained the whole region with the two boundaries of the front wall of the liquid column even during the oscillation takes place. Measurements were made in a vertical laser plane parallel to the front wall of the liquid column through the centre of the column as shown in Fig. 3-6. The image recording was started approximately 60 seconds after switching on the motor to let the forced oscillation to establish a fairly steady surface wave motion within the

liquid column. Image recording and data acquisition were continued for a sufficiently long time to catch the various modes and stages of the liquid oscillatory motion. The dynamic velocity field within the oscillating liquid medium was calculated by processing the acquired images using PIVlab as explained in section 3.2.2.1.

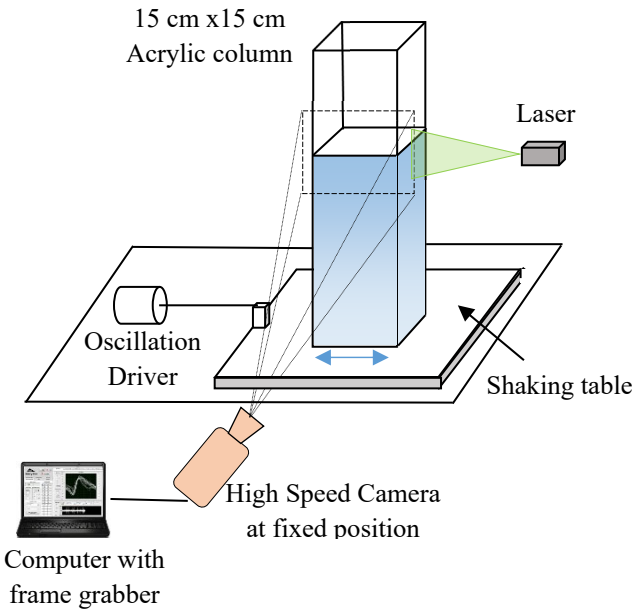

Figure 3-6: Sketch of the experimental setup for the sub-study of horizontal oscillation

Data analysis

A special MATLAB program was written to re-confirm the oscillatory properties that supplied to the liquid column and to quantify the resulting properties of the wave surface using image analysis, while the PIV technique was used for the visualization of dynamic velocity profiles and different features of the oscillatory system.

The effect of shaking frequency on the rheology of the fluid medium was investigated with different visual models. Accurate quantification of oscillation frequency and the horizontal shaking velocity of the liquid-

filled square cross-sectional column was very important since those quantities affect the dynamic velocity magnitude within the bulk liquid medium.

According to the image analysis performed to detect the motion of the liquid-filled column, it could be easily observed that the displacement of the liquid column due to the oscillation could be represented by Eq. (2-2). Even though Eq. (2-2) was defined initially for a vertical system, it is still valid for the horizontal displacement of this liquid column qualitatively and similarly, the velocity could be estimated by the Eq. (2-3). Knowing the horizontal velocity of the liquid-filled column, the bulk velocity magnitudes within the liquid medium that was obtained by PIV were corrected as depicted by the following Eq. (3-3);

$$U_{bulk\ liquid\ medium} = U_{obtained\ by\ PIV} - U_{liquid\ column}, \qquad (3\text{-}3)$$

where U represents the horizontal velocity component.

3.3.4 Numerical study to investigate the effect of oscillation on the dynamic velocity field

For this sub-study, 2-dimensional, two-phase CFD simulations were performed to investigate the effect of frequency and amplitude of vertical oscillatory motion on the velocity field of a liquid column.

ANSYS DesignModeler 18.0 and ANSYS Meshing 18.0 were used for the geometry and mesh generation, respectively. The new experimental setup for the core study was designed and under construction by this time and it was decided to adhere to the real dimensions of the new setup as far as the computational time permits it. Therefore, a geometry of the vertical pipe with an internal diameter of 50 mm and a length of 850 mm was used for the simulations as shown in Fig. 3-7. A piston arrangement was made to provide the sinusoidal oscillatory motion to the liquid body itself and an air layer was considered on top of the liquid surface to study

the interface behaviour during oscillations. Both Newtonian (water) and non-Newtonian fluids were simulated. For the non-Newtonian case 2 g/L and 4 g/L Poly-Anionic Cellulose (PAC) in water was used. The viscosity of the PAC solution was defined as a non-Newtonian power-law fluid in ANSYS Fluent.

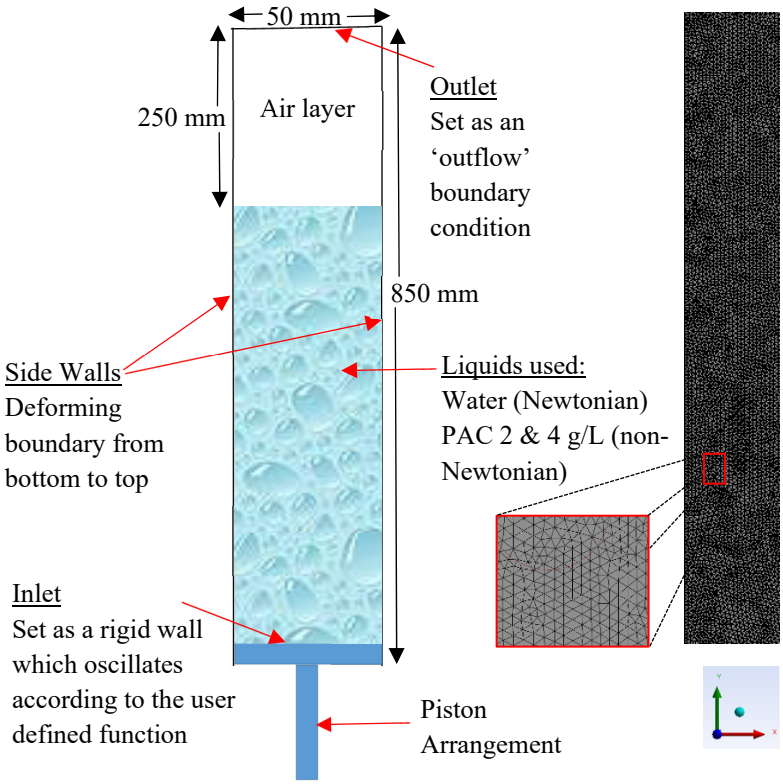

Figure 3-7: The geometry and the grid used for the numerical study

A grid independence study was carried out by performing several simulations with different grid sizes to ensure satisfactory results without any influence on the grid size used. In this way, a grid size of 1 mm was selected as the maximum element size and the geometry was meshed with triangular cells. The outlet boundary was set as an 'outflow' and the sidewalls were defined as deforming boundaries. The physical and

rheological properties of the test fluids are listed in Table 3-6. The values for water and air are from the ANSYS Fluent database and for PAC are from laboratory experiments at 21 °C.

Table 3-6: Properties of the test materials.

Material			Non-Newtonian power-law parameters			
	A	B	C	D	E	F
Water	998.2	0.0010	-	-	-	-
Air	1.225	1.79e-5	-	-	-	-
PAC 2 g/L	1000	-	0.057	0.78	0.013	0.036
PAC 4 g/L	1000	-	0.194	0.71	0.024	0.124

Where,
A – Density [kg/m^3]
B – Newtonian Viscosity [Pa.s]
C – Consistency Index (K) [Pa.s^n]
D – Behaviour Index (n) [-]
E – Minimum viscosity limit [Pa.s]
F – Maximum viscosity limit [Pa.s]

3.3.4.1 CFD model

The governing equations, which form the basis of the flow for a generalized incompressible Newtonian fluid in a pipe, can be written as [24];

Continuity $$\nabla . \boldsymbol{U} = 0 \quad (3\text{-}4)$$

Motion $$\rho \frac{D\boldsymbol{U}}{Dt} = -\nabla \mathrm{p} + [\nabla . \eta\dot{\gamma}] + \rho \boldsymbol{g} \quad (3\text{-}5)$$

Where $\boldsymbol{U}$ is the velocity vector, t is the time, $\boldsymbol{g}$ is the gravitational acceleration. The term on the left-hand side of Eq. (3-5) represents the mass per unit volume times acceleration, while the right hand side represents the pressure force, viscous force and the gravity force per unit

volume respectively. The non-Newtonian fluids considered in the simulations are of power-law type as described in Eq. (3-1).

The transverse sinusoidal oscillatory motion was imposed on the liquid body itself mimicking a piston arrangement from the bottom in the y-direction normal to the pipe cross-section as shown in Fig. 3-7. In the same way, as described in section 2.2.4.1, the oscillating/vibrational Reynolds number was employed based on Eq. (2-6) to identify the hydrodynamic regime of the flow within the pipe section. For all the test cases for this sub-study, the values of oscillatory Reynolds number were in the laminar regime (< 455) for both PAC fluids and in turbulent regime (> 9000) for water. The test conditions for the different simulation cases with different oscillation properties are given in Table 3-7.

Table 3-7: Conditions for the different simulation cases

Case #	Frequency (f) [Hz]	Velocity Amplitude of the piston ($\lvert V_P \rvert$)[m/s]
Case 1	0.25	0.1
Case 2	0.50	0.1
Case 3	0.75	0.1
Case 4	1.00	0.1
Case 5	5.00	0.1
Case 6	1.00	0.2
Case 7	1.00	0.3

It should be noted that the velocity amplitude ($\lvert V_P \rvert$) here is the product of a and ω of the piston following the same definition as expressed in Eq. (2-2). The inlet was defined as a 'rigid body' to facilitate the provision of different properties (frequency and velocity amplitude) of the oscillatory motion using a user defined function (UDF). The user defined function was important to define the geometry and motion with time since the zone adjacent to the inlet wall is deforming and moving at the same time.

The multiphase volume of fluid (VOF) method was employed to specify the air and fluid phases. For the pressure based cases, a realizable $k - \varepsilon$ turbulent model was used for all the cases with water and the test cases for non-Newtonian fluids were simulated under laminar conditions. Under the dynamic mesh settings, a diffusion-based smoothing method with a diffusion parameter of 2 was utilized to update the volume mesh in the deforming regions.

All the simulation cases were solved over five oscillation periods to acquire more generalized results. It did not affect the accuracy of the result but increased the simulation time in proportion. The time step size and the number of time steps were determined after a considerable amount of computational experimentation based on the frequency of the particular simulation case and solution convergence. The simulated liquid velocities and shear rates were extracted along a radial line located 200 mm below the initial air-liquid interface.

3.4 Experimental procedures and data treatment methods within the core study

A newly designed and developed experimental setup was used for the core study. Three sub-studies were conducted within this section and mainly they are twofold; the experiments to visualize the dynamics of the vertical oscillatory motion of the Newtonian and non-Newtonian liquid medium without settling particles and the experiments associated with settling particles when the liquid medium is oscillating. The same experimental setup was used by making necessary adjustments. Fig. 3-8 shows the sketch of the U-shaped experimental setup.

The test section on the left limb of the U-tube has a circular cross-section with an internal diameter of 50 mm and a total length of 1200 mm. The bottom and the right limbs of the U-tube were also circular in cross-section and 30 mm in internal diameter. The whole U-tube including the

piston cylinder (with an internal diameter of 50 mm) was made up of transparent acrylic due to visualization purposes.

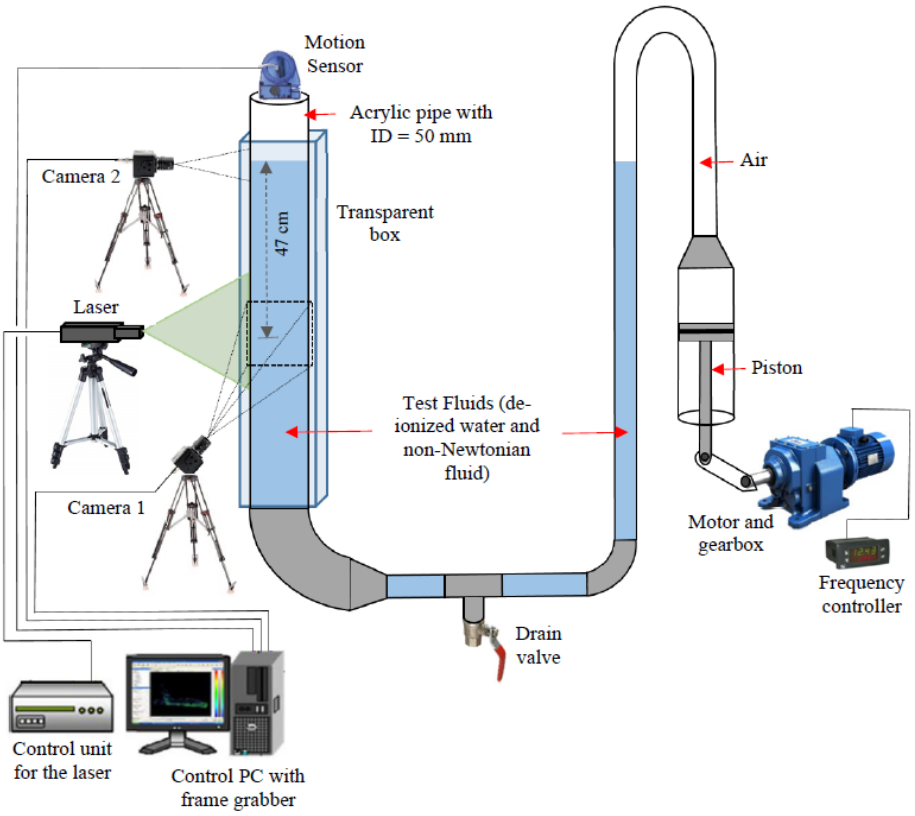

Figure 3-8: Sketch of the experimental setup used for the core study

The harmonic oscillations were provided by the piston attached to the right limb of the U-tube, which is driven by a motor-gearbox unit. The rotary motion of the gearbox is converted to a reciprocating motion of the piston by mechanically projecting it into the arm of the piston. The revolution speed of the motor and the gearbox was controlled by a frequency controller in such a way that, the required output frequency was set to the piston. A tachometer was used to confirm the frequency of the piston. To avoid optical aberrations, the test section was placed inside a second recipient of transparent acrylic, of square cross-section (15 x 15

cm^3), filled with the same deionized water to match the refractive index of the acrylic walls.

3.4.1 Visualization of oscillatory flow conditions in Newtonian and non-Newtonian fluids and estimation of shear rate change

For the first part of the core study, experiments with four different oscillation frequencies were tested as 0.1, 0.25, 0.5 and 0.75 Hz. Several combinations of the length of the rotating arm allowed the oscillating amplitude to be varied as 15, 20 and 25 mm. Out of that, the oscillation amplitude ratio (A) was determined as a/D = 0.3, 0.4 and 0.5, where a is the displacement amplitude of the piston and D is the pipe diameter. Since the piston impacts on the elastic air column instead of directly to the liquid, it was necessary to install separate monitoring of the resulting liquid motion. Therefore, the fast-ultrasonic distance measurements from the motion sensor (described in section 3.2.4) was used to confirm the high-speed imaging results. See **Paper V** for further details. The test conditions for the first part of the core study are summarized in Table 3-8.

The density of the test fluids was measured using Anton Paar DMA-4500 density meter. All the experiments were carried out and the liquid properties were measured at the room temperature of 21$\pm$0.5 °C and atmospheric pressure. The number of test cases concerned for each investigation was based on the aim of each sub-study. (See **Paper V** and **VI** in Part II of this thesis for more details.) According to the rheological characterization of the test fluids described in section 3.2.1, the properties of the three slightly viscoelastic non-Newtonian test fluids are presented in Table 3-9.

Table 3-8: Test fluids and conditions for the first part of the core study

State variable	Range and unit
Test Fluids (see section 3.1.1 for details)	Deionized water (density – 997.60 kg/m^3) Fluid 1 (density – 998.26 kg/m^3) Fluid 2 (density – 999.01 kg/m^3) Fluid 3 (density – 1000.13 kg/m^3)
Oscillation frequencies (f)	0.1, 0.25, 0.5 and 0.75 Hz
Oscillation amplitude ratio ($A = a/D$)	0.3, 0.4 and 0.5 [-]
Measured variables	Velocity from PIV Air-liquid interface movement by high-speed imaging Air-liquid interface movement by ultrasonic distance measurements (motion sensor)

Table 3-9: Rheological parameters for the non-Newtonian test fluids in 1st part of the core study

	K [mPa.s^n]	n [-]	λ [s]
Fluid 1	36.21	0.82	0.037
Fluid 2	192.13	0.68	0.021
Fluid 3	667.33	0.59	0.016

Table 3-10 provides more specific details about the used measurement techniques for this part of the study.

Table 3-10: Specific details for the different measurement techniques used for the 1st part of the core study

Measurement technique	Details
PIV technique	
- Measurement area	470 mm below the equilibrium air-liquid interface (see Fig. 3-8)
- Camera	Basler acA800-510um USB 3.0 camera with ON Semiconductor
- Lens	Nikon AF Nikkor 50 mm – f/1.4D
- Acquisition rate	200 fps
- View of interest	560 x 460 pixels^2
- Laser	Photop LDC-2500S continuous wave laser (wavelength 532 nm)
- Type of seeding	PSP50, Dantec Dynamics
High-speed imaging	
- Measurement area	Air-liquid interface in the test section
- Camera	Basler acA800-510um USB 3.0 camera with ON Semiconductor
- Lens	Basler C125-0818-5M F1.8 f/8mm
- Acquisition rate	100 fps
- View of interest	256 x 360 pixels^2
- Illumination	Using a LED lamp without disturbing the PIV system
Level measurements by the motion sensor	
- Measurement area	Air-liquid interface in the test section
- Acquisition rate	100 fps

The two cameras were synchronized using a LabView program and triggered by a separate control switch.

3.4.1.1 Data treatment

To obtain the full-field velocity distribution and the profiles of the air-liquid interface motions, a series of image analysis steps were further undertaken. The time-varying air-liquid interface was detected from the high-speed images using a MATLAB program which was specifically

made for this analysis. This was accomplished by selecting a vertical line as the observation "path" – given as one fixed column of the matrix array in the high-speed images. A line located close to the centreline (axis) of the pipe was selected as shown in Fig. 3-9. The air-liquid interface was found by setting an intensity threshold value to track the first brightest pixel from top to bottom along the pixel column. This was chosen as the air-liquid interface at any time instant.

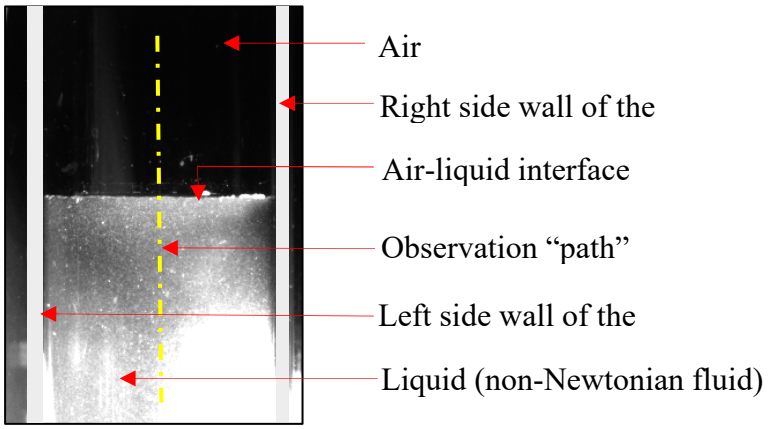

Figure 3-9: Illustration of the observation path in a high-speed image at the interface

It is to be noted that the pixel threshold value was varied from one experimental case to another based on the light conditions. The interface position at this "observation path" was tracked for 10 seconds with the recorded image sequence, and thus a time series of the air-liquid interface was obtained as shown in Fig. 3-10. It is to be noted that, the interface detection procedure shown in this figure has been illustrated only for 500 frames, which correspond to 5 seconds at 0.5 Hz for the non-Newtonian fluid. The detected air-liquid interface for both Newtonian and non-Newtonian fluids for the four frequencies are shown in Fig. 4-7.

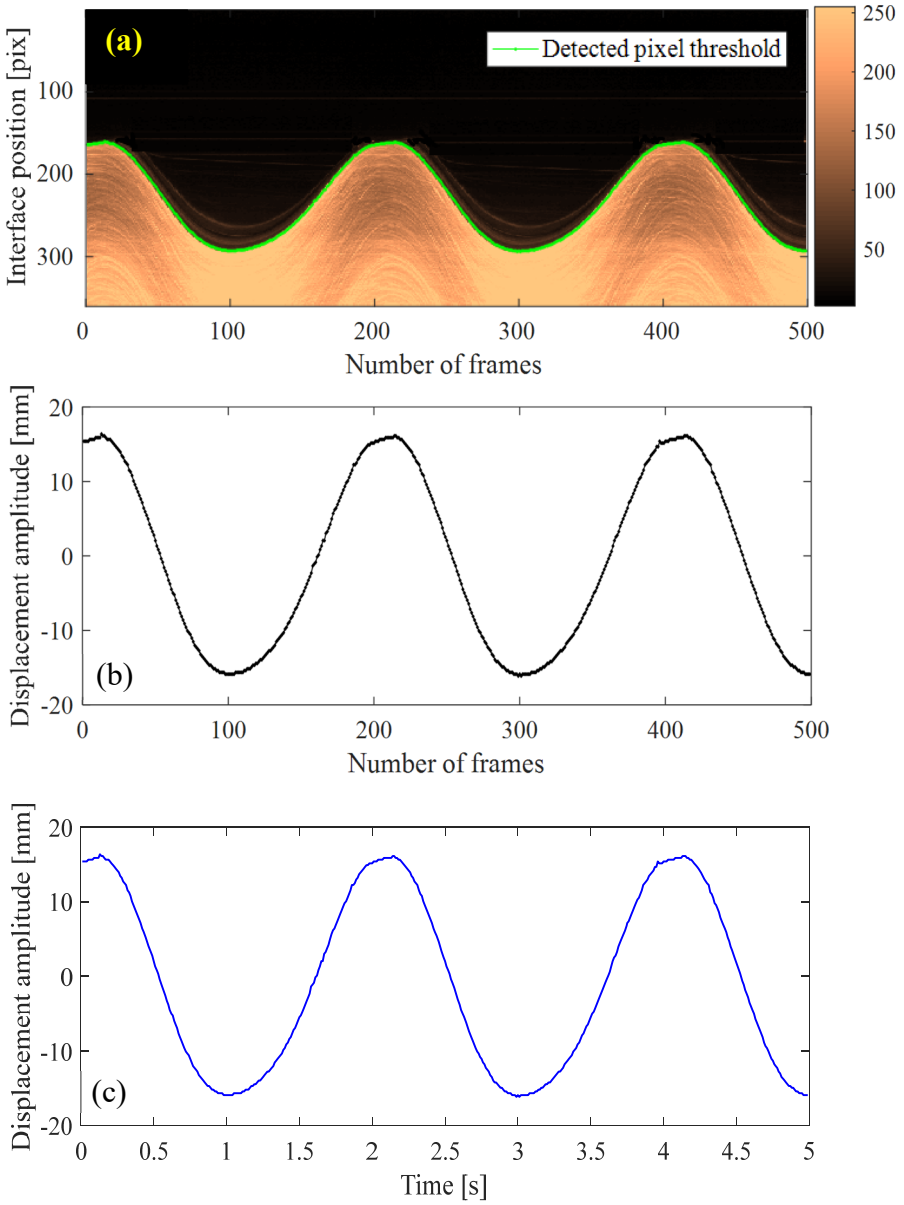

Figure 3-10: Tracking of air-liquid interface: (a) detected pixel threshold (b) displacement amplitude with frame number (c) displacement amplitude with time

The dynamic velocity field within the oscillating liquid medium was calculated by processing the acquired images using PIVlab as explained

in section 3.2.2.1. Full details of the experiment and the data treatment method are mentioned clearly in [40, 118] and some main remarks are highlighted in Chapter 4.2.1.

3.4.2 Investigation of particle settling in vertically oscillating Newtonian and non-Newtonian fluids

The effect of low-frequency oscillatory motion on particle settling in water and shear-thinning non-Newtonian fluids was investigated. The same experimental setup shown and described in section 3.4 was used for this last part of the core study with some minor changes as listed below.

- Settling particles (glass beads) were incorporated in this sub-study to investigate the particle settling in the presence of oscillatory motion.
- The motion sensor was replaced with the particle dropping tube which was partly immersed in the liquid surface. (See **Paper VII** for expanded view).

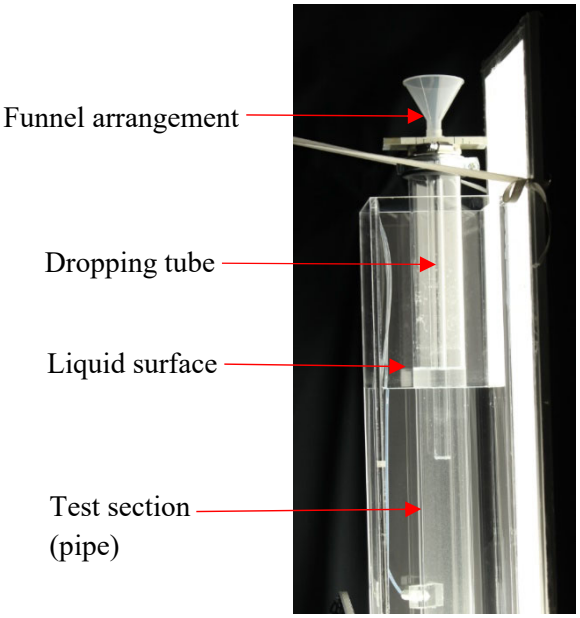

Figure 3-11: Illustration of the particle releasing mechanism

After switching on the driving motor, at least 2 minutes were left in order to the oscillatory motion to become visually harmonic. Then the particles were carefully released manually into the funnel on top of the dropping tube. The funnel arrangement helped the particle to be directed at the intended dropping location within the test section and the small metal net at the bottom of the dropping tube helped the particle to reduce its initial velocity as low as possible.

- The arrangement of the two cameras was altered in such a way that the view of interest for one camera was covering the whole trajectory of the falling particle along the vertical liquid column and the other camera captures the motion of the piston.
- The laser was not employed and the particle motion was captured solely by high-speed imaging.

Three different sizes of glass beads were employed in the experiment series to study the settling rate under oscillatory conditions as described in section 3.1.2. The primary focus was to study the effects of oscillation frequency on the settling rate without any wall effects. Therefore, the particles were released along the axis of the vertical test section; which was considered as the "Location 1" – (L1). Then, two other locations within the test section which are more closer to the pipe walls were selected (L2 and L3) as illustrated in Fig. 3-12 to investigate the effect of shear region on particle settling in non-Newtonian fluids.

Therefore, L1 $\approx R$, L2 $\approx 0.5R$ and L3 $\approx 0.2R$, where R is the pipe radius measured from the pipe wall. It is to be noted that Fig. 3-12 is just for the illustration purpose and not in scale.

All the experiments were carried out and the liquid properties were measured at the room temperature of 22 ± 0.5 °C and atmospheric pressure. The test conditions for the last part of the core study are summarized in Table 3-11.

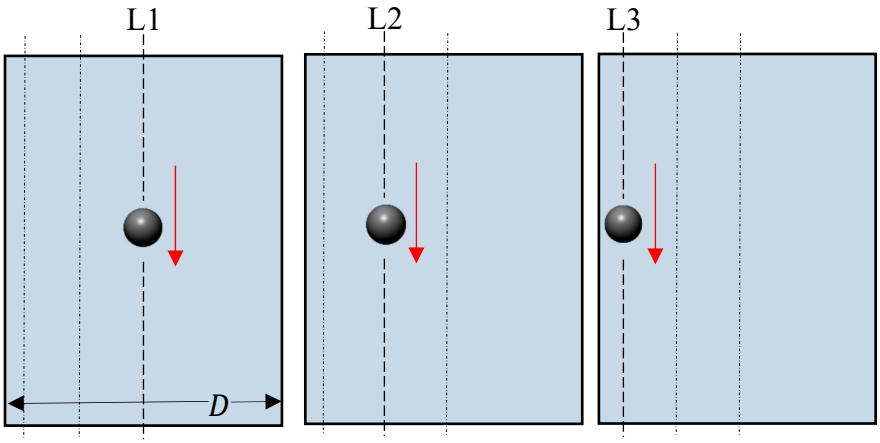

Figure 3-12: Particle falling in test fluids at different locations within the test section

Table 3-11: Test conditions for the last part of the core study

State variable	Range and unit
Test Fluids (see section 3.1.1 for details)	Deionized water (density – 997.55 kg/m^3) Fluid 1 (density – 999.47 kg/m^3) Fluid 2 (density – 1000.25 kg/m^3) Fluid 3 (density – 1000.01 kg/m^3)
Particles (as stated in Table 3-3)	1 mm 2 mm 3 mm
Oscillation frequencies (f)	0 (stationary fluid), 0.25, 0.5 and 0.75 Hz
Oscillation amplitude ratio ($A = a/D$)	0.4 [-]
Particle releasing locations	L1, L2 and L3 (See Fig. 3-12)
Measured variables	Particle displacement along the vertical column by high-speed imaging

Based on the variables, 144 different experimental cases were tested for 4 different frequencies (including still condition), 3 different particle

sizes, 4 different fluid types and 3 different locations within the pipe as presented in Table 3-11. Each experiment case was repeated three times to achieve a better averaged result and to check the repeatability.

All the rheological properties were measured just after the corresponding experimental run and are presented in Table 3-12.

Table 3-12: Rheological parameters for the non-Newtonian test fluids for the last part of the core study

	K [mPa.s^n]	n [-]	λ [s]
Fluid 1	26.99	0.85	0.037
Fluid 2	168.68	0.71	0.019
Fluid 3	397.38	0.66	0.015

Table 3-13 provides more specific details about the measurement technique for this part of the study.

Table 3-13: Specific details for the different measurement techniques used for the last part of the core study

Measurement technique	Details
High-speed imaging	
- Measurement area	Camera 1 - trajectories between two reference points 15 cm and 63 cm below the tip of the dropping tube Camera 2 - the motion of the piston
- Camera (both)	Basler acA800-510um USB 3.0 camera with ON Semiconductor
- Lens (both)	Basler C125-0818-5M F1.8 f/8mm
- Acquisition rate	25 - 200 fps depending on the speed of the particles (identical for both cameras)
- View of interest	Camera 1 - 256 x 616 pixels^2 Camera 2 - 128 x 370 pixels^2
- Illumination	Using LED lamps

The two cameras were synchronized using a LabView program and triggered by a separate control switch. Each experiment case was performed at least three times to ensure consistency and the quality of results. All the experimental cases allocated for a single fluid type were conducted within each day to avoid any inconsistency.

3.4.2.1 Data treatment and estimation of particle settling velocity

The high-speed image analysis was performed using Tracker – version 4.11.0 (http://physlets.org/tracker/). The whole image was used without specifying any region of interest (ROI) since the full trajectory of the particle is preferred. Specific colour adjustments were performed on each image to achieve accurate tracking. Piston movement was also tracked using the same software simultaneously for all the experimental cases incorporating oscillatory conditions.

Since the velocity of the particle is fluctuating with the oscillatory motion, it was challenging to determine the velocity of each particle directly. However, the trajectory of any particle is a function of space and its gradient is the instantaneous velocity of it. Therefore, the obtained particle trajectory (vertical component of the displacement) is fitted to a linear curve to achieve its average settling velocity within the test section as depicted in Fig. 3-13. The trajectories are shown for the whole span of the image frame with time and not based on the phase positions. Number of data points are different due to the different acquisition rates and data filtering in plotting the figure. The y- axis is positive downwards. See **Paper VII** for more details.

Based on the calculations on the oscillatory Reynolds number (Re_δ) for the same experimental setup and conditions (See **Paper V**), it was found that the oscillatory boundary layer close to the pipe wall was laminar in all cases.

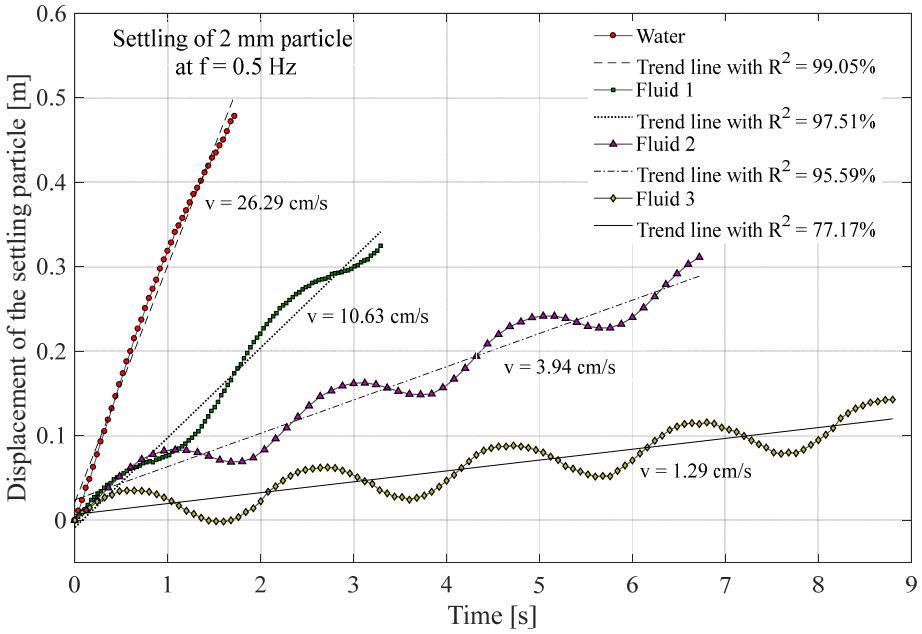

Figure 3-13: Illustration of the data treatment and analysis method to achieve the average settling velocity of particles

3.5 Dimensionless phase position used to discuss the results and main remarks

3.5.1 Based on the piston movement

The characteristic sinusoidal harmonic motion of the piston was also identified by tracking its displacement on the vertical plane. Fig. 3-14 shows a typical sinusoidal movement of the piston together with its phase angle and used as the basis to introduce the notation system adopted to discuss the results and the main remarks of this thesis.

The phase position/angle (ωt) was normalized by the angle value ($\pi/4$), and the value for $\omega t/(\pi/4)$ has been utilized in presenting and discussing further results. From the visual observations, great care was taken to release the particle at a moment of the piston movement

corresponds to $\omega t/(\pi/4) = 2$ or 10. Once the sinusoidal phase position of the piston is identified and tracked in data analysis, the displacement of the particle is started to track from the moment that corresponds to $\omega t/(\pi/4) = 0$ of the piston movement. Based on the preliminary investigations related to the experiment, the authors verify that both steady and periodic regimes are reached by the particles within the span of the trajectory image frame.

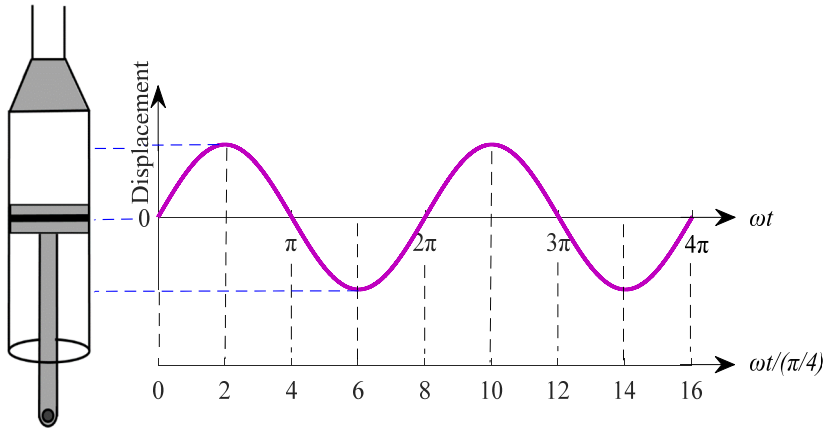

Figure 3-14: Introduction of the different phase positions within the oscillation period based on the displacement of the piston

Note: This same basis of notation has been used in discussing the main remarks of the numerical study in chapter 4.1.4 and the study of horizontal oscillation movement in chapter 4.1.3.

3.5.2 Based on the axial velocity of the bulk liquid medium

The two sub-studies of the first part of the core study were carried out without capturing the motion of the piston. Since the pipe centreline is the best location to identify the maximum up and down motion of the fluid with the least possible viscous and wall effects, the axial (or the

centreline) velocity was used to represent the different positions within the oscillation period as shown in Fig. 3-15. It presents the axial velocity profiles of Fluid 1 and 2, along the pipe centreline when they are oscillated at a frequency of 0.75 Hz and a piston amplitude ratio of A = 0.5.

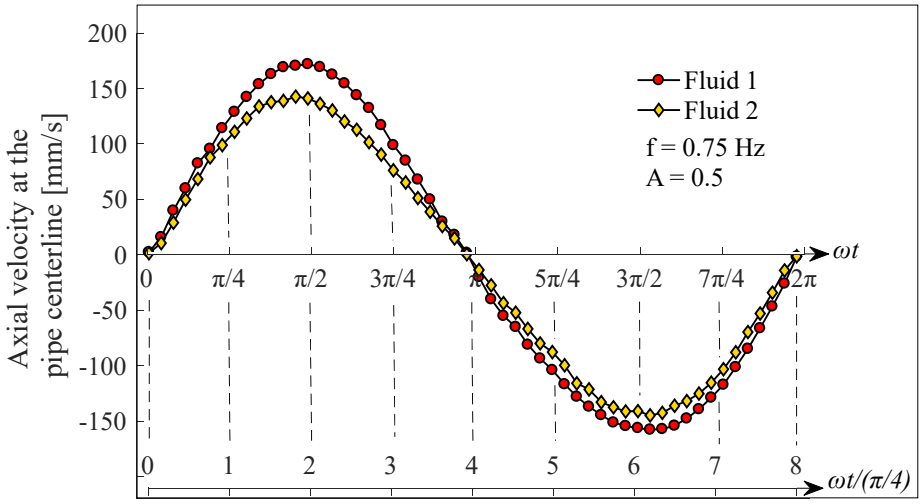

Figure 3-15: Introduction of the dimensionless phase positions within the phase cycle based on centreline axial velocity

Qualitatively, the periodical shape of the curves obtained from the PIV measurements confirms the successful transmission of energy from the mechanical piston to the fluid system via the gas buffer in between them. The quantitative description of the different velocity curves plotted in Fig. 3-15 is provided in section 4.2.1.2 under main remarks. However, the asymmetry of the axial velocity between the first and second half of the cycle for Fluid 1 demonstrates some local friction exerted on the piston motion especially on its decelerating phase.

4 Main Remarks

4.1 Pre-study

4.1.1 Rheological characterization of model drilling fluids to achieve desired properties

This sub-study was basically to investigate the effect of Xanthan gum (Xg) concentration on the rheological properties of Polyanionic Cellulose (PAC).

4.1.1.1 Shear viscosity at steady shear conditions

According to the shear viscosity curves presented in **Paper I**, it can be seen that the viscosity of PAC has increased due to the addition of Xg as expected. This rise of shear viscosity could be linked to the separate contribution of Xg itself, but quite likely also due to the intermolecular interactions between PAC and Xg molecules.

A significant influence of Xg concentration on the shear viscosity of PAC at the low shear region was observed. Even at low shear rates such as 0.1 s^{-1}, many of the combined polymer samples have not reached the constant shear viscosity or the zero-shear region. This observation is much more significant when the added Xg concentration is increased where the combined polymers tend to be more inter-linked and elastic (or gel type) rather than being viscous. The influence of Xg concentration on the PAC viscosity is less significant at the high shear region, where the shear rate is somewhat similar to that within the drilling pipe according to Bui et al. [16].

4.1.1.2 Shear-thinning behaviour

It is of primary importance to check the influence on the shear-thinning behaviour of the polymer mixtures based on the power-law rheological

model compared to that of the individual polymers. Since the experimental data show a non-linear pattern for the viscosity curves at the very low shear region, the power-law model was used over a selected shear rate domain to visualize how the experimental results fit with rheological models. See **Paper I** for illustrated figures. The results show that the added Xg concentration has increased the shear-thinning behaviour of the polymer mixture. At high shear rates, this is more visible since the flow encounters less resistance. The disentanglement of the polymer coils in solution or the increased orientation of the polymer coils in the direction of flow could have influenced this behaviour of the samples at the higher shear region.

As per the intention of this study, the impact of Xg on the rheological properties of PAC solutions is illustrated in Fig. 4-1, concerning the K and n values obtained from the power-law. It is to find out the relationship between K and n values together with the individual sample concentrations and how far it is possible to predict the properties of polymer mixtures.

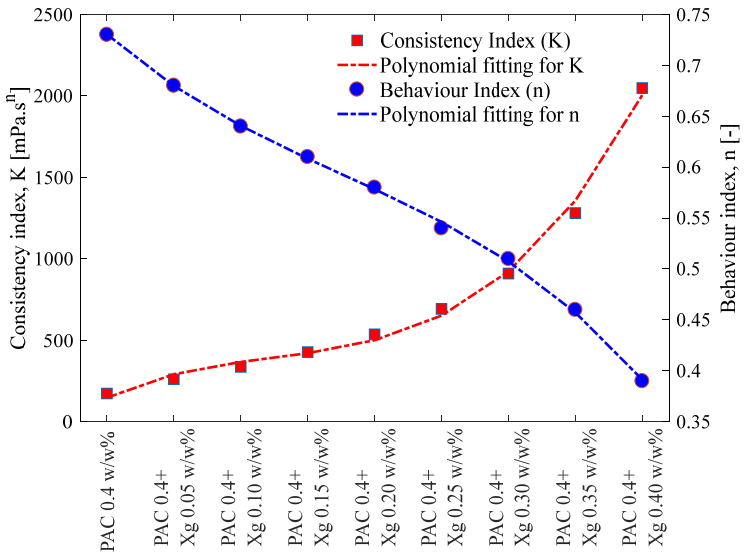

Figure 4-1: Behaviour of K and n according to the added Xg concentration

The K and n values have been fitted into third-order polynomials as shown in Fig. 4-1. The experimental results are in good agreement with the fitted polynomial having R^2 values for both the curves better than 99%. This means that it is possible to predict the behaviour of any combined polymer with PAC 0.4 w/w% and Xg, using the below mentioned two correlations.

$$n = -6.061\ {C_{Xg}}^3 + 3.199\ {C_{Xg}}^2 - 1.157\ C_{Xg} + 0.7303 \quad (4\text{-}1)$$

$$K = 6.236 * 10^4\ {C_{Xg}}^3 - 2.302 * 10^4\ {C_{Xg}}^2 + 3871\ C_{Xg} + 148.3 \quad (4\text{-}2)$$

Here C_{Xg} is the Xg concentration in w/w%. Furthermore, this particular rheological study was supplemented with some other experimental results (obtained by the author) to develop a more generalized correlation for predicting the K value as presented in Eq. 4-3.

$$K' = {}^{K}/_{M} \quad (4\text{-}3)$$

where $M = 2.47.(10\ C_{PAC})^{-0.65}$ and C_{PAC} is the PAC concentration in w/w% and K' is the generalized consistency index of any blended polymer solution in mPa.s^n which contains PAC and Xg. A separate rheological investigation was carried out to validate the presented correlations for K and n of a polymer mixture as explained in **Paper I** and it was observed that the model represents the viscosity curves well for combined polymers with errors less than 14% within the shear-thinning range.

4.1.1.3 Dynamic state results

As described in section 3.2.1.1, oscillatory rheological experiments were performed to determine the LVE range and the structural characteristics of samples. See **Paper I** for the illustrated results. Based on the oscillatory amplitude sweep test data, it can be seen that the LVE range

of the individual PAC and the combined polymers is generally very low at an angular frequency of 10 rad/s. According to Ferry [119], this could be due to the entanglement of long-chain molecules in a concentrated polymer solution results in a transient network structure, which can lead to the viscoelasticity of the samples, even though they show very little slight viscoelastic properties.

Knowing such properties is of paramount importance to determine and keep the required degree of particles in suspension. A larger viscoelastic range and gel formation are desired to prevent the settling of particles and enhance the cuttings carrying capacity. Therefore, viscoelasticity is a desired property in drilling operations and thus, the possibility of predicting the behaviour in advance would be an advantage.

4.1.2 Investigation of low-frequency acoustic field on Newtonian and non-Newtonian fluids

4.1.2.1 Transient flow development

According to the results illustrated in **Paper II**, it can be observed that the streaming is highest along the beam centreline. Maximum flow velocity is reached at a certain distance from the transducer, and beyond this distance, the streaming is gradually diffused. This velocity "smearing" is attributed to the attenuation effects within the liquid medium. Strong streaming is formed in the direction of the beam-axis immediately after the transducer is switched on (at t = 0 s) and the spatial distribution of the velocity vectors is complex with several local peaks and vortices.

4.1.2.2 Velocity magnitude at steady state

According to the study, it was observed that the streaming velocity is dying out in the fluid medium when it is moving away from the transducer. The peak velocity (V_{pk}) is obtained only one time along the

beam axis (horizontally) closer to the acoustic source and some other minor peaks that are not so strong can also present confirming that the acoustic streaming is significant in the proximity of the transducer and decreases as the flow moves away from the transducer. This is due do the attenuation of the acoustic wave and this attenuation increases with the distance from the transducer. This quick damping of the streaming even within Newtonian fluids was not desirable in achieving the aim of the research where it was expected to obtain an alteration of the particle settling rate. However, it was noted that the peak streaming velocity increases when the applied frequency of the transducer and the input electrical power to the acoustic source are increased.

4.1.2.3 Effect of fluid rheology on acoustic streaming

As described in the methodology, Polyanionic Cellulose (PAC) was used to investigate how the fluid rheology influences acoustic streaming. That is one of the main objectives of this preliminary sub-study to use acoustic streaming effect on non-Newtonian liquids where to investigate whether the settling rate of particles is affected and if so in which way. Known quantities of 1 g/L PAC were added gradually to the water container in small portions. The streaming flow was then checked for each case as done for the pure water. Fig. 4-2 shows the influence of PAC concentration on axial (horizontal) streaming velocity only for some selected cases for brevity.

It can be seen that the axial streaming velocity has been reduced with the added PAC concentration. When the overall PAC concentration within the liquid channel reached 0.19 g/L, the streaming flow had completely disappeared. Similar to that seen for pure water, the streaming velocity is dying out in the non-Newtonian fluid medium also further away from the transducer.

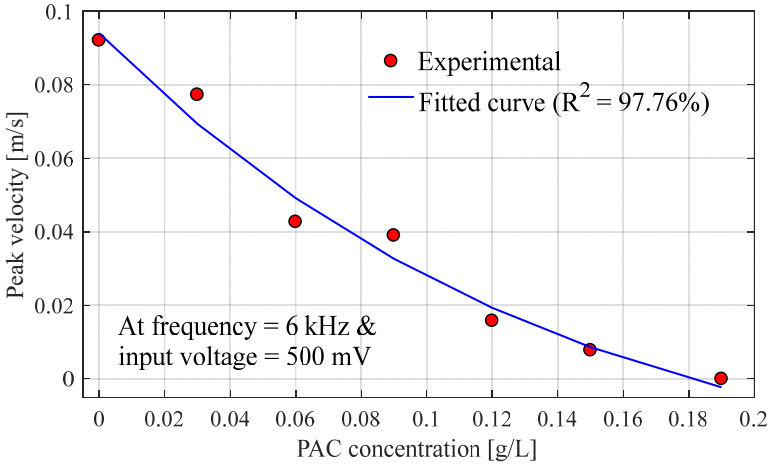

Figure 4-2: Peak velocity variation with PAC concentration (test condition: frequency = 6 kHz and input voltage = 700 mV; which equals to an electrical input power of 25.1 W_{RMS})

However, it is important to notice that the flow induced by the acoustic waves within the non-Newtonian medium is smearing out quickly at a lower axial distance than that we observed for pure water (See **Paper II**). This phenomenon is attributed to the strong attenuation property of non-Newtonian liquids. It is observed that the peak velocity is obtained only one time along the beam axis closer to the acoustic source before it smears out. The results confirmed that employing a low-frequency acoustic pressure field is not adequate in fulfilling the aim of the research successfully. It was then decided to approach a mechanical oscillatory mechanism with even lower driving frequencies.

4.1.3 Study on the effects of horizontal oscillatory motion on non-Newtonian rheology

As the first attempt, this sub-study was performed by providing a horizontal oscillatory motion to a liquid-filled column as described in section 3.3.3.

4.1.3.1 Velocity variation within the liquid medium

Based on the results shown in **Paper III**, it can be seen that the fluctuation of bulk velocity within the liquid column impacts liquid shear when non-Newtonian fluids present and thus the forces acting upon the immersed particles. It could be noted that the velocity magnitude is reduced when the oscillation frequency is reduced. With increased liquid velocity, the variation of shear rate is also higher due to the impact on the viscous resistance of the polymer liquid.

To obtain an informative visualization of the velocity distributions Fig. 4-3 presents the velocity vectors close to the liquid surface when the tank is filled with PAC 2 g/L and is oscillated at 1.75 Hz for brevity. The four points A, B, C, and D are selected to represent four typical positions on the tank movement as illustrated on top of the figure based on the definition of notations illustrated in Fig. 3-14. The colour indicates the velocity magnitude while the vectors give the flow direction. All velocities are corrected for the tank oscillatory motion, as given by Eq. (3-3).

According to Fig. 4-3, it is seen that the bulk liquid medium achieves its maximum velocity and kinetic energy when the tank passes its middle position. The motion of the bulk liquid is driven by the surface wave. The direction of the velocity vectors illustrates how the fluid is directed point to point at a given instant. Close to the sidewalls, the fluid motion is nearly one dimensional, directed vertically upward or downward. This generates an oscillating shear rate that affects the fluid rheology due to the vertical motion of liquid relative to the walls. This type of periodic oscillations within the drilling fluid is common when it is in drill pipe, within the annulus or in the shale shaker. Usually, the drilling fluids experience a wide range of shear rates during circulation.

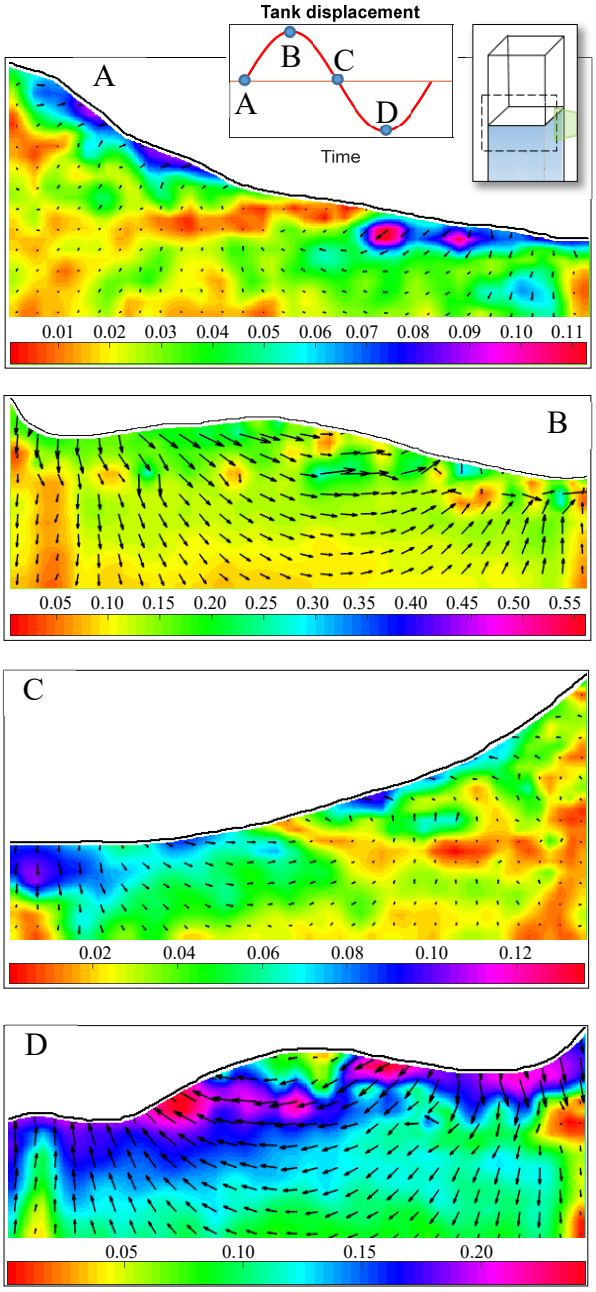

Figure 4-3: A typical flow visualization with velocity vectors close to the liquid surface

For instance, drilling fluids confronts shear rates of order 1000 s^{-1} within the drill pipe where the shear field is reduced to about 100 s^{-1} when it comes to the annulus [16]. It could be observed that increased oscillation frequency leads to different dynamic patterns and a range of velocity magnitudes.

4.1.3.2 Change of shear rate due to periodic oscillations

The change of shear rate due to periodic oscillations within the bulk liquid medium was also derived from the PIV analysis. The secondary flow structures in oscillatory motion, and the associated shear rate is very important from the rheological point of view of the drilling fluids. This influences both flow dynamics, as well as local settling velocities of cuttings particles. According to the results, it could be seen that the change of shear rate is higher in high concentrations of PAC solutions compared to that of low concentrations of PAC. Furthermore, it could be observed that the shear rate is fluctuating along the wall and the fluctuation is reached a maximum close to the surface, but suddenly drops when it touches the surface. These consequences of shear rate variation due to the oscillatory motion are quantified and presented in detail under the main remarks of core study.

4.1.4 Computational study on vertical oscillation in Newtonian and non-Newtonian fluids

4.1.4.1 Effect of oscillation frequency on the velocity magnitude

The variation of the velocity field within the bulk liquid medium is a better way to understand the impact of the oscillatory motion. Fig. 4-4 shows the dynamic velocity profiles only for PAC 2 g/L and PAC 4 g/L fluids at different frequencies and different positions within an oscillation period for a fixed piston velocity amplitude (V_P) (Cases 1 – 5). Note that the velocity values given by ANSYS Fluent are absolute values, so that phase positions represented by $\omega t/(\pi/4)$ = 4 and 6 are

downwards flow (negative in "real" values). The two vertical panels of Fig. 4-4 represent the laminar cases investigated in this computational study.

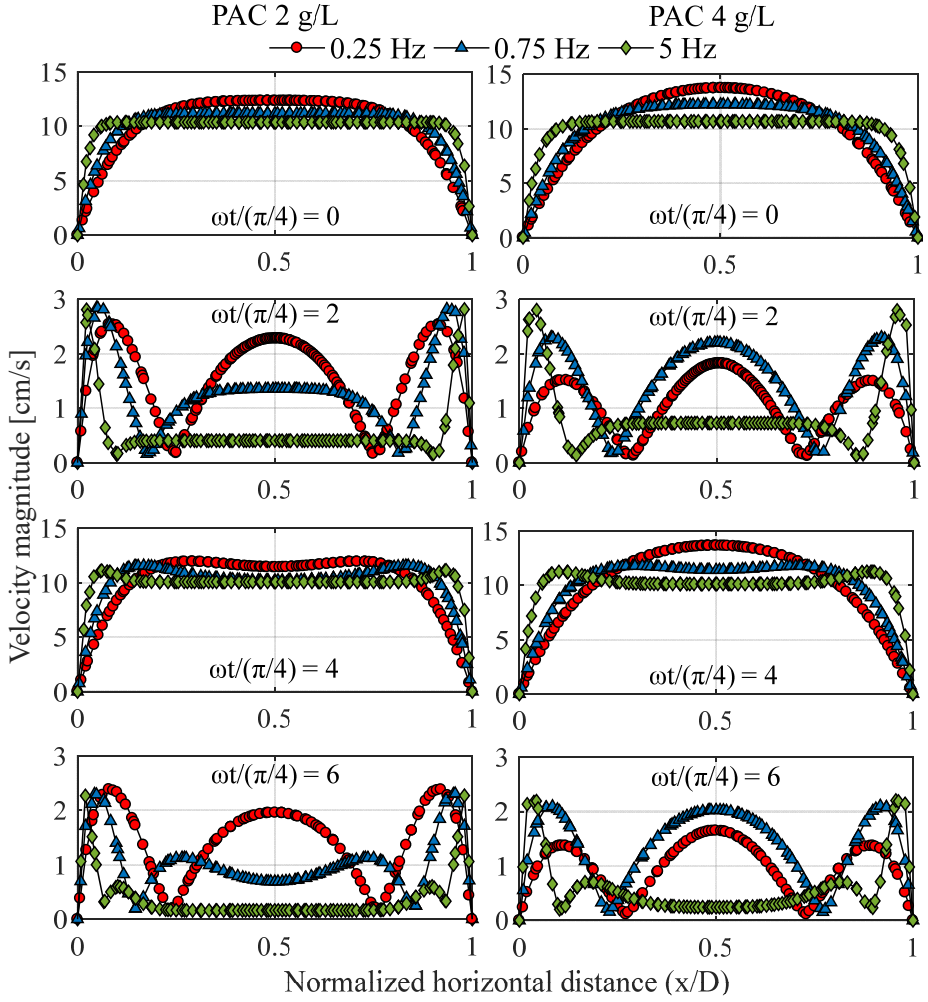

Figure 4-4: Velocity variation with frequency of oscillation at different phase positions within an oscillation period ($|V|$ = 0.1 m/s)

It could be noted that irrespective of the flow condition whether it is laminar or turbulent (see **Paper IV**), the patterns/shapes of the velocity

profiles for all the test fluids at different phase positions are slightly qualitatively similar. Furthermore, when the piston is in the middle position of its way ($\omega t/(\pi/4)$ = 0 and 2), the radial velocity profiles for both non-Newtonian fluids show plug-type behaviour with increasing frequency, deviating from the usual parabolic shape. The non-dimensional phase positions 2 and 6 are the moments where the piston comes to rest to change its direction and so the bulk liquid medium also lowers its velocity to change the direction. As a result of this, a bell-shaped velocity profile could be seen at those phase positions for all the liquids concerned here, where a local velocity maximum (and sometimes a minimum too) can be observed close to the wall region and that propagates towards the centre of the pipe with increasing driving frequency. Moreover, it is to be noted that, the peak velocity magnitudes achieved by non-Newtonian fluids are lower than that of water, which could be attributed to the higher viscous resistance of the non-Newtonian liquids and also the laminar flow conditions.

Similarly, the results indicate that when the excitation velocity amplitude is increased, the achieved instantaneous velocity magnitudes are also increased (refer to **Paper IV**). This increased velocity magnitudes at high excitation velocity amplitudes could be attributed to the increased kinetic energy provided by the excitation via the piston. For almost all the cases, the velocity gradient close to the wall is greater compared to that within the middle area of the pipe. It can be depicted that, the effect of excitation velocity amplitude on fluids oscillated vertically lead to significant variations in the radial velocity profiles revealing the presence of an alternating upward/downward motion. This complexity is significant in non-Newtonian fluids since these varying velocity magnitudes and hence the velocity gradients change the shear field of the non-Newtonian fluids.

4.1.4.2 Variation of shear rate with the frequency of oscillation and velocity amplitude

The transient results shown in **Paper IV** are consistent with the interpretation of the phenomenon, in that the shear rate is maximum when the velocity gradient (see Eq. (2-17)) is maximum and vice versa. Shear rate is normally highest close to the pipe wall in both steady-state and transient flows with boundary layer build-up. This is specially termed as the 'shear layer' and greatly proven by the profiles of the shear rate shown in section 4.2.1.8 under the main remarks of core study (and also in **Paper IV**). The maximum shear rate is near the wall region of the pipe is achieved at the maximum position of the oscillation period, where the axial velocity also possesses its highest magnitude. The thickness of the shear region seems to increase with the increasing excitation velocity amplitude irrespective of the fluid type. The thickness of the shear region decreases with the increase in driving frequency. At higher excitation velocity amplitudes, the most viscous fluid (PAC 4 g/L) has reported a maximum change in shear rate and hence the maximum reduction of viscosity due to its shear-thinning behaviour as an effect of the oscillatory motion.

Therefore, the superimposition of a sinusoidal oscillatory motion on a bulk liquid medium contained in a pipe leads to a change in apparent local shear viscosity of the shear-thinning non-Newtonian fluids. Consequently, the solids carrying capacities and solids separation capacities of such fluid are altered considerably as described in section 4.2.2.5 under the main remarks of the core study.

4.2 Core study

4.2.1 Dynamics in vertical oscillatory motion

4.2.1.1 Movement of the air-liquid interface

According to the data treatment procedure described in section 3.4.1.1, the detected air-liquid interface of the Newtonian and non-Newtonian fluid (only for Fluid 3) at different frequencies by the high-speed camera is shown in Fig. 4-5 for a time duration of 10 s.

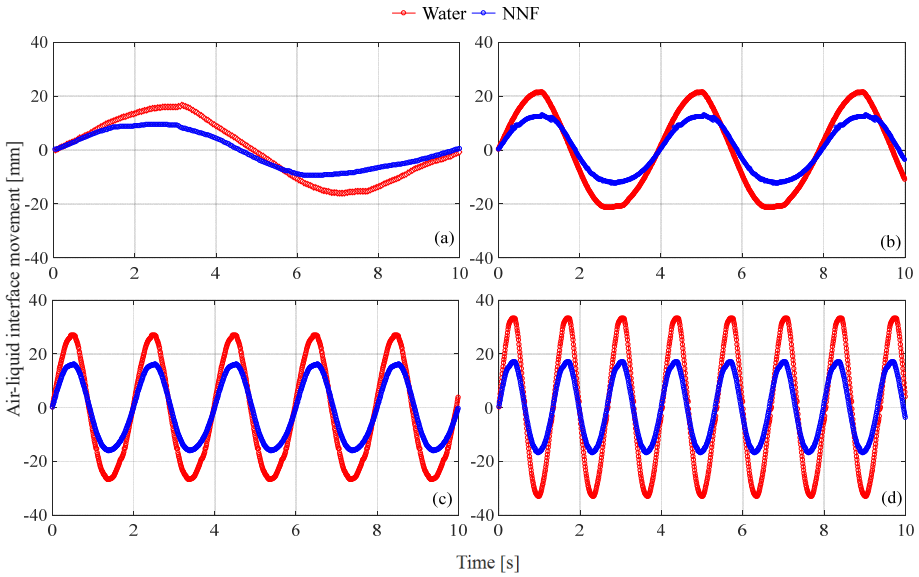

Figure 4-5: Air-liquid interface movement detected from high-speed image analysis (a) at 0.1 Hz (b) at 0.25 Hz (c) at 0.5 Hz (d) at 0.75 Hz

According to Fig. 4-5, it can be seen that the displacement amplitude of the air-liquid interface of water is always greater than that of Fluid 3 (NNF in the figure). This is as expected since the non-Newtonian fluids have a higher viscosity than pure water and thus have higher flow resistance against the air-cushion drive. A bit more counter-intuitive is perhaps that, as the frequency is increased, the interface displacement

amplitude is also increased, irrespective of the liquid type. When the frequency is increased, the momentum transfer from the piston via the air-buffer to the liquid is increased and the kinetic energy achieved by the fluid system is also increased. When the kinetic energy of the fluid system is increased, the viscous resistance of the fluid medium reduces, and hence the displacement of the interface is increased with frequency.

4.2.1.2 Axial velocity component of the pipe centreline

The best location to identify the maximum of the characteristic sinusoidal fluid motion within the vertical pipe (as expressed in Eq. (2-1)) is along the pipe axis.

4.2.1.3 Velocity amplitude variation based on axial velocity

4.2.1.3.1 Comparison between Newtonian and non-Newtonian fluid

Fig. 4-6 shows all the velocity amplitudes at different frequencies only for water and Fluid 3. See **Paper V** for more details. According to Fig. 4-6, it can be seen that the velocity amplitude achieved by water is greater than that of non-Newtonian fluid in almost all the frequencies except at the highest oscillation frequency. When the oscillation period is decreased, the velocity ampltude also increased, for both the liquids. This is a vertical set up where the elevation changes from point to point and the PIV measurements have been obtained at a location of 47 cm below the air-liquid interface (see Fig. 3-8). Even though the displacement amplitude for water was twice as high as for the non-Newtonian fluid at the interface, both fluids showed only a slight difference in velocity amplitudes calculated from PIV analysis.

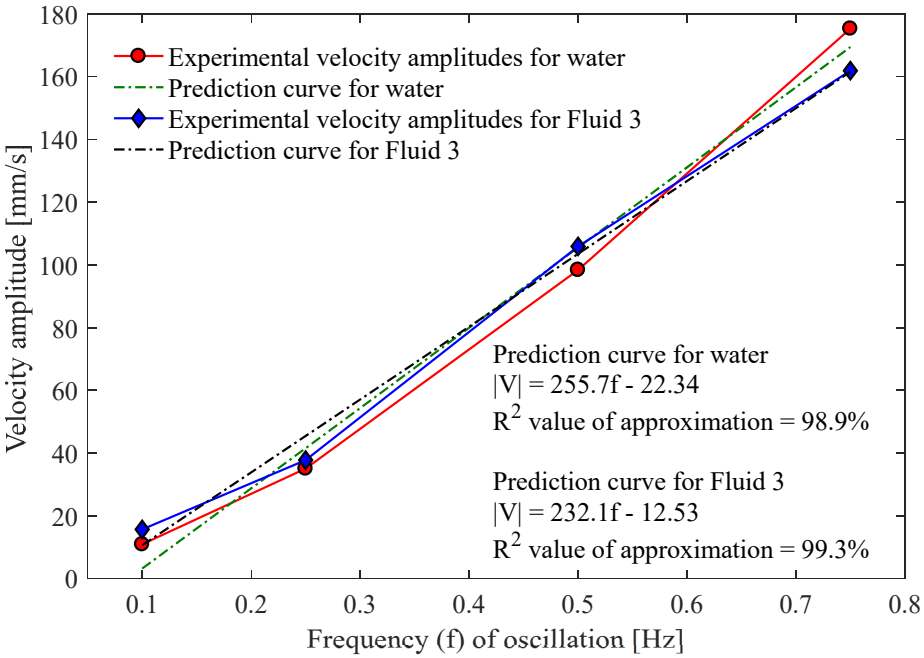

Figure 4-6: Comparison of velocity amplitudes at different frequencies for both the liquids based on PIV measurements

4.2.1.3.2 Comparing the non-Newtonian fluids

According to the results presented in **Paper VI**, it could be observed that when n decreases (or the fluid becomes more viscous) the achieved velocity amplitude of the liquid medium is decreased for a particular piston displacement amplitude ratio and frequency. This situation was visible at all the experimental conditions with a small deviation at A = 0.5. This could be attributed to the increased viscous resistance exerted by the non-Newtonian fluids that acts as a negative impact on particle settling in drilling fluids by increasing the drag force.

However, to reveal the nonlinearities caused by shear-thinning behaviour more evident, the axial velocity amplitudes achieved by the non-Newtonian fluids have been normalized by the piston velocity amplitude

and calculated as a velocity amplitude ratio (β') which can be expressed as;

$$\beta' = \frac{Axial\ velocity\ amplitude\ of\ the\ liquid\ medium}{Velocity\ amplitude\ of the\ piston\ at\ the\ particular\ driving\ condition} \quad (4\text{-}4)$$

The β' values at different driving frequencies are presented in Fig. 4-7. Here, the axial velocity amplitude of the liquid medium is obtained from the PIV measurements and the piston velocity amplitude is calculated as the product of a and ω. According to Fig. 4-7, for all the three non-Newtonian fluids, the β values for the first two piston (displacement) amplitude ratios (A = 0.3 and 0.4) are almost the same for all the driving frequencies. That implies the absence of nonlinearities between the first two lower driving amplitudes studied here. However, at higher driving amplitudes, the β' values deviate from the other two, revealing the nonlinearity caused by the shear-thinning of the non-Newtonian fluids. All the experimental cases except a couple of low-frequency cases show an increment of β' value with the increased driving frequency.

4.2.1.4 Evaluation of the flow field associated with the experiments

Based on the rheological characterization provided in section 3.2.1.1, the test fluids are slightly viscoelastic and show power-law characteristics in their linear region. First, they are evaluated for their De (= $\lambda\omega$) based on the oscillation frequency and values are reported in Table 4-1.

All the values for the calculated De are less than unity and not large enough for resonances to occur [120]. According to Casanellas and Ortin [72], these small De make the attenuation length of the viscoelastic waves essentially identical to their wavelength and the oscillating boundary layer of these fluids could be mostly similar to that of a Newtonian case without resonances.

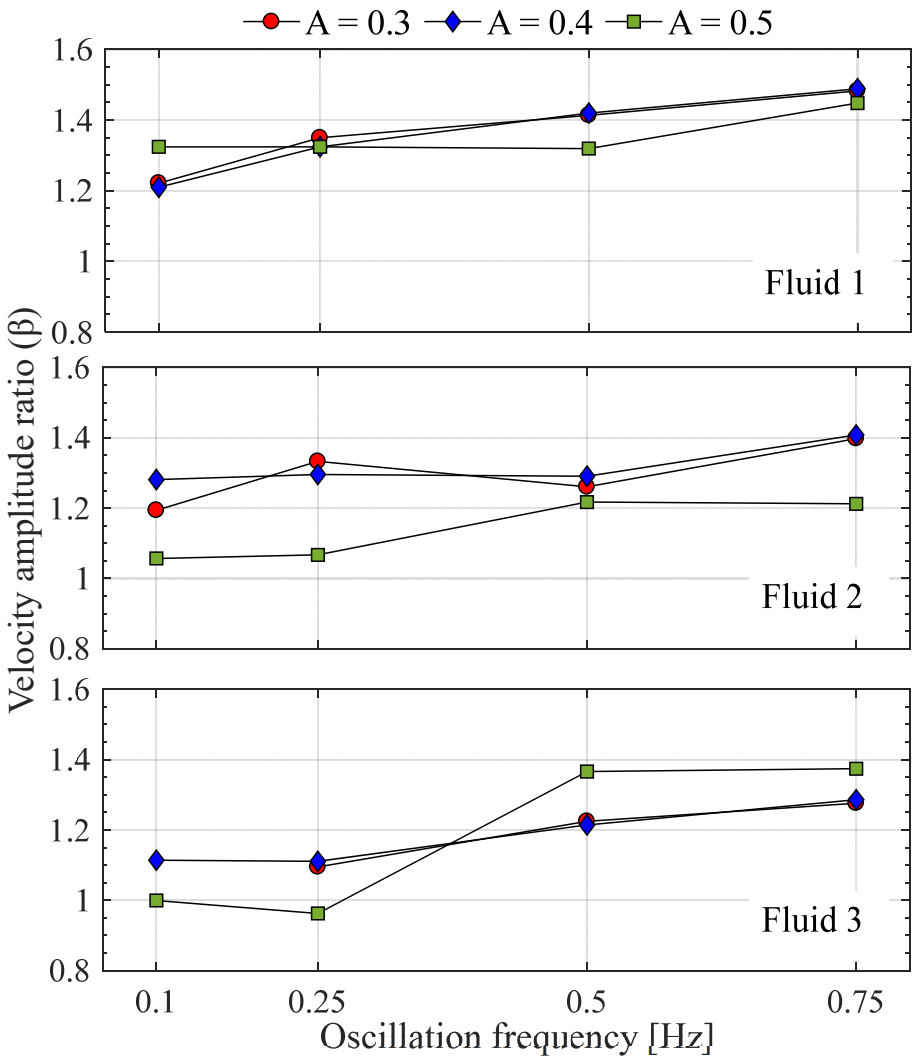

Figure 4-7: Velocity amplitude ratio (β) for different non-Newtonian fluids at different oscillating conditions

In addition to De, the evaluation of the viscoelastic Stokes parameter (Λ_{ve}) for the non-Newtonian experimental cases could be seen in **Paper VI** with a better illustration.

Table 4-1: *De* for the test fluids at different driving frequencies

	f_1	f_2	f_3	f_4
F 1	0.0229	0.0575	0.1149	0.1724
F 2	0.0132	0.0329	0.0658	0.0987
F 3	0.0103	0.0258	0.0517	0.0775

∗ F 1, F 2, and F 3 represent Fluid 1, Fluid 2, and Fluid 3 respectively. f_1, f_2, f_3 and f_4 represent the frequency values of 0.1 Hz, 0.25 Hz, 0.5 Hz, and 0.75 Hz respectively.

However, to identify the flow features more precisely, it is important to determine the correct hydrodynamic flow regime which each experimental case belongs to. Table 4-2 reports the Reynolds number values for all the experimental cases and all the test fluids of the core study of this research. For the non-Newtonian fluids, Re_δ based on δ_{ve} is used for the determination of oscillatory Reynolds number as depicted by Eq. (2-13). The shear viscosity value of each test fluid corresponding to $\dot{\gamma}$ = 100 s^{-1} was employed. Further, the maximum velocity amplitude values reported in section 4.2.1.3 have been utilized for the calculations. See **Paper VI** for more details.

Table 4-2: Oscillating Reynolds number (Re_δ) values for all the experimental cases

	A_1				A_2				A_3			
	f_1	f_2	f_3	f_4	f_1	f_2	f_3	f_4	f_1	f_2	f_3	f_4
W	-	-	-	-	-	-	-	-	19.77	40.03	79.38	115.46
F1	5.27	9.52	14.93	20.31	6.95	12.45	19.99	27.18	9.52	15.56	23.23	33.06
F2	2.99	5.39	7.45	10.46	4.29	6.98	10.17	14.04	4.39	7.23	11.99	15.12
F3	-	2.91	4.73	6.202	2.47	3.94	6.25	8.330	2.76	4.26	8.80	11.12

∗ W, F1, F2, and F3 represent Water, Fluid 1, Fluid 2, and Fluid 3 respectively. f_1, f_2, f_3 and f_4 represent the frequency values of 0.1 Hz, 0.25 Hz, 0.5 Hz, and 0.75 Hz respectively. A_1, A_2 and A_3 represent the amplitude ratio values of 0.3, 0.4, and 0.5 respectively.

Based on these calculations, it can be concluded that all the experimental cases belong to the laminar regime, and also the nonlinearities of the oscillating flow are due to the rheological properties of the fluids and not due to the inertial effects. Even if the decrease in viscosity due to the shear-thinning is considered, they are well within the laminar regime.

4.2.1.5 Cross-sectional average velocity distribution versus normalized axial velocity

The velocity profiles and the corresponding amplitudes of velocity shown in Figs. 4-6 and 4-7 are calculated at the pipe centreline. However, in common pipe flow experiments, if the velocity across the cross-section is unevenly distributed, it becomes difficult to compare different scenarios, especially with non-Newtonian fluids. Because, for the non-Newtonian fluids (even for slightly viscoelastic fluids as investigated in this research), the flow resolves into annular regions of alternating upward and downward motion. It is important to know that these annular regions are separated by quiescent boundaries where the shear stress reaches local maxima. Since the velocity profile of non-Newtonian fluids can take several shapes, either parabolic or the so-called 'Mexican hat type', the individual axial velocity components along with the radial distance and also the magnitude of the velocity amplitude do not provide a clear picture about the correct distribution of the velocity across the cross-section. Therefore, a new parameter called the cross-sectional average velocity (V_{ave}) [32] can then be defined for a pipe flow in a circular cross-section as;

$$V_{ave} = \frac{1}{\pi R^2} \int_0^R V(r).\, 2\pi r.\, dr\,, \tag{4-5}$$

where r is the radial position between 0 and R. By calculating the cross-sectional average velocity as given by Eq. (4-5) it allows us to obtain an indication of how the bulk velocity at that particular moment is established both qualitatively (direction-wise) and quantitatively. For instance, even the axial velocity is showing a higher positive magnitude in a case of a non-Newtonian fluid, the magnitude close to the shear region may have achieved two negative peaks in axial velocity which reduces the overall cross-sectional average velocity and results with a

lower value. This scenario has been illustrated in detail in **Paper V** and **VI** for all the test fluids.

4.2.1.6 Axial velocity distribution along the pipe diameter

Fig. 4-8 shows the instantaneous axial velocity distribution of water and Fluid 3 along the diameter of the pipe only for two selected cases for brevity. Note that the vertical axis of Fig. 4-8 represents the colour scheme.

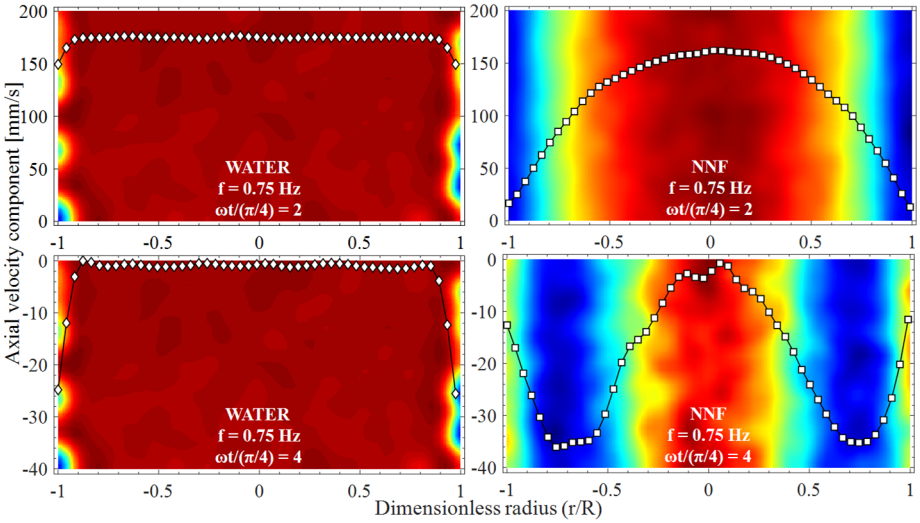

Figure 4-8: Instantaneous axial velocity distribution of water and non-Newtonian fluid along the diameter of the pipe (at f = 0.75 Hz)#

The colour background of the analysed PIV images shown in Fig. 4-8 clearly shows the significance of shear forces. See **Paper VI** for a comparison between the non-Newtonian fluids. For water, these shear forces are much more localized near the wall and the majority of the individual axial flow jets obtain mostly similar velocity values. They occupy the majority of pipe cross-section to retain as a plug-type flow. However, it is different in the non-Newtonian fluid where the effect of wall shear is propagating towards the central axis of the pipe and as a

result, different colour regions have appeared. According to Gerrard and Hughes [68], for Newtonian fluids, the flow outside the central region can be described as an oscillating boundary layer where this boundary layer becomes thinner as the frequency increases.

4.2.1.7 Temporal evolution of the axial velocity distribution along the pipe diameter

The primary data for PIV measurements in the form of instantaneous velocity fields for some specific positions of the phase cycle is presented in Fig. 4-9 for Fluid 3. It is drawn based on the centreline axial velocities for Fluid 3 and refer **Paper V** for a similar illustration for water.

The axial velocity profiles shown in Fig. 4-9 seem to be quite irregular, but parabolic like only within the core region of the pipe. Continuous flow reversal is the reason for not attaining the full parabolic profile along the whole diameter. In the cases of flow reversal with non-Newtonian fluid, if the net axial velocity profile remains positive in the core region of the pipe, some part of the velocity profile seems to be negative in a very small region near the wall. The thickness of this region decreases with the increase of frequency. It was observed that the velocity amplitude of the centreline axial velocity component increased with increasing frequency for both water and non-Newtonian fluid. Moreover, it can be concluded that the PIV technique provides more promising results at slightly higher frequencies compared to that at very low frequencies. While analysing the PIV images, it could be seen that the streamwise (axial) velocity component is greatly affected by the imposed oscillations and the impact on transverse (horizontal) velocity component is not that significant. Despite the theoretically well known no-slip condition at the wall, when it comes to the practical situation it appears as if the velocity “at the wall” is not exactly equal to zero. This is simply a consequence of the limited spatial resolution of our PIV

measurements. We would need micrometer resolution to measure at the wall.

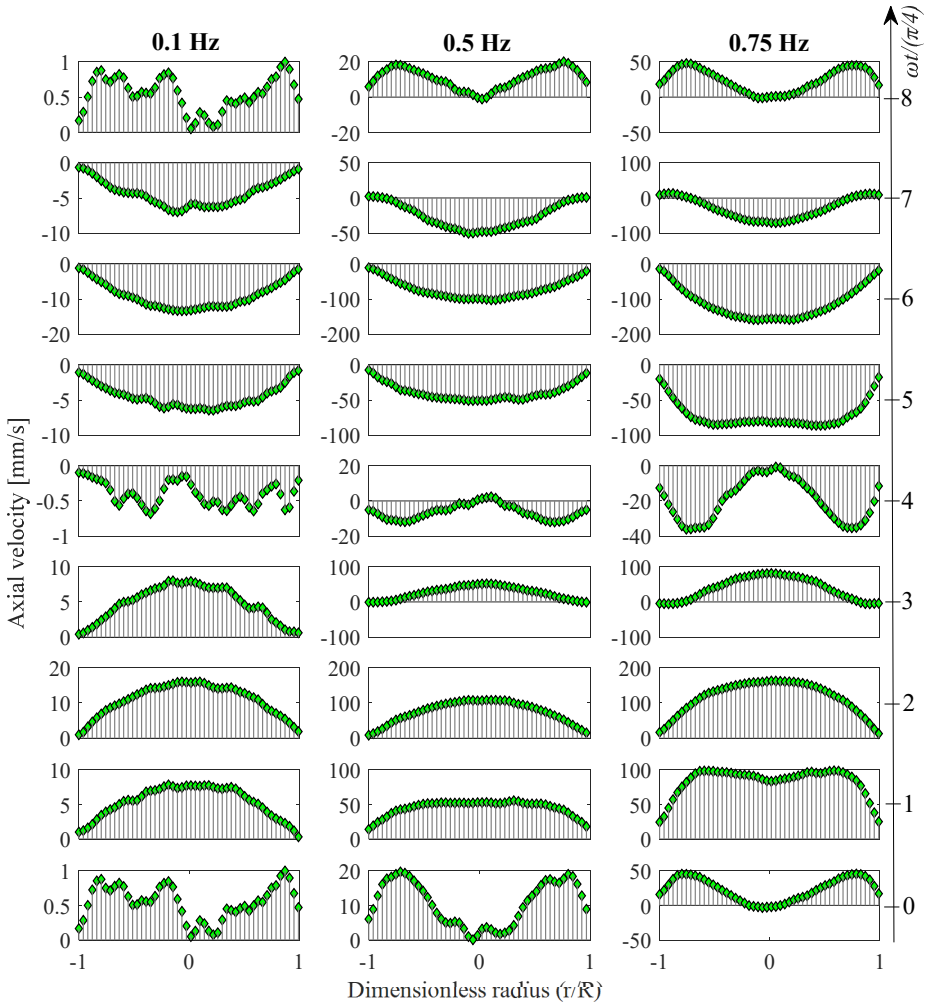

Figure 4-9: Temporal evolution of the axial velocity distribution for Fluid 3#

Fig. 4-10 illustrates the instantaneous axial velocity amplitudes (v_f) normalized by the cross-sectional average velocity (V_{ave}) in the radial direction of the pipe for Fluid 3.

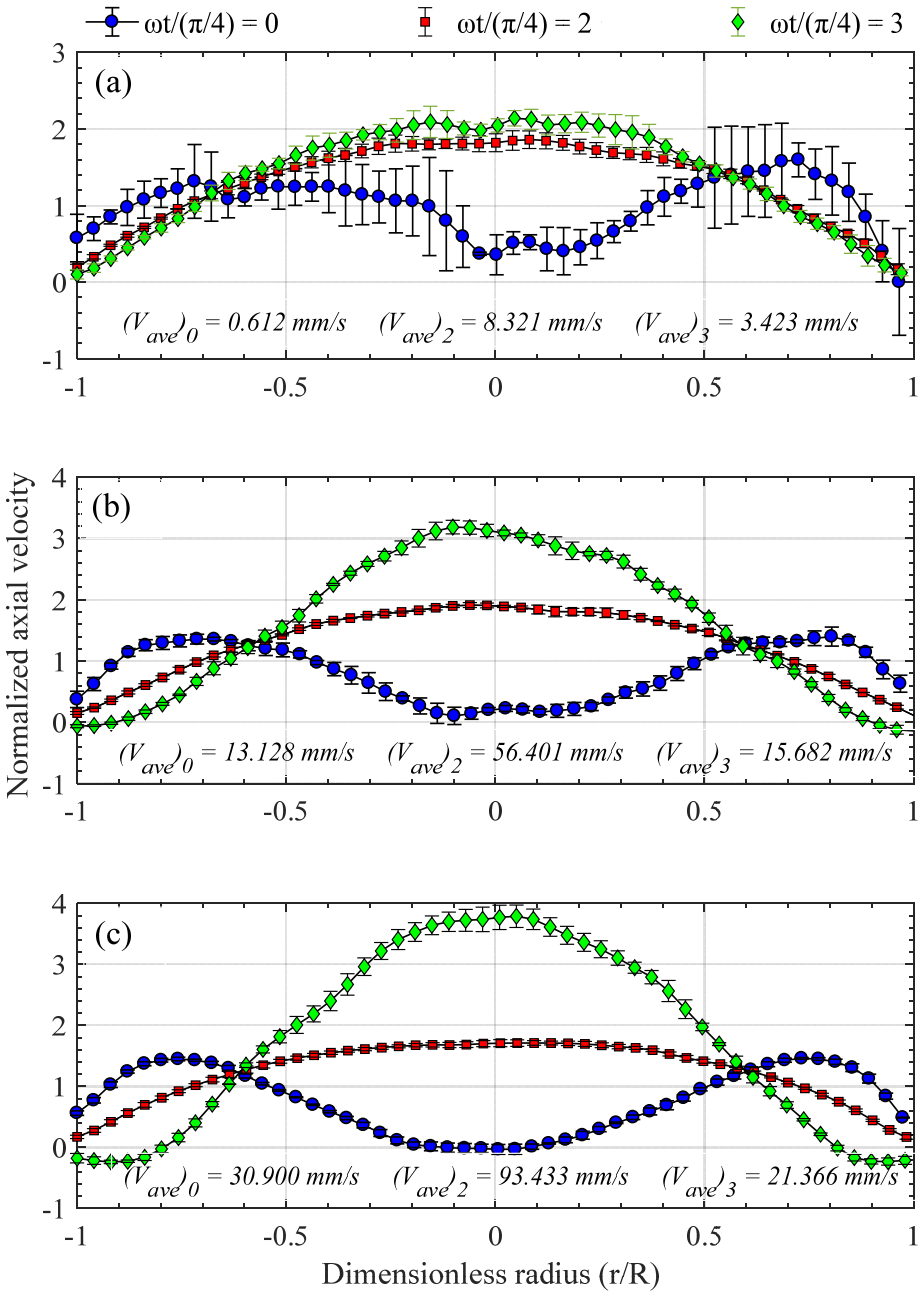

Figure 4-10: Normalized velocity profiles for the Fluid 3 (a) f = 0.1 Hz (b) f = 0.5 Hz (c) f = 0.75 Hz

Only three positions of the phase cycle within the acceleration half of the oscillation period have been selected for brevity in illustration. $(V_{ave})_k$ in Fig. 4-6 refers to $(V_{ave})_{[\omega t/(\pi/4)]=k}$, where k = 0, 2 and 3. See **Paper V** for a similar illustration for water.

According to Fig. 4-10, it could be observed that the normalized axial velocity distributions for the non-Newtonian fluid achieve a maximum in the core (or the axis) of the pipe while the normalized velocity near the pipe wall region tends to be zero. When the period of oscillation is decreased, the normalized axial velocity component for non-Newtonian fluid is increased accordingly.

The error bars drawn in Fig. 4-10 illustrate the calculated standard deviation of those readings taken at three different levels within the region of interest (ROI). It is to be noted that, these different levels within the ROI have been chosen in such a way that, it does not reflect the velocity variation with height but, to reflect the accuracy of the PIV measurements. It can be seen that the standard deviation of the PIV measurements taken at lower frequencies is greater than that taken at higher frequencies. Furthermore, the error bars shown in Fig. 4-10 are much more significant in the core region of the pipe. That can be attributed to the shear layer effect of the non-Newtonian fluid and thus it exerts a resistance for the motion close to the wall. Therefore, the velocity magnitudes for non-Newtonian fluid close to the wall region estimated by PIV analysis tend to be unchanged compared to those taken within the core region of the pipe. This provided some insight on further studies to be carried out within the near-wall region where the PIV technique is a promising non-intrusive method for estimation of wall shear stress and also the change of shear rate.

4.2.1.8 Variation of shear rate due to oscillatory motion

One of the main objectives of this study is to investigate how the shear rate is varying in the presence of oscillatory motion. The shear rate was

defined in Eq. (2-17), linked directly to the velocity gradient [74]. It is obvious here that, unlike in conventional unidirectional steady pipe flow, unsteady oscillatory pipe flow undergoes flow reversal continuously, and thus the axial velocity is varying both in magnitude and direction. Thus, the shear rate is time-varying and has more pronounced impact for non-Newtonian fluids.

Fig. 4-11 shows how the instantaneous shear rate of Fluid 3 is varying along the radial position when the fluid undergoes through the different positions of the phase cycle oscillating at f = 0.75 Hz and A = 0.5. For illustration purpose and brevity, only a single test case has been used for this figure, and the raw experimental data has been regressed with a R^2 value greater than 95% for clarity. The non-dimensional phase position $\omega t/(\pi/4)$ has been denoted as k in the figure caption.

According to the profiles shown in Fig. 4-11, it can be seen that there is a significant variation in shear rate throughout the pipe cross-section. This is very important to understand with respect to the particle settling/separation point of view. The variation of rate of shear directly affects the viscosity of the shear-thinning non-Newtonian fluids and consequently on the drag reduction. At phase positions where the velocity profiles show some "Mexican hat" type distribution (see Fig. 4-9), there seem to be two or three points where the change in shear rate becomes zero. The shear rate profiles are even steeper close to the wall regions in some phase positions such as $\omega t/(\pi/4)$ = 0, and 4. When the flow reaches to its maximum phase position where $\omega t/(\pi/4)$ = 2 or 6, the distribution of the rate of shear seems to show more or less linear profile from the wall to the centre region which makes the settling particles in such a system experience differences in viscosity of the fluid medium. However, the maximum change of shear rate is achieved at the maximum position of the phase cycle ($\omega t/(\pi/4)$ = 2 or 6), where the axial velocity also possesses the highest magnitude.

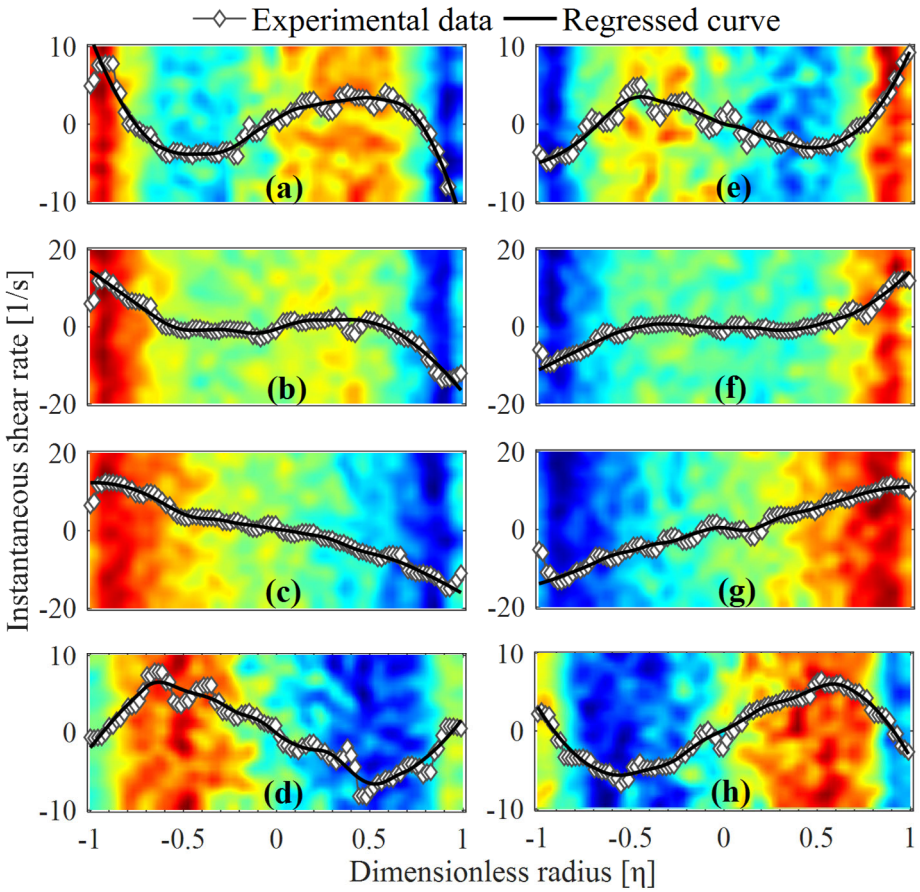

Figure 4-11: Change of instantaneous shear rate for Fluid 3 with the phase position at f = 0.75 Hz and A = 0.5#

(a) k = 0; (b) k = 1; (c) k = 2; (d) k = 3; (e) k = 4; (f) k = 5; (g) k = 6; (h) k = 7 [* The color scale for each subfigure is defined by the magnitude of each plot itself – vertical axis]

The different PIV generated colour patterns in the background of the shear rate profiles shown in Fig. 4-11 illustrate the shear rate magnitudes for a case of De = 0.078 and δ_{ve} = 18 mm. The red colour (or dark blue colour for the opposite direction) indicates the peak shear region and it could be seen that the wall shear tends to propagate towards the pipe

centreline through the oscillation cycle. This experimental observation possesses a deviated behaviour from the theoretical explanation provided in section 2.2.4.4 regarding the definition of 'wide' systems as explained by Casanellas and Ortin [72]. This could be attributed specifically to the rheological characterization of the test fluids where they are not pure Maxwellian fluids and also to the highly reversing flow phenomena in the experimental setup. The test fluids were slightly viscoelastic according to section 3.2.1.1. Therefore, they neither behave similar to pure Maxwell fluids nor show the properties of pure Newtonian fluids.

The variation of the shear rate close to the pipe walls is illustrated and described with more details in **Paper VI**.

4.2.2 Dynamics of spherical particles settling in oscillating Newtonian and non-Newtonian fluids

4.2.2.1 Settling velocity at stationary conditions (in quiescent fluid) along pipe axis (Location 'L1')

To assess the experimental data and results of the present analysis in comparison to the well-established knowledge on particle settling in stationary Newtonian and non-Newtonian fluids, the settling of spherical particles was captured by the high-speed camera under stationary conditions before imposing any oscillatory motion. The results could be seen in **Paper VII**.

4.2.2.2 Validation of particle tracking method and the experimental results

To validate the experimental measurements captured by the high-speed imaging system, and to prove the accuracy of the particle tracking method, the terminal settling velocities (at quiescent conditions) of the three particles in water at quiescent conditions (also at Location 'L1') were used. Based on the terminal settling velocities for those three sizes

of glass beads, the drag coefficient was calculated using Eq. (4-6), which is just a re-arrangement of Eq. (2-18);

$$C_{D0} = \frac{4}{3}\frac{gd(\rho_p - \rho_f)}{\rho_f v_{p0}^2} \tag{4-6}$$

The terminal velocity Reynolds number of the particle ($Re_{p0} = \rho_f v_p d/\mu_f$) was then calculated as described in section 3.4.2.1. The calculated C_{D0} values were plotted upon the drag coefficient ($C_{D0-correlation}$) versus Re_{p0} correlation [121] graph as shown in Fig. 4-12. This correlation is shown in Eq. (4-7).

$$C_{D0-correlation} = \frac{24}{Re_{p0}} + \frac{2.6\left(\frac{Re_{p0}}{5.0}\right)}{1+\left(\frac{Re_{p0}}{5.0}\right)^{1.52}} + \frac{0.411\left(\frac{Re_{p0}}{26300}\right)^{-7.94}}{1+\left(\frac{Re_{p0}}{26300}\right)^{-8.00}} + \frac{0.25\left(\frac{Re_{p0}}{10^6}\right)}{1+\left(\frac{Re_{p0}}{10^6}\right)} \tag{4-7}$$

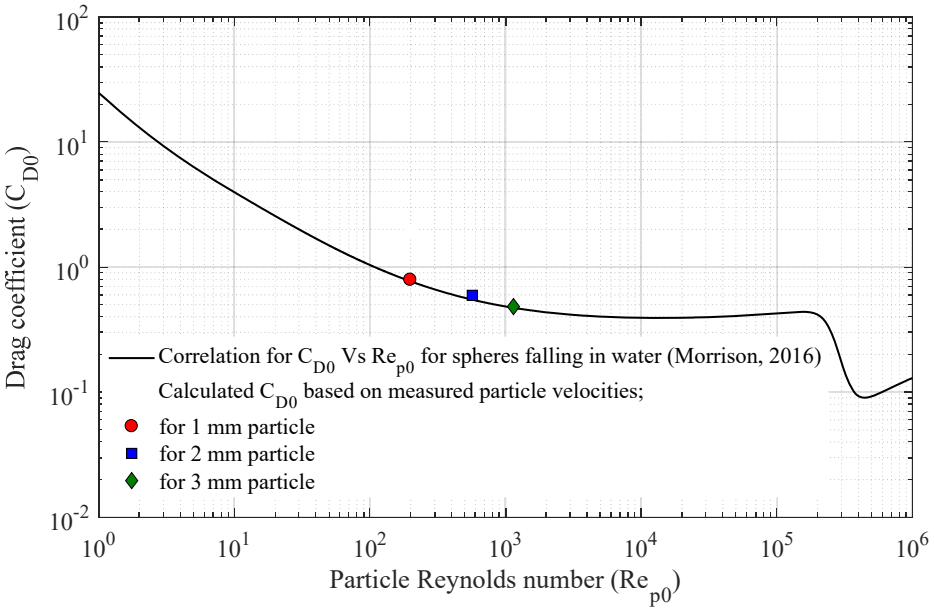

Figure 4-12: Drag coefficient versus particle Reynolds number

According to Fig. 4-12, it can be seen that all the drag coefficient values calculated from experimentally measured terminal settling velocity values (using high-speed imaging technique and the particle tracking method) are within 5% deviation from the data correlation presented by Morrison [121], which is an acceptable variance.

4.2.2.3 Particle displacement in oscillatory conditions along pipe axis (Location 'L1')

Particle tracking velocimetry (PTV) is a proven technique to analyze and study the particle motion in unsteady oscillatory conditions while the observation of wake patterns provides more in-depth details regarding the hydrodynamics.

4.2.2.3.1 Variation of particle displacement with the frequency of oscillation

According to the plots presented in **Paper VII** to check how the particles move downwards (or upwards) at different frequencies, it could be seen that the time development of the particle displacement at stationary conditions are pretty straight forward and determination of their terminal settling velocity is easy. Moreover, the settling velocity of particles in water does not show to be much affected by the oscillation at lower frequencies.

When the frequency is increased the displacement curves for water tend to show some response to the oscillatory motion. However, it could be seen that the vertical component of the displacement curves of the particles in non-Newtonian fluids is significantly affected at all frequencies. When the oscillatory motion is present, the frictional force or the drag force together with lift force on the particle act either in the same direction as the buoyancy force or in the opposite direction. The magnitude of each force depends on the viscosity of the fluid medium and the size of the particle.

The slopes of the particle displacement curves provide the settling velocity of each particle and since in some cases, more than one oscillation period is considered, it could be termed as 'average velocity'. Thus, it could be seen that large-sized particles have achieved higher settling velocities at all the oscillation frequencies and all sized particles tend to settle faster in water than in any non-Newtonian fluid even at oscillatory conditions.

4.2.2.3.2 Variation of particle displacement with different fluid types

Fig. 4-13 shows the vertical component of the particle displacement for different fluid types, for all the particle sizes and for the oscillation frequency equal to 0.75 Hz. According to Fig. 4-13, it can be seen that the displacement of the particles in water is not affected significantly even at higher frequencies; especially for the large-sized particles. In comparison to that, all particle sizes are greatly affected and influenced by the oscillatory motion in such a way that they alter their displacement direction (vertically as downwards and upwards) from time to time within the oscillation period in the course of settling. According to the plots of displacement evolution of the particles shown in Fig. 4-13, a condition of partial stability (or stagnation) of the particles could be observed in some instances especially at higher fluid viscosities and also for smaller sized particles. This temporary stability is simply due to the initial relaxation of the particle to align with the action of the combined gravitational force (downwards) and the viscous drag (oscillating). If the liquid was purely oscillating in absence of gravitation the particles would follow nearly the same motion. The only difference would be the particle inertia. If the liquid flowed with constant speed in absence of gravity, the particle would follow more or less completely aligned, except for local liquid perturbations. An alternative but fully equivalent way to depict the motion would be to take the numerical time derivative of the displacement trajectories to give the "falling speed" of the particles. However we chose to show the displacement as these are the raw data, and the numerical derivative could be too fluctuating.

4.2.2.4 Settling velocity of particles in different oscillatory conditions along pipe axis (Location 'L1')

As explained in section 3.4.2.1, the average settling velocity of the particles at different oscillatory conditions was approximated by fitting the vertical component of the displacement profiles of the particles into a linear curve and considering its slope.

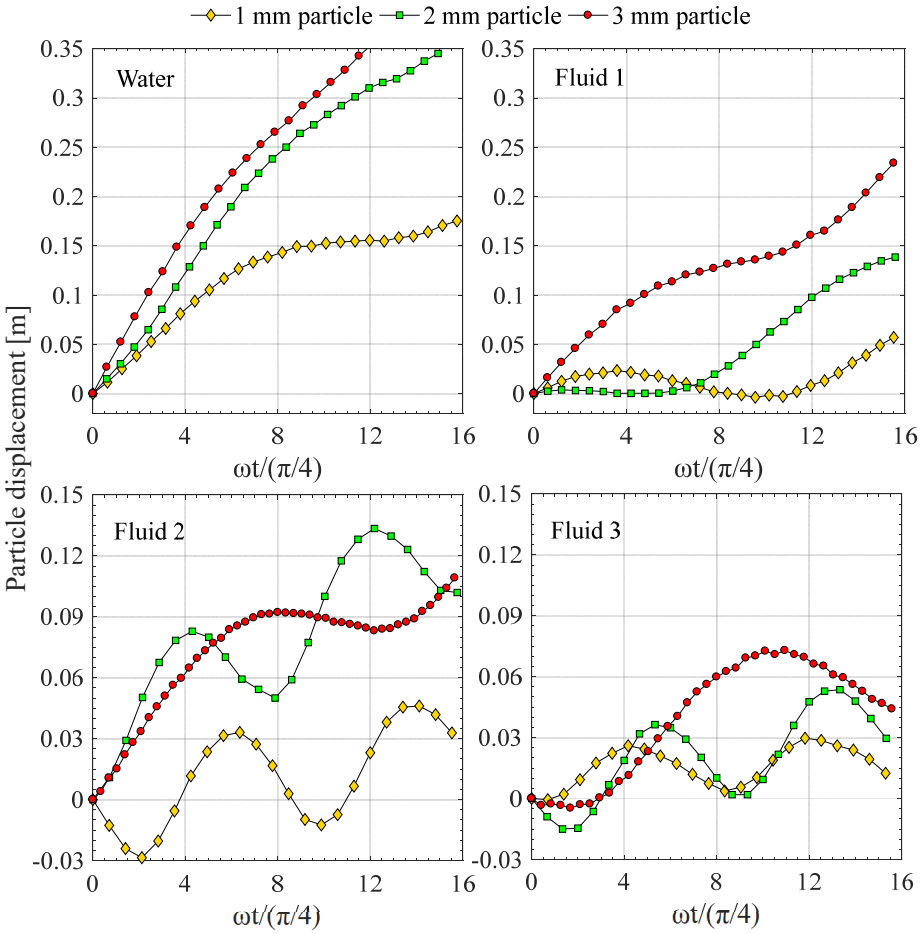

Figure 4-13: Vertical component of the particle displacement in all test fluids at f = 0.75 Hz

To provide a clear idea about the changes in settling velocity of particles at each oscillating condition by comparing those with the non-oscillating condition, a velocity ratio (β) is defined as;

$$\beta = \frac{v_p}{v_{p0}} \tag{4-8}$$

where, v_p is the settling velocity of given particle size at a particular oscillation frequency settled along the pipe axis ('L1') in a particular test fluid. Then v_{p0} is selected as the terminal settling velocity (at non-oscillating conditions) of the same sized particle settled along 'L1'

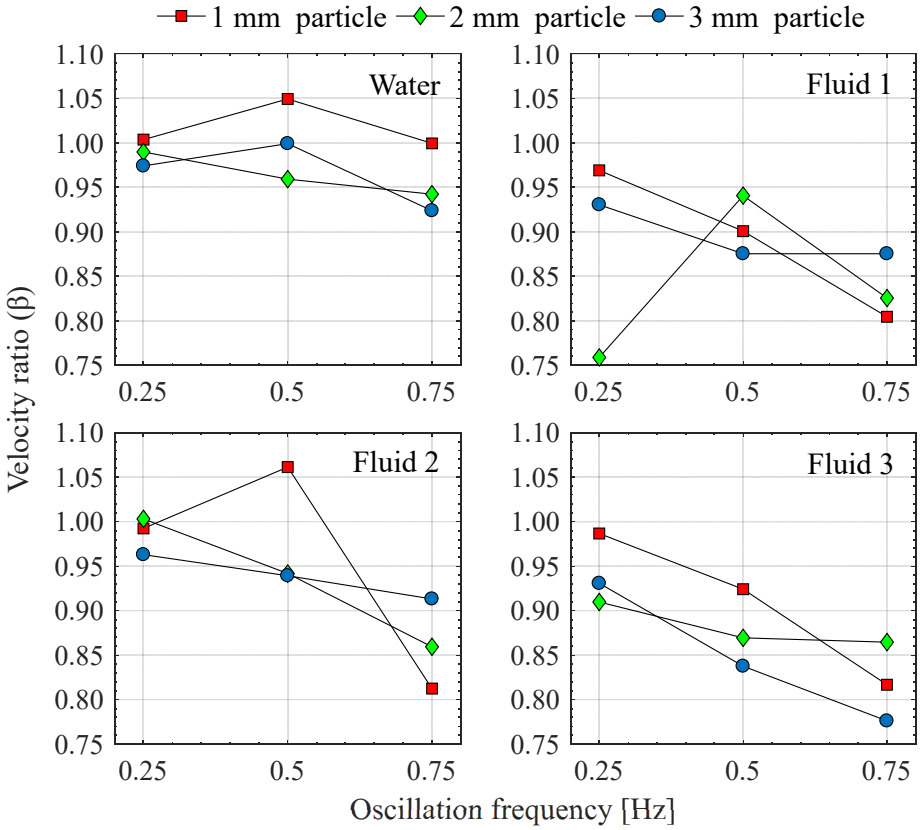

Figure 4-14: Variation of β at different oscillation frequencies for different particle sizes

within the same test fluid. Fig. 4-14 shows how β varies with the changing of oscillation frequency for different particle sizes while Fig. 4-15 shows the same for different fluid types for better understanding.

According to Figs. 4-14 and 4-15, it can be observed that the settling velocity of the particles at oscillatory conditions has been reduced from that at stagnant condition except for a couple of outlier values for the combinations of 2 mm particle in Fluid 1 and 1 mm particle in Fluid 2. The slight variance in velocity ratio β at oscillatory conditions compared to the terminal settling velocities presented in **Paper VII** could be due to the uncertainty effects related to slight variations in particle shape. Also the exact radial position could perhaps be masked by azimuthal movement. Moreover, it could also be attributed to a condition of adverse pressure-gradient where the wake becomes unstable and fluctuations of the drag force appear even though the flow is laminar for all the test cases based on the oscillatory Reynolds number explained by Mazzuoli et al. [63] and Amaratunga et al. [118].

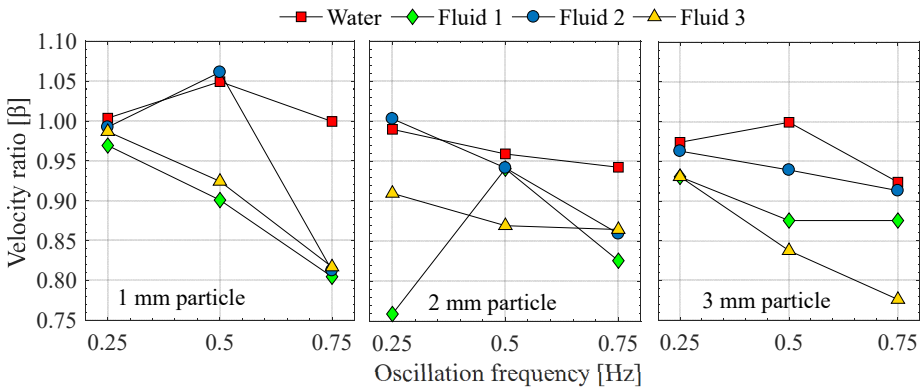

Figure 4-15: Variation of β at different oscillation frequencies in different fluid types

However, Figs. 4-14 and 4-15 again prove the fact that water being a Newtonian fluid appears to be the least affected by the oscillations in terms of the velocity reduction. On the other hand the significance of retardation becomes increased when the non-Newtonian fluids become

more viscous with increased shear-thinning effects. The variation of β within water always lies close to unity, which ranges from 1.05 to 0.92 for all the particle sizes. That indicates that there has been only a slight drag enhancement on the particles due to the oscillations when they are settled in the water. However, a reduction of β in the range from 4 – 23% could be observed in non-Newtonian fluids where the maximum reduction is achieved when the particles are settled in Fluid 3. This reduction of velocity could be attributed to the oscillation-induced increases in the drag coefficient on the particles at unbounded shear conditions and the unstable wake due to the continuous changing of the oscillatory flow [122]. The drag force on the particles in oscillatory conditions is significantly modified by the instantaneous relative velocity between the particles and fluids [102] because of the continuous flow changes within the flow.

Furthermore, particle inertia is not negligible with respect to that of the fluid in this scenario and the drag coefficient is most likely be affected by the unsteadiness of the wake. Refer **Paper VII** for more details.

4.2.2.5 Effect of the shear region on settling velocity (settling at 'L2' and 'L3')

Since the unsteady oscillatory pipe flow undergoes flow reversals continuously and thus the axial velocity is varying both in magnitude and direction, the shear rate is time-varying and effects from that become more pronounced for non-Newtonian fluids.

The same approach has been taken as described in Eq. (4-8) to quantify the effect of walls at stationary conditions and the effect of the shear region at oscillatory conditions where the instantaneous settling velocity of the particle (v_p) refers to the value either along 'L2' or 'L3'. v_{p0} is the same as that measured along 'L1' for resting fluid.

4.2.2.5.1 Wall effects at stationary conditions

When spherical particles settle within pipes and conduits, they experience retardation effects from the walls which reduce its settling velocity. This effect is quantified in terms of a wall factor which is defined as the ratio of the settling velocity in the presence of confining walls to the unbounded settling velocity in the same fluid.

According to the results presented in **Paper VII**, it can be seen that the wall effects are significant when smaller sized particles settle in both Newtonian and non-Newtonian fluids. When a 1 mm particle settles in water, the velocity ratio (β) shows a reduction of around 25% while it is just around 3% when a 3 mm particle settles in water. Furthermore, it is observed that the wall retardation becomes less significant when the non-Newtonian fluids become more viscous and it becomes less severe in power-law fluids than in Newtonian fluids. However, the effect of particle size on oscillation-induced retardation is more significant than that observed for the wall-effect in the absence of oscillation.

4.2.2.5.2 Effect of the shear region at oscillatory conditions

In comparison to the wall-effects at stationary conditions, a particle which moves parallel to a wall in an oscillatory flow behaves in a slightly different manner since it does not experience a transverse (lift) force, at least within the Stokes region [122]. Fig. 4-16 shows how the velocity ratio (β) varies when the particle can settle closer to the pipe wall in oscillatory conditions.

It could be seen that when the particle is close to the wall in water, β tends to reduce. But, when it is allowed to settle in non-Newtonian fluids closer to the wall and at oscillating conditions, β tends to show a slight increase. This slight increase may not be sufficient to overcome the terminal settling velocity at stationary conditions, but that is considerable and interesting to study since it is expected to have an increased drag as a result of both shear flow and the wall-effect. Despite the slight

anomalies shown by the 1 mm particle from the above-mentioned observation, 2 mm and 3 mm particles are in good agreement. This slight increase in β could be attributed to the increased shear effects and the

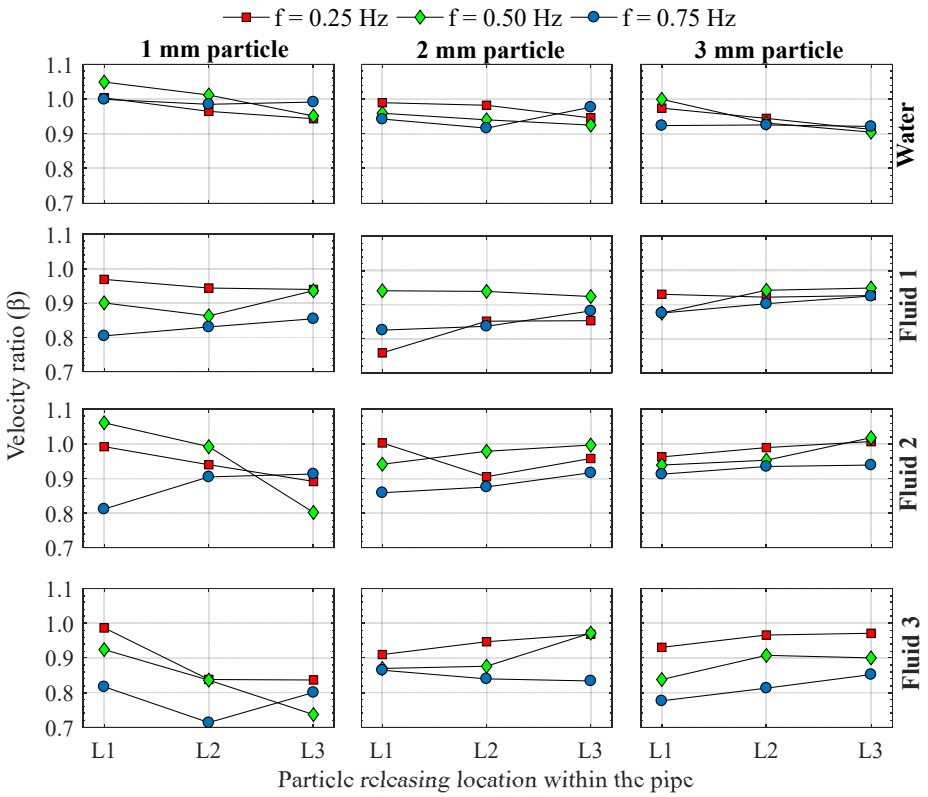

Figure 4-16: Effect of the shear region on particle settling at oscillatory conditions in different fluid types

slight drag reduction within the Stokes region [122, 123] in the presence of the oscillations, which can be elucidated as follows.

The viscosity of most water-based drilling fluids is formulated by a combination of polymers similar to the test fluids in the current study. In addition, water-based drilling fluids may contain some additives to achieve desired agglomeration effects. The structural units and surface charges between those particles in polymeric liquids may get weakened by the oscillations/vibrations and that leads to a reduction of internal liquid viscosity. It is to be noted that the cyclic maximum shear rate

change occurs mostly near the pipe wall, and thus the resulting viscosity reduction is more pronounced in the near-wall regions [118].

This explains the fact that, when the shear-thinning non-Newtonian fluids (primarily water-based polymeric liquids) are subjected to oscillatory motion, there will be a substantial reduction of viscosity of the fluid and that will result in the reduction of the drag force on the settling particles and consequently experiences faster settling. Furthermore, it is important to know that there exist some interactions of the particle with the coherent vortex structures in the near-wall region as explained by Mazzuoli et al. [63] and the hydrodynamic force on the sphere is characterized by such complex time development. Since the particles are released fairly close to the wall at L3 (see Fig. 3-12), their trajectory (and thus the average velocity) is largely influenced by the vorticity present in the vicinity of the wall. Vortices are generated in the boundary layer during some positions of the oscillation period.

Therefore, the non-linear dependence of the drag force on the relative velocity of the particle to fluid becomes apparent in the presence of oscillatory motion since the shear effects come into action and the shear rate increases closer to the walls. It can be concluded that the mean relative velocity of settling (or rising) of particles in a liquid medium is reduced if the liquid medium is made to undergo sinusoidal vertical oscillations. However, the settling particles in that oscillating fluid medium closer to the pipe wall would experience a slight reduction in drag within the shear region than that in the core region.

4.2.2.6 Error analysis

As stated previously, it is important to discuss the error associated with the current analysis since it contains some approximations in averaging the settling velocity at oscillatory conditions, which is the significant parameter in the present study. The error sources associated with this study could be two-fold; namely, (i) the experimental (or the random)

error when capturing the position of the settling particle and (ii) the error associated with approximating the slope for the displacement profile of the particles when they are settling in oscillatory conditions. In a way, the latter could be considered as a 'systematic' error since it is obvious to deviate from the linear curve. On the other hand, the size of the particles is not exactly 1, 2 or 3 mm (as shown in Table 3-3) could also be a slight contribution to the systematic error of the experiment. However, it is of great importance to mention here that, the vertical displacement of the particles has been recorded for a time long enough to estimate the average slope with precision. The authors wanted to investigate the behaviour of the falling particle throughout its whole path within the test section rather than just calculating the average velocity at the bottom of the test section as 'a specified distance divided by the time spent'.

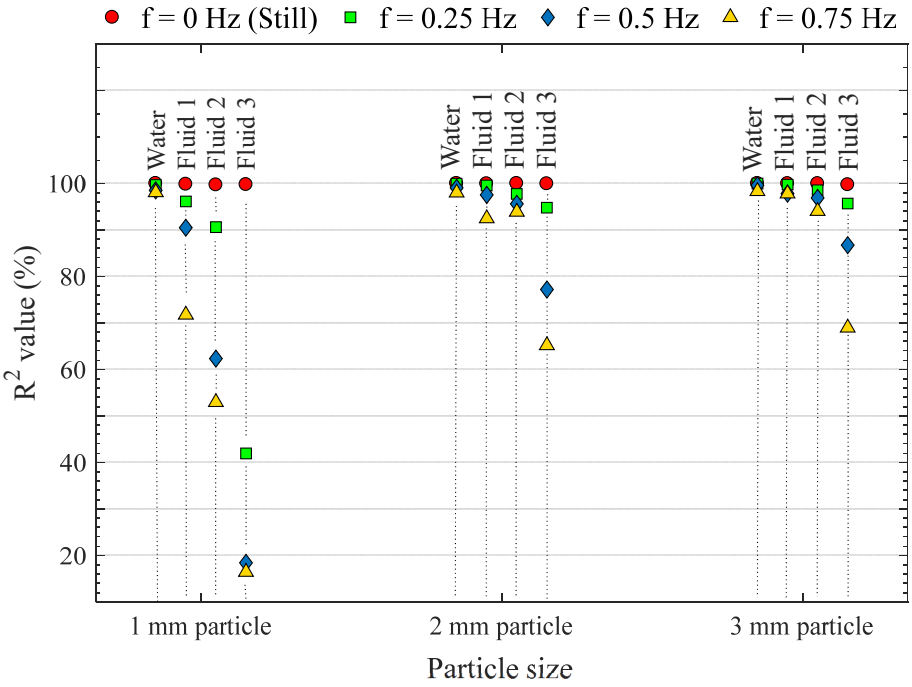

Figure 4-17: Resulted R^2 value in approximating the slope for the displacement profiles of particles in oscillatory conditions

To assess the associated error and to enhance the accuracy of results, all the experimental cases were repeated three times. Out of those trials, it could be observed that the terminal settling velocities at stationary conditions has the lowest standard deviation of 0.000437 m/s when 3 mm particle settles in Fluid 3 and the largest standard deviation of 0.0387 m/s when 1 mm particle settles in water. Even for the oscillatory cases, the random error was not significant in such a way that their standard deviations are comparably too small. This indicates that the random error which is associated with the results of this particular study would be not that significant.

Furthermore, when approximating the slope for the displacement profile of the particles under oscillatory conditions, some cases exhibited significant deviations as shown in Fig. 4-17. It can be seen that R^2 values are within the acceptable range (> 90%) for still fluids, and also when they oscillated at very low frequencies. Further increase in the frequency enhances the deviation especially for the smaller sized particles when they are settling in highly viscous non-Newtonian fluids. The lowest R^2 values recorded are around 17% when 1 mm particle settles in Fluid 3. As stated in section 4.2.2.3.2, the condition of partial stability or the temporary stagnation of the particles within its course of settling is the closest reason for this increased deviation (or lower R^2 value) for smaller-sized particles in high viscous non-Newtonian fluids. As earlier mentioned, it was found to have certain oscillation frequencies where the absolute downward displacement of the particle is smaller than its displacement in the opposite direction, regardless of the gravitational force. And so, the displacement profile of the particle also showed more or less sinusoidal pattern which consequently reduces the R^2 value of the fitted linear curve. The authors understand the necessity of performing additional tests for each experimental condition to achieve better convergence statistics and a comprehensive investigation would require observing the velocity field around the particle during its motion, for instance utilizing PIV measurements.

However, taking the average settling velocity even with such low R^2 values were successful in quantifying the oscillation-induced reduction of settling velocity of particles in Newtonian and non-Newtonian fluids.

5 Conclusions

The conclusions are derived based on all the sub-studies and considering the whole research as an overall.

When a particle is allowed to settle through an unsteady liquid, additional forces arise as a result of the changes in the flow patterns around the particle. Thus, these forces may create a significant effect on both the instantaneous relative velocity of the particle to the fluid and also on the mean transport velocity of the particle. Therefore, the settling at oscillatory conditions is quite different from that at steady conditions. This research was carried out to study how the viscous properties of shear-thinning non-Newtonian fluids alter when exposed to oscillatory conditions and the effects of oscillatory motion on the settling of spherical particles in Newtonian and non-Newtonian fluids. Different limited studies were performed within the project, employing different measurement techniques. Also a computational study was carried out for quantification and visualization of related parameters.

The research concludes that;

- Optimal drilling performance depends strongly on the optimum dosage of different polymers into the drilling fluids. The addition of Xg into water-based drilling mud should be carried out carefully to achieve the required properties of the drilling fluid.
- Low-frequency acoustic streaming is not much effective in providing a considerable effect on settling particles especially when they are settled in non-Newtonian fluids.
- PIV is a very good non-intrusive technique to analyse oscillatory flow both for Newtonian and non-Newtonian fluids. It provides insight into the velocity profile at the near-wall regions as well as in the core region. It is fair to say that presently there are no other experimental techniques that can measure velocity profiles with such resolution in

space and time. The colour maps obtained through PIV analysis are useful in identifying the shear regions and fluctuations in such a study.

- The combined (near wall) shear force and liquid inertia cause the velocity profile of non-Newtonian fluids to become a complicated radial function quite different from the plug flow imposed by the oscillating piston.
- The thickness of the shear region decreases with increasing oscillation frequency. The axial velocity in the shear region either lags or leads the axial velocity in the central pipe region by a small amount and tends to be zero at some certain positions of the phase cycle.
- The centreline velocity amplitude increases with increasing frequency and with increasing oscillating amplitude ratio. This is irrespective of the fluid type.
- The axial velocity profile of water across the cross-section is plug-type with a peak appears between the axis and the wall and this peak approaches the wall with increasing frequency. At higher frequencies, the viscous effects are confined to the Stokes layer and the central core is plug-type with increased velocity amplitudes.
- The viscous resistance of the non-Newtonian fluid and the presence of shear layer contribute much to generate an uneven distribution of the velocity across the cross-section. Cross-sectional average velocity provides a more complete picture of the kinematic structure of oscillating flow and its dynamic distribution across the cross-section.
- Tracking of particles from high-speed images is a very useful and informative way to study the settling of particles in both Newtonian and non-Newtonian fluids at steady and unsteady conditions.
- When the fluids are at rest, the terminal settling velocity of particles within Newtonian fluids is larger than that within the non-Newtonian fluids due to the increased viscosity of non-Newtonian fluids. Both theoretically (from literature) and experimentally, it is shown that oscillations lead to increased drag force exerted on the particles.
- The increased drag effect becomes significant in stagnant conditions when the non-Newtonian fluids are more viscous and shear-thinning.

This reduction of terminal settling velocity could also be attributed to the negative wake that is perceived to happen only in shear-thinning viscoelastic fluids.

- In quiescent fluids, the rate of increase in terminal settling velocity (with increasing particle size) is higher for water and low viscous NNFs compared to that in high viscous NNFs. This means that larger particles settle down at a slower rate than the smaller particles when the shear-thinning of the NNF is increasing (when n becomes low). Therefore, increasing shear viscosity may be an effective solution to achieve suspensions of large-sized particles.
- A condition of partial stability (or stagnation) of the particles within its course of settling could be observed in some instances especially at higher fluid viscosities and also for smaller sized particles under oscillatory conditions. Such temporary stable condition could be seen only when the fluid medium moves upward in its oscillating cycle due to the neutralization of finite buoyancy forces by the gravitational and drag forces acting on the particle.
- The settling velocity of particles in both Newtonian a non-Newtonian fluids experiences a reduction under oscillatory conditions. This reduction of settling velocity may be primarily related to increased drag forces induced by the fluid oscillations. However, the effects of phase lag between the particle and the fluid medium, the velocity field around the particle during its motion, and wake dynamics could be considered as secondary influences. More detailed PIV studies supported by CFD simulations could explain this in more detail.
- Velocity retardation effect under oscillatory conditions becomes significant by reduction of the power-law index, n and with relatively large-sized particles.
- The impact of wall retardation at steady conditions becomes less significant when the non-Newtonian fluids become more viscous and it becomes less severe in power-law fluids than in Newtonian fluids.

- The effect of particle size on oscillation-induced retardation is more significant than that observed for the wall-effect in the absence of oscillation.
- When the shear-thinning non-Newtonian fluids (primarily water-based polymeric liquids) are exposed to oscillatory motion, there will be a reduction of viscosity of the fluid closer to the pipe walls where the shear region exists and that will result in the reduction of the drag force on the settling particles.
- Even though the approximation of average settling velocity from particle displacement profile (as described in section 3.4.2.1) seems less accurate in some instances, it is a successful way in quantifying the oscillation-induced retardation of settling velocity of particles in Newtonian and non-Newtonian fluids.

As an overall idea, the research reveals that an enhancement of suspension in Newtonian and non-Newtonian fluids could occur in oscillatory flows. However, when the particles are settled close to the pipe wall in the oscillatory non-Newtonian fluid medium, they could experience a slight reduction in drag due to the increase in shear rate. Furthermore, the author expects that this work will stimulate further experimentation on different aspects especially in understanding the hydrodynamics forces on the particles being settled in oscillatory shear-thinning, non-Newtonian fluids.

6 Recommendations for future work

Accurate measurement demands plenty of time and money. In addition to that, processing and analyzing the experimental data are also time-consuming and need proper techniques. While performing the experiments and analyzing the experimental data, many new ideas were queued in the author's mind for further implementation.

The U-shaped experimental setup used for the core study of this research is some sort of a fertile turf to any investigator to perform both fundamental and applied research. The author could only perform the expected experimental work that is within the aim of the research whereas many other aspects still stimulate careful experimental analysis. If any suggestions for further work should be made the author would like to recommend the following areas for further investigations.

- The yield stress of the non-Newtonian fluids can help to retain the particles up to some extent. In shear-thinning fluids, understanding the effect of yield stress on particle settling is limited. Therefore, it is recommended to use some shear-thinning non-Newtonian fluids with sufficient yield stress and perform these oscillatory experiments, so that it would be interesting to see the influence on particle settling in such fluid at different oscillatory conditions.
- The preliminary rheological characterization at the beginning of the research (first sub-study within the pre-study) with Xg was carried out having the aim of designing the test fluids with some intended rheological characteristics (K and n values in power-law). However, since Xg makes the water-based polymer solution a little opaque, the use of optical measuring techniques such as PIV was limited. Therefore, it is recommended to use a transparent viscosifier such as Xanvis^{TM} (a brand name modified Xanthan polymer) for better visualization and at the same time can be incorporated to design the test fluid with intended characteristics.

- The rheological measurements for all the sub-studies in this research were tested using the concentric cylinder mode of the rheometer. It is recommended to use the other modes such as double-gap, cone-plate, parallel-plate, etc. for comparison. Furthermore, more time should be allowed in rheological measurements to achieve very low shear rates (less than 0.1 s^{-1}), so that the signs of plateau value of zero-shear viscosity could also be visible. For example, Brookfield viscometers provide accurate results for such types of very low shear rates [124].
- Non-Newtonian test fluids with high viscoelasticity effect could be employed in the experiments to investigate the effects of viscoelasticity on particle settling in oscillatory conditions. Similar to that, one can extend the experiments to check the effect of fluid elasticity by using Boger fluids.
- Instead of water-based polymeric solutions, oil-based model drilling muds (transparency is desirable for PIV) can be used to investigate the difference in different mud types when particles are settled in oscillatory conditions.
- The patterns and shapes of the air-liquid interface at different oscillatory conditions could be further studied for different non-Newtonian fluids.
- As explained within the thesis, the extents of laminar to turbulent in terms of the oscillating Reynolds number is not exact in the current literature. The U-tube experimental setup can be employed to investigate the laminar to turbulent transition. The visualization could be carried out easily by incorporating a coloured dye into the test section when the oscillation takes place.
- It will be very exciting to use stereoscopic PIV and later tomographic PIV to yield more information in a larger flow domain. That will help avoid the light refraction effects from the curved pipe walls and obtaining more accurate flow phenomena even with the settling particles. This requires a pulsed laser instead of the continuous laser used in the present work.

- Instead of single-particle settling, the experiments can be extended with a cluster of particles with the same size or with different sizes.
- Particles with different shapes can be used to investigate the effect of particle shape on settling rate in the presence of oscillatory motion.
- The retardation of settling velocity at oscillatory conditions is due to the shedding of a large wake during each oscillation. It would be very informative to investigate and observe this alternating wake by coating the settling spheres with a dye.
- The air gap between the liquid medium and the piston can be avoided and the piston can be arranged in such a way that it directly transfers the oscillatory motion to the liquid medium.
- The motor and the piston can be attached to the smaller vertical pipe (the right limb of the U-tube), so that the piston moves vertically downwards and could be checked for any differences in the results compared to the current arrangement.
- A more controllable cushioned linear piston can be used to provide the oscillatory motion to avoid any type of hammer effects at the peaks and troughs of the phase cycle.
- The same experiment can be carried out with different pipe sizes to study the effect of channel or pipe diameter.
- Pressure transmitters could be incorporated to get pressure data and correlate them with the pressure drop to predict the inline rheometry.
- Temperature measurements along the pipe (starting from the piston cylinder) could be used to study any adiabatic effects of the oscillatory motion.
- The main part of the current research was carried out by keeping the oscillation amplitude constant. However, the experiments can be extended to study the effect of oscillation amplitude on particle settling while keeping the driving frequency constant.
- The same experiment can be repeated in a non-circular duct. Since the secondary flow located near to the corner of the noncircular duct is unique, it will be interesting to see the effect on particle settling in a non-circular duct.

- Fully resolved numerical simulations using computational fluid mechanics can be performed to understand and unearth the physical mechanism at a few strategic points in the vast parameter space.

7 References

[1] R. Caenn, G. V. Chillingar, and engineering, "Drilling fluids: State of the art," *Journal of Petroleum Science and Engineering,* vol. 14, no. 3-4, pp. 221-230, 1996.

[2] T. H. Omland, "Particle settling in non-newtonian drilling fluids," *PhD Thesis*, University of Stavanger, Norway, 2009.

[3] S. N. Shah, N. H. Shanker, and C. C. Ogugbue, "Future challenges of drilling fluids and their rheological measurements," in *AADE fluids conference and exhibition, Houston, Texas*, 2010: sn.

[4] A. Saasen and H. Hodne, "Influence of Vibrations on the Rheological Properties of Drilling Fluids and Its Consequence an Solids Control," *Journal of Applied Rheology,* vol. 26, no. 2, pp. 28-33, 2016.

[5] A. Fard, T. H. Omland, and A. Saasen, "Shale shaker's effect on drilling fluids rheological properties," *Annual transactions of Nordic Rheology Society,* vol. 15, p. 227, 2007.

[6] P. Banfill, X. Yongmo, and P. Domone, "Relationship between the rheology of unvibrated fresh concrete and its flow under vibration in a vertical pipe apparatus," *Magazine of Concrete Research,* vol. 51, no. 3, pp. 181-190, 1999.

[7] P. Frantzis and R. Baggott, "Effect of vibration on the rheological characteristics of magnesia phosphate and ordinary Portland cement slurries," *Cement concrete research,* vol. 26, no. 3, pp. 387-395, 1996.

[8] A. Saasen and G. Løklingholm, "The effect of drilling fluid rheological properties on hole cleaning," in *IADC/SPE Drilling Conference*, 2002: Society of Petroleum Engineers.

[9] S. B. Hamed and M. Belhadri, "Rheological properties of biopolymers drilling fluids," *Journal of Petroleum Science and Engineering,* vol. 67, no. 3-4, pp. 84-90, 2009.

[10] M. Edali, M. N. Esmail, and G. H. Vatistas, "Rheological properties of high concentrations of carboxymethyl cellulose solutions," *Journal of Applied Polymer Science,* vol. 79, no. 10, pp. 1787-1801, 2001.

[11] J. Herraez-Dominguez, F. G. G. De León, O. Diez-Sales, and M. Herráez-Domínguez, "Rheological characterization of two viscosity grades of methylcellulose: an approach to the modeling of the thixotropic behaviour," *Journal of Colloid and Polymer Science,* vol. 284, no. 1, pp. 86-91, 2005.

[12] A. Benchabane and K. Bekkour, "Rheological properties of carboxymethyl cellulose (CMC) solutions," *Journal of Colloid and Polymer Science,* vol. 286, no. 10, p. 1173, 2008.

[13] S. K. Arnipally and E. Kuru, "Effect of Elastic Properties of the Fluids on the Particle Settling Velocity," in *ASME 2017 36th International Conference on Ocean, Offshore and Arctic Engineering*, 2017: American Society of Mechanical Engineers Digital Collection.

[14] S. K. Arnipally and E. Kuru, "Settling Velocity of Particles in Viscoelastic Fluids: A Comparison of the Shear Viscosity vs Elasticity Effect," presented at the SPE Annual Technical Conference and Exhibition, San Antonio, Texas, USA, 2017/10/9, 2017.

[15] R. W. Time and A. Rabenjafimanantsoa, "On the relevance of laboratory scale rheometric measurements for calculation of complex large scale flows in well drilling and pipe flows," *Annual Transactions of Nordic Rheology Society,* vol. 22, 2013.

[16] B. Bui *et al.*, "Viscoelastic properties of oil-based drilling fluids," *Annual Transactions of Nordic Rheology Society,* vol. 20, pp. 33-47, 2012.

[17] A. Kumar, T. Kumaresan, A. B. Pandit, and J. B. Joshi, "Characterization of flow phenomena induced by ultrasonic horn," *Chemical Engineering Science,* vol. 61, no. 22, pp. 7410-7420, 2006.

[18] S. J. Lighthill, "Acoustic streaming," *Journal of Sound and Vibration,* vol. 61, no. 3, pp. 391-418, 1978/12/08/ 1978, doi: https://doi.org/10.1016/0022-460X(78)90388-7.

[19] W. L. Nyborg, "Acoustic streaming due to attenuated plane waves," *The journal of the acoustical society of America,* vol. 25, no. 1, pp. 68-75, 1953.

[20] A. S. Dukhin and P. J. Goetz, "Acoustic theory for particulates," in *Studies in Interface Science*, vol. 24: Elsevier, 2010, pp. 127-185.

[21] S. Juradin, "Determination of rheological properties of fresh concrete and similar materials in a vibration rheometer," *Journal of Materials Research,* vol. 15, no. 1, pp. 103-113, 2012.

[22] T. W. Chow, L. V. McIntire, K. R. Kunze, and C. E. Cooke, "The rheological properties of cement slurries: Effects of vibration, hydration conditions, and additives," *Journal of SPE production engineering,* vol. 3, no. 04, pp. 543-550, 1988.

[23] A. Saasen and H. Hodne, "The Influence of Drilling Fluid Rheological Properties on Primary Solids Control," in *ASME 2015 34th International Conference on Ocean, Offshore and Arctic Engineering*, 2015: American Society of Mechanical Engineers Digital Collection.

[24] R. B. Bird, R. C. Armstrong, and O. Hassager, *Dynamics of polymeric liquids. Vol. 1: Fluid mechanics*. John Wiley and Sons Inc., New York, 1987.

[25] H. Barnes, P. Townsend, and K. Walters, "On pulsatile flow of non-Newtonian liquids," *Rheologica Acta,* vol. 10, no. 4, pp. 517-527, 1971.

[26] O. Manero, B. Mena, and R. Valenzuela, "Further developments on non-Newtonian flow in oscillating pipes," *Rheologica Acta,* vol. 17, no. 6, pp. 693-697, 1978.

[27] B. Mena, O. Manero, and D. Binding, "Complex flow of viscoelastic fluids through oscillating pipes: Interesting effects and applications," *Journal of Non-Newtonian Fluid Mechanics,* vol. 5, pp. 427-448, 1979.

[28] W. Chan, S. Lee, and C. Liu, "Effects of frequency and amplitude of oscillation on low Reynolds number pulsating flow in a circular pipe," *Journal of Engineering Computations,* 2002.

[29] M. Eesa and M. Barigou, "CFD analysis of viscous non-Newtonian flow under the influence of a superimposed rotational vibration," *Computers and fluids,* vol. 37, no. 1, pp. 24-34, 2008.

[30] M. Torralba, J. Castrejón-Pita, A. Castrejón-Pita, G. Huelsz, J. Del Río, and J. Ortín, "Measurements of the bulk and interfacial velocity profiles in oscillating Newtonian and Maxwellian fluids," *Physical Review E,* vol. 72, no. 1, p. 016308, 2005.

[31] P. R. Hoskins, "Estimation of blood velocity, volumetric flow and wall shear rate using Doppler ultrasound," *Ultrasound,* vol. 19, no. 3, pp. 120-129, 2011.

[32] L. Fishler and R. Brodkey, "Transition, turbulence and oscillating flow in a pipe a visual study," *Experiments in fluids,* vol. 11, no. 6, pp. 388-398, 1991.

[33] S. P. Singh, A. K. Srivastava, and J. F. Steffe, "Vibration induced settling of a sphere in a Herschel-Bulkley fluid," *Journal of food engineering,* vol. 13, no. 3, pp. 181-197, 1991.

[34] M. Y. Gundogdu and M. O. Carpinlioglu, "Present State of Art on Pulsatile Flow Theory : Part 1:Laminar and Transitional Flow Regimes," *JSME International Journal Series B,* vol. 42, no. 3, pp. 384-397, 1999, doi: 10.1299/jsmeb.42.384.

[35] I. Ramadan, A. Abd El-Rahman, A. Ibrahim Essawey, and E. Abdel-Rahman, "Transition to turbulence in oscillating flows," in *Proceedings of the 24th International Congress on Sound and Vibration*, 2017, pp. 23-27.

[36] G. Yamanaka, H. Kikura, Y. Takeda, and M. Aritomi, "Flow measurement on an oscillating pipe flow near the entrance using the UVP method," *Experiments in fluids,* vol. 32, no. 2, pp. 212-220, 2002.

[37] J. Harris, G. Peev, and W. Wilkinson, "Velocity profiles in laminar oscillatory flow in tubes," *Journal of Physics E: Scientific Instruments,* vol. 2, no. 11, p. 913, 1969.

[38] M. Ohmi, M. Iguchi, K. Kakehashi, and T. Masuda, "Transition to turbulence and velocity distribution in an oscillating pipe flow," *Bulletin of The Japan Society of Mechanical Engineers,* vol. 25, no. 201, pp. 365-371, 1982.

[39] M. Teufel, D. Trimis, A. Lohmüller, Y. Takeda, and F. Durst, "Determination of velocity profiles in oscillating pipe-flows by using laser Doppler velocimetry and ultrasonic measuring devices," *Journal of Flow measurement & Instrumentation,* vol. 3, no. 2, pp. 95-101, 1992.

[40] M. Amaratunga, H. A. Rabenjafimanantsoa, and R. W. Time, "Comparison of oscillatory flow conditions in Newtonian and non-Newtonian fluids using PIV and high-speed image analysis," *Journal of Flow measurement & Instrumentation,* vol. 70, p. 101628, 2019.

[41] Y. Su, J. H. Davidson, and F. Kulacki, "Fluid flow and heat transfer structures of oscillating pipe flows," *International*

Journal of Mechanical, Aerospace, Industrial, Mechatronic & Manufacturing Engineering, vol. 5, no. 9, pp. 1813-1822, 2011.

[42] M. Hino, M. Sawamoto, and S. Takasu, "Experiments on transition to turbulence in an oscillatory pipe flow," *Journal of Fluid Mechanics,* vol. 75, no. 2, pp. 193-207, 1976.

[43] M. Y. Gundogdu and M. O. Carpinlioglu, "Present state of art on pulsatile flow theory: Part 2: Turbulent flow regime," *JSME International Journal Series B Fluids; Thermal Engineering,* vol. 42, no. 3, pp. 398-410, 1999.

[44] M. Iguchi, M. Ohmi, and K. Maegawa, "Analysis of free oscillating flow in a U-shaped tube," *Bulletin of the Japan Society of Mechanical Engineers,* vol. 25, no. 207, pp. 1398-1405, 1982.

[45] D. M. Eckmann and J. B. Grotberg, "Experiments on transition to turbulence in oscillatory pipe flow," *Journal of Fluid Mechanics,* vol. 222, pp. 329-350, 1991.

[46] K. H. Ahn and M. B. Ibrahim, "Laminar/turbulent oscillating flow in circular pipes," *International Journal of Heat & Fluid Flow,* vol. 13, no. 4, pp. 340-346, 1992.

[47] R. Trip, D. Kuik, J. Westerweel, and C. Poelma, "An experimental study of transitional pulsatile pipe flow," *Physics of fluids,* vol. 24, no. 1, p. 014103, 2012.

[48] S. Sergeev, "Fluid oscillations in pipes at moderate Reynolds numbers," *Journal of Fluid dynamics,* vol. 1, no. 1, pp. 121-122, 1966.

[49] D. Drake, "On the flow in a channel due to a periodic pressure gradient," *The Quarterly Journal of Mechanics & Applied Mathematics,* vol. 18, no. 1, pp. 1-10, 1965.

[50] S. Tsangaris and N. Vlachakis, "Exact solution of the Navier-Stokes equations for the fully developed, pulsating flow in a rectangular duct with a constant cross-sectional velocity," *Journal of Fluids Engineering,* vol. 125, no. 2, pp. 382-385, 2003.

[51] R. Blythman, T. Persoons, N. Jeffers, and D. Murray, "Effect of oscillation frequency on wall shear stress and pressure drop in a rectangular channel for heat transfer applications," in *Journal of Physics: Conference Series*, 2016, vol. 745, no. 3: IOP Publishing, p. 032044.

[52] G. B. Thurston, "Theory of oscillation of a viscoelastic medium between parallel planes," *Journal of Applied Physics,* vol. 30, no. 12, pp. 1855-1860, 1959.

[53] G. B. Thurston, "Theory of oscillation of a viscoelastic fluid in a circular tube," *The Journal of the Acoustical Society of America,* vol. 32, no. 2, pp. 210-213, 1960.

[54] Y. A. Andrienko, D. Siginer, and Y. G. Yanovsky, "Resonance behavior of viscoelastic fluids in Poiseuille flow and application to flow enhancement," *International Journal of non-linear Mechanics,* vol. 35, no. 1, pp. 95-102, 2000.

[55] M. F. Letelier, D. A. Siginer, D. L. Almendra, and J. S. Stockle, "Resonance in laminar pipe flow of non-linear viscoelastic fluids," *International Journal of Non-Linear Mechanics,* vol. 115, pp. 53-60, 2019.

[56] L. Casanellas and J. Ortín, "Vortex ring formation in oscillatory pipe flow of wormlike micellar solutions," *Journal of Rheology,* vol. 58, no. 1, pp. 149-181, 2014.

[57] J. Del Rio, M. L. De Haro, and S. Whitaker, "Enhancement in the dynamic response of a viscoelastic fluid flowing in a tube," *Physical Review E,* vol. 58, no. 5, p. 6323, 1998.

[58] J. Castrejón-Pita, J. Del Río, A. Castrejón-Pita, and G. Huelsz, "Experimental observation of dramatic differences in the dynamic response of Newtonian and Maxwellian fluids," *Physical Review E,* vol. 68, no. 4, p. 046301, 2003.

[59] D. Tsiklauri and I. Beresnev, "Enhancement in the dynamic response of a viscoelastic fluid flowing through a longitudinally vibrating tube," *Physical Review E,* vol. 63, no. 4, p. 046304, 2001.

[60] H. A. Barnes, J. F. Hutton, and K. Walters, *An introduction to rheology*. Elsevier, 1989.

[61] D. Quemada, "Rheological modelling of complex fluids. I. The concept of effective volume fraction revisited," *The European Physical Journal-Applied Physics,* vol. 1, no. 1, pp. 119-127, 1998.

[62] M. Clamen and P. Minton, "An experimental investigation of flow in an oscillating pipe," *Journal of Fluid Mechanics,* vol. 81, no. 3, pp. 421-431, 1977.

[63] M. Mazzuoli, G. Seminara, and G. Vittori, "Settling of heavy particles in a turbulent Stokes layer: Numerical simulations," *Journal of Advances in water resources,* vol. 72, pp. 2-14, 2014.

[64] M. Mazzuoli, A. G. Kidanemariam, and M. Uhlmann, "Direct numerical simulations of ripples in an oscillatory flow," *Journal of Fluid Mechanics,* vol. 863, pp. 572-600, 2019.

[65] A. Still, "Multiphase phenomena in a vibrating column reactor," Oklahoma State University, 2012.

[66] E. Khabakhpasheva, V. Popov, A. Kekalov, and E. Mikhailova, "Pulsating flow of viscoelastic fluids in tubes," *Journal of non-Newtonian Fluid Mechanics,* vol. 33, no. 3, pp. 289-304, 1989.

[67] T. Zhao and P. Cheng, "The friction coefficient of a fully developed laminar reciprocating flow in a circular pipe," *International Journal of Heat & Fluid Flow,* vol. 17, no. 2, pp. 167-172, 1996.

[68] J. Gerrard and M. Hughes, "The flow due to an oscillating piston in a cylindrical tube: a comparison between experiment and a simple entrance flow theory," *Journal of Fluid Mechanics,* vol. 50, no. 1, pp. 97-106, 1971.

[69] J. R. Womersley, *An elastic tube theory of pulse transmission and oscillatory flow in mammalian arteries*. Wright-Patterson Air Force Base, Ohio: Wright Air Development Center (in English), 1957.

[70] M. Ohmi and M. Iguchi, "Critical Reynolds number in an oscillating pipe flow," *Bulletin of the Japan Society of Mechanical Engineers,* vol. 25, no. 200, pp. 165-172, 1982.

[71] R. J. Poole, "The Deborah and Weissenberg numbers," *Rheology Bulletin, British Society of Rheology,* no. 53(2), pp. 32 -39, 2012.

[72] L. Casanellas and J. Ortı, "Laminar oscillatory flow of Maxwell and Oldroyd-B fluids: Theoretical analysis," *Journal of non-Newtonian Fluid Mechanics,* vol. 166, no. 23-24, pp. 1315-1326, 2011.

[73] R. P. Chhabra and J. F. Richardson, *Non-Newtonian flow in the process industries: fundamentals and engineering applications*. Butterworth-Heinemann, 1999.

[74] M. Amaratunga, R. Nybø, and R. W. Time, "PIV analysis of dynamic velocity profiles in non-Newtonian drilling fluids exposed to oscillatory motion," in *ASME 2018 37th International*

Conference on Ocean, Offshore and Arctic Engineering, 2018: American Society of Mechanical Engineers Digital Collection.

[75] R. Clift, J. R. Grace, and M. E. Weber, *Bubbles, drops, and particles*. Academic Press, 1978 - New York., 1978.

[76] A. Haider and O. Levenspiel, "Drag coefficient and terminal velocity of spherical and nonspherical particles," *Journal of Powder Technology,* vol. 58, no. 1, pp. 63-70, 1989.

[77] R. Chhabra, L. Agarwal, and N. K. Sinha, "Drag on non-spherical particles: an evaluation of available methods," *Powder Technology,* vol. 101, no. 3, pp. 288-295, 1999.

[78] R. Kehlenbeck and R. D. Felice, "Empirical relationships for the terminal settling velocity of spheres in cylindrical columns," *Journal of Chemical Engineering,* vol. 22, no. 4, pp. 303-308, 1999.

[79] P. P. Brown and D. F. Lawler, "Sphere drag and settling velocity revisited," *Journal of environmental engineering,* vol. 129, no. 3, pp. 222-231, 2003.

[80] N.-S. Cheng, "Comparison of formulas for drag coefficient and settling velocity of spherical particles," *Powder Technology,* vol. 189, no. 3, pp. 395-398, 2009.

[81] S. Zhiyao, W. Tingting, X. Fumin, and L. Ruijie, "A simple formula for predicting settling velocity of sediment particles," *Journal of Water Science Engineering,* vol. 1, no. 1, pp. 37-43, 2008.

[82] H. Sharma, "Creeping Motion of a Non-Newtonian Fluid Past a Sphere," *Indian Journal of Pure & Applied Mathematics,* vol. 10, no. 12, pp. 1565-1575, 1979.

[83] V. C. Kelessidis, "An explicit equation for the terminal velocity of solid spheres falling in pseudoplastic liquids," *Chemical engineering science,* vol. 59, no. 21, pp. 4437-4447, 2004.

[84] S. Malhotra and M. M. Sharma, "Settling of spherical particles in unbounded and confined surfactant-based shear thinning viscoelastic fluids: An experimental study," *Chemical Engineering Science,* vol. 84, pp. 646-655, 2012.

[85] S. K. Arnipally and E. Kuru, "Settling velocity of particles in viscoelastic fluids: a comparison of the shear-viscosity and elasticity effects," *SPE Journal,* vol. 23, no. 05, pp. 1,689-1,705, 2018.

[86] S. N. Shah, "Proppant settling correlations for non-Newtonian fluids under static and dynamic conditions," *Society of Petroleum Engineers Journal,* vol. 22, no. 02, pp. 164-170, 1982.

[87] S. N. Shah, "Proppant-settling correlations for non-Newtonian Fluids," *SPE Production Engineering,* vol. 1, no. 06, pp. 446-448, 1986.

[88] A. R. Acharya, "Particle transport in viscous and viscoelastic fracturing fluids," *SPE Production Engineering,* vol. 1, no. 02, pp. 104-110, 1986.

[89] L. Jin and G. S. Penny, "Dimensionless methods for the study of particle settling in non-Newtonian fluids," *Journal of Petroleum Technology,* vol. 47, no. 03, pp. 223-228, 1995.

[90] L. Childs, A. Hogg, and D. Pritchard, "Dynamic settling of particles in shear flows of shear-thinning fluids," *Journal of Non-Newtonian Fluid Mechanics,* vol. 238, pp. 158-169, 2016.

[91] L. J. Harrington, R. R. Hannah, and D. Williams, "Dynamic experiments on proppant settling in crosslinked fracturing fluids," in *SPE Annual Technical Conference and Exhibition*, 1979: Society of Petroleum Engineers.

[92] B. Van den Brule and G. Gheissary, "Effects of fluid elasticity on the static and dynamic settling of a spherical particle," *Journal of non-newtonian fluid mechanics,* vol. 49, no. 1, pp. 123-132, 1993.

[93] L. Becker, G. McKinley, H. K. Rasmussen, and O. Hassager, "The unsteady motion of a sphere in a viscoelastic fluid," *Journal of Rheology,* vol. 38, no. 2, pp. 377-403, 1994.

[94] P. F. Fischer, G. K. Leaf, and J. M. Restrepo, "Forces on particles in oscillatory boundary layers," *Journal of Fluid Mechanics,* vol. 468, pp. 327-347, 2002.

[95] P. Cherukat and J. B. McLaughlin, "The inertial lift on a rigid sphere in a linear shear flow field near a flat wall," *Journal of Fluid Mechanics,* vol. 263, pp. 1-18, 1994.

[96] H. Lee and S. Balachandar, "Drag and lift forces on a spherical particle moving on a wall in a shear flow at finite Re," *Journal of Fluid Mechanics,* vol. 657, pp. 89-125, 2010.

[97] R. Herringe and L. Flint, "Particle motion in vertically oscillated liquids," in *5th Australian Conference on Hydraulics and Fluid Mechanics*, 1974, pp. 103-110.

[98] J. Bailey, "Particle motion in rapidly oscillating flows," *Chemical Engineering Science,* vol. 29, no. 3, pp. 767-773, 1974.

[99] G. Houghton, "The behaviour of particles in a sinusoidal velocity field," *Proceedings of the Royal Society of London. Series A. Mathematical & Physical Sciences,* vol. 272, no. 1348, pp. 33-43, 1963.

[100] G. Houghton, "Particle trajectories and terminal velocities in vertically oscillating fluids," *The Canadian Journal of Chemical Engineering,* vol. 44, no. 2, pp. 90-95, 1966.

[101] G. Houghton, "Particle retardation in vertically oscillating fluids," *The Canadian Journal of Chemical Engineering,* vol. 46, no. 2, pp. 79-81, 1968.

[102] P. A. Hwang, "Fall velocity of particles in oscillating flow," *Journal of Hydraulic Engineering,* vol. 111, no. 3, pp. 485-502, 1985.

[103] L. Boyadzhiev, "On the movement of a spherical particle in vertically oscillating liquid," *Journal of Fluid Mechanics,* vol. 57, no. 3, pp. 545-548, 1973.

[104] P. Schöneborn, "The interaction between a single particle and an oscillating fluid," *International Journal of Multiphase Flow,* vol. 2, no. 3, pp. 307-317, 1975.

[105] S. Hassan, T. P. Lyubimova, D. V. Lyubimov, and M. Kawaji, "Effects of vibrations on particle motion near a wall: Existence of attraction force," *International Journal of Multiphase Flow,* vol. 32, no. 9, pp. 1037-1054, 2006.

[106] V. Sorokin, I. Blekhman, and V. Vasilkov, "Motion of a gas bubble in fluid under vibration," *Journal of Nonlinear Dynamics,* vol. 67, no. 1, pp. 147-158, 2012.

[107] M. Saadatmand, "A Study on Vibration-Induced Particle Motion under Microgravity," University of Toronto, 2012.

[108] M. K. Hill, "Behavior of spherical particles at low Reynolds numbers in a fluctuating translational flow," California Institute of Technology, 1973.

[109] G. Gheissary and B. Van den Brule, "Unexpected phenomena observed in particle settling in non-Newtonian media," *Journal of Non-Newtonian Fluid Mechanics,* vol. 67, pp. 1-18, 1996.

[110] A. Talmon and M. Huisman, "Fall velocity of particles in shear flow of drilling fluids," *Journal of Tunnelling & underground space technology,* vol. 20, no. 2, pp. 193-201, 2005.

[111] S. N. Shah, Y. El Fadili, and R. Chhabra, "New model for single spherical particle settling velocity in power law (visco-inelastic) fluids," *International journal of multiphase flow,* vol. 33, no. 1, pp. 51-66, 2007.

[112] T. G. Mezger, *The rheology handbook: for users of rotational and oscillatory rheometers*. Vincentz Network GmbH & Co KG, 2006.

[113] W. Thielicke and E. Stamhuis, "PIVlab–towards user-friendly, affordable and accurate digital particle image velocimetry in MATLAB," *Journal of Open Research Software,* vol. 2, no. 1, 2014.

[114] K. D. Jensen and Engineering, "Flow measurements," *Journal of the Brazilian Society of Mechanical Sciences,* vol. 26, no. 4, pp. 400-419, 2004.

[115] R. J. Adrian, "Particle-imaging techniques for experimental fluid mechanics," *Annual Review of Fluid Mechanics,* vol. 23, no. 1, pp. 261-304, 1991.

[116] J. Westerweel and technology, "Fundamentals of digital particle image velocimetry," *Journal of Measurement science,* vol. 8, no. 12, p. 1379, 1997.

[117] H. Huang, D. Dabiri, and M. Gharib, "On errors of digital particle image velocimetry," *Measurement Science Technology,* vol. 8, no. 12, p. 1427, 1997.

[118] M. Amaratunga, H. A. Rabenjafimanantsoa, and R. W. Time, "Estimation of shear rate change in vertically oscillating non-Newtonian fluids: Predictions on particle settling," *Journal of Non-Newtonian Fluid Mechanics,* vol. 277, p. 104236, 2020.

[119] J. D. Ferry, "Viscoelastic properties of polymer solutions," *Journal of research of the National Bureau of Standards,* vol. 41, no. 1, pp. 53-62, 1948.

[120] M. Torralba, A. Castrejón-Pita, G. Hernández, G. Huelsz, J. Del Rio, and J. Ortín, "Instabilities in the oscillatory flow of a complex fluid," *Physical Review E,* vol. 75, no. 5, p. 056307, 2007.

[121] F. A. Morrison, *An introduction to fluid mechanics*. Cambridge University Press, 2013.

[122] L. Zeng, F. Najjar, S. Balachandar, and P. Fischer, "Forces on a finite-sized particle located close to a wall in a linear shear flow," *Physics of fluids,* vol. 21, no. 3, p. 033302, 2009.

[123] L. Zeng, S. Balachandar, and P. Fischer, "Wall-induced forces on a rigid sphere at finite Reynolds number," *Journal of Fluid Mechanics,* vol. 536, pp. 1-25, 2005.

[124] F. García-Ochoa and J. Casas, "Apparent yield stress in xanthan gum solutions at low concentrations," *The Chemical & Biochemical Engineering Journal,* vol. 53, no. 3, pp. B41-B46, 1994.

- End of Part I –

Part II

Scientific Articles

Paper I

Predicting rheological properties of water-based polymer mixtures from their component properties – Polyanionic Cellulose and Xanthan gum

Maduranga Amaratunga, Milad Khatibi, Nikita Potokin and Rune W. Time

University of Stavanger, Norway.

This paper was initially presented in the *27th Nordic Rheology Conference (NRC 2018) held in Trondheim, Norway, in June 2018*.

The paper was then selected to be published in the Annual Transactions of the Nordic Rheology Society, vol. 26, pp 31 – 39.

This paper is not in Brage for copyright reasons

Paper II

Visualization of acoustic streaming using PIV in Newtonian and non-Newtonian liquids

Maduranga Amaratunga and Rune W. Time

University of Stavanger, Norway.

This paper was initially presented in the *18th International Conference on Computational Methods and Experimental Measurements (CMEM 2017) held in Alicante, Spain, in July 2017*.

The paper was then selected to be published in the International Journal of Computational Methods and Experimental Measurements, Volume 6, Issue 4, pp 814 – 826.

This paper is not in Brage for copyright reasons

Paper III

PIV analysis of dynamic velocity profiles in non-Newtonian drilling fluids exposed to oscillatory motion

Maduranga Amaratunga[a], Roar Nybø[b] and Rune W. Time[a]

[a]University of Stavanger, Norway.
[b]SINTEF Petroleum Research, Bergen, Norway

This paper was initially presented in the *ASME 2018 - 37th International Conference on Ocean, Offshore and Arctic Engineering (OMAE 2018) in Madrid, Spain, in June 2018*.

The paper was then published in the Proceedings of the ASME 2018 - 37th International Conference on Ocean, Offshore and Arctic Engineering. Volume 8 under the section of Polar and Arctic Sciences and Technology; Petroleum Technology.

This paper is not in Brage for copyright reasons

Paper IV

CFD Analysis of low frequency oscillations in Newtonian and non-Newtonian fluids in a vertical pipe

Maduranga Amaratunga, H. A.
Rabenjafimanantsoa and Rune W. Time

University of Stavanger, Norway.

This paper was initially presented in the *41st International Conference on Boundary Elements and other Mesh Reduction Methods (BEM/MRM 41) in New Forest, UK, in September 2018*.

The paper was then published in the WIT Transactions on Engineering Sciences, 125, pp 37-48 in 2019.

This paper is not in Brage for copyright reasons

Paper V

Comparison of oscillatory flow conditions in Newtonian and non-Newtonian fluids using PIV and high-speed image analysis

Maduranga Amaratunga, H. A.
Rabenjafimanantsoa and Rune W. Time

University of Stavanger, Norway.

The paper was published in the *Journal of Flow Measurement and Instrumentation*, 70: 101628 in 2019.

Flow Measurement and Instrumentation 70 (2019) 101628

Contents lists available at ScienceDirect

Flow Measurement and Instrumentation

journal homepage: www.elsevier.com/locate/flowmeasinst

Comparison of oscillatory flow conditions in Newtonian and non-Newtonian fluids using PIV and high-speed image analysis

Maduranga Amaratunga*, Herimonja A. Rabenjafimanantsoa, Rune W. Time

Department of Energy and Petroleum Engineering, University of Stavanger, Norway

ARTICLE INFO

Keywords:
Critical Reynolds number
Frequency
Oscillating flow
Particle image velocimetry
Unsteady flow
Velocity amplitude

ABSTRACT

Oscillatory flow in pipelines is common in many industrial applications, including oil well drilling. An experimental investigation of oscillatory flow inside a vertical U-shaped circular pipe is presented in this paper to mimic the practical scenario takes place within a vertical oil well. Flow visualization was deployed to compare the velocity distributions in Newtonian (deionized water) and non-Newtonian fluid (a mixture of three water-based polymeric liquids). The experiments were performed in a 1.2 m high, 50 mm diameter transparent test section, at room temperature (21 °C) and atmospheric pressure.

Particle image velocimetry (PIV) technique was used to obtain non-invasive instantaneous flow velocity profiles. Based on local velocities, the streamwise (axial) velocity component within the pipe across its diameter was determined and the cross-sectional average velocity together with the normalized axial velocity were also calculated. In addition, high-speed motion pictures were used to determine the displacement of the air-liquid interface at the top of the U-tube limb. This enabled comparison of the flow field with the overall volumetric oscillating flow. A piston was driven at harmonic motion via a gas buffer, to provide the driving force for the test fluids at four different low frequencies ranging from 0.1 to 0.75 Hz. Oscillatory Reynolds number (Re_S) based on Stokes layer thickness was used as the criteria for determining the specific flow regime. According to the literature, the critical value for the oscillating Reynolds number was considered to be 500, and with this as reference all the experimental cases were within the laminar regime. Eight different experimental cases were tested within the ranges of ($4 < Re_S < 116$) and Womersley number ($3 < Wo < 55$).

At higher frequencies, the viscous effects for the Newtonian fluid are confined to the Stokes layer and the central core of the velocity profile is plug-type. At the same time, higher frequencies resulted with increased velocity amplitudes. The viscous resistance of the non-Newtonian fluid and the presence of shear layer contribute to an uneven velocity profile across the pipe cross-section. Cross-sectional average velocity provides a more complete picture of the kinematic structure of oscillating flow and its dynamic distribution across the cross-section. Non-Newtonian fluid tends to achieve higher normalized axial velocities compared to that for Newtonian fluid, which is more or less equals to unity.

The study was partly motivated by challenges associated with operational procedures during drilling and maintenance of petroleum wells. Furthermore, this study is also part of a comprehensive study aimed at investigating the influence of low frequency oscillations on particle settling in non-Newtonian drilling fluids.

1. Introduction

The majority of pipe flow investigations available in scientific literature are related to steady flow. However, more attention should be paid to unsteady flows, since there are many industrial and biological applications in the fields of applied fluid mechanics. As an example, even local geometrical variations and gas kicks in real oil-well drilling operations might cause flow instabilities and fluctuations along the pipe trajectory. For intermittent regimes of two-phase flow, this is particularly important.

According to literature, there are two major types of unsteady flows: namely, pulsating (or pulsatile) flow and pure oscillating flow [1–3]. The pulsatile flow is an oscillating flow superimposed on a steady flow with a non-zero mean velocity, whereas the pure oscillating flow is an oscillating flow with zero mean velocity. This study focuses on the latter type of the oscillatory flows where there is pure oscillating flow without any mean velocity.

The kinematic structure of the flow is noticeably altered with the

* Corresponding author.
E-mail address: amaratunga.maduranga@uis.no (M. Amaratunga).

https://doi.org/10.1016/j.flowmeasinst.2019.101628
Received 25 June 2019; Received in revised form 20 August 2019; Accepted 16 September 2019
Available online 17 September 2019

occurrence of any oscillatory motion within a pipe. It can significantly deform the velocity profile within the pipe [4–6] or can influence the turbulent characteristics [1] by leading to a change of integral flow parameters such as hydraulic resistance and heat transfer [7]. Further, it can produce a boundary layer on the bottom of a channel by the progressive liquid waves and cause liquid hammer [8] too, which can be detrimental to the durability of the pipeline. Furthermore, if the fluid in the oscillatory environment which is at least close to turbulent, the process becomes even more complicated from a rheological point of view.

Some theoretical, numerical and experimental approaches to investigate this oscillatory motion within pipes could be seen in the literature. Many of them have studied the transition from the laminar region to the turbulent region [1–3,5,8–14] and some of them have studied different geometries such as rectangular ducts [15,16], whereas circular pipes are more common. Importantly, many of them have developed theoretical expressions for oscillatory flows that occur in horizontal pipelines [8,15] and validated them with experimental results.

Since many of the researchers have discussed the transition to turbulence in oscillatory pipe flow, it is worth to look into how the extents of laminar to turbulent transition are described.

1.1. Oscillating Reynolds number

If the sinusoidal oscillatory movement is imposed in the transversal y-direction parallel to the flow as shown in Fig. 1, the vertical displacement (y) of any particular liquid point along the centerline of the pipe can be written as;

$$y(t) = |a| \sin(\omega t) \tag{1}$$

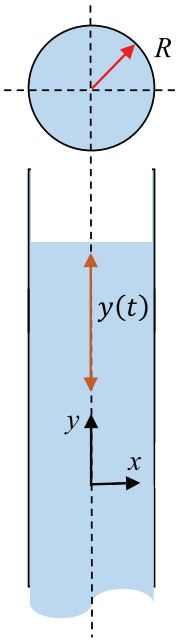

Fig. 1. Sinusoidal oscillatory motion imposed on the fluid in a vertical pipe.

where, a is the displacement amplitude, t is the time and $\omega = 2\pi f$, where f is the frequency of oscillation. The vertical linear velocity of the bulk liquid medium at the centerline of the pipe $V(t)$ due to the oscillation is therefore,

$$V(t) = \frac{dy}{dt} = |V| \cos(\omega t) \tag{2}$$

where, $|V| = |a|\omega$ is the amplitude of the centerline velocity in the axial direction.

According to the general approach for steady flow, the Reynolds number for a circular pipe flow (Re_D) is given for example by Clamen and Minton [17];

$$Re_D = \frac{|V|D}{\nu} \tag{3}$$

where, D is the pipe diameter and ν is the kinematic viscosity of the fluid concerning within the circular pipe. However, since the oscillatory flow is of main focus in this study, it is important to introduce the basic parameter of an oscillating flow, as proposed by Womersley [18], which is namely, the "Womersley number" (Wo) [3,11,14]. Different terminology has been used in literature to denote this same parameter, such as "non-dimensional frequency" [2,5,13,19] or the "frequency parameter" (α) [17], which can be written as;

$$Wo = \alpha = \frac{D/2}{\sqrt{\nu/\omega}} \tag{4}$$

This non-dimensional frequency (α) expressed in Eq. (4) is a measure of the ratio of the pipe radius to the distance through which vorticity diffuses away from the wall in one period of oscillation [19]. Further, Fishler and Brodkey [1] state the physical interpretation of α as the ratio of the time of a cycle ($1/\omega$) to the time necessary for the amplification of disturbances (R^2/ν). They claim that increasing α should lead to a stable state of the flow if Re_D is held constant.

However, based on the oscillating boundary layer (Stokes layer), the most important non-dimensional parameter for this study which is called the oscillating Reynolds number (Re_δ) can be derived by combining the expressions in Eqs. (3) and (4);

$$Re_\delta = \frac{|V|\delta}{\nu} \tag{5}$$

where, δ is called the Stokes boundary layer or the viscous penetration depth and can be written as [1,3];

$$\delta = \sqrt{\frac{2\nu}{\omega}} \tag{6}$$

Thus, Gundogdu and Carpinliogu [2] and Hino et al. [8] state another parameter called Stokes parameter (λ) as the ratio of radius to the viscous penetration depth, δ. Notation-wise, λ can be written as;

$$\lambda = \frac{D}{2}\sqrt{\frac{\omega}{2\nu}} \tag{7}$$

where, the relation between Re_D and Re_δ can be written as;

$$Re_D = 2\lambda\, Re_\delta \tag{8}$$

In addition to that since $|V| = |a|\omega$, Re_D in Eq. (3) can be re-written including the oscillatory behavior [9] as;

$$Re_D = \frac{(|a|\omega)D}{\nu} \tag{9}$$

which is by definition higher in value than Re_δ expressed in Eq. (5) (since $D \gg \delta$). Some other researchers have presented the oscillating Reynolds number with some slight changes to the expression presented in Eq. (5). For an instance, Khabakhpasheva et al. [20] have introduced the pulsating/oscillating Reynolds number (Re_f) as the ratio of time scale for the diffusion of momentum to the time scale of oscillation. Notation-wise, Re_f can be written as;

$$Re_f = \frac{R^2/\nu}{1/f} = \frac{R^2 f}{\nu} \tag{10}$$

Zhao and Cheng [21] state that the pulsating Reynolds number (Re_ω) can be written as;

$$Re_\omega = \frac{\omega D^2}{\nu} \tag{11}$$

This version is slightly higher than Eq. (10), and both Eqs. (10) and (11) result in a very large value compared to that of Re_δ.

The common pipe flow Reynolds number (Re_D) can be used to specify the extent of the laminar regime. $Re_D = 2100$ is considered as the critical Reynolds number for fully developed unidirectional steady pipe flow [12], where the transition from laminar to turbulent starts. However, different values for the critical oscillating Reynolds number (Re_δ) are reported in the literature by different authors. For an instance, Merkli and Thomann [22] have found that the value of the critical oscillating Reynolds number for frequencies higher than 20 Hz is 280, whereas the value was found to be around 500 at "sub-acoustic" frequencies. According to the study performed by Eckmann and Grotberg [11] to investigate the effects of intrusivity of hot-wire probe on oscillating flow, the critical Reynolds number has been reported as 300 and 500 with and without the probe respectively. Fishler and Brodkey [1] who describe different flow structures and events that are responsible for the turbulence generation in the oscillating flow, have defined a range for the value of critical Reynolds number as $650 < Re_\delta < 1000$. The experimental investigations on the transition to turbulence in oscillating flow performed by Ramadan et al. [3] reveal that the critical Reynolds number (Re_δ) is 500. Sergeev [9] used flow visualization and strain gauge measurements to obtain a value of 495. Based on their experiments using hot-wire anemometry on transition to turbulence in a purely oscillatory pipe flow, Hino et al. [8] reported a value of $Re_\delta = 565$ for the Stokes layer on a smooth wall, a significantly lower value of $Re_\delta = 160$ for the modified Stokes layer or wavy boundary layer and a value of $Re_\delta = 500$ for oscillatory pipe flow. Ohmi et al. [5] and Ohmi and Iguchi [23] have presented the value for the critical Reynolds number as a function of non-dimensional frequency which equals to 800α. The summary of experimental and theoretical results on the critical Reynolds number for oscillatory flow mentioned in Hino et al. [8] is very useful with this regard.

Taking into consideration all these different literature values, we have concluded to use $Re_\delta = 500$ as the critical Reynolds number for this study of oscillatory flow in a vertical pipe. The evaluation on Reynolds number for the different cases of this study is mentioned under the section of results validation at the latter part of this paper.

1.2. Particle image velocimetry (PIV) as a measurement technique

The complex kinematic structure of oscillating flows in pipes is associated with large amounts of flow detail variation in both time and space. In that sense, particle image velocimetry (PIV) is a great non-intrusive optical measuring technique used to solve such complex problems, which allows obtaining the spatial distributions of velocity, vorticity, shear stress etc. instantaneously in a single measurement [24]. The principles of PIV have been covered in many research papers [24–26].

Even though PIV has been employed in the measurement of single-phase flows in many research studies since the 1970s, there are not many reported for oscillatory flows. For an instance, the early researchers who investigated the oscillatory of pulsatile flow have used the hot wire anemometry [5,22,23] for the velocity measurements and it is one of the intrusive techniques, which is a drawback in some cases. According to the investigations by Merkli and Thomann [22], the disturbances of the flow by the hot-wire probe becomes larger for higher frequencies as high as 85 Hz and becomes less significant for lower frequencies. The non-intrusivity of the PIV technique has made it more popular among recent researchers who have studied the velocity distributions or the transition to turbulence in oscillatory flows. Trip et al. [14] have utilized the PIV technique extensively to investigate how the critical Reynolds number is affected by different pulsatile conditions in a horizontal pipe flow and on the transition to turbulence. Based on the experimental study performed by Amaratunga et al. [27] on the horizontal oscillatory motion of a fluid medium in a vertical rectangular column, the influence of oscillatory motion on the dynamic velocity profiles in non-Newtonian drilling fluids is discussed together with the influence on particle settling.

1.3. Aim and scope of the study

As shown from the aforementioned brief literature survey, several studies have investigated the oscillatory motion in horizontal pipes. However, the dynamics of oscillating flow in vertical pipes with free gas-liquid surface at the top is not well understood and sparse. Non-steady and oscillating flows are very common industrially and also scientifically loaded with challenges; especially in the low frequency range and even more so for non-Newtonian flows. Therefore, the aim of this study is to investigate the dynamic velocity profiles of both Newtonian and non-Newtonian fluids oscillated vertically with a zero mean velocity within a rigid, straight cylindrical geometry. Further, it is aimed to study the fluid dynamics of unsteady flows in a local scale to mimic the dynamics take place within a vertical oil well.

The time-resolved PIV system is utilized with this study to obtain a full-field non-intrusive analysis of the fluid system. The rigid straight cylindrical geometry is a vertical U-shaped pipe to represent a practical drilling well in laboratory scale. Based on the performed measurements, the authors have constructed and analyzed the fields of average flow velocity and the displacement of air-liquid interface during the period of imposed oscillations.

2. Methodology

The experiments were performed in the multi-phase flow laboratory at University of Stavanger (UiS), Norway.

2.1. Experimental set up

Fig. 2 shows a sketch of the U-shaped experimental set up. Eight different experimental cases were tested within the ranges of $(4 < Re_\delta < 116)$ and $(3 < Wo < 55)$. The test section on the left limb of the U-tube has a circular cross-section with an internal diameter of 50 mm and a total length of 1200 mm. The bottom and the right limbs of the U-tube were also circular in cross-section and 30 mm in internal diameter. The whole U-tube including the piston cylinder (with an internal diameter of 50 mm) was made up of transparent acrylic due to visualization purposes. It should be noted that the origin of the axes (x, y and z) is located at the middle-center of the pipe.

The harmonic oscillations were provided by the piston attached to the right limb of the U-tube, which is driven by a motor-gearbox unit. The rotary motion of the gearbox is converted to a reciprocating motion of the piston by mechanically projecting it into the arm of the piston. The revolution speed of the motor (model: 3DF56-2S7032 from ABM Greiffenberger, Germany) and the gearbox from David Brown (Radicon series), UK was controlled by a frequency controller (model: Micromaster 420 from Siemens) in such a way that, the required output frequency was set to the piston. A tachometer (model: AT-6L from Clas Ohlson, Norway) was used to confirm the frequency of the piston. Experiments with four different oscillation frequencies were tested as 0.1, 0.25, 0.5 and 0.75 Hz. The piston oscillation was set to a fixed displacement amplitude of 25 mm before starting the experiments. An acrylic transparent visualization box filled with deionized water with dimensions of $15 \times 15 \times 100\ cm^3$ was used around the test section to minimize the light refraction through the curved pipe walls. Since the

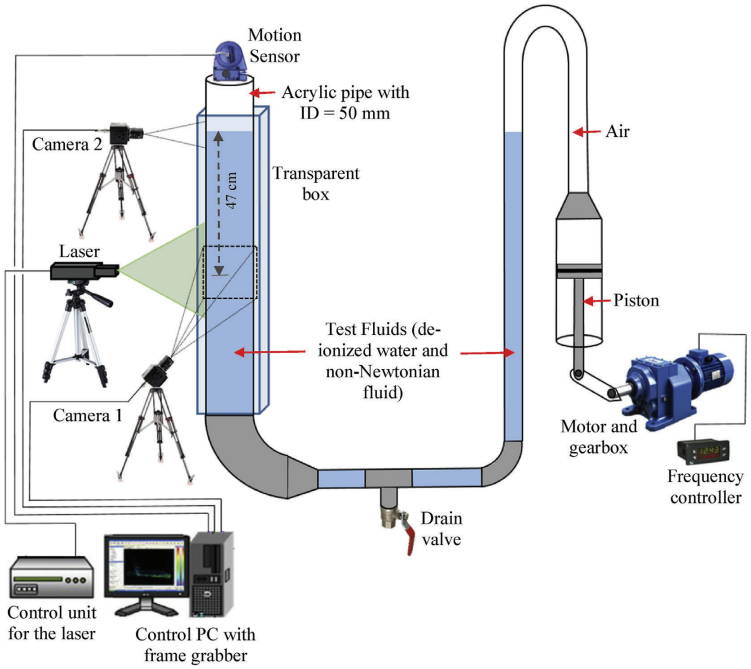

Fig. 2. Sketch of the experimental set up.

piston impacts on the elastic air column instead of directly to the liquid, it was necessary to install separate monitoring of the resulting liquid motion. Two systems were used; high-speed video imaging and a fast ultrasonic distance measurement unit. This is explained further in the coming section 2.3.3.

2.2. Materials and fluids

Deionized water was used as Newtonian fluid and also to make the shear-thinning non-Newtonian Fluid (NNF). The non-Newtonian Fluid is a mixture of three water based polymers namely Poly-anionic Cellulose (PAC) called PolyPAC, low viscous Carboxymethyl Cellulose (LV-CMC) and high viscous Carboxymethyl Cellulose (HV-CMC) provided by Sigma-Aldrich. The viscosity of the NNF was measured by Anton Paar MCR 302 rotational rheometer and the rheological properties are described in section 3.1 with Fig. 6. The density of the two fluids was measured to be 997.60 kg/m^3 for water and 1000.13 kg/m^3 for NNF using Anton Paar DMA-4500 density meter. All the experiments were carried out and the liquid properties were measured at the room temperature of 21 °C and atmospheric pressure. There were eight different experimental cases tested as two fluids and four different frequencies each, as explained before. Both water and non-Newtonian fluid were assumed to be incompressible.

2.3. Measurement techniques

2.3.1. The PIV system

The measurement area by the PIV system was centered at 470 mm below the equilibrium air-liquid interface (see Fig. 2), so that the end-effects from the free surface and the bend of the U-tube was minimized. Two Basler cameras of the same type (Model: acA800-510 µm USB 3.0 camera with the ON Semiconductor) were used for the acquisition of images. Their maximum frame rate is 500 fps at full resolution of 800 × 600 pixel^2. High-speed images for the PIV analysis were acquired at 200 fps by camera 1 that was equipped with a Nikon AF Nikkor 50 mm – f/1.4D lens. The images were cropped to a reduced section of 560 × 460 pixel^2 to fit the view of interest. The measurement area of the PIV system was illuminated with a Photop LDC-2500S continuous wave laser (class 3B) at wavelength 532 nm (green light spectrum) and variable output up to 200 mW. The thickness of the laser beam was set to approximately 1 mm using a lens and the collimator system. The laser sheet was aligned such that it illuminates the vertical plane through the center of the pipe (see Fig. 2). In order to illuminate the fluid motion, Polyamide seeding particles were used (Model: PSP50, Dantec Dynamics), with mean particle diameter = 50 µm and specific density = 1.03 as the tracer particles. The Stokes number (Stk) for the seeding particles were approximately $5.5 \times 10^{-4} \ll 0.1$ and the settling speed of the seeding particles are very small, typically less than 10^{-7} m/s.

2.3.2. High-speed imaging

The motion of the air-liquid interface was captured by camera 2 (Basler lens of model: C125-0818-5 M F1.8 f/8 mm) at a rate of 100 fps. The top part of the test section close to the air-liquid interface was sufficiently illuminated using a LED lamp without disturbing the PIV system. The two cameras were synchronized using a LabView program and triggered by a separate control switch. The results were acquired after allowing the system to oscillate at least for 1 min to achieve a

stable periodic motion up and down.

2.3.3. Level measurements by the motion sensor

The motion sensor of model PS-2103A from PASCO scientific instruments was mounted on top of the test section (see Fig. 2) in such a way that, the sensor is about 28 mm higher than the equilibrium air-liquid interface. A set of zero flow measurements were always recorded initially for calibration and reference. The motion sensor uses an ultrasonic electrostatic transducer (directed along the axis of the pipe) as both an emitter and receiver. For each measured distance (liquid height), the transducer transmits a burst of 16 ultrasonic pulses with a frequency of about 49 kHz, which are reflected off the air-liquid interface and returned to the sensor. Time-of-flight between the trigger-rising edge and the echo-rising edge is measured, and the distance to the interface calculated based on the present speed of sound.

The motion sensor was connected to the PC through the PASCO control unit (PS-850) and provided a good indication to get an initial observation on stability (well-developed) of the oscillatory flow before starting image acquisition. The measurements from the motion sensor confirmed the oscillation frequency provided by the piston to the fluid system.

2.4. Data treatment and analysis

In order to obtain the full-field velocity distribution and the profiles of the air-liquid interface motions, a series of image analysis steps were further undertaken.

2.4.1. Analysis of PIV images

The PIV analysis was performed using PIVlab – version 2.01 [28], which is a digital particle image velocimetry (DPIV) tool developed in MATLAB. As shown in Fig. 3, the region of interest (ROI) was limited to the pipe cross section rather than the entire image captured. The size of the smallest interrogation area for the present analysis was selected as 16 × 8 pixels based on the guidelines provided by Jensen [24].

As explained by Adrian [25] and Westerweel [26], the most probable displacement of the tracer particles which is homogeneously seeded in a small interrogation area can be inferred from the cross-correlation of two successive captures of the flow field. It is a statistical pattern matching technique that tries to find the particle pattern from the interrogation area A (at $t = t_0$) back in the interrogation area B (at $t = t_0 + nt$). In PIVlab, it is accomplished with the discrete cross-correlation (DCC) function [29] and the location of the intensity peak in the resulting correlation matrix gives the most probable displacement of the particles from A to B [28]. All the images were pre-processed using contrast limited adaptive histogram equalization (CLAHE) method and some of the background noise was removed using high pass filter. For the PIV settings a FFT window deformation was adopted. The axial velocity component of the vertically oscillating fluid medium along the centerline of the pipe and along the diameter of the pipe was distinguished separately from the velocity magnitudes obtained from PIV analysis for further processing.

2.4.2. Analysis of high-speed images

The time varying air-liquid interface was detected from the high-speed images using a MATLAB program which was specifically made for this analysis.

This was accomplished by selecting a vertical line as observation "path" – given as one fixed column of the matrix array in the high-speed images. A line located close to the centerline (axis) of the pipe was selected as shown in Fig. 4. The air-liquid interface was found by setting an intensity threshold value to track the first brightest pixel from top to bottom along the pixel column. This was chosen as the air-liquid interface at any time instant.

It is to be noted that the pixel threshold value was varied from one experimental case to another based on the light conditions. The interface position at this "observation path" was tracked for 10 s with the recorded image sequence, and thus a time series of the air-liquid interface was obtained (see Fig. 5). It is to be noted that the interface detection procedure shown in Fig. 5 has been illustrated only for 500 frames, which correspond to 5 s at 0.5 Hz for the non-Newtonian fluid. The detected air-liquid interface for both Newtonian and non-Newtonian fluids for the four frequencies are shown in Fig. 7.

3. Results and discussion

In this section, the rheological properties of the non-Newtonian fluid, the motion of the air-liquid interface obtained from high-speed

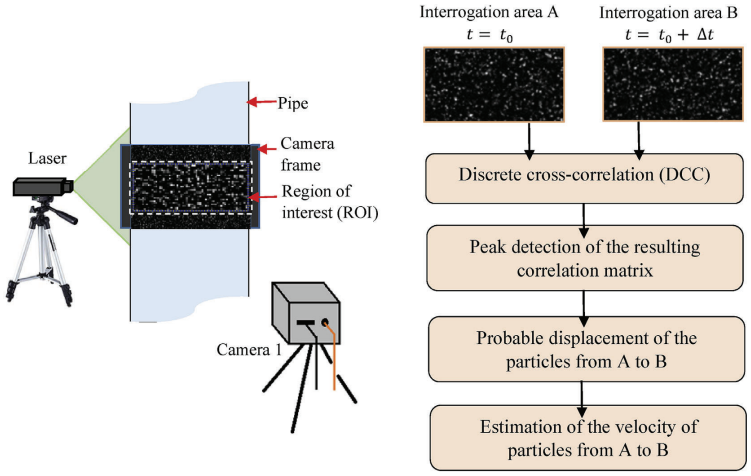

Fig. 3. Steps of PIV analysis using PIVlab.

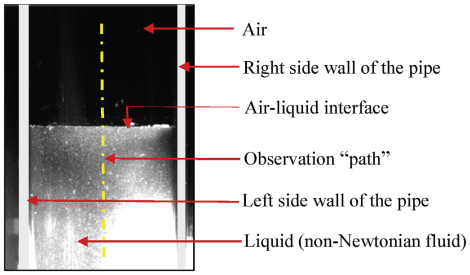

Fig. 4. Illustration of the observation path in a high-speed image at the interface.

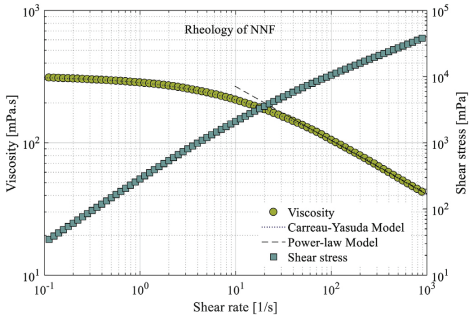

Fig. 6. Viscosity and shear stress of non-Newtonian fluid at varying shear rate.

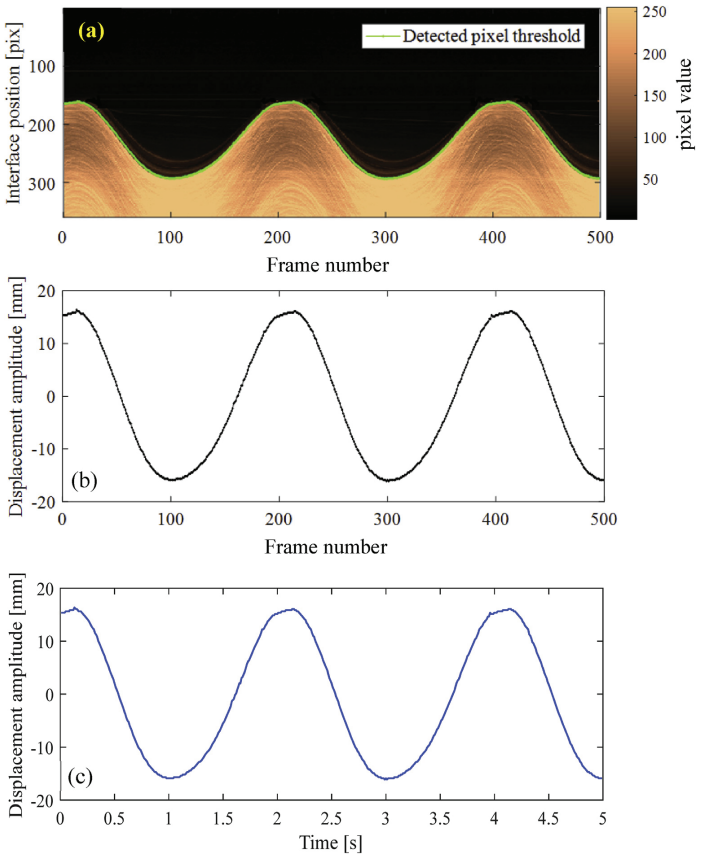

Fig. 5. Tracking of air-liquid interface: (a) detected pixel threshold (b) displacement amplitude with frame number (c) displacement amplitude with time.

images and the motion sensor and axial velocity distributions of both axial and radial directions are presented. The influence of low frequency oscillation on Newtonian and non-Newtonian fluids is also illustrated and discussed.

3.1. Rheology of the non-Newtonian fluid

The rheological properties of the non-Newtonian fluid were measured by the modular compact rheometer (Anton Paar - MCR 302), using a concentric cylinder configuration (CC27). Fig. 6 shows the flow curve and the viscosity curve against the varying shear rate for the non-Newtonian fluid, which was used in the experiment.

The viscosity curve shown in Fig. 6 clearly shows the shear-thinning behavior of the non-Newtonian fluid. The power-law and Carreau-Yasuda (CY) rheological models used for curve fitting the experimental data are expressed in Eq. (12) and Eq. (13) respectively;

$$\mu_{PL} = K\,\dot{\gamma}^{n-1} \tag{12}$$

$$\mu_{CY} = \mu_{\infty} + (\mu_{O} - \mu_{\infty})\,[1 + (\lambda_c \dot{\gamma})^{a\,c}]^{\frac{n_c-1}{a\,c}} \tag{13}$$

where, μ_{PL} is the apparent viscosity predicted by the power-law model, μ_{CY} is the apparent viscosity predicted by the Carreau-Yasuda model, K is the consistency index, n is the behavioral index for the power-law, $\dot{\gamma}$ is the shear rate, μ_{∞} and μ_{0} are the upper and lower limits of the viscosity corresponding to the low and high shear rates. The coefficients λ_c and n_c are empirically determined. a_c has also been determined empirically for this experiment, where $a_c = 2$ for the classical Carreau model. The values for all these coefficients are mentioned in Table 1 with their corresponding units.

It is to be noted that, the power-law model has been applied only for the linear region of the experimental data of non-Newtonian fluid. The viscosity of water was measured to be 0.9764 mPa s at 21 °C.

3.2. Movement of the air-liquid interface

According to the procedure described in section 2.4.2, the detected air-liquid interface of the Newtonian and non-Newtonian fluid at different frequencies is shown in Fig. 7 for a time duration of 10 s.

According to Fig. 7, it can be clearly seen that the displacement amplitude of the air-liquid interface of water is always greater than that of non-Newtonian fluid. This is as expected since the NNF has a higher viscosity than pure water and thus has higher flow resistance against the air-cushion drive. A bit more counter-intuitive is perhaps that, as the frequency is increased, the interface displacement amplitude is also increased, irrespective of the liquid type. When the frequency is increased, the momentum transfer from the piston via the air-buffer to the liquid is increased and the kinetic energy achieved by the fluid system is also increased. When the kinetic energy of the fluid system is increased, the viscous resistance of the fluid medium reduces and hence the displacement of the interface is increased with frequency. For water however, the viscosity is constant, and thus the behavior seems puzzling. It could be observed that the air-liquid interface profiles generated by the damped harmonic oscillating system is very regular.

The interface profiles from high-speed images were compared with those obtained with the motion sensor. Fig. 8 shows only the air-water interface movement obtained from the level measurements by the motion sensor at different frequencies. The profiles for the non-Newtonian fluid were also qualitatively similar to the plots in Fig. 8, but quantitatively they differ.

Similar to the observations from Fig. 7, it can be seen that when the oscillation frequency is increased, the displacement amplitude of the interface also increases. One important fact to emphasize here is that the interface is strongly impacted by the inertia of the whole liquid column when it comes to the highest level. It was also observed that the flow just below the liquid interface is not radially symmetric and it is influenced by the circular geometry of the pipe. Especially with the non-Newtonian fluid runs, the flow around the axis of the pipe exhibited a 'Mexican hat' type convened interface abiding to the strong viscous effects close to the wall.

It is to be noted that the achieved amplitude of the air-water interface is not similar to that provided by the piston (which is 25 mm). This could be attributed to the damped harmonic oscillator system that has been employed for the experiment, which is not completely "stiff" since the air pocket in between the liquid and the piston is compressible. However, it was observed during the experiments and the analysis that the air-liquid interface follows the piston motion with a higher degree and there is fairly a good transmission from the piston to the liquid system. Therefore, the liquid system concerned in this study has its own behavior in oscillatory motion. Furthermore, according to Fig. 8, it can be seen that the maximum displacement of the air-water interface is as low as 17 mm at the lowest oscillation frequency concerned and the output signals from the motion sensor have been suffered very little from noise compared to the higher frequency cases. Readings of the motion sensor for the non-Newtonian fluid also show a similar trend as with respect to the noise in the measurements. The presence of this noise within the motion sensor reading could also be due to the manifestations of compressibility of the air gap in between the oscillating liquid column and the driving piston. However, the raw data has been regressed with a value of R^2 greater than 90% for all the cases and based on the regressed curves, it can be seen that the flows were very close to sinusoidal.

It is worth to cross-check the achieved frequency and the displacement amplitude of the fluid system corresponding to the frequency and the oscillation amplitude provided by the piston. Fig. 9(a) summarizes the system-achieved frequency of the interface detected from high-speed images and level measurements against the frequency provided by the piston. Fig. 9(b) summarizes the phase-averaged displacement amplitude of the air-liquid interface detected from high-speed images and level measurements against the frequency provided by the piston.

It can be clearly seen that the mechanical piston arrangement has successfully transmitted the simple harmonic motion to the liquid system without any noticeable change in its frequency of oscillation. According to Fig. 9(a), the deviation of the system-achieved oscillation frequency from that provided by the piston is less than 5% and that enables the authors to discuss the results based on the frequency values supplied to the fluid system. However, the scenario is different when the displacement amplitude of the air-liquid interface is concerned.

As stated before, the displacement amplitude of the piston was preset to 25 mm before all the experimental runs. However, the interface displacement of water and non-Newtonian fluid have achieved different amplitudes at different frequencies. According to Fig. 9(b), it can be seen that the displacement amplitude of the air-liquid interface is always higher for water than for the non-Newtonian fluid. Apparently, the amplitude of water seems to be twice in value of the amplitude of non-Newtonian fluid. This could be attributed to the viscous resistance and the mass inertia that restrict the free motion of non-Newtonian

Table 1
Parameters of the two rheological models.

	K[mPa.s^n]	n[−]	μ_0[mPa.s]	μ_∞[mPa.s]	λ_c[s]	n_c[−]	a_c[−]
Power-law model	667.34	0.59	–	–	–	–	–
Carreau-Yasuda model	–	–	310.18	7.07	0.054	0.456	0.662

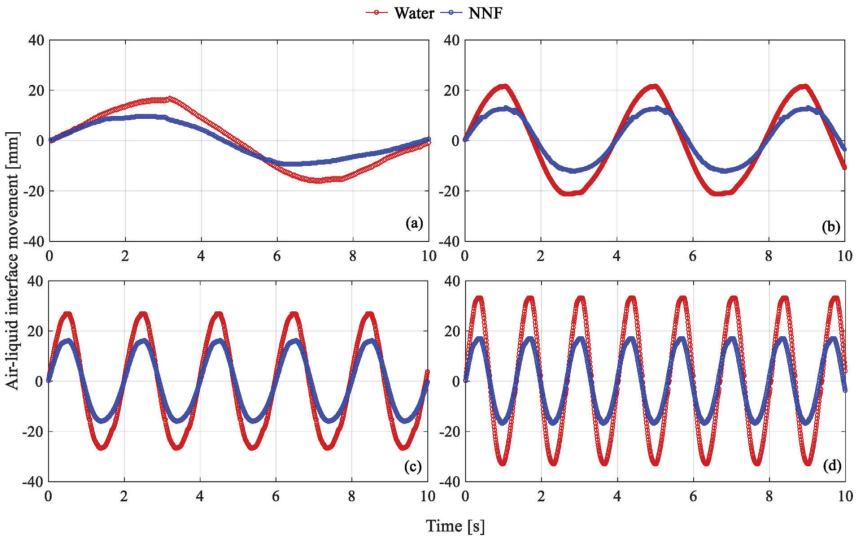

Fig. 7. Air-liquid interface movement detected from high-speed image analysis (a) at 0.1 Hz (b) at 0.25 Hz (c) at 0.5 Hz (d) at 0.75 Hz.

fluid at the interface.

Furthermore, it can be seen that the level measurements performed by the motion sensor always detect a higher displacement amplitude compare to that of high-speed image analysis for water. It is not exactly the same for non-Newtonian fluid, but in general, it can be said that the level measurements tend to result in a greater value than image analysis. This can be due to the fact that, in high-speed image analysis, the air-liquid interface is detected based on the image which has been captured just in front of the pipe wall and the edge could be actually the interface level at the pipe wall at that particular moment in concern. However, in level measurements, it is a transducer mounted in the path of the axis and the transmitted ultrasonic pulses are along the axis of the pipe. In the cases of oscillated non-Newtonian fluid, the presence of some “peaks” and “troughs” in the core region of the pipe due to the viscous shear layer could be the reason for detecting a higher displacement amplitude than in image analysis. It is to be highlighted that irrespective of the fluid type, the resulted displacement amplitude of the air-liquid interface has been increased when the frequency of oscillation is increased. The reason for this has been discussed earlier within this same section 3.2.

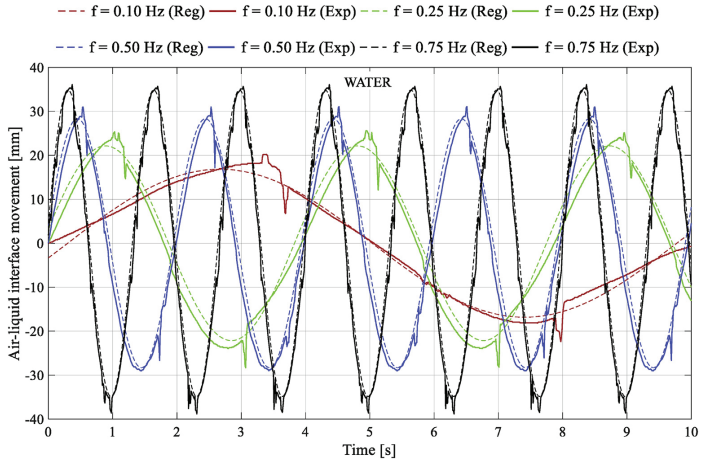

Fig. 8. Air-water interface movement detected by level measurements.

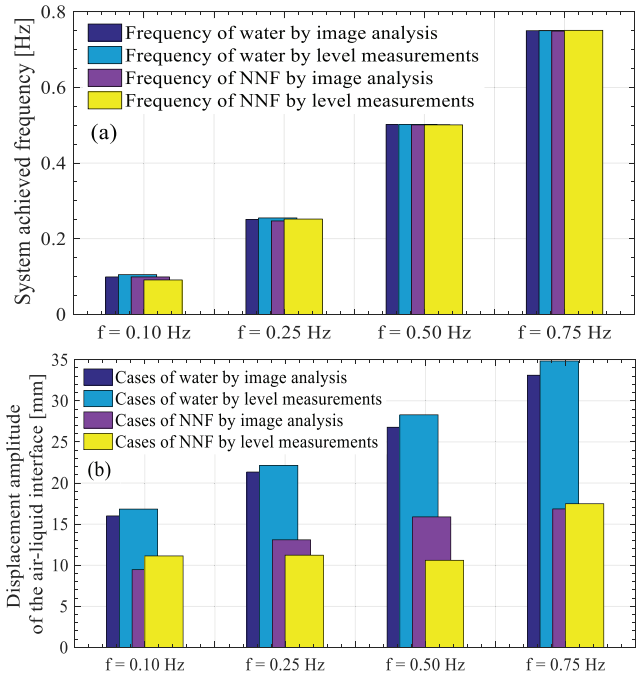

Fig. 9. Comparison of interface detection techniques (a) achieved frequency by the fluid system (b) phase-averaged displacement amplitude of the interface.

3.3. Evaluation on the oscillating Reynolds number

According to the expression stated in Eq. (5), it is important to check whether the experimental cases belong to the laminar regime or to the turbulent regime. Table 2 shows the Reynolds number values for all the experimental cases of this study. It is to be noted that since the non-Newtonian fluid has a shear rate dependent viscosity, the lower limit of the viscosity which corresponds to the least possible shear rate change (see Fig. 6) has been considered in the calculations. That assumes that the non-Newtonian fluid encounters a minimum shear rate change of $\dot{\gamma} = 0.1\ s^{-1}$. Further, the maximum velocity amplitude values reported in section 3.4.1 have been utilized within the calculation of Re_δ based on Stokes layer thickness.

Further, the calculated Re_δ is based on the PIV measurements performed 470 mm below the equilibrium air-liquid interface (see Fig. 2), which is the best possible location of the vertical test section to minimize the end effects of the pipe. Therefore, it can be concluded that all the experimental cases are within the laminar regime.

Table 2
Reynolds number values for all the experimental cases.

Fluid	Experimental case Number	Oscillating Reynolds number (Re_δ)	Womersley Number (Wo)
Water	1–0.1 Hz	19.77	20.3
	2–0.25 Hz	40.03	31.67
	3–0.5 Hz	79.38	44.79
	4–0.75 Hz	115.46	54.86
Non-Newtonian Fluid	5–0.1 Hz	4.39	3.11
	6–0.25 Hz	6.68	4.91
	7–0.5 Hz	13.25	6.95
	8–0.75 Hz	16.53	8.51

3.4. Validation of the PIV results

If the radial velocity profile is given by $V(r)$, the cross-sectional average velocity (V_{ave}) is then defined [1,30] as;

$$V_{ave} = \frac{1}{A}\int_A V(r)\,dA \tag{14}$$

where A is the cross section area of the duct in the direction of the flow. For a pipe flow in a circular cross-section, this implies;

$$V_{ave} = \frac{1}{\pi R^2}\int_0^R V(r).\ 2\pi r.\ dr \tag{15}$$

where, r is any radial position between 0 and R. The cross-sectional space and time averaged velocity ($V_{cs-mean}$) can further be expressed as;

$$V_{cs-mean} = \frac{1}{T}\sum_0^T V_{ave} \tag{16}$$

where, T is the time selected for averaging and is normally chosen large enough to average out all the time-dependent variations.

Modelling oscillatory flows analytically is difficult due to the complexity. There are many aspects such as fluid properties, wall properties and entrance length, transition to turbulence [2] etc. to be accounted in

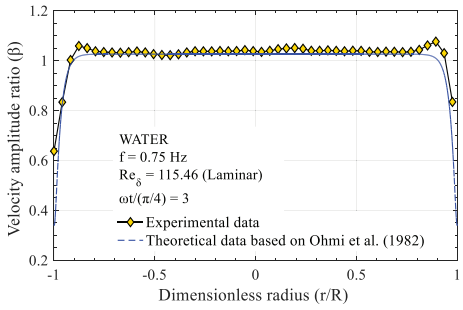

Fig. 10. Validation of experimental PIV results with literature.

such an approach. There exists some studies, which describe the theoretical approach to develop some correlations for the radial velocity profile of oscillatory flow in laminar regime [2,5,30] and for the wall shear stress which includes an acceleration term [10] etc. For example, Ohmi et al. [5] have developed a theoretical expression for the velocity amplitude ratio (β), for the oscillating flow of a Newtonian fluid in laminar regime as;

$$\beta = \frac{|V(t)|}{|V_{cs-mean}|} = \frac{M_0(\alpha)}{M_2(\alpha)}\sqrt{1+\left\{\frac{M_0(r'\alpha)}{M_0(\alpha)}\right\}^2 - 2\frac{M_0(r'\alpha)}{M_0(\alpha)}\cos\{\theta_0(r'\alpha) - \theta_0(\alpha)\}} \quad (17)$$

Here r' is the non-dimensional radius equal to r/R and $M_m(\alpha)$ and $\theta_m(\alpha)$ are the modulus and the phase of the first kind of Bessel function of order m respectively, which can in generally be written as $J_m\left(i^{2/3}\alpha\right)$. This theoretical expression shown in Eq. (17), which is developed for the oscillating flow of a Newtonian fluid in the laminar regime, has been used to validate the PIV results of this present study. Fig. 10 shows both the theoretical prediction and the experimental result obtained for water, which was used as the Newtonian fluid in the experiment. It is to be noted that, only one specific position of the phase cycle and a specific case out of the eight different flow conditions has been used for the validation as highlighted in Fig. 10.

According to Fig. 10, it can be seen that the amplitude ratio (β) in the pipe agrees reasonably well with the theoretical velocity amplitude ratio proposed by Ohmi et al. [5], only within the core area of the pipe. The agreement becomes limited when it comes closer towards the wall regions where the experimental values show a slightly higher velocity amplitude ratio at the walls and slight deviations from the theoretical prediction. Despite of that, it could be calculated that the total deviation of the experimental data from the theoretical prediction was not more than 5%. Therefore, it is concluded that the PIV results presented in this study are valid and trusted. Note that, both experimental and theoretical results overshadow the no-slip condition at the walls, which is usually assumed in pipe flow investigations.

3.5. Axial velocity component of the pipe centerline

The best location to identify the maximum of the characteristic sinusoidal fluid motion within the vertical pipe (as expressed in Eq. (2)) is along the pipe axis. Therefore, this section summarizes some results obtained along the pipe centerline (axis) from the PIV analysis. The axial velocity at the pipe centerline shown in Fig. 11 is used as a basis to introduce the notation system adopted by the authors to discuss the results in the latter part of this paper.

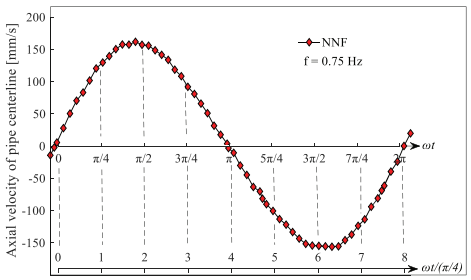

Fig. 11. Introduction of the different positions within the phase cycle based on the centerline axial velocity.

As illustrated, different positions within a complete phase cycle of the centerline axial velocity variation for each fluid and at each frequency are identified. The phase position (ωt) has made dimensionless using the angle value ($\pi/4$) and the value for $\omega t/(\pi/4)$ has been utilized in presenting and discussing further results. Fig. 12 shows the centerline axial velocity profiles of water and non-Newtonian fluid when they were oscillated at a frequency of 0.5 Hz.

It is apparent from the graphs that PIV measurements adequately reflect the periodical character of the flow velocity. This periodical characteristic is visible for all the experimental cases and only two examples are illustrated here in Fig. 12 for brevity. However, each of them differs from the magnitude of velocity amplitude, which is affected by the oscillation frequency provided by the piston and the liquid type. The shape of the curves shows some inequality between the acceleration and deceleration amplitudes that demonstrates some local friction exerted on the piston motion especially on its accelerating phase. That elucidates the features of the mechanical piston arrangement that could not be overcome, thus providing a reliable driving mechanism.

3.5.1. Maximum velocity amplitude

The importance of plotting the centerline axial velocity profiles similar to Fig. 12 is to get an idea on how the velocity amplitude is varying with the provided oscillation frequency. Fig. 13 shows all the velocity amplitudes at different frequencies and for both the liquids. According to Fig. 13, it can be seen that the velocity amplitude achieved by water is greater than that of non-Newtonian fluid in almost all the frequencies except at the highest oscillation frequency. When the period of oscillation is decreased, the amplitude of velocity has been increased for both the liquids assuring the same qualitative observation as for the displacement amplitude shown in Fig. 9(b). This is a vertical set up where the elevation changes from point to point and the PIV measurements have been obtained at a location of 47 cm below the air-liquid interface. Even though water has achieved doubled values in displacement amplitude compared to non-Newtonian fluid at the interface, at the place of PIV measurements, both fluids show only a slight difference between the velocity amplitudes. As explained earlier, all the test runs are within the laminar regime and thus the viscous effects dominate. Therefore, these finite amplitude differences in velocity could be due to the viscous effects of the two liquids.

3.5.2. Cross-sectional average axial velocity Vs normalized axial velocity

The velocity profiles shown in Fig. 12 and the amplitudes of velocity shown in Fig. 13 are calculated at the centerline of the pipe. However, in a usual pipe flow experiment, if the velocity across the cross-section is unevenly distributed, it becomes difficult to compare different scenarios, especially with non-Newtonian fluids. Because, the viscous resistance and the presence of shear layer contribute much to generate an

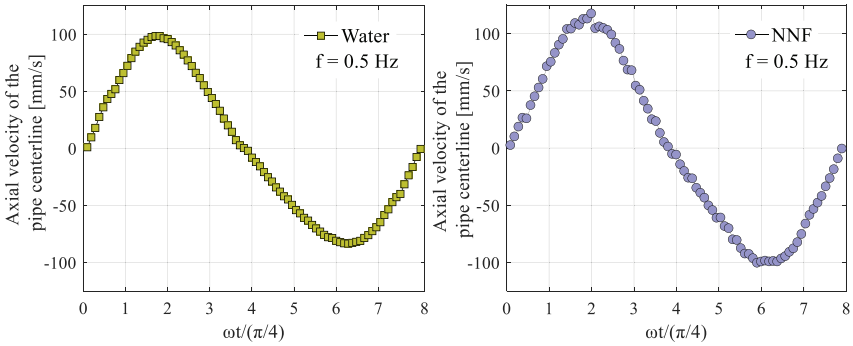

Fig. 12. Axial velocity of the pipe centerline for water and non-Newtonian fluid at 0.5 Hz.

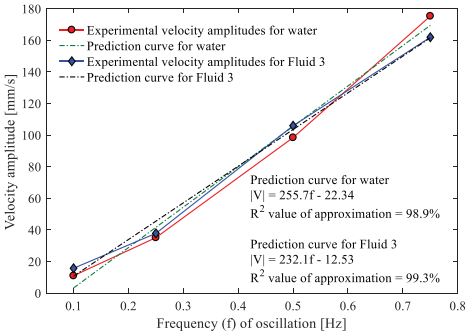

Fig. 13. Comparison of velocity amplitudes at different frequencies for both the liquids based on PIV measurements.

uneven distribution of the velocity across the cross-section. Therefore, it is worth to discuss the variation of axial velocity based on the concept of cross-sectional average velocity as expressed in Eq. (13). When the instantaneous axial velocity components are normalized by the cross-sectional average velocity, a more complete picture of the kinematic structure of oscillating flow and its dynamics can be obtained.

Fig. 14 shows six different cases where the cross-sectional average velocity and also the normalized axial velocity are illustrated based on the instantaneous values of the centerline axial velocities. All the six sub-figures depict the periodical structure of the flow due to the oscillatory motion where the cross-sectional average velocity becomes maximum at $\omega t/(\pi/4) = 2$ and minimum at $\omega t/(\pi/4) = 6$. Furthermore, it is noted that the maximum magnitude of the cross-sectional average velocity is increased with increasing frequency irrespective of the type of fluid. However, the values of the cross-sectional average velocity of the non-Newtonian fluid is always lower than that of water providing some insights on the uneven distribution of the velocity across the cross-section for the non-Newtonian fluid cases.

In Fig. 14, the normalized axial velocity is also drawn together with the cross-sectional average velocity to get a clear picture on the contribution of the average velocity. It can be seen that the normalized axial velocity of water is more or less equals to unity in all the positions of the phase cycle except at $\omega t/(\pi/4) = 0$, 4 and 8. For these three positions, the instantaneous axial velocity component at the centerline of the pipe is zero or very close to zero and thus the normalization process would end up in zero (or even less than zero), even though the cross-sectional average velocity has a magnitude due to the motion of the Stokes layer. The value of unity for other phase positions implies that, the instantaneous velocity distributions for water are more flattened and the cross-sectional average velocity is also very close to the magnitude of instantaneous axial velocity amplitudes at the axis.

However, the normalized velocity values for the centerline axial velocity distribution of the non-Newtonian fluid seem to be spread among different values without being localized around unity or zero. The main reason behind this is the uneven distribution of velocity across the cross-section due to the effect of the shear layer within the non-Newtonian fluid. Two common peaks in the normalized axial velocity plot could be identified at $\omega t/(\pi/4) = 3$ and 7 for non-Newtonian fluid, where the lowest cross-sectional average velocity is resulted due to the change in flow direction of the flow and thus the radial velocity profiles show opposite velocities in the core region and around the shear region close to the wall.

3.6. Axial velocity distribution along the pipe diameter

In order to properly understand the effect of cross-sectional average velocity, it is important to observe the distribution of the axial velocity component along the diameter of the pipe. Fig. 15 shows the instantaneous axial velocity distribution of water and non-Newtonian fluid along the diameter of the pipe only for two selected cases for brevity.

The color background of the analyzed PIV images shown in Fig. 15 clearly shows the zones of the shear layer. In a classical pipe flow motion, the individual axial jet motions are determined by both total pressure drop and by the shear forces imposed by the walls. This study has considered a vertical pipe and the total pressure drop is of course changing time to time due to oscillations. However, the total pressure drop is the same at a similar position of the phase cycle for both Newtonian and non-Newtonian fluids. Therefore, since all the cases considered in this study are within the laminar flow regime, these shear forces and hence the frictional stresses of the wall on the flow velocity becomes significant in non-Newtonian fluid compared to water.

The different color themes used in the background of the PIV image shown in Fig. 15 illustrate this significance of shear forces. For water, these shear forces are much more localized near the wall and the majority of the individual axial flow jets obtain mostly similar velocity values. They occupy the majority of pipe cross-section to retain as a plug-type flow. However, it is different in non-Newtonian fluid where the effect of wall shear is propagating towards the central axis of the pipe and as a result, different color regions have appeared. According to

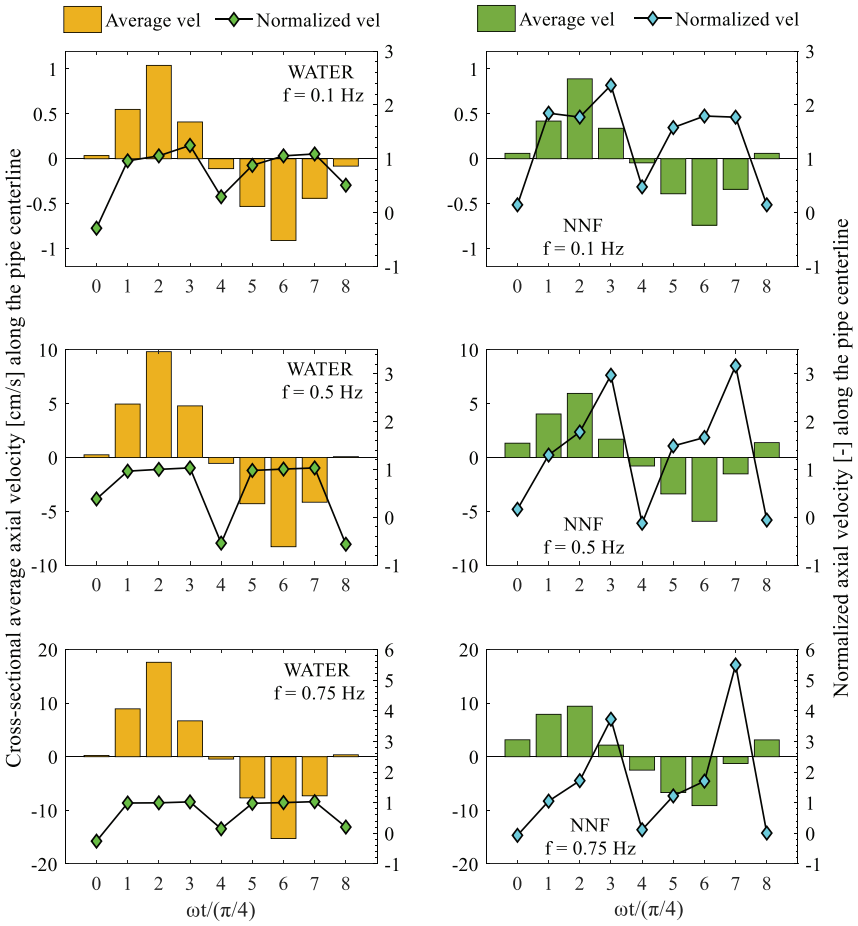

Fig. 14. Comparison of cross-sectional average axial velocity Vs normalized axial velocity for both water and non-Newtonian fluid.

Gerrard and Hughes [19], the flow outside the central region can be described as an oscillating boundary layer where, this boundary layer becomes thinner as the frequency increases.

3.6.1. Temporal evolution of the axial velocity distribution along the pipe diameter

The primary data for PIV measurements in the form of instantaneous velocity fields for some specific positions of the phase cycle are presented in Fig. 16 for water and in Fig. 17 for the non-Newtonian fluid. It is to be highlighted that the two plots are drawn based on the centerline axial velocities for both the fluids.

One of the common features that can be observed from the two figures is that, the flow field could be identified as two parts, namely as a wall region and an outer (or core) region. This could be experienced even by visual observations during the experiments where, the most excited radial and rotational motions of tracer particles were observed near the wall region. In addition to that, it was observed that the fluid near the wall turned its direction faster than the fluid within the core region, when the piston changes its direction of the motion. This could be attributed to the flow friction exerted on the fluid layers adjacent to the wall and the higher momentum achieved by the flow within the core region. This visual observation is reflected especially in the velocity profiles plotted for water shown in Fig. 16. There, the velocity profiles become flatter in the core of the flow. The degree of the fullness of the velocity profile increases with the increase of Re_δ and the frequency of the imposed oscillations. This increased fullness of the velocity profile at higher frequencies (for instance at 0.5 Hz or 0.75 Hz) could be attributed to the tendency of the flow to achieve more turbulent characteristics compared with the low frequency cases.

However, the axial velocity profiles for the non-Newtonian fluid

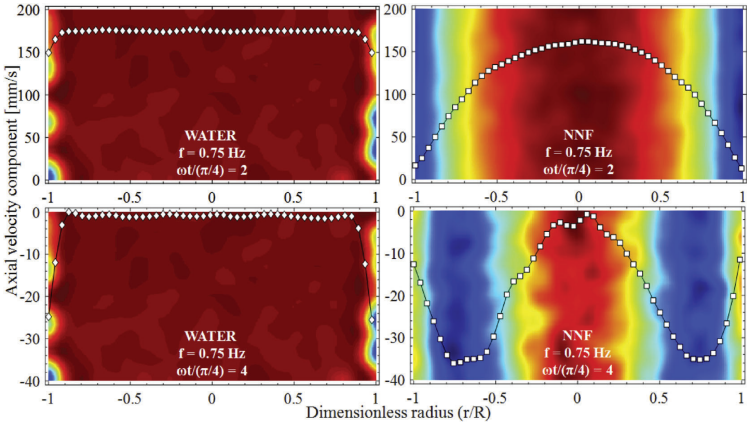

Fig. 15. Instantaneous axial velocity distribution of water and non-Newtonian fluid along the diameter of the pipe (at f = 0.75 Hz) – vertical axis represents the color scheme. (For interpretation of the references to color in this figure legend, the reader is referred to the Web version of this article.)

shown in Fig. 17 seem to be much irregular but more parabolic only within the core region of the pipe. Continuous flow reversal is the reason for not attaining the full parabolic profile along the whole diameter. In the cases of flow reversal with non-Newtonian fluid, if the net axial velocity profile remains positive in the core region of the pipe, some part of the velocity profile seems to be negative in a very small region near the wall. The thickness of this region goes on decreasing with increase of frequency. It is observed that the velocity amplitude of the centerline axial velocity component is increased with increasing frequency for both water and non-Newtonian fluid.

According to Figs. 16 and 17, it can be identified that PIV technique provides more promising results at slightly higher frequencies compared to that at very low frequencies. While analyzing the PIV images, it could be seen that the streamwise (axial) velocity component is greatly affected by the imposed oscillations and the impact on transverse (horizontal) velocity component is not that significant. It is a known fact that the velocity on the walls should be equal to zero based on the no-slip condition. However, when it comes to the practical situation, it can be seen that velocity on the walls is not exactly equal to zero, but has a value higher than that.

3.6.2. *Normalized velocity profiles for some selected phase positions*

Figs. 18 and 19 illustrate the normalized velocity profiles in the radial direction of the pipe for both Newtonian and non-Newtonian fluids. In order to get a clear picture on how the axial velocity is distributed across the cross-section, the instantaneous axial velocity components are normalized by the cross-sectional average velocity of the concerning phase position. Only three positions of the phase cycle within the acceleration half have been selected for brevity in illustration. $(V_{ave})_k$ in Figs. 18 and 19 refers to $(V_{ave})_{[\omega t/(\pi/4)]=k}$, where $k = 0$, 2 and 3.

The initial observation which can be made from the two figures is that, the normalized axial velocity of water within the core region of the pipe is not strongly affected by the low frequency of oscillation provided in this set of experiments. It is just because of the plug-type behavior of the axial velocity distribution of water in the core region. The curves for water show a steep velocity gradient near the wall and a flat plug flow region in the center indicating that the normalized velocity is not responding to the increased frequency within this core region. It always gets the value of 0 at $\omega t/(\pi/4) = 0$ and unity at $\omega t/(\pi/4) = 2$ & 3.

However, the patterns of normalized axial velocity distributions for the non-Newtonian fluid differ from those of water. The normalized axial velocity distributions achieve a maximum in the core (or the axis) of the pipe while the normalized velocity near the pipe wall region tends to be zero. According to the curves in Fig. 19, it can be read that the maximum normalized axial velocity is 2.2 at the lowest frequency and 3.8 at the highest frequency tested in this set of experiments. That reveals the fact that, when the period of oscillation is decreased, the normalized axial velocity component for non-Newtonian fluid is increased accordingly.

It is to be highlighted the significance of considering the normalized axial velocity here. Unlike water, the velocity distribution of non-Newtonian fluid is not uniform over the cross-section and it can take several shapes either parabolic or the so called 'Mexican hat type'. For water, it is mostly plug-type except near the wall region and therefore, the individual axial velocity components along the radial distance do not provide a clear picture about the correct distribution of the velocity across the cross-section. By calculating the cross-sectional average velocity as depicted by Eq. (13), it allows us to obtain an indication on how the bulk velocity at that particular moment of time is established in both qualitatively (direction-wise) and quantitatively. For an instance, even the axial velocity is showing a higher positive velocity magnitude in a case of the non-Newtonian fluid, the magnitude close to the Stokes layer may have achieved two negative peaks in axial velocity which reduces the overall cross-sectional average velocity and results with a lower value. However, if the cross-sectional average velocity results in a very low magnitude, the resulting normalized axial velocity magnitudes may end up with higher values than the corresponding instantaneous velocity components at each radial position. That is what reflected in both Figs. 18 and 19 and the cross-sectional average velocity plays a vital role here.

To report the uncertainty, three readings were taken from the analyzed PIV image. The error bars drawn in Figs. 18 and 19 illustrate the calculated standard deviation of those readings taken at different levels within the region of interest (ROI). It is to be noted that, these different levels within the ROI have been chosen in such a way that, it does not reflect the velocity variation with height but, to reflect the accuracy of the PIV measurements. It can be seen that standard deviation of the PIV measurements taken at lower frequencies are greater

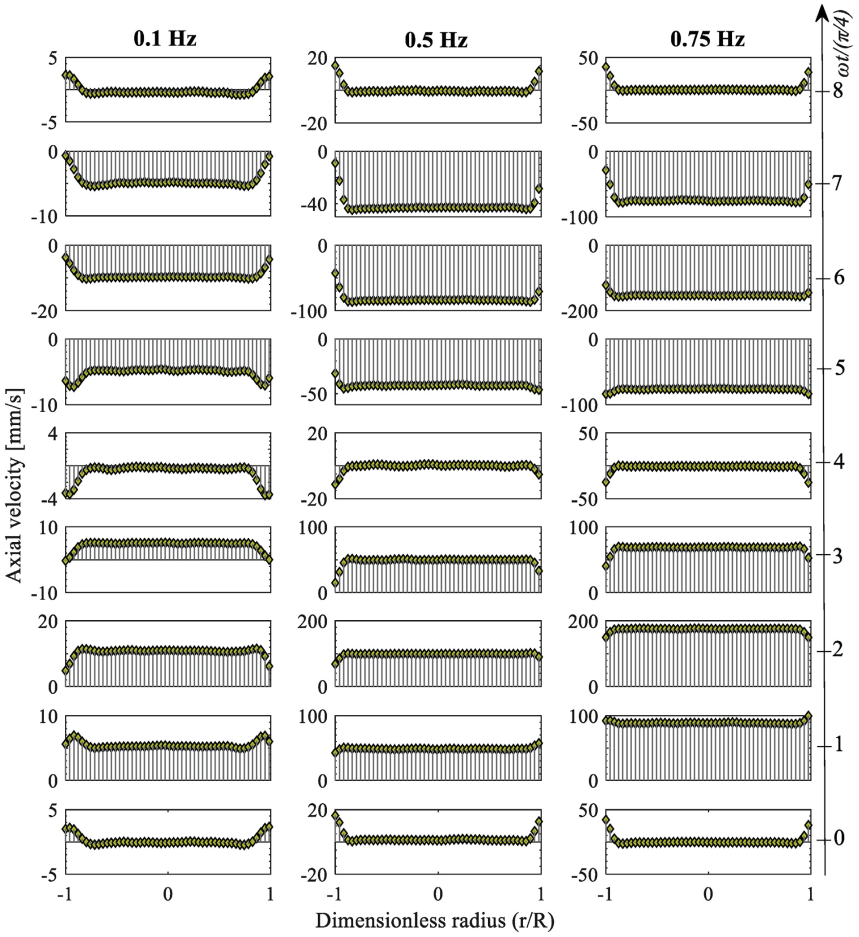

Fig. 16. Temporal evolution of the axial velocity distribution for water.

than that taken at higher frequencies. It is common for both Newtonian and non-Newtonian fluids where, the standard deviation values for water are smaller in magnitude in comparison to the same frequency cases of non-Newtonian fluid.

According to the profiles drawn for water in Fig. 18, at least some significant amount of error bars could be seen only close to the wall region of the pipe. However, when it comes to the non-Newtonian fluid, the error bars are much more significant in the core region of the pipe. That can be attributed to the shear layer effect of the non-Newtonian fluid and thus it exerts a resistance for the motion close to the wall. Therefore, the velocity magnitudes for non-Newtonian fluid close to the wall region estimated by PIV analysis tend to be unchanged compared to those taken within the core region of the pipe. This gives some insights and hopes on further studies to be carried out within the near-wall region where the PIV technique is a promising non-intrusive method for estimation of wall shear stress and also the change of shear rate.

Khabakhpasheva et al. [20] state that, the significance of this type of oscillatory flow could be the manifestation of the effects of non-linear viscoelastic properties of the shear-thinning non-Newtonian fluid by allowing one to judge whether one or another rheological equation of state reflects the actual behavior of the viscoelastic fluid in concern. However, according to the experimental study performed by Manero et al. [31], it appears that the dominating factor in the oscillating flow of non-Newtonian fluids in pipes is the shear dependent viscosity and the elastic properties of the liquid are virtually of no importance in the phenomenon. This is currently being studied by the authors to investigate the effect of viscoelasticity on oscillatory flow and its relation to the settling of solids in shear-thinning fluids.

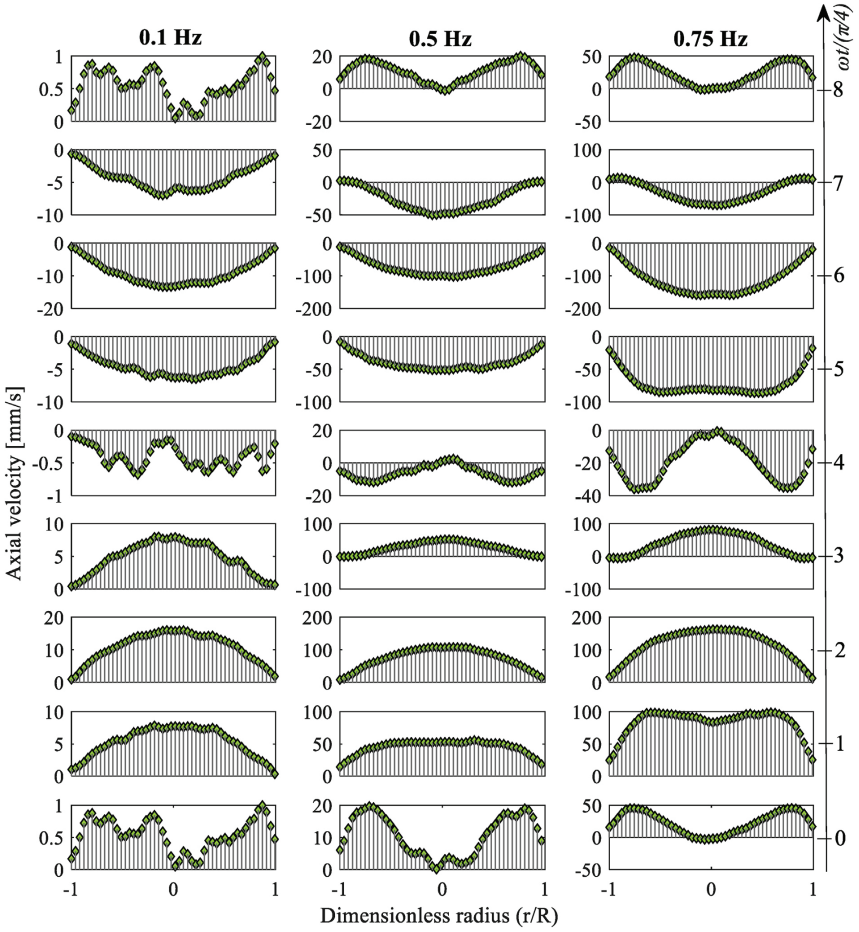

Fig. 17. Temporal evolution of the axial velocity distribution for non-Newtonian fluid.

4. Conclusion

A system of PIV measurements within a vertical pipe flow with externally imposed oscillations has been developed from this study. The system allows investigating the dynamics of the processes in oscillatory flows of both Newtonian and non-Newtonian that mimics several industrial applications including drilling in the oil and gas industry. The streamwise (axial) velocity distribution in a circular vertical pipe is measured at different low frequency values which are less than 1 Hz and this experimental study demonstrates the applicability of non-intrusive PIV technique for such low frequency oscillatory flows which enables to study the process more clearly and accurately.

The high-speed image analysis was also carried out to detect the air-liquid interface and compared that with the measurements from a motion sensor. The two readings were in good agreement with a deviation less than 5% for both the fluid types and confirmed the frequency supplied by the piston arrangement to the fluid system.

Oscillatory Reynolds number and the non-dimensional frequency (in other words the Womersley number) are the two governing non-dimensional parameters in oscillatory flow. Therefore, accurate evaluation of critical Reynolds number to determine whether the oscillatory flow is laminar or turbulent is very important since it may lead to a change in the kinematic structure of the flow.

The experimental analysis reveals that, the axial velocity profile of water across the cross-section is plug-type with a peak appears between the axis and the wall and this peak approaches the wall with increasing frequency. At higher frequencies, the viscous effects are confined to the Stokes layer and the central core is plug-type with increased velocity amplitudes. The viscous resistance of the non-Newtonian fluid and the presence of shear layer contribute much to generate an uneven

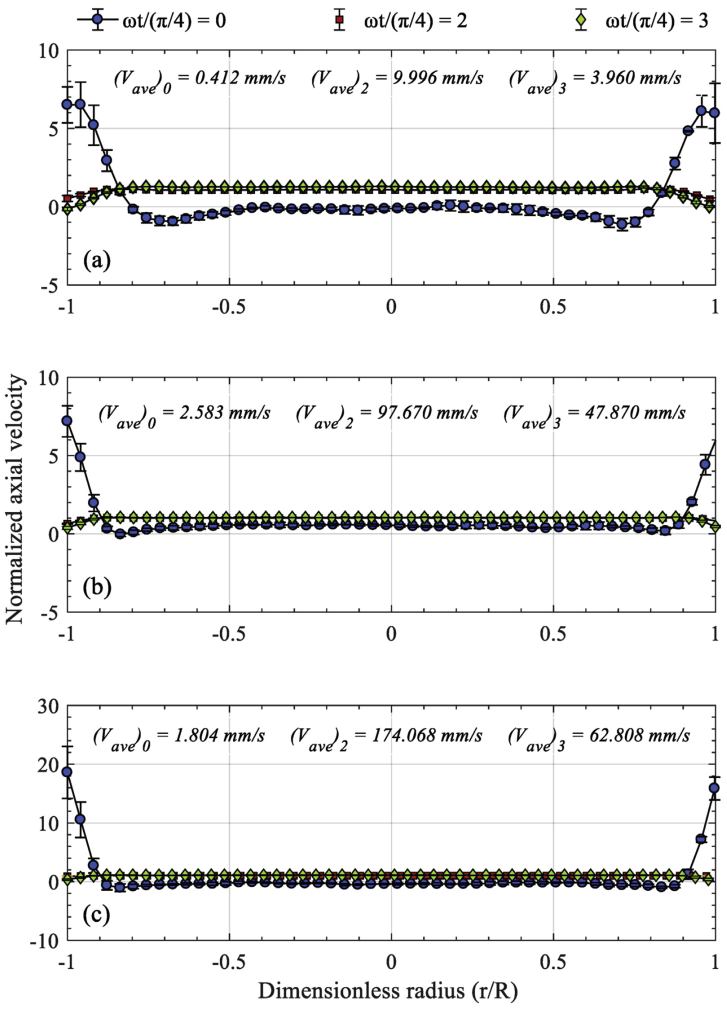

Fig. 18. Normalized velocity profiles for water, (a) f = 0.1 Hz (b) f = 0.5 Hz (c) f = 0.75 Hz.

distribution of the velocity across the cross-section. Cross-sectional average velocity provides a more complete picture of the kinematic structure of oscillating flow and its dynamic distribution across the cross-section. The normalized axial velocity is important in discussing the presence of shear layer especially in non-Newtonian fluids. When the period of oscillation is decreased, the normalized axial velocity component for non-Newtonian fluid is increased accordingly.

PIV is a great non-intrusive optical measuring technique that can be used to visualize the velocity distribution of non-steady flows in vertical pipe systems. The streamwise (axial) velocity component is significantly affected by the imposed oscillations compared to the horizontal velocity component. At higher frequencies, the significance of the transverse velocity component (in the horizontal direction) becomes very low in both water and non-Newtonian fluid. PIV technique provides more promising results for the velocity distributions at higher frequencies for both Newtonian and non-Newtonian fluids. According to the analysis, PIV shows some quantifiable uncertainty close to the wall region for water and within the core region for non-Newtonian fluid. However, the effect of the low frequency oscillation on the shear layer of the fluid and thus on the viscosity of the non-Newtonian fluids and the consequence in solids separation will be investigated and discussed in the next study by the authors.

Acknowledgement

Authors gratefully acknowledge the Norwegian Research Council

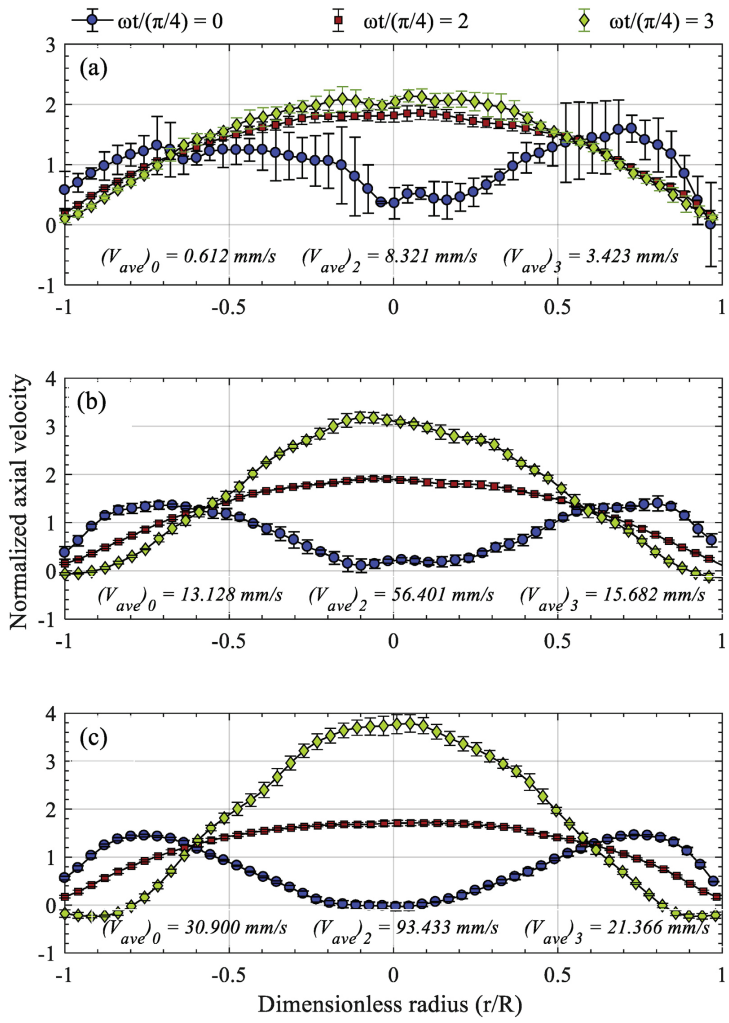

Fig. 19. Normalized velocity profiles for the non-Newtonian fluid, (a) f = 0.1 Hz (b) f = 0.5 Hz (c) f = 0.75 Hz.

for funding this study under the project "NFR Improved Model Support in Drilling Automation". We appreciate the valuable support provided by Jon Arne Evjenth, from the Department of Energy & Petroleum Engineering at the University of Stavanger in preparing the data acquisition system for the experiments. The advice and encouragement provided by Roar Nybø and Knut S. Bjørkevoll from SINTEF, Bergen are also greatly appreciated.

Notation

CMC	Carboxymethyl Cellulose
CLAHE	Contrast limited adaptive histogram equalization
CY	Carreau-Yasuda rheological model
DCC	Discrete cross-correlation function
DPIV	Digital particle image velocimetry
NNF	Non-Newtonian fluid
PAC	Poly-anionic Cellulose
PIV	Particle image velocimetry
PIVlab	Software tool developed in MATLAB to perform PIV analysis
PL	Power-law rheological model
ROI	Region of interest
a	Displacement amplitude
a_c	Empirical coefficient for the CY model
A	Cross-sectional area of the pipe

D	Diameter of the pipe
f	Frequency of oscillation, Hz; $\omega/2\pi$
K	Consistency index of the non-Newtonian fluid
$M_m(\alpha)$	and $\theta_m(\alpha)$ Modulus and the phase of the first kind of Bessel function of order m respectively, $J_m\left(i^{2/3}\,\alpha\right)$
n	Behavioral index for the power-law
n_c	Empirical coefficient for the CY model
r'	Non-dimensional radius, r/R
R	Radius of the pipe
Re_δ	Oscillatory Reynolds number based on stokes layer thickness; $\lvert V\rvert\,\delta/\nu$
Re_D	Reynolds number for the general pipe flow; $\lvert V\rvert\,D/\nu$
Re_f	Oscillatory Reynolds number based on the oscillating frequency; $R^2 f/\nu$
Re_ω	Pulsating Reynolds number; $D^2\omega/\nu$
t	Time
T	Time selected for averaging
$V(t)$	Linear velocity with time in the axial direction at the centerline
$\lvert V\rvert$	Velocity amplitude in the axial direction at the centerline, $\lvert V\rvert = \lvert a\rvert\omega$
$y(t)$	Displacement with time in the axial direction at the centerline
V_{ave}	Cross-sectional average velocity
$V_{cs-mean}$	Cross-sectional mean average velocity
Stk	Stokes number for seeding particles
Wo	Womersley number; $R\sqrt{\omega/\nu}$

Greek Letters

α	Frequency parameter or non-dimensional frequency; $R\sqrt{\omega/\nu}$
β	Velocity amplitude ratio, $\lvert V\rvert/\,V_{cs-mean}$
$\dot{\gamma}$	Shear rate
δ	Oscillating boundary layer (Stokes layer); $\sqrt{2\nu/\omega}$
ω	Angular frequency; $2\pi f$
ν	Kinematic viscosity of the fluid
λ	Stokes parameter; $R\sqrt{\omega/2\nu}$
λ_c	Empirical coefficient for the CY model
μ	Dynamic viscosity of the fluid
μ_0	Lower limit of dynamic viscosity corresponding to the low shear rate
μ_∞	Upper limit of dynamic viscosity corresponding to the high shear rate

References

[1] L.S. Fishler, R.S. Brodkey, Transition, turbulence and oscillating flow in a pipe a visual study, Exp. Fluids 11 (6) (October 01 1991) 388–398.

[2] M.Y. Gundogdu, M.O. Carpinlioglu, Present state of art on pulsatile flow theory: Part 1: laminar and transitional flow regimes, JSME Int. J. Ser. B Fluids Therm. Eng. 42 (3) (1999) 384–397.

[3] I.A. Ramadan, A.I.A. El-Rahman, A.H. Ibrahim, Transition to turbulence in oscillating flow, 23 - 27 July, 2017, Presented at the 24th International Congress on Sound and Vibration, London, 2017.

[4] J. Harris, G. Peev, W. Wilkinson, Velocity profiles in laminar oscillatory flow in tubes, J. Phys. E Sci. Instrum. 2 (11) (1969) 913.

[5] M. Ohmi, M. Iguchi, K. Kakehashi, T. Masuda, Transition to turbulence and velocity distribution in an oscillating pipe flow, Bull. JSME 25 (201) (1982) 365–371.

[6] M. Teufel, D. Trimis, A. Lohmüller, Y. Takeda, F. Durst, Determination of velocity profiles in oscillating pipe-flows by using laser Doppler velocimetry and ultrasonic measuring devices, Flow Meas. Instrum. 3 (2) (1992) 95–101.

[7] Y. Su, J.H. Davidson, F. Kulacki, Fluid Flow and Heat Transfer Structures of Oscillating Pipe Flows, (2011).

[8] M. Hino, M. Sawamoto, S. Takasu, Experiments on transition to turbulence in an oscillatory pipe flow, J. Fluid Mech. 75 (2) (1976) 193–207.

[9] S. Sergeev, Fluid oscillations in pipes at moderate Reynolds numbers, Fluid Dyn. 1 (1) (1966) 121–122.

[10] M. Iguchi, M. Ohmi, K. Maegawa, Analysis of free oscillating flow in a U-shaped tube, Bull. JSME 25 (207) (1982) 1398–1405.

[11] D.M. Eckmann, J.B. Grotberg, Experiments on transition to turbulence in oscillatory pipe flow, J. Fluid Mech. 222 (1991) 329–350.

[12] K.H. Ahn, M.B. Ibrahim, Laminar/turbulent oscillating flow in circular pipes, Int. J. Heat Fluid Flow 13 (4) (1992) 340–346.

[13] M.Y. Gundogdu, M.O. Carpinlioglu, Present state of art on pulsatile flow theory: Part 2: turbulent flow regime, JSME Int. J. Ser. B Fluids Therm. Eng. 42 (3) (1999) 398–410.

[14] R. Trip, D. Kuik, J. Westerweel, C. Poelma, An experimental study of transitional pulsatile pipe flow, Phys. Fluids 24 (1) (2012) 014103.

[15] D. Drake, On the flow in a channel due to a periodic pressure gradient, Q. J. Mech. Appl. Math. 18 (1) (1965) 1–10.

[16] S. Tsangaris, N. Vlachakis, Exact solution of the Navier-Stokes equations for the fully developed, pulsating flow in a rectangular duct with a constant cross-sectional velocity, J. Fluids Eng. 125 (2) (2003) 382–385.

[17] M. Clamen, P. Minton, An experimental investigation of flow in an oscillating pipe, J. Fluid Mech. 81 (3) (1977) 421–431.

[18] J.R. Womersley, An Elastic Tube Theory of Pulse Transmission and Oscillatory Flow in Mammalian Arteries, Aerospace Research Labs Wright-Patterson AFB OH, 1957.

[19] J. Gerrard, M. Hughes, The flow due to an oscillating piston in a cylindrical tube: a comparison between experiment and a simple entrance flow theory, J. Fluid Mech. 50 (1) (1971) 97–106.

[20] E. Khabakhpasheva, V. Popov, A. Kekalov, E. Mikhailova, Pulsating flow of viscoelastic fluids in tubes, J. Non-Newtonian Fluid Mech. 33 (3) (1989) 289–304.

[21] T. Zhao, P. Cheng, The friction coefficient of a fully developed laminar reciprocating flow in a circular pipe, Int. J. Heat Fluid Flow 17 (2) (1996) 167–172.

[22] P. Merkli, H. Thomann, Transition to turbulence in oscillating pipe flow, J. Fluid Mech. 68 (3) (1975) 567–576.

[23] M. Ohmi, M. Iguchi, Critical Reynolds number in an oscillating pipe flow, Bull. JSME 25 (1982) 165–172 200.

[24] K.D. Jensen, Flow measurements, J. Braz. Soc. Mech. Sci. Eng. 26 (4) (2004) 400–419.

[25] R.J. Adrian, Particle-imaging techniques for experimental fluid mechanics, Annu. Rev. Fluid Mech. 23 (1) (1991) 261–304.

[26] J. Westerweel, Fundamentals of digital particle image velocimetry, Meas. Sci. Technol. 8 (12) (1997) 1379.

[27] M. Amaratunga, R. Nybø, R.W. Time, PIV analysis of dynamic velocity profiles in non-Newtonian drilling fluids exposed to oscillatory motion, ASME 2018 37th International Conference on Ocean, Offshore and Arctic Engineering, American Society of Mechanical Engineers, 2018V008T11A058-V008T11A058.

[28] W. Thielicke, E. Stamhuis, PIVlab–towards user-friendly, affordable and accurate digital particle image velocimetry in MATLAB, J. Open Res. Softw. 2 (1) (2014).

[29] H. Huang, D. Dabiri, M. Gharib, On errors of digital particle image velocimetry, Meas. Sci. Technol. 8 (12) (1997) 1427.

[30] S. Uchida, The pulsating viscous flow superposed on the steady laminar motion of incompressible fluid in a circular pipe, Z. Angew. Math. Phys. ZAMP 7 (5) (1956) 403–422.

[31] O. Manero, B. Mena, R. Valenzuela, Further developments on non-Newtonian flow in oscillating pipes, Rheol. Acta 17 (6) (1978) 693–697.

Paper VI

Estimation of shear rate change in vertically oscillating non-Newtonian fluids: Predictions on particle settling

Maduranga Amaratunga, H. A. Rabenjafimanantsoa and Rune W. Time

University of Stavanger, Norway.

The paper was published in the *Journal of Non-Newtonian Fluid Mechanics 277: 104236* in 2020.

Journal of Non-Newtonian Fluid Mechanics 277 (2020) 104236

Contents lists available at ScienceDirect

Journal of Non-Newtonian Fluid Mechanics

journal homepage: www.elsevier.com/locate/jnnfm

Estimation of shear rate change in vertically oscillating non-Newtonian fluids: Predictions on particle settling

Maduranga Amaratunga*, Herimonja A. Rabenjafimanantsoa, Rune W. Time

Department of Energy and Petroleum Engineering, University of Stavanger, Norway

ARTICLE INFO

Keywords:
Oscillatory motion
Shear viscosity
Shear rate change
Non-Newtonian fluids
Particle settling

ABSTRACT

This study investigates the effect of oscillatory motion on velocity and shear rate change within different non-Newtonian, slightly viscoelastic fluids oscillated in a vertical U-shaped circular pipe. An estimation to quantify the influence on particle settling in an oscillatory environment is also presented. Flow visualization using particle image velocimetry (PIV) technique was deployed to compare the two-dimensional velocity field in the vertical plane of the U-tube axis and the resulting shear rate change in three different non-Newtonian fluids. The experiments were performed in a 1.2 m high, 50 mm diameter transparent test section, at room temperature (21 ± 0.5 °C) and atmospheric pressure.

A piston was driven at harmonic motion via a gas buffer, to provide the driving force for the test fluids at four different low frequencies ranging from 0.1 – 0.75 Hz and at three different piston oscillation amplitude ratios of $A = a/D = 0.3$, 0.4 and 0.5, where a is the displacement amplitude of the piston and D is the pipe diameter. Oscillatory Reynolds number (Re_δ) based on Stokes layer thickness was used as the criteria for determining the specific flow regime. 36 different experimental cases were tested within the range of $2 < Re_\delta < 34$, and all the experimental cases exhibited the laminar flow regime.

The study reveals that the axial velocity amplitude along the pipe centerline increases with the increasing frequency and with increasing oscillation amplitude irrespective of the non-Newtonian fluid type. The thickness of the shear region decreases with the increase of frequency. The change of shear rate is maximum near the wall region of the pipe and that is achieved at the maximum position of the phase cycle, where the axial velocity also possesses its highest magnitude. The most viscous and the least elastic fluid have reported a maximum reduction of viscosity as an effect of the oscillatory motion and the viscosity reduction becomes insignificant when the non-Newtonian fluids become less viscous.

1. Introduction

Oscillating flow is a special case of pulsatile flow where, the velocity of the flow is varied with time and there is no steady velocity superposed on that [1,2]. Harmonic oscillating flow is the most simple unsteady flow [3] and similar to fully-developed pipe flow, the oscillatory flow in pipes can also be either laminar, transitional or turbulent [4–6]. In industrial applications, the occurrence of any oscillatory motion within a pipe can be characterized as a cause-and-effect relationship where both ways are possible: system vibrations and noise themselves can cause flow oscillations while the flow pulsations can appear in the mode of self-oscillations due to unattenuated local fluctuations.

Many applications can be found where the oscillatory motion and self-induced vibrations could be identified such as blood flow in the large arteries [7], respiratory flow in the trachea [1], oil pressure engineering, reciprocating compressors, gas kicks and pressure oscillations in oil well drilling [8], food transportation [9], etc. Furthermore, oscillatory motion is employed deliberately in many applications such as solid control techniques, situations where an enhancement of heat and mass transfer is expected [10], for stimulation of oil reservoirs [11], design of pumps and other process equipment with transient flow patterns and for treatment of groundwater aquifers contaminated by organic liquids [12], etc.

1.1. Past work regarding the oscillatory flow

Many researchers have investigated this unsteady, oscillatory flows in horizontal ducts and pipes. However, the majority of those studies are hydrodynamic flow regime testing experiments for Newtonian fluids [1,2,5,6,13–17], where they mostly talk about the transition from laminar to turbulent flow regime. In addition to these, Iguchi et al. [14] have considered a free oscillating flow of a viscous Newtonian fluid in a U-shaped tube and developed an analytical representation for the wall shear stress for the case of laminar flow. However, a significant con-

* Corresponding author.
E-mail address: amaratunga.maduranga@uis.no (M. Amaratunga).

https://doi.org/10.1016/j.jnnfm.2020.104236
Received 20 July 2019; Received in revised form 29 November 2019; Accepted 9 January 2020
Available online 22 January 2020

Notations

CMC	Carboxymethyl Cellulose
CLAHE	contrast limited adaptive histogram equalization
DPIV	digital particle image velocimetry
LVE	linear viscoelastic range
NNF	non-Newtonian fluid
PAC	poly-anionic Cellulose
PIV	particle image velocimetry
PIVlab	software tool developed in MATLAB to perform PIV analysis
PL	power-law rheological model
ROI	region of interest
SAOS	small amplitude oscillation shear
a	displacement amplitude
A	amplitude ratio based on the displacement amplitude of the piston
D	diameter of the pipe
De	Deborah number
f	frequency of oscillation, Hz; $\omega/2\pi$
G'	elastic (or storage) modulus
G''	viscous (or loss) modulus
k	non-dimensional phase position; $\omega t/(\pi/4)$
K	consistency index of the non-Newtonian fluid
n	behavior index for the non-Newtonian fluid
r	radial position
R	radius of the pipe
L	entry length for an oscillatory pipe flow
t	time
t_ν	viscous time scale
T	oscillation period
$V(t)$	linear velocity with time in the axial direction at the centerline
$\lvert V\rvert$	velocity amplitude in the axial direction at the centerline, $\lvert V\rvert = \lvert a\rvert\omega$
V_{ave}	cross-sectional average velocity
Re_δ	oscillatory Reynolds number based on stokes layer thickness; $\lvert V\rvert\,\delta/\nu$
Wi	Weissenberg number
Wo	Womersley number

Greek Letters

γ	strain
$\dot{\gamma}$	shear rate
δ	oscillating boundary layer (Stokes layer); $\sqrt{2\nu/\omega}$
δ_{ve}	viscous penetration depth for a viscoelastic fluid
ω	angular frequency; $2\pi f$
ν	kinematic viscosity of the fluid
ϑ	phase shift angle (or loss angle) for the viscoelastic fluid
λ	relaxation time of the viscoelastic non-Newtonian fluid
μ	dynamic viscosity of the fluid
$\lvert\mu^*\rvert$	complex dynamic viscosity
γ_L	limiting value of the shear strain
η	non-dimensional radius; $2r/D$
ρ	density of the fluid
Λ	Stokes parameter
Λ_{ve}	viscoelastic Stokes parameter

tribution could be found in literature where several researchers have employed different non-Newtonian fluids in their studies regarding oscillatory laminar flow. Such studies could be either between infinitely large parallel plates [18] or in a rigid tube of infinite length and circular cross-section [19]. The non-Newtonian fluids used in such studies have different rheological characteristics such as highly viscous and shear-thinning, constant viscosity but elastic (Boger fluids), viscoelastic, etc. For example, Khabakhpasheva et al. [20] have studied the pulsating flow of viscoelastic fluids while Balmer and Florina [21] have studied the same as an inelastic power-law fluid. After the early works of Barnes et al. [22,23] on the effects of pressure gradient oscillations around the non-zero mean in the straight circular pipe, Siginer [24] has provided a very detailed and a comprehensive piece of theoretical work which was useful for the future researchers. Instabilities [25], and nonlinearity [26] have received great attention related to the oscillatory flow of a complex fluid. Theoretical work presented by Rio et al. [27,28] and also the studies on worm-like micellar solutions subjected to pulsating flow [29,30] provide more insight on the oscillatory flow of non-Newtonian fluids in many aspects. Furthermore, the study performed by Mitran et al. [31] on the extensions of the Ferry shear wave model [32,33] and the studies performed by Lindley et al. [34] on the spatial stress and strain distributions of viscoelastic layers in oscillatory shear are also remarkable with this regard. However, the studies on pulsating turbulent flows [35,36] have also become increasingly popular in the recent past.

1.2. Effect of oscillatory motion on non-Newtonian fluids

The oscillatory flow of a non-Newtonian fluid is remarkably different from that of a Newtonian fluid, even at low driving frequencies. Particularly, viscoelastic fluids could exhibit both viscous dissipative behavior of simple fluids and also the elastic response characteristic of solids which originates from the re-orientation and stretching of the fluid molecules. When subjected to oscillatory motion highly viscoelastic non-Newtonian fluids could be resulted in a resonance behavior [37,38] and also with a vortex ring formation [39]. There could be dramatic differences in the dynamic response of a non-Newtonian fluid [27,40–42] compared with Newtonian fluid. As explained in Section 1.1, non-Newtonian fluids that are highly viscoelastic exhibit significant resonance peaks at particular driving frequencies. The shear-induced instabilities in nonlinear complex (viscoelastic) fluids lead to the formation of complex non-symmetric structures by making the vortex structures more unstable at higher driving frequencies and amplitudes. This type of formation of vortex structures or resonance behavior of viscoelastic oscillatory pipe flow systems is highly noticeable in comparison with the purely dissipative response of a Newtonian fluid in the same experimental conditions.

Furthermore, oscillatory motion naturally leads shear-thinning non-Newtonian fluids to experience shear rate related changes in rheological parameters such as shear viscosity, gel formation and extensional viscosity [43], etc. For example, in the drilling industry, the use of primary solids control devices such as shakers leads to an alteration of the rheological properties of the drilling fluids [44]. Most of the water-based drilling fluids usually have a strong gel structure since they possess a high extensional viscosity. According to Saasen and Hodne [44,45], such drilling fluids having high extensional viscosity are generally not that affected by vibrations/oscillations. Furthermore, they explain that oil-based drilling fluids are much more sensitive to the oscillatory effects than water-based drilling fluids. In the concrete industry, the provision of vibrations with the correct amplitude reduces the viscosity of the cement paste [46]. The reason for this type of viscosity change could be explained using the structural units that contain within the polymeric non-Newtonian fluids [47]. These structural units are local agglomerations of particles and polymers that form the viscosity of the fluid. The agglomerations are usually stabilized by the interaction of surface charges of the different particles and when any vibrational field is applied to the fluid, these structural units are partially destroyed and the viscosity is altered.

1.3. Governing non-dimensional parameters for an oscillatory flow

A number of relevant dimensionless parameters that characterize the oscillatory flow at a given driving frequency and amplitude are reported here.

1.3.1. Oscillating Reynolds number (Re$_\delta$)

Many researchers have discussed the extent of laminar to turbulent transition in oscillatory flows [5,15,16,48] with the use of the critical value of oscillatory Reynolds number [1,4–6,14,49] mainly for the Newtonian fluids. The Reynolds number measures the ratio of inertial forces to viscous forces where the oscillating Reynolds number (Re_δ) based on the Stokes boundary layer thickness (δ) is [1,50];

$$Re_\delta = \frac{|V|\delta}{\nu} \tag{1}$$

Here, $|V| = |a|\omega$ is the amplitude of the centerline velocity in the axial direction, a is the displacement amplitude, $\omega = 2\pi f$, where f is the frequency of oscillation and ν is the kinematic viscosity of the fluid concerning within the circular pipe. This Stokes boundary layer or the viscous penetration depth is defined as [1];

$$\delta = \sqrt{\frac{2\nu}{\omega}} \tag{2}$$

It is to be noted that, δ is particularly defined for a Newtonian fluid where transverse oscillations are therefore overdamped (cannot propagate into the fluid). However, since things are different for viscoelastic non-Newtonian fluids, this special notion has been successfully extended to adapt for the simplest viscoelastic fluid (a Maxwell fluid) as described in Section 1.3.4.

In literature, different researchers have used different terminology to define this oscillatory Reynolds number [4,20,25,51] and thus the critical value where the transition from laminar to turbulent flow takes place. Taking into consideration all the different literature vales, authors have concluded that, $Re_\delta = 500$ (based on viscoelastic Stokes boundary layer which will be defined later in this paper) is to be considered as the critical Reynolds number for this study of oscillatory flow in a vertical pipe. The evaluation of the Reynolds number for the different cases of this study is mentioned under Section 3.2.1.

1.3.2. Womersley number (Wo)

It is a measure of the ratio of the pipe radius to the distance through which vorticity diffuses away from the wall in one period of oscillation [52]. It was introduced by Womersley [53]. It is the basic parameter of an oscillatory flow (sometimes referred to as the "non-dimensional frequency" [13,52] and can be expressed as [48];

$$Wo = \frac{D/2}{\sqrt{\nu/\omega}} \tag{3}$$

It is claimed that increasing (Wo) should lead to a stable state of the flow if Re_δ is held constant [1].

1.3.3. Stokes parameter (Λ)

The Stokes parameter measures the ratio of the pipe radius ($R = D/2$) to the viscous penetration depth (δ) for oscillatory viscous flow in a pipe. Thus, Λ can be expressed as [2,5];

$$\Lambda = \frac{D/2}{\delta} = \frac{D}{2}\sqrt{\frac{\omega}{2\nu}} \tag{4}$$

Here, Λ is defined based on δ for a Newtonian fluid and relevant adaptations for a non-Newtonian fluid are explained in Section 1.3.4.

1.3.4. Deborah number (De)

This is one of the main dimensionless parameters to describe the flow of any non-Newtonian viscoelastic fluid. For a simple viscoelastic fluid (a Maxwell fluid), since the stress relaxation can be described by a single time constant which we call the relaxation time (λ) of the fluid, it has been employed in defining the non-dimensional parameters related to non-Newtonian oscillatory flows. De is the measure of the relative importance of the relaxation time (λ) of any viscoelastic fluid to the scale of the flow which is the same as the characteristic time or the oscillation period ($T = \frac{2\pi}{\omega}$) for the deformation process [54]. De can be expressed as;

$$De = \frac{2\pi\lambda}{T} = \lambda\omega \tag{5}$$

As explained in Section 1.3.1, since the behavior of non-Newtonian fluids are different from that of simple dissipative Newtonian fluids, the viscous penetration depth for a viscoelastic fluid (δ_{ve}) is expressed as [55];

$$\delta_{ve} = \delta\left(De + \sqrt{1 + De^2}\right) \tag{6}$$

It is clear that the difference between Eqs. (2) and (6) is imposed by the elasticity of the fluid ($De > 0$), so that the transverse oscillations can effectively propagate before they are attenuated.

Furthermore, the viscoelastic Stokes parameter (Λ_{ve}) can be expressed as [55];

$$\Lambda_{ve} = \frac{R}{\delta} \tag{7}$$

In analogy to Λ, the parameter Λ_{ve} is the ratio of the radius to the extension of the shear waves generated by the pipe walls. In the theoretical analysis performed on the laminar oscillatory flow of Maxwell and Oldroyd-B fluids, Casanellas and Ortin [55] characterize the non-Newtonian oscillatory systems into two main categories as; (1) 'narrow' systems for $\Lambda_{ve} < 1$, when viscoelastic shear waves extend through the whole system and (2) 'wide' systems for $\Lambda_{ve} > 1$, when an inviscid core is present at the center of the pipe.

1.3.5. Viscous to relaxation time ratio

This is another important non-dimensional parameter that characterizes the flow of any non-Newtonian viscoelastic fluid. The viscous time scale (t_v) to relaxation time ratio is expressed as;

$$\text{Viscous to relaxation time ratio} = \frac{t_v}{\lambda} = \frac{R^2/\nu}{\lambda} \tag{8}$$

Following a similar characterization method, Casanellas and Ortin [55] state that, at $t_v/\lambda << 1$ (where highly viscoelastic fluids are oscillated in narrow tubes) the resonant behavior could occur. At $t_v/\lambda = 1$ the velocity magnitude at the center is strongly decreased and for $t_v/\lambda >> 1$ the resonances could completely disappear.

1.3.6. Weissenberg number (Wi)

The ratio of the relaxation time of the fluid to the characteristic inverse shear rate is defined as the Weissenberg number. Wi is expressed as [54];

$$Wi = \lambda\dot{\gamma} \tag{9}$$

Here, $\dot{\gamma}$ is the shear rate and can be calculated as is the relative velocity of two fluid layers moving with respect to each other [56,57] and is expressed as;

$$\dot{\gamma} = \frac{dV}{dr} \tag{10}$$

where, r denotes the radial distance. A value of higher Wi indicates the elastic stresses become large and the onset of elastic instabilities.

1.4. Measurements using PIV technique

Particle image velocimetry (PIV) technique is a non-intrusive optical technique, which has been used widely in literature to visualize the two-dimensional velocity distributions [58]. The non-intrusivity of the PIV technique is important in investigating scientific and engineering applications when it is necessary to avoid disturbances to the flow itself. Even though PIV has been employed in the measurement of single-phase flows in many research studies since the 1970s, it has only recently been applied in oscillatory flows [25,50]. Trip et al. [17] have utilized the PIV technique extensively to investigate how the critical Reynolds number is affected by different pulsatile conditions in horizontal pipe flow and on

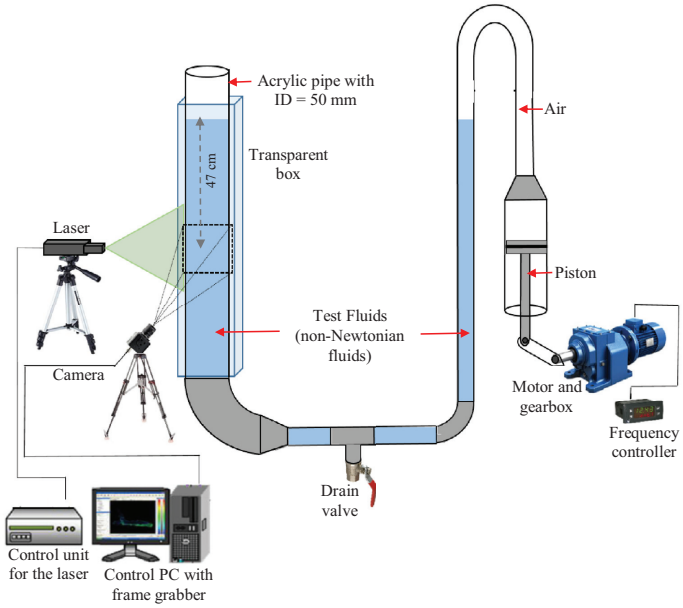

Fig. 1. Sketch of the experimental setup.

the transition to turbulence. Based on the experimental study performed by Amaratunga et al. [57] on the horizontal oscillatory motion of a fluid medium in a vertical rectangular column, the influence of oscillatory motion on the dynamic velocity profiles in non-Newtonian drilling fluids is discussed together with the influence on particle settling. The PIV technique has been used by Blythman et al. [59] to characterize the dependence of wall shear stress and pressure gradient with frequency for oscillatory flow in a two-dimensional rectangular channel. The study performed by Torralba et al. [42] using PIV to present dynamic velocity profiles in a Newtonian and a viscoelastic Maxwell fluid driven by an oscillating pressure gradient in a vertical cylindrical pipe seems to render some valuable input for this current investigation.

1.5. Objective and scope of the study

It has been identified that the free oscillating flow in a U-shaped tube is a fundamental and generic flow setup to study the various types of unsteady motion of fluids [14]. However, the present study is employed with a piston-driven forced oscillation having the objective of obtaining a better visual picture of the phenomena occurring in oscillatory flow in a vertical pipe system.

There are several studies in the literature that depicts the macroscopic manifestations, such as the changes in flow properties flow enhancements [60], etc. impacted by vibrations and oscillations on non-Newtonian liquids. However, neither the effect of oscillatory flow on non-Newtonian fluid rheology nor the impact on particle settling is fully understood in highly reversed flows like those investigated in this study. This paper focuses on utilizing PIV to visualize the oscillatory flow in a more quantitative and systematic manner. It describes how the shear-thinning non-Newtonian drilling fluid rheological properties alter when they are exposed to oscillatory motion within a pipeline and predicts the consequences on particle settling. This investigation is partly motivated by challenges associated with operational procedures during drilling and maintenance of petroleum wells and it is also part of a comprehensive study aimed at investigating the influence of low-frequency oscillations on particle settling in non-Newtonian drilling fluids.

2. Methodology

The experiments were performed in the multi-phase flow laboratory at the University of Stavanger (UiS), Norway.

2.1. Experimental set up

Fig. 1 shows a sketch of the U-shaped experimental set up used for the investigation of the effect of low-frequency oscillatory motion on non-Newtonian fluids. The test section on the left limb of the U-tube has a circular cross-section with an internal diameter of 50 mm and a total length of 1200 mm. The bottom and the right limbs of the U-tube were also circular in cross-section and 30 mm in internal diameter. The whole U-tube including the piston cylinder (with an internal diameter of 50 mm) was made of transparent acrylic for visualization purposes.

Harmonic oscillations were provided by the piston attached to the right limb of the U-tube, which is driven by a motor-gearbox unit. The rotary motion of the gearbox is converted to a reciprocating motion of the piston by mechanically projecting it into the arm of the piston. The revolution speed of the motor (model: 3DF56-2S7032 from ABM Greiffenberger, Germany) and the gearbox from David Brown (Radicon series), UK was controlled by a frequency controller (model: Micromaster 420 from Siemens) in such a way that the required output frequency was set to the piston. A tachometer (model: AT-6 L from Clas Ohlson, Norway) was used to confirm the frequency of the piston. Experiments with four different oscillation frequencies were tested as 0.1, 0.25, 0.5 and 0.75 Hz. Several combinations of the length of the rotating arm allowed

Table 1
Specific details of the polymers and the mixture configuration.

Polymer type	Viscosity at 25 °C	Used weight (g) to dissolve in 5 L of deionized water		
		Fluid 1	Fluid 2	Fluid 3
PolyPAC	800–1200 mPa.s (1% H_2O)	0.5	5	4.5
MV-CMC	400–1000 mPa.s (2% H_2O)	7.5	5	7.5
HV-CMC	1500–3000 mPa.s (1% H_2O)	22.5	5	2.5

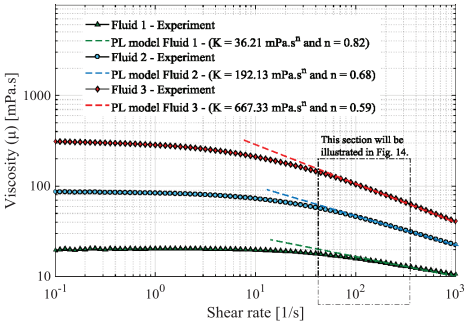

Fig. 2. Viscosity curves for the test fluids at 21 °C.

the oscillating amplitude to be varied as 15, 20 and 25 mm. Out of that, the oscillation amplitude ratio (A) was determined as $a/D = 0.3$, 0.4 and 0.5, where a is the displacement amplitude of the piston and D is the pipe diameter. In order to avoid optical aberrations, the test section was placed inside a second recipient of transparent acrylic, of square cross-section (15 × 15 cm^3), filled with the same deionized water to match the refractive index of the acrylic walls.

2.2. Materials and fluids

Deionized water was used to prepare three polymeric non-Newtonian Fluids (NNF), later referred to as "Fluid 1", "Fluid 2" and "Fluid 3". They are a mixture of three water-based polymers namely Poly-anionic Cellulose (PAC) called PolyPAC-R provided by MI-Swaco, Norway, medium viscous Carboxymethyl Cellulose (MV-CMC) and high viscous Carboxymethyl Cellulose (HV-CMC) provided by Sigma-Aldrich. The specific details of the polymers and the mixture configuration are mentioned in Table 1.

The viscosity of the NNF was measured by Anton Paar MCR 302 rotational rheometer and the rheological properties are described in Section 3.1 with Fig. 2. The density values of the fluids measured using Anton Paar DMA-4500 density meter were 998.26, 999.01 and 1000.13 kg/m^3 for Fluid 1, Fluid 2 and Fluid 3, respectively. All experiments were carried out and liquid properties were measured at room temperature of 21 ± 0.5 °C and atmospheric pressure. Based on these variables, 36 different experimental cases were tested within the range of $2 < Re_\delta < 34$ as shown in Table 2. All the non-Newtonian fluids were assumed to be incompressible.

2.3. The PIV system

2D PIV technique was employed in measuring the velocity fields in a vertical plane, along the symmetry axis of the test limb of the U-tube. The measurement area for the PIV system was centered at 470 mm below the equilibrium air-liquid interface (see Fig. 1), so that the end-effects from the free surface and the bend of the U-tube was minimized.

Table 2
Test matrix.

State variable	Range and unit
Test Fluids	Fluid 1, Fluid 2 and Fluid 3
Oscillation frequencies (f)	0.1, 0.25, 0.5 and 0.75 Hz
Oscillation amplitude ratio (A)	0.3, 0.4 and 0.5 (-)
Measured variables	Velocity from PIV

Replacing δ by δ_{we} accordingly, the present experimental set up has provided sufficient entry lengths from both sides as explained by Gerrard and Hughes [52] and Yamanaka et al. [3] for Newtonian fluids, which is $L = 0.3\ \delta Re_\delta$, where L is meant to be the entry length for an oscillatory pipe flow. A Basler camera (Model: acA800-510um USB 3.0 camera with the ON Semiconductor) with a maximum frame rate of 500 fps at full resolution of 800 × 600 $pixel^2$ was used for the acquisition of images. The images for the PIV analysis were acquired at 200 fps by the camera that was equipped with a Nikon AF Nikkor 50 mm – f/1.4D lens. The images were cropped to a reduced section of 560 × 460 $pixel^2$ to fit the view of interest. The measurement area of the PIV system was illuminated with a Photop LDC-2500S continuous-wave laser (class 3B) at wavelength 532 nm (green light spectrum) and variable output up to 200 mW. The thickness of the laser beam was set to approximately 1 mm using a lens and the collimator system. The laser sheet was aligned such that it illuminates the vertical plane through the center of the pipe (see Fig. 1). In order to illuminate the fluid motion, Polyamide seeding particles were used (Model: PSP50, Dantec Dynamics), with mean particle diameter = 50 μm and specific density = 1.03 g/m^3 as the tracer particles. The Stokes number (Stk) for the seeding particles were approximately $5.5 \times 10^{-4} \ll 0.1$ and the settling speed of the seeding particles are very small, typically less than 10^{-7} m/s. The change of rheology of the test fluids due to the addition of seeding is negligible. The results were acquired after allowing the system to oscillate at least for 1 min to achieve a stable periodic motion up and down.

2.3.1. Data treatment and analysis

The PIV analysis was performed using PIVlab – version 2.01 [61], which is a digital particle image velocimetry (DPIV) tool developed in MATLAB. A region of interest (ROI) that was limited to the pipe cross-section rather than the entire image was selected. Also, the size of the smallest interrogation area for the present analysis was selected as 16 × 8 pixels based on the guidelines provided by Jensen [62]. All the images were pre-processed using contrast limited adaptive histogram equalization (CLAHE) method and some of the background noise was removed using high-pass filter. For the PIV settings, a FFT window deformation was adopted as explained by Thielicke and Stamhuis [61]. The axial velocity component of the vertically oscillating fluid medium along the centerline of the pipe and along the diameter of the pipe was distinguished separately from the velocity magnitudes obtained from PIV analysis for further processing.

3. Results and discussion

The significance of the different fluids selected for this study in a rheological context is described in the following section. In particular,

Table 3
Rheological parameters for the test fluids.

	K (mPa.s^n)	n (-)	λ (s)
Fluid 1	36.21	0.82	0.037
Fluid 2	192.13	0.68	0.021
Fluid 3	667.33	0.59	0.016

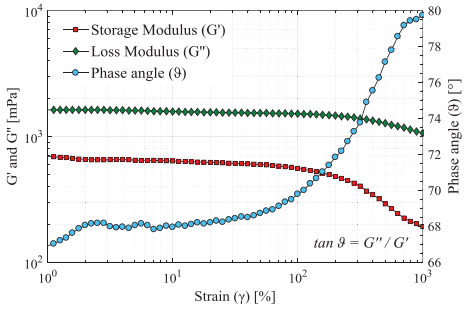

Fig. 3. Amplitude sweep test for Fluid 3 at a constant angular frequency of $\omega = 10$ rad/s.

this regards how local velocity and the corresponding shear rate vary with different oscillatory conditions.

3.1. Rheology of non-Newtonian fluids

The rheological properties of the non-Newtonian fluids were measured by a modular compact rheometer (Anton Paar – MCR 302), using the concentric cylinder configuration (CC27). Fig. 2 shows the dynamic viscosity (μ) curves for the all the three fluids used in the experiment, together with their corresponding power-law parameters. The power-law rheological model was used to model the viscous and the shear-thinning behavior of the test fluids as shown in Eq. (11);

$$\mu_{PL} = K\dot{\gamma}^{n-1} \tag{11}$$

Here, μ_{PL} is the viscosity predicted by the power-law model, K is the consistency index, n is the behavioral index and $\dot{\gamma}$ is the shear rate. The parameters for the model are mentioned in Fig. 2 and also summarized in Table 3.

The shear-thinning behavior of the test fluids can be easily distinguished from the viscosity curves where Fluid 3 is the most shear-thinning fluid with the lowest n value. It is to be noted that, the power-law model has been applied only for the linear region of the experimental viscosity data and that does not cover the constant viscosity plateau observed in the low values of shear rate. The highlighted section will be further illustrated in Fig. 14, in Section 3.4.2.

The viscoelastic properties of the test fluids were also measured in small amplitude oscillation shear (SAOS) tests as part of the rheological investigation. In order to determine the linear viscoelastic (LVE) region at low strain amplitudes, and also to investigate the viscoelastic behavior of the samples, strain amplitude sweeps and frequency sweeps were conducted. Fig. 3 shows the results of the amplitude sweep test only for Fluid 3, over a given strain (γ) range. It was ramped up logarithmically from 1 to 1000%, at a constant angular frequency of $\omega = 10$ rad/s.

It can be observed that the viscous (same as loss) modulus (G'') of Fluid 3 is larger than its elastic (or storage) modulus (G'), and the calculated phase angle (ϑ) is varying from approximately 65° to 80°. The variation of moduli curves for the two other test fluids also shows a similar trend, where there is no crossover point between the moduli curves.

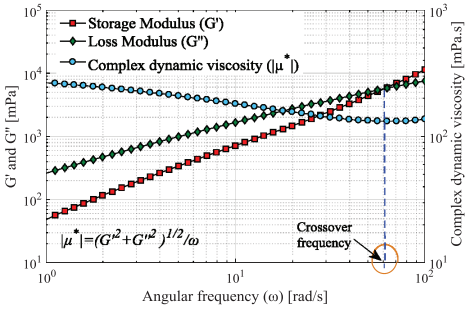

Fig. 4. Frequency sweep test for Fluid 3 at a constant strain at $\gamma = 1\%$.

Therefore, it could be concluded that all three test fluids are slightly viscoelastic at the corresponding low shear region. The G' curve for Fluid 3 starts to lose its plateau value at around 10% of shear strain which corresponds to a shear rate value of $\dot{\gamma} = 1$ 1/s. That is identified as the limiting value of the shear strain (γ_L) for Fluid 3 which defines the LVE range. Other test fluids have shorter LVE ranges than Fluid 3 where Fluid 1 has the shortest with its G' starts to decrease at much lower strain around ($\gamma < 2\%$).

The viscoelastic property of any polymer solution in its LVE range is reflected in the frequency sweep data, which can be used to investigate the time-dependent deformation behavior of any sample. It is a direct measure of elasticity [63]. Fig. 4 shows the results of the frequency sweep test for Fluid 3 over a given angular frequency (ω) range (ramped down logarithmically from 100 to 1 rad/s) at a constant strain 1%.

It can be seen from Fig. 4 that, both the elastic and the viscous moduli increase when the frequency is increased. However, the elastic modulus (G') increases faster than the viscous modulus (G'') and the solid-like behavior of the fluid becomes dominant after the crossover frequency as illustrated in Fig. 4. The inverse of this crossover frequency represents the longest characteristic relaxation time (λ) of the polymer solution [64] and the corresponding λ values for the three fluids are mentioned in Table 3. According to the values presented in Table 3, it can be observed that Fluid 1 has the highest relaxation time of the test fluids and therefore has the highest elasticity. Since the λ values are very small, it could be concluded that the test fluids are only slightly viscoelastic. All the aforementioned rheological properties were measured just after the corresponding experimental run.

3.2. Axial velocity variation at the pipe centerline

The characteristic driving sinusoidal harmonic motion was identified by determining the axial velocity along the centerline of the pipe. The centerline is the best location to identify the maximum up and down motion of the fluid with the least possible viscous and wall effects. Fig. 5 presents the axial velocity profiles of Fluid 1 and 2, along the pipe centerline when they are oscillated at a frequency of 0.75 Hz and at a piston amplitude ratio (defined previously) of $A = 0.5$. The axial velocity at the pipe centerline shown in Fig. 5 is used as a basis to introduce the notation system adopted by the authors to discuss the results in the latter part of this paper.

The phase position/angle (ωt) was made dimensionless using the angle value ($\pi/4$), and the value for $\omega t/(\pi/4)$ has been utilized in presenting and discussing further results. Qualitatively, the periodical shape of the curves obtained from the PIV measurements confirms the successful transmission of energy from the mechanical piston to the fluid system via the gas buffer in between them. The quantitative description of the

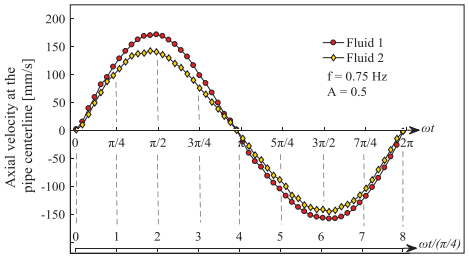

Fig. 5. Introduction of the different phase positions within the phase cycle based on centerline axial velocity.

Table 4
De for the test fluids and different driving frequencies.

	f_1	f_2	f_3	f_4
F 1	0.0229	0.0575	0.1149	0.1724
F 2	0.0132	0.0329	0.0658	0.0987
F 3	0.0103	0.0258	0.0517	0.0775

*F 1, F 2 and F 3 represent Fluid 1, Fluid 2 and Fluid 3 respectively. f_1, f_2, f_3 and f_4 represent the frequency values of 0.1 Hz, 0.25 Hz, 0.5 Hz and 0.75 Hz, respectively.

different velocity curves plotted in Fig. 5 is provided in Section 3.2.3. However, the asymmetry of the axial velocity between the first and second half of the cycle for Fluid 1 demonstrates some local friction exerted on the piston motion especially on its decelerating phase.

3.2.1. Evaluation of the flow field associated with the experiments

Based on the rheological characterization provided in Section 3.1, the test fluids are slightly viscoelastic and show power-law characteristics in their linear region. First, they are evaluated for their *De* (= $\lambda\omega$) based on the oscillation frequency and values are reported in Table 4.

All the values for the calculated *De* are less than unity and not large enough for resonances to occur [25]. According to Casanellas and Ortin [55], these small *De* make the attenuation length of the viscoelastic waves essentially identical to their wavelength and the oscillating boundary layer of these fluids could be mostly similar to that of a Newtonian case without resonances.

In addition to *De*, it is useful to evaluate the viscoelastic Stokes parameter (Λ_{ve}) for the experimental cases to get a better understanding of the oscillating system in concern. According to Eq. (6), it can be easily understood that the viscous penetration depth for viscoelastic fluids is greater than that of Newtonian fluids because of the presence of relaxation time (λ) in viscoelastic fluids. To illustrate the difference, we consider the ratio of Stoke parameters for both Newtonian and viscoelastic fluids as;

$$\frac{\Lambda}{\Lambda_{ve}} = \frac{R/\delta}{R/\delta_{ve}} = \frac{\delta_{ve}}{\delta} \tag{12}$$

and Fig. 6 shows a plot of δ_{ve}/δ as a function of *De* for the driving frequencies and test fluids concerned within this study.

According to Fig. 6, it can be seen that δ_{ve}/δ (similar Λ/Λ_{ve}) is increasing linearly with *De* and is always greater than unity for all the driving frequencies of this study. It confirms the fact depicted by Eq. (6) also that the viscous penetration depth for viscoelastic fluids is greater than that of Newtonian fluids because of the presence of relaxation time in viscoelastic fluids. Since the test fluids concerned within this study are slightly viscoelastic, it can be seen that δ_{ve}/δ is just over unity, but still it is increasing with *De*. However, since $\Lambda_{ve} > 1$ for all the test cases, the system could be considered as a 'wide' system according to Casanellas and Ortin [55].

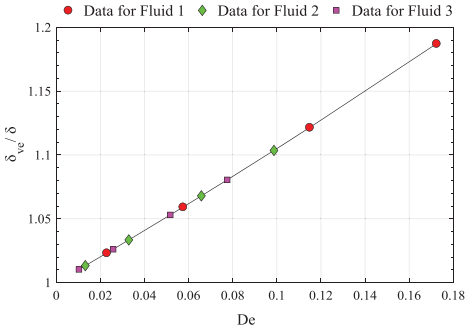

Fig. 6. Variation of δ_{ve} with respective to δ at different *De*.

Furthermore, with the introduction of experimental setup length (which is the pipe radius in our case), the ratio of viscous time scale to the relaxation time scale (t_v/λ) is calculated for further characterization of the experimental system. Fig. 2 showed that all the test fluids are shear-thinning non-Newtonian fluids and they have a shear rate dependent viscosity. Since $\dot{\gamma} = 100$ 1/s represents the shear rate value within a typical drilling pipe [65], the shear viscosity value of each test fluid corresponding to $\dot{\gamma} = 100$ 1/s has been utilized in the calculation of t_v/λ. For the test fluids and conditions considered, the ratio of viscous to relaxation time yields 1072.8 for Fluid 1, 646.9 for Fluid 2 and 361.9 for Fluid 3, which are greatly larger than the unity. Therefore, the possibilities of occurring resonance are disappeared while the system can be considered as a 'wide' system where the oscillation takes place comparably in a large geometry ($D = 50$ mm) and the flow in the central core could be inviscid [55].

However, the differences in piston driving amplitude and the consequences of that were not taken into account in the above non-dimensional parameter evaluations. Therefore, in order to identify the flow features more precisely, it is important to determine the correct hydrodynamic flow regime which each experimental case belongs to. Table 5 reports the Reynolds number values for all the experimental cases of this study. The oscillating Reynolds number (Re_δ) based on viscoelastic Stokes boundary layer (δ_{ve}) is used for this determination as depicted by Eq. (6). Similar to that used in t_v/λ calculation, the shear viscosity value of each test fluid corresponding to $\dot{\gamma} = 100$ 1/s was employed. Further, the maximum velocity amplitude values reported in Section 3.2.3 have been utilized for the calculations.

It is to be noted that the calculated Re_δ is based on the PIV measurements performed through the fixed observation window centered 470 mm below the equilibrium air-liquid interface (see Fig. 1). This is the optimal location in the vertical test section to minimize the end and entrance effects in the pipe. According to Torralba et al. [42], Re_δ could have been even lower if the measurement was carried out closer to the air-liquid interface. Therefore, based on these calculations, it can be concluded that all the experimental cases belong to the laminar regime and also the nonlinearities of the oscillating flow is due to the rheological properties of the fluids and not due to the inertial effects. Even if the decrease in viscosity due to the shear-thinning is considered, they are well within the laminar regime.

3.2.2. Temporal evolution of the axial velocity distribution along the pipe diameter

The primary data for PIV measurements in the form of instantaneous velocity fields for some specific positions of the phase cycle are presented in Fig. 7. It is to be highlighted that, the velocity profiles are drawn based on the centerline axial velocities of Fluid 2 only which is

Table 5
Oscillating Reynolds number (Re_δ) values for all the experimental cases.

	A_1				A_2				A_3			
	f_1	f_2	f_3	f_4	f_1	f_2	f_3	f_4	f_1	f_2	f_3	f_4
F 1	5.27	9.52	14.93	20.31	6.95	12.45	19.99	27.18	9.52	15.56	23.23	33.06
F 2	2.99	5.39	7.45	10.46	4.29	6.98	10.17	14.04	4.39	7.23	11.99	15.12
F 3	–	2.91	4.73	6.202	2.47	3.94	6.25	8.330	2.76	4.26	8.80	11.12

*F 1, F 2 and F 3 represent Fluid 1, Fluid 2 and Fluid 3 respectively. f_1, f_2, f_3 and f_4 represent the frequency values of 0.1 Hz, 0.25 Hz, 0.5 Hz and 0.75 Hz, respectively. A_1, A_2 and A_3 represent the amplitude ratio values of 0.3, 0.4 and 0.5, respectively.

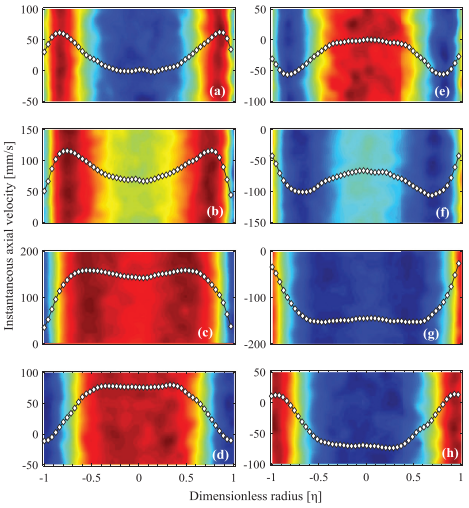

Fig. 7. Instantaneous axial velocity distribution profiles of Fluid 2 with time and phase position at $f = 0.75$ Hz and $A = 0.5$ (a) $k = 0$; (b) $k = 1$; (c) $k = 2$; (d) $k = 3$; (e) $k = 4$; (f) $k = 5$; (g) $k = 6$; (h) $k = 7$ (* The color scale for each subfigure is defined by the magnitude of each plot itself – vertical axis).

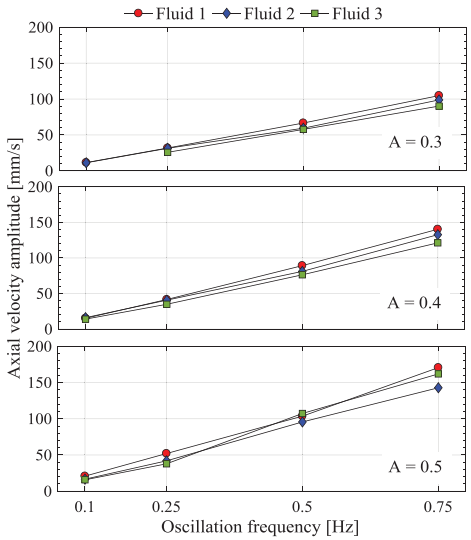

Fig. 8. Axial velocity amplitude variation with different non-Newtonian fluids for different piston amplitude ratios.

oscillated at $f = 0.75$ Hz and $A = 0.5$. The non-dimensional phase position $\omega t/(\pi/4)$ has been denoted as k in the figure caption.

The presented axial velocity profiles seem to be somewhat irregular in shape but almost symmetrical along the pipe centerline. For a fully established steady-state laminar flow, the profile would be parabolic throughout the whole pipe cross-section. However, due to the continuing oscillations and also the highly reversing nature of the flow in the present study, the velocity profile is deviated from the parabolic shape in most of the phase positions and at certain instants with minor similarities to a parabolic shape in the core region of the pipe. At the stage of flow reversal it was observed that while the net axial velocity profile remains positive in the core region, some part of the velocity profile seems to be negative (returns) in a very small region near the wall. This is basically due to the complex structure of the non-Newtonian fluids and even though they are only slightly viscoelastic, they exhibit annular regions within the pipe with alternating upward/downward motion. The thickness of this shear region decreases with increasing frequency. The axial velocity in the shear region either lags or leads the axial velocity in the central region by a small amount, which tends to zero at certain positions of the phase cycle.

As expected, the centerline axial velocity varies periodically in magnitude and direction following the pattern of the imposed oscillations. At higher frequencies, there is an extensive region in the center of the fully developed flow in which vorticity is very small, that is, where the velocity is almost independent of the radial position. The color theme used in the background of the PIV image shown in Fig. 7 illustrates this significance of shear forces. For the non-Newtonian fluid where the effect of wall shear is propagating towards the central axis of the pipe and as a result, different color regions have appeared. However, it is somewhat deviating from the theoretical idea presented in Section 1.3.4 for the system to be 'wide' and the flow in the central core is inviscid. This deviation could be attributed to the highly reversing nature of the system and also to the presence of a compressible air pocket in between the fluid and piston arrangement.

It could be seen from Fig. 7(c) and (g) that, when the piston is at its equilibrium position (where the flow velocity is maximum or minimum), the flow velocity outside the Stokes layer has a Poiseuille velocity profile with different peak velocity magnitudes depending on the frequency.

3.2.3. Velocity amplitude variation based on centerline axial velocity

Since Fig. 7 shows the radial velocity variation only for a single experimental case, it is important to investigate how the amplitude of velocity is varying in non-Newtonian fluids with different n values (or polymer concentrations) and with different oscillatory conditions. Fig. 8

compares the velocity amplitude achieved by the liquid medium (at the location of PIV measurements) for different frequencies and at different piston displacement amplitudes. Furthermore, it depicts the impact of the different non-Newtonian fluids on the velocity amplitude.

According to Fig. 8, it can be clearly seen that the axial velocity amplitude along the centerline of the pipe increases with the increasing frequency irrespective of the displacement amplitude of the piston and the fluid type. This can be explained as follows: when the oscillation frequency is increased for fixed piston amplitude, the momentum transfer from the piston to the liquid via the air-buffer is increased and the kinetic energy achieved by the fluid system is also increased. When the kinetic energy of the fluid system is increased, the viscous resistance of the fluid medium reduces and hence the velocity amplitude is increased. A similar scenario could be observed with respect to the displacement amplitude ratios, where the magnitude of the velocity amplitude of the liquid medium increases with increasing piston amplitude ratio.

It is also interesting to see the effect of different shear-thinning non-Newtonian fluids on the nonlinearities of the non-Newtonian liquid medium in terms of the achieved velocity amplitude. It can be observed from Fig. 8 that, when n decreases (or the fluid becomes more viscous) the achieved velocity amplitude of the liquid medium is decreased for a particular piston displacement amplitude ratio and frequency. This situation was visible at all the experimental conditions with a small deviation at $A = 0.5$. This could be attributed to the increased viscous resistance exerted by the non-Newtonian fluids that act as a negative impact on particle settling in drilling fluids by increasing the drag force.

However, to reveal the nonlinearities caused by shear thinning more evident, the axial velocity amplitudes presented in Fig. 8 have been normalized by the piston velocity amplitude and calculated as a velocity amplitude ratio (β) which can be expressed as;

$$\beta = \frac{\text{Axial velocity amplitude of the liquid medium}}{\text{Velocity amplitude of the piston at the particular driving conditions}} \tag{13}$$

The β values at different driving frequencies are presented in Fig. 9. Here, the axial velocity amplitude of the liquid medium is obtained from the PIV measurements and the piston velocity amplitude is calculated as the product of a and ω.

According to Fig. 9, for all the three non-Newtonian fluids, the β values for the first two piston (displacement) amplitude ratios ($A = 0.3$ and 0.4) are almost the same for all the driving frequencies. That implies the absence of nonlinearities in between the first two lower driving amplitudes studied here. However, at higher driving amplitudes, the β values are deviated from the other two, revealing the nonlinearity caused by the shear-thinning of the non-Newtonian fluids. All the experimental cases except a couple of low-frequency cases show an increment of β value with the increased driving frequency.

3.3. Cross-sectional average velocity distribution

As explained by Amaratunga et al. [50], the instantaneous velocity field of a Newtonian fluid has the same sign everywhere within its spatial domain. However, for the non-Newtonian fluids (even for slightly viscoelastic fluids as investigated in this study), the flow resolves into annular regions of alternating upward and downward motion. It is important to know that these annular regions are separated by quiescent boundaries where the shear stress reaches local maxima. This could be easily seen from Fig. 7. Since the velocity distribution of non-Newtonian fluids can take several shapes, either parabolic or the so-called 'Mexican hat type', the individual axial velocity components along the radial distance and also the magnitude of the velocity amplitude do not provide a clear picture about the correct distribution of the velocity across the cross-section. Therefore, a new parameter called the cross-sectional average velocity (V_{ave}) [1] can then be defined for a pipe flow in a circular

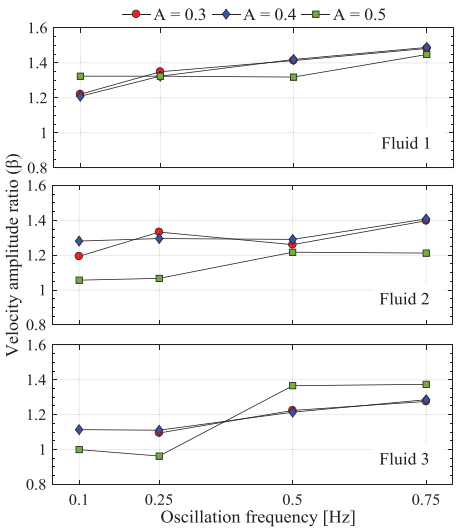

Fig. 9. Velocity amplitude ratio (β) for different non-Newtonian fluids at different oscillating conditions.

cross-section as;

$$V_{ave} = \frac{1}{\pi R^2} \int_0^R V(r).\, 2\pi r.dr \tag{14}$$

where r is the radial position between 0 and R. By calculating the cross-sectional average velocity as given by Eq. (14) it allows us to obtain an indication of how the bulk velocity at that particular moment of time is established both qualitatively (direction-wise) and quantitatively. For instance, even the axial velocity is showing a higher positive magnitude in a case of a non-Newtonian fluid, the magnitude close to the shear region may have achieved two negative peaks in axial velocity which reduces the overall cross-sectional average velocity and results with a lower value. In order to illustrate this better, the instantaneous velocity amplitudes (V) at specific positions of the phase cycle have been normalized by the calculated cross-sectional average velocity (V_{ave}) as;

$$\text{Normalized axial velocity} = \frac{V}{V_{ave}} \tag{15}$$

Fig. 10(a) and (b) show the normalized axial velocity for six different test cases where the phase positions are based on the notation plot presented in Fig. 5. Here, the V_{ave} is calculated based on the instantaneous axial velocities along the radial distance of the pipe.

The normalized axial velocity values of all the six test cases depict the periodical structure of the flow due to the oscillatory motion where $\omega t/(\pi/4) = 2$ and $\omega t/(\pi/4) = 6$ are the closest to unity. It means that at $\omega t/(\pi/4) = 2$ and 6, the instantaneous velocities along the radial direction manifest a profile close to parabolic and they are almost unidirectional without having any alternating upward and downward motions among the small annular regions. According to Fig. 10(a), it can be seen that V_{ave} is increasing and hence the normalized axial velocity is decreasing with the increasing displacement amplitude ratio of the piston for the same fluid type. This could be attributed to a low degree of fullness in its own profile, and deviation from the parabolic shape is considerable at lower piston amplitude ratio (A) values. It can be observed that the magnitude of V_{ave} is increased with increasing frequency

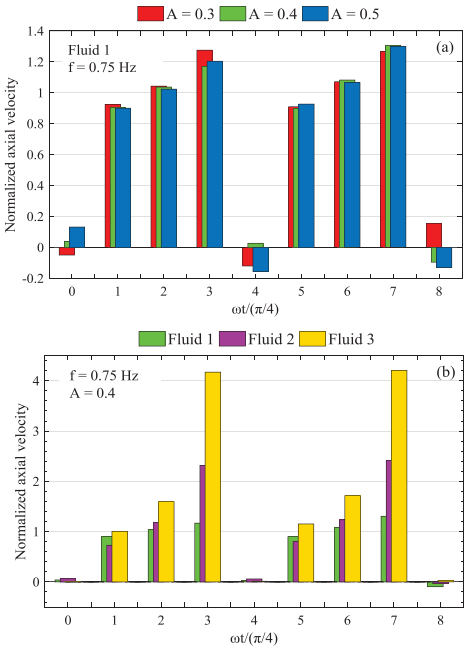

Fig. 10. Comparison of normalized axial velocity at (a) different driving amplitude ratios, but same fluid type (b) different non-Newtonian fluids, but the same driving amplitude.

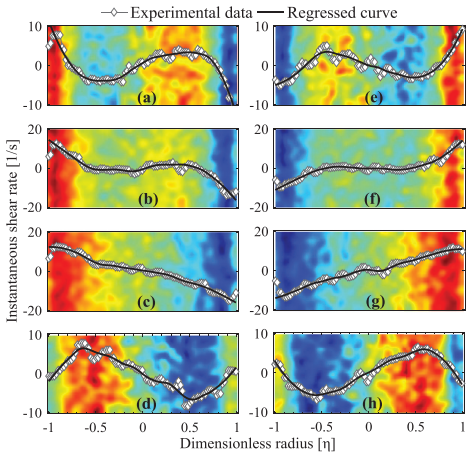

Fig. 11. Change of instantaneous shear rate for Fluid 3 with the phase position at $f = 0.75$ Hz and $A = 0.5$ (a) $k = 0$; (b) $k = 1$; (c) $k = 2$; (d) $k = 3$; (e) $k = 4$; (f) $k = 5$; (g) $k = 6$; (h) $k = 7$ (* The color scale for each subfigure is defined by the magnitude of each plot itself – vertical axis). (For interpretation of the references to color in this figure legend, the reader is referred to the web version of this article.)

irrespective of the type of fluid. However, according to Fig. 10(b), it can be further confirmed that, when the flow behavior index (n) value of the non-Newtonian fluid is decreasing, the fluid becomes more viscous and the normalized axial velocity is increasing at all the phase positions for a particular amplitude ratio. The explanation is that when the fluid viscosity and hence friction increases, the uneven distribution of the velocity profile becomes more pronounced. Therefore, V_{ave} becomes lower for the highly viscous fluids compared to that of low viscous fluids, which results in an increment of the normalized axial velocities.

3.4. Variation of the shear rate due to oscillatory motion

One of the main objectives of this study is to investigate how the shear rate is varying in the presence of oscillatory motion. The shear rate was defined in Eq. (10), linked directly to the velocity gradient [57]. It is obvious here that, unlike in conventional unidirectional steady pipe flow, unsteady oscillatory pipe flow undergoes flow reversals continuously and thus the axial velocity is varying both in magnitude and direction. Thus, the shear rate is time-varying and effects from that become more pronounced for non-Newtonian fluids.

In the following section, we try to evaluate and illustrate the impact of the oscillatory motion of a shear-thinning non-Newtonian fluid on the shear rate. Fig. 11 shows how the instantaneous shear rate of Fluid 3 is varying along with the radial position when the fluid undergoes through the different positions of the phase cycle oscillating at $f = 0.75$ Hz and $A = 0.5$. For illustration purpose and brevity, only a single test case has been used for this figure, and the raw experimental data has been regressed with a R^2 value greater than 95% for clarity. The non-dimensional phase position $\omega t/(\pi/4)$ has been denoted as k in the figure caption.

According to the profiles shown in Fig. 11, it can be seen that there is a significant variation in shear rate throughout the pipe cross-section. This is so important to understand with respect to the particle settling/separation point of view since the variation of rate of shear directly affects the viscosity of the shear-thinning non-Newtonian fluids and consequently on the drag reduction. At phase positions where the velocity profiles show some "Mexican hat" type distribution (see Fig. 7), there seem to be two or three points where the change in shear rate becomes zero. The shear rate profiles are even steeper close to the wall regions in such phase positions such as $\omega t/(\pi/4) = 0$, and 4. When the flow reaches to its maximum phase position where $\omega t/(\pi/4) = 2$ or 6, the distribution of the rate of shear seems to show more or less linear profile from the wall to the center region which makes the settling particles in such a system experience differences in viscosity of the fluid medium. However, the maximum change of shear rate is achieved at the maximum position of the phase cycle ($\omega t/(\pi/4) = 2$ or 6), where the axial velocity also possesses the highest magnitude.

The different PIV generated color patterns in the background of the shear rate profiles shown in Fig. 11 illustrate the shear rate magnitudes for a case of $De = 0.078$ and $\delta_{ve} = 18$ mm. The red color (or dark blue color for the opposite direction) indicates the peak shear region and it could be seen that the wall shear tends to propagate towards the pipe centerline through the oscillation cycle. This experimental observation possesses a deviated behavior from the theoretical explanation provided in Section 1.3.4 regarding the definition of 'wide' systems as explained by Casanellas and Ortin [55]. This could be attributed specifically to the rheological characterization of the test fluids where they are not pure Maxwellian fluids and also to the highly reversing flow phenomena in the experimental setup. The test fluids were slightly viscoelastic according to Section 3.1. Therefore, they neither behave similar to pure Maxwell fluids nor show the properties of pure Newtonian fluids.

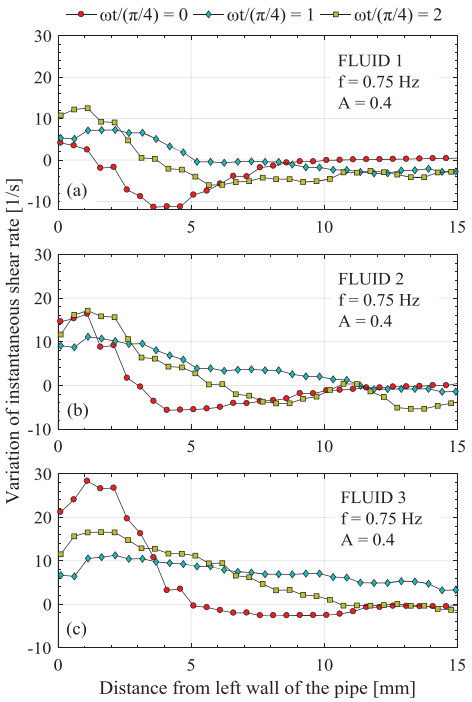

Fig. 12. Instantaneous shear rate profile close to the pipe wall for different non-Newtonian fluids.

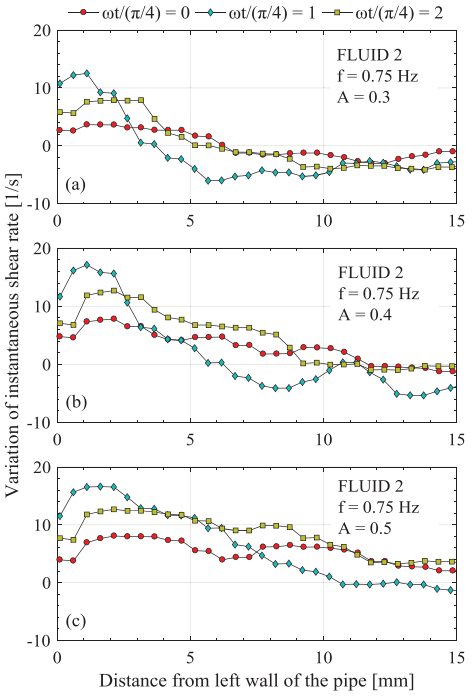

Fig. 13. Instantaneous shear rate profile close to the pipe wall for different oscillation amplitude ratios.

3.4.1. Variation of instantaneous shear rate with different non-Newtonian fluids under different oscillatory conditions

As seen in Fig. 11, the thickness of the shear region is changing through the phase cycle. Since the shear rate change is a key parameter in this study, it is important to check how the shear rate varies with respect to the different non-Newtonian fluids with different viscosities and also with different oscillatory conditions. Fig. 12 illustrates the shear rate profiles with different non-Newtonian fluids with different n values close to the left wall of the pipe, only for three different phase positions.

The shear rate profiles for the presented phase positions in Fig. 12 seem to reach zero with a much shorter distance from the wall for less viscous fluids (with higher n values) compared to that of high viscous fluids (with lower n values). That provides some insight on the thickness of the shear region where it increases with decreasing n value. The thickness of the shear region is estimated by calculating the shear rate from the velocity data obtained from PIV analysis and plotting them in color maps such as shown in Fig. 11. Specifically, at $\omega t/(\pi/4) = 0$, the shear rate variation becomes more significant within the first 5 mm from the wall, for high viscous fluids than that of less viscous fluids. A similar trend could be observed from Fig. 13 which illustrates the shear rate variation close to the left wall of the pipe with different (displacement) amplitude ratios of the piston, only for three different phase positions.

It confirms the fact that the change of shear rate is maximum near the wall region of the pipe. The thickness of the shear region seems to increase with the increasing oscillation amplitude ratio for a particular fluid type. Furthermore, the profile of the shear rate becomes linear with approximately a constant gradient with the increasing oscillation amplitude ratio.

Figs. 12 and 13 show that the influence of the wall (shear layer and resulting shear resistance) on the flow velocity may be considered localized in a near-wall area at a distance of 5 – 10 mm. These shear rate variations greatly affect the viscosity of the oscillating fluid within the pipe and hence influences the solids settling rate significantly.

3.4.2. Predictions on the effect on particle settling/solids control in drilling fluids

Particle settling and solids control is a comprehensive topic when it comes to non-Newtonian fluids for drilling purposes. The removal efficiency of cuttings from the well and also the solids separation efficiency through primary solids control devices are strongly dependent on the properties of the drilling mud that is circulated through the well. According to Saasen and Hodne [45], viscosity profile, gel formation and extensional viscosity of the fluid are the main aspects to this regard. This study also tries to provide a prediction on how viscosity profiles due to the oscillatory motion would influence the particle settling with non-Newtonian fluids. Fig. 14 shows an enlarged section of previously presented viscosity curves of the test fluids in Fig. 2.

It is magnified around $\dot{\gamma}$ = 100 1/s to emphasize the applicability of present experimental results into the practical operating shear rate [65] in a drilling pipe. Based on the shear rate profiles for all the test

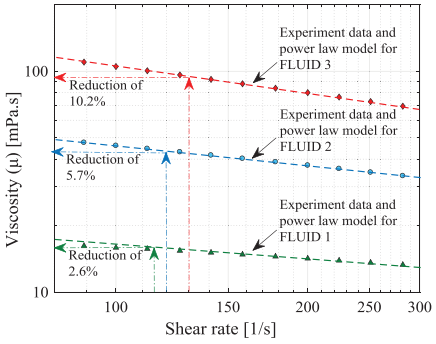

Fig. 14. Illustration of viscosity change due to the variation in shear rate.

cases, the authors have decided to quantify the maximum amount of shear rate change for Fluid 1, Fluid 2 and Fluid 3 to be approximately 15, 20 and 30 1/s respectively. This is slightly less than the reduction approximated by Saasen and Hodne [44] in their experiment, where they have applied the vibration directly to the viscosity measuring cup. With that information, Fig. 14 illustrates how an increment of shear rate (at $\dot{\gamma}$ = 100 1/s) would result in the change in viscosity of the shear-thinning non-Newtonian drilling fluid.

It can be observed from Fig. 14 that a considerable amount of viscosity reduction occurs as a result of the oscillatory motion. The maximum reduction of viscosity has been reported for the most viscous and the least elastic fluid (Fluid 3) and the viscosity reduction becomes insignificant when the non-Newtonian fluids become less viscous. The viscosity of most water-based drilling fluids is formulated by a combination of polymers similar to the test fluids in the current study. In addition, water-based drilling fluids may contain some additives to achieve desired agglomeration effects. However, Saasen and Hodne [45] state that, the structural units and surface charges between those particles in polymeric liquids may get weakened by the oscillations/vibrations and that leads to a reduction of internal liquid viscosity. It is to be noted that the cyclic maximum shear rate change occurs mostly near the pipe wall, and thus the resulting viscosity reduction is more pronounced in the near-wall regions. This explains the fact that, when the shear-thinning non-Newtonian fluids (primarily water-based polymeric liquids) are subjected to oscillatory motion, there will be a substantial reduction of viscosity of the fluid and that will result in the reduction of the drag force on the settling particles and consequently in increased particle settling. It is important to identify that, this increased settling could mostly be expected close to the wall regions and not at the core of the pipe based on the radial shear rate profiles shown in Figs. 12 and 13. This could be contradictory to the typical wall-effects described in many of the particle settling studies performed in quiescent fluid systems. The major difference here is the application of a highly reversing oscillatory flow field and thus a high degree of agitation-disturbance compared to those quiescent Newtonian or non-Newtonian liquid columns.

4. Conclusion

This experimental investigation was carried out to study how the viscous properties of shear-thinning non-Newtonian fluids alter when being exposed to oscillatory conditions. Three different non-Newtonian fluids were tested for four different low frequencies and for three different oscillation amplitudes. The study concludes that;

- PIV is a very good non-intrusive technique to analyze oscillatory flow both for Newtonian and non-Newtonian fluids. It provides insight into the velocity profile at the near-wall regions as well as in the core region. It is fair to say that presently there are no other experimental techniques that can measure velocity profiles with such resolution in space and time. The color maps obtained through PIV analysis are useful in identifying the shear regions and fluctuations in such a study.
- The combined (near wall) shear force and liquid inertia cause the velocity profile to become a complicated radial function quite different from the plug flow imposed by the oscillating piston.
- The thickness of the shear region decreases with increasing oscillation frequency. The axial velocity in the shear region either lags or leads the axial velocity in the central pipe region by a small amount, and tends to be zero at some certain positions of the phase cycle.
- The centerline velocity amplitude increases with increasing frequency and with increasing oscillating amplitude ratio. This is irrespective of the non-Newtonian fluid type.
- With increasing viscosity, the resistance increases and the axial velocity amplitude and V_{ave} reduces. Associated with this the velocity profile becomes more complex and uneven due to the interplay of viscous and inertial forces.
- The change of shear rate is maximum near the wall region and occurs at the maximum position of the phase cycle ($\omega t/(\pi/4)$ = 2 or 6), where the axial velocity is also maximum.
- The shear rate profile becomes linear from the pipe wall to the centerline at the maximum position of the phase cycle ($\omega t/(\pi/4)$ = 2 or 6).
- During low-frequency oscillations, the maximum reduction of viscosity has been reported for the most viscous and the least elastic fluid (Fluid 3). The viscosity reduction becomes insignificant when the non-Newtonian fluids become less viscous.
- The evaluation of the oscillating Reynolds number based on viscoelastic Stokes boundary layer for this particular study revealed that inertia is not responsible for the destabilization of the basic flow and it is basically the viscous forces that dominate within the oscillatory flow system.

Therefore, the presented application of the PIV technique to give velocity distribution and shear rate variation in oscillatory flow in a vertical pipe may bring more detailed information on oscillatory flow characteristics together with a detailed rheological characterization.

Acknowledgment

Authors gratefully acknowledge the Norwegian Research Council for funding this study under the project “NFR Improved Model Support in Drilling Automation”. We appreciate the valuable support provided by Jon Arne Evjenth, from the Department of Energy & Petroleum Engineering at the University of Stavanger in preparing the data acquisition system for the experiments. The advice and encouragement provided by Roar Nybø and Knut S. Bjørkevoll from SINTEF, Bergen are also greatly appreciated.

References

[1] L. Fishler, R. Brodkey, Transition, turbulence and oscillating flow in a pipe a visual study, Exp Fluids 11 (6) (1991) 388–398.
[2] M.Y. Gundogdu, M.O. Carpinlioglu, Present state of art on pulsatile flow theory: part 1: laminar and transitional flow regimes, JSME Int. J. Ser. B Fluids Therm. Eng. 42 (3) (1999) 384–397.
[3] G. Yamanaka, H. Kikura, Y. Takeda, M. Aritomi, Flow measurement on an oscillating pipe flow near the entrance using the UVP method, Exp Fluids 32 (2) (2002) 212–220.
[4] S. Sergeev, Fluid oscillations in pipes at moderate Reynolds numbers, Fluid Dyn. 1 (1) (1966) 121–122.
[5] M. Hino, M. Sawamoto, S. Takasu, Experiments on transition to turbulence in an oscillatory pipe flow, J. Fluid Mech. 75 (2) (1976) 193–207.
[6] M. Ohmi, M. Iguchi, K. Kakehashi, T. Masuda, Transition to turbulence and velocity distribution in an oscillating pipe flow, Bull. JSME 25 (201) (1982) 365–371.
[7] P.R. Hoskins, Estimation of blood velocity, volumetric flow and wall shear rate using Doppler ultrasound, Ultrasound 19 (3) (2011) 120–129.

[8] R.W. Time, A. Rabenjafimanantsoa, On the relevance of laboratory scale rheometric measurements for calculation of complex large scale flows in well drilling and pipe flows, Ann. Trans. Nordic Rheol. Soc. 22 (2013).

[9] S.P. Singh, A.K. Srivastava, J.F. Steffe, Vibration induced settling of a sphere in a Herschel-Bulkley fluid, J. Food Eng. 13 (3) (1991) 181–197.

[10] Y. Su, J.H. Davidson, F. Kulacki, Fluid flow and heat transfer structures of oscillating pipe flows, Int. J. Mech. Aerosp. Ind. Mechatron. Manuf. Eng. 5 (9) (2011) 1813–1822.

[11] A. Aarts, G. Ooms, Net flow of compressible viscous liquids induced by travelling waves in porous media, J. Eng. Math. 34 (4) (1998) 435–450.

[12] A. Lambert, G. Ibáñez, S. Cuevas, J. Del Río, Optimal behavior of viscoelastic flow at resonant frequencies, Phys. Rev. E 70 (5) (2004) 056302.

[13] M.Y. Gundogdu, M.O. Carpinlioglu, Present state of art on pulsatile flow theory: part 2: turbulent flow regime, JSME Int. J. Ser. B Fluids .Therm. Eng. 42 (3) (1999) 398–410.

[14] M. IGUCHI, M. OHMI, K. MAEGAWA, Analysis of free oscillating flow in a U-shaped tube, Bull. JSME 25 (207) (1982) 1398–1405.

[15] D.M. Eckmann, J.B. Grotberg, Experiments on transition to turbulence in oscillatory pipe flow, J. Fluid Mech. 222 (1991) 329–350.

[16] K.H. Ahn, M.B. Ibrahim, Laminar/turbulent oscillating flow in circular pipes, Int. J. Heat Fluid Flow 13 (4) (1992) 340–346.

[17] R. Trip, D. Kuik, J. Westerweel, C. Poelma, An experimental study of transitional pulsatile pipe flow, Phys. Fluids 24 (1) (2012) 014103.

[18] G.B. Thurston, Theory of oscillation of a viscoelastic medium between parallel planes, J. Appl. Phys. 30 (12) (1959) 1855–1860.

[19] G.B. Thurston, Theory of oscillation of a viscoelastic fluid in a circular tube, J. Acoust. Soc. Am. 32 (2) (1960) 210–213.

[20] E. Khabakhpasheva, V. Popov, A. Kekalov, E. Mikhailova, Pulsating flow of viscoelastic fluids in tubes, J. Non Newton. Fluid Mech. 33 (3) (1989) 289–304.

[21] R. Balmer, M. Florina, Unsteady flow of an inelastic power-law fluid in a circular tube, J. Non Newton. Fluid Mech. 7 (2–3) (1980) 189–198.

[22] H. Barnes, P. Townsend, K. Walters, Flow of non-Newtonian liquids under a varying pressure gradient, Nature 224 (5219) (1969) 585.

[23] H. Barnes, P. Townsend, K. Walters, On pulsatile flow of non-Newtonian liquids, Rheol. Acta 10 (4) (1971) 517–527.

[24] A. Siginer, Oscillating flow of a simple fluid in a pipe, Int. J. Eng. Sci. 29 (12) (1991) 1557–1567.

[25] M. Torralba, A. Castrejón-Pita, G. Hernández, G. Huelsz, J. Del Rio, J. Ortín, Instabilities in the oscillatory flow of a complex fluid, Phys. Rev. E 75 (5) (2007) 056307.

[26] P.A. Vasquez, Y. Jin, K. Vuong, D.B. Hill, M.G. Forest, A new twist on stokes' second problem: partial penetration of nonlinearity in sheared viscoelastic layers, J. Non Newton. Fluid Mech. 196 (2013) 36–50.

[27] J. Del Rio, M.L. De Haro, S. Whitaker, Enhancement in the dynamic response of a viscoelastic fluid flowing in a tube, Phys. Rev. E 58 (5) (1998) 6323.

[28] J.A. del Río, M. López de Haro, and S. Whitaker, Erratum: enhancement in the dynamic response of a viscoelastic fluid flowing in a tube [Phys. rev. e 58, 6323 (1998)], Phys. Rev. E, vol. 64, no. 3, p. 039901, 08/27/ 2001, doi:10.1103/PhysRevE.64.039901.

[29] E.E. Herrera, F. Calderas, A. Chávez, O. Manero, Study on the pulsating flow of a worm-like micellar solution, J. Non Newton. Fluid Mech. 165 (3–4) (2010) 174–183.

[30] L. Casanellas, J. Ortín, Experiments on the laminar oscillatory flow of wormlike micellar solutions, Rheol. Acta 51 (6) (2012) 545–557.

[31] S.M. Mitran, M.G. Forest, L. Yao, B. Lindley, D.B. Hill, Extensions of the ferry shear wave model for active linear and nonlinear microrheology, J. Non Newton. Fluid Mech. 154 (2–3) (2008) 120–135.

[32] J.D. Ferry, Studies of the mechanical properties of substances of high molecular weight I. a photoelastic method for study of transverse vibrations in gels, Rev. Sci. Instrum. 12 (2) (1941) 79–82.

[33] J.D. Ferry, Mechanical properties of substances of high molecular weight. ii. rigidities of the system polystyrene-xylene and their dependence upon temperature and frequency, J. Am. Chem. Soc. 64 (6) (1942) 1323–1329.

[34] B.S. Lindley, M.G. Forest, B.D. Smith, S.M. Mitran, D.B. Hill, Spatial stress and strain distributions of viscoelastic layers in oscillatory shear, Math. Comput. Simul. 82 (7) (2012) 1249–1257.

[35] S. He, J. Jackson, An experimental study of pulsating turbulent flow in a pipe, Eur. J. Mech.-B/Fluids 28 (2) (2009) 309–320.

[36] P. Papadopoulos, A. Vouros, Pulsating turbulent pipe flow in the current dominated regime at high and very-high frequencies, Int. J. Heat Fluid Flow 58 (2016) 54–67.

[37] Y.A. Andrienko, D. Siginer, Y.G. Yanovsky, Resonance behavior of viscoelastic fluids in Poiseuille flow and application to flow enhancement, Int. J. Non Linear Mech. 35 (1) (2000) 95–102.

[38] M.F. Letelier, D.A. Siginer, D.L. Almendra, J.S. Stockle, Resonance in laminar pipe flow of non-linear viscoelastic fluids, Int. J. Non Linear Mech. 115 (2019) 53–60.

[39] L. Casanellas, J. Ortín, Vortex ring formation in oscillatory pipe flow of wormlike micellar solutions, J. Rheol. (N Y) 58 (1) (2013) 149.

[40] J. Castrejón-Pita, J. Del Río, A. Castrejón-Pita, G. Huelsz, Experimental observation of dramatic differences in the dynamic response of Newtonian and Maxwellian fluids, Phys. Rev. E 68 (4) (2003) 046301.

[41] D. Tsiklauri, I. Beresnev, Enhancement in the dynamic response of a viscoelastic fluid flowing through a longitudinally vibrating tube, Phys. Rev. E 63 (4) (2001) 046304.

[42] M. Torralba, J. Castrejón-Pita, A. Castrejón-Pita, G. Huelsz, J. Del Río, J. Ortín, Measurements of the bulk and interfacial velocity profiles in oscillating Newtonian and Maxwellian fluids, Phys. Rev. E 72 (1) (2005) 016308.

[43] H.A. Barnes, J.F. Hutton, K. Walters, An Introduction to Rheology, Elsevier, 1989.

[44] A. Saasen, H. Hodne, Influence of vibrations on the rheological properties of drilling fluids and its consequence a solids control, Appl. Rheol. 26 (2) (2016) 28–33.

[45] A. Saasen, H. Hodne, The influence of drilling fluid rheological properties on primary solids control, in: Proceedings of the 34th International Conference on Ocean, Offshore and Arctic Engineering, ASME 2015, American Society of Mechanical Engineers, 2015 pp. V010T11A037-V010T11A037.

[46] L. Børgesson, A. Fredriksson, 32 INFLUENCE of vibrations on the rheological properties of cemenT, in: Proceedings of the International Conference on Rheology of Fresh Cement and Concrete, Liverpool, 1990, CRC Press, 2014, p. 313.

[47] D. Quemada, Rheological modelling of complex fluids. I. THE concept of effective volume fraction revisited, Eur. Phys. J.-Appl. Phys. 1 (1) (1998) 119–127.

[48] M. OHMI, M. Iguchi, Critical reynolds number in an oscillating pipe flow, Bull. JSME 25 (200) (1982) 165–172.

[49] P. Merkli, H. Thomann, Transition to turbulence in oscillating pipe flow, J. Fluid Mech. 68 (3) (1975) 567–576.

[50] M. Amaratunga, H.A. Rabenjafimanantsoa, R.W. Time, Comparison of oscillatory flow conditions in Newtonian and non-Newtonian fluids using PIV and high-speed image analysis, Flow Meas. Instrum. 70 (2019) 101628.

[51] T. Zhao, P. Cheng, The friction coefficient of a fully developed laminar reciprocating flow in a circular pipe, Int. J. Heat Fluid Flow 17 (2) (1996) 167–172.

[52] J. Gerrard, M. Hughes, The flow due to an oscillating piston in a cylindrical tube: a comparison between experiment and a simple entrance flow theory, J. Fluid Mech. 50 (1) (1971) 97–106.

[53] J.R. Womersley, An Elastic Tube Theory of Pulse Transmission and Oscillatory Flow in Mammalian Arteries, Aerospace Research Labs Wright-Patterson AFB OH, 1957.

[54] R.J. Poole, The Deborah and Weissenberg numbers, Rheol. Bull. 53 (2) (2012) 32–39.

[55] L. Casanellas, J. Ortı, Laminar oscillatory flow of Maxwell and Oldroyd-b fluids: theoretical analysis, J. Non Newton. Fluid Mech. 166 (23–24) (2011) 1315–1326.

[56] R.P. Chhabra, J.F. Richardson, Non-Newtonian Flow in the Process Industries: Fundamentals and Engineering Applications, Butterworth-Heinemann, 1999.

[57] M. Amaratunga, R. Nybø, R.W. Time, PIV analysis of dynamic velocity profiles in non-newtonian drilling fluids exposed to oscillatory motion, in: Proceedings of the ASME 2018 37th International Conference on Ocean, Offshore and Arctic Engineering, American Society of Mechanical Engineers, 2018 pp. V008T11A058-V008T11A058.

[58] R.J. Adrian, Particle-imaging techniques for experimental fluid mechanics, Ann. Rev. Fluid Mech. 23 (1) (1991) 261–304.

[59] R. Blythman, T. Persoons, N. Jeffers, D. Murray, Effect of oscillation frequency on wall shear stress and pressure drop in a rectangular channel for heat transfer applications, J. Phys. Conf. Ser. 745 (3) (2016) 032044 IOP Publishing.

[60] J.A. Goshawk, N. Waters, G. Rennie, E. Staples, Enhancement of the drainage of non-Newtonian liquid films by oscillation, J. Non Newton. Fluid Mech. 51 (1) (1994) 21–60.

[61] W. Thielicke, E. Stamhuis, PIVlab–towards user-friendly, affordable and accurate digital particle image velocimetry in MATLAB, J Open Res. Softw. 2 (1) (2014).

[62] K.D. Jensen, Flow measurements, J. Braz. Soc. Mech. Sci. Eng. 26 (4) (2004) 400–419.

[63] T.G. Mezger, The Rheology Handbook: For Users of Rotational and Oscillatory Rheometers, Vincentz Network GmbH & Co KG, 2006.

[64] S.K. Arnipally, E. Kuru, Settling velocity of particles in viscoelastic fluids: a comparison of the shear-viscosity and elasticity effects, SPE J. 23 (5) (2018) 17.

[65] B. Bui, et al., Viscoelastic properties of oil-based drilling fluids, Ann. Trans. Nordic Rheol. Soc. 20 (2012) 33–47.

Paper VII

Influence of low-frequency oscillatory motion on particle settling in Newtonian and shear-thinning non-Newtonian fluids

Maduranga Amaratunga, H. A.
Rabenjafimanantsoa and Rune W. Time

University of Stavanger, Norway.

The paper has been accepted (on 11th August 2020) by the *Journal of Petroleum Science and Engineering* and currently the article is in press for online publication.

Influence of low-frequency oscillatory motion on particle settling in Newtonian and shear-thinning non-Newtonian fluids

Maduranga Amaratunga*, Herimonja A. Rabenjafimanantsoa*, Rune W. Time*
*Department of Energy and Petroleum Engineering, University of Stavanger, Norway

Abstract

An experimental study is performed to observe the effect of vertical fluid oscillations on the mean settling velocity of single spherical glass particles released into mixtures of water and polymeric fluids which exhibit shear-thinning behaviour for "non-zero" shear rates. The influence of the shear region in shear-thinning non-Newtonian fluids on the settling rate of spherical particles at different oscillatory conditions is also discussed.

A transparent, U-shaped pipe with a circular cross-section of 50 mm inner diameter is used. Visualizations are captured along one of the two vertical branches of the pipe while a piston generates pressure gradient oscillations in the other branch at three different low frequencies (0.25, 0.5, and 0.75 Hz). Tests at still fluid are also carried out for comparison. Four fluids are considered: water and three mixtures of water-based polymeric solutions which provide the mixture with viscoelastic properties and shear-thinning behaviour. Spherical particles of diameter d = 1 mm, 2 mm and 3 mm are released at three different distances from the center of the cross-section: 0, $0.5R$, and $0.8R$, where R is the pipe radius. Particles are released one-by-one and their trajectory is captured from the high-speed camera.

The settling velocity was found smaller if particles were released close to the pipe wall, independently on the rheology of the fluid. A significant reduction of the settling velocity was observed in the presence of an oscillatory flow when a fluid characterized by shear-thinning viscosity is used. According to the results, it was found that the liquid oscillations brought a decrement of up to 7% in the average settling velocity in Newtonian fluid and a 23% decrement of that in non-Newtonian fluids. Moreover, when the fluid oscillates, the combination of the shear-layer associated with the particle wake and with the pipe wall does not result in any reduction of the settling velocity. In other words, the effect of the near-wall shear layer, which reduces the viscosity of shear-thinning fluids, dominates over the other effects that would not keep the particle longer in suspension.

Keywords: Oscillatory motion; particle settling; velocity reduction; non-Newtonian fluids; shear rate; drag force

1. Introduction

After the first introduction of Stokes law for the creeping flow regime by George Stokes in 1851, many researchers have worked a lot on settling of particles in Newtonian fluids even in higher Reynolds numbers (Clift et al., 1978, Khan and Richardson, 1987, Haider and Levenspiel, 1989, Chhabra et al., 1999, Kehlenbeck and Felice, 1999, Brown and Lawler, 2003, Zhiyao et al., 2008, Cheng, 2009). Even the works related to the settling of particles in shear-thinning non-Newtonian fluids are also omnipresent in the literature (Sharma, 1979, Shah, 1982, Shah, 1986, Acharya, 1986, Jin and Penny, 1995, Kelessidis, 2004, Malhotra and Sharma, 2012, Arnipally and Kuru, 2018). However, all the above-mentioned studies are related to the

settling of particles in stationary fluids while dynamic settling (Harrington et al., 1979, Van den Brule and Gheissary, 1993, Becker et al., 1994, Childs et al., 2016) has become an interesting topic concerning its practicality and the importance in industrial applications.

Particle settling in oscillatory systems is a practically important example under dynamic settling. Sinusoidal oscillatory fluid motion exhibits a condition of continuously changing acceleration and thus the flow patterns and drag phenomena could be significantly different from those at steady state. Theory and experiments have shown that oscillating or continuously accelerating such systems could exhibit a variety of complicated flow phenomena (Amaratunga et al., 2019b) including periodic vortex shedding (Schöneborn, 1975, Herringe, 1976), boundary layer separation, secondary streaming and wake turbulence (Tunstall and Houghton, 1968), etc.

When talking about the particle settling, it is important to have a fundamental understanding of the comprehensive picture of the forces which results from the fluid on the particles, namely, lift, drag, and buoyancy (Fischer et al., 2002, Zeng et al., 2009). When a spherical particle is moving steadily in a stagnant fluid medium, the forces exerted on the particle can be predicted from the well-known drag coefficient-Reynolds number relationship since the terminal settling velocity occurs when the net gravitational force (gravity minus buoyancy) equals the drag force. However, if the same particle is allowed to settle through an unsteady fluid medium, the contribution of the lift and drag forces to the dynamics of the particles becomes much more significant (Fischer et al., 2002, Cherukat and McLaughlin, 1994, Lee and Balachandar, 2010) as a result of the changes in the flow patterns around the particle. Those will eventually have a considerable impact on both the instantaneous relative velocity of the particle to the fluid and also on the mean transport velocity of the particle (Herringe and Flint, 1974).

The settling velocity of particles suspended in vibrating/oscillating liquids is of great importance in a wide variety of natural geophysical environments and industrial applications including drilling. According to (Baird et al., 1967), low-frequency oscillations have been used nearly for two centuries in the processing of mineral ores. There are many instances where devices have been used to disperse particles such as bubbles, droplets, and solid particles in liquids by shaking or vibrating the mixtures. The dynamic behavior of such particles in the oscillating continuous phase can impose a significant effect on mass or heat transfer characteristics of the resulting two-phase systems or on mixing and separation in particle-fluid systems (Harbaum and Houghton, 1960, Bailey, 1974, Still, 2012). Ultrasonic fields with short wavelengths are used to enhance mixing to increase the interfacial area in pulse liquid-liquid extraction columns. Furthermore, (Bailey, 1974) states that periodic flow pulsations could be used to accelerate ore flotation as well as to speed-up the particle deposition in settling tanks if quick settling is preferred. (Singh et al., 1991) mention that the settling of spheres suspended in non-Newtonian fluid with yield stress under the influence of vibrations is of great practical importance while transporting liquid food systems such as soups, sauces, and jams.

1.1 Past work related to particle settling in oscillatory flow

Interest in the geophysical as well as in the industrial problems has spawned many theoretical and experimental studies on particle settling in oscillatory Newtonian fluids in the past. Such studies reveal that the drag forces in unsteady systems tend to exceed the average forces that might be expected from the laws of drag under steady conditions (Bailey, 1974). That means, due to the increased drag forces, the settling velocity of particles in oscillatory fluid systems

could be reduced (Tunstall and Houghton, 1968, Hwang, 1985, Ikeda and Yamasaka, 1989) and thus the settling velocity under oscillatory conditions is less than the terminal settling velocity under stationary conditions.

In a fascinating series of papers (Houghton, 1963, Houghton, 1966, Houghton, 1968), Houghton describes deeply about the velocity profile around a particle in a sinusoidal field and introduces a hydrodynamic model based on the non-linear Langevin equation to predict the directional motion of particles by applying a sinusoidal velocity to the continuous phase in which the particles are suspended. Thereafter, (Herringe and Flint, 1974) have studied the free fall of particles through a vertically oscillated Newtonian fluid both theoretically and experimentally and state that the motion of the particle is most accurately predicted when the 'history' and 'added mass' terms are preceded by empirical coefficients which are functions of the instantaneous acceleration number.

1.1.1 Mechanism of retardation

If we consider a vortex free situation, based on the non-linear Langevin equation presented by (Houghton, 1963), the motion of a spherical particle settling in a vertically unsteady flow can be written as;

$$\left(\rho_p + \chi\rho_f\right)\frac{\pi d^3}{6}\frac{dv_p}{dt} = \left(\rho_p - \rho_f\right)g\frac{\pi d^3}{6} - \frac{1}{2}\rho_f C_D\frac{\pi d^2}{4}\,(v_p - v_f)|v_p - v_f|$$

$$+ \rho_f(1+\chi)\frac{\pi d^3}{6}\frac{dv_f}{dt} + B(t), \qquad (1)$$

where, ρ_p is the density of the particle, ρ_f is the density of the oscillating fluid (continuous phase), d is the diameter of the spherical particle, v_p is the instantaneous velocity of the particle taken as positive downwards, v_f is the velocity of the fluid taken as positive downwards, g is the gravitational acceleration, C_D is the drag coefficient, t is the time, χ is the added mass coefficient and $B(t)$ is the Basset term. It is assumed that the continuous phase experiences a uniform velocity (v_f), which is sinusoidal with an angular frequency of ω in the direction of particle motion so that,

$$v_f(t) = a'\omega\cos(\omega t), \qquad (2)$$

where, a' is the displacement amplitude of the oscillation. The term on the left-hand side of Eq. (1) represents the inertial forces on the particle. The added mass coefficient (χ) is required to account for the virtual mass that is slightly larger than the ordinary mass of the particle by a fraction of χ of the displaced fluid. In this analysis, χ is taken to be 0.5 (Ikeda and Yamasaka, 1989). The first term on the right-hand side of the Eq. (1) gives the buoyancy forces on the particle while the second term represents the frictional (drag) forces on the particle. The third term on the right-hand side of the Eq. (1) corresponds to the effects of the pressure gradient in the accelerating fluid phase combined with the virtual mass of the fluid displaced by the particle. According to (Houghton, 1963), the simple form of this term arises from the assumption that there are no velocity gradients in the fluid perpendicular to the direction of motion. The Basset term $B(t)$ has been introduced to allow the effects of deviations of the flow pattern around the particle from that at steady state. If the particle diameter is small and the fluid density is small

compared with that of the particle, then $B(t)$ becomes insignificant. Even though ρ_f is not that small compared to ρ_p in this analysis and $B(t)$ is neglected.

The terminal settling velocity of a particle (v_{p0}) in a stationary fluid can be easily derived from Eq. (1) as;

$$v_{p0} = \sqrt{\frac{4}{3}\frac{(\rho_p - \rho_f)}{\rho_f C_{D0}} g d}\,. \tag{3}$$

Hereafter, the subscript '0' denotes the value in the stationary fluid. If we consider a temporal average of Eq. (1) over a period of fluid motion, with the aid of Eq. (3), it yields (Ikeda and Yamasaka, 1989);

$$C_{D0}.v_{p0}^2 = \overline{C_D\left(v_p - v_f\right)\left|v_p - v_f\right|}\,. \tag{4}$$

The overbar hereafter denoting temporal averaging over a period of fluid oscillation. From Eq. (4), it can be easily derived that the temporally averaged settling velocity of spheres in a sinusoidally oscillating fluid is equal to that in a stationary fluid as long as the fluid drag obeys Stokes' law. The relative velocity ($v_p - v_f$) can be divided into two parts as a stationary velocity component ($\overline{v_{ps}}$) and a periodic velocity component (v_{pp}). Here, v_{pp} is a function of phase ωt and has following characteristics (Ikeda and Yamasaka, 1989): (i) it is a periodic function with a period of $2\pi/\omega$, (ii) the functional dependence on phase ωt is not given in terms of a simple harmonic but is rather skewed in time and (iii) the temporal average over one-period vanishes (since $\overline{v_{ps}}$ takes up the averaged effect). Therefore, ($v_p - v_f$) can then be written as;

$$v_p - v_f = \overline{v_{ps}} + v_{pp}\,. \tag{5}$$

For derivation, consider another limiting case for which the instantaneous Reynolds number is always sufficiently large (> 1000) to obey Newton's law of resistance. So, it can be written as (Ikeda and Yamasaka, 1989);

$$C_D = C_{D0} \approx 0.4. \tag{6}$$

With the help of Eq. (6), we substitute Eq. (5) into Eq. (4) and yields;

$$C_{D0}.v_{p0}^2 = C_{D0}\left[\overline{v_{ps}}^2 + \overline{v_{pp}{}^2}\right]. \tag{7}$$

Based on Eq. (7), it can be concluded that $v_{p0} > \overline{v_{ps}}$ and the settling velocity of particles is caused by the nonlinearity of the fluid drag and the particles exhibit a retardation in oscillatory environments.

However, (Baird et al., 1967) state that the reduction of the settling velocity at oscillatory conditions is due to the shedding of a large wake during each oscillation. That shedding replaces the relatively small vortices which are periodically shed from spheres moving steadily. Moreover, the resisting force opposing the motion of a sphere could be attributed to the break-off of the eddies alternately on either side of the sphere in a periodic manner that exerts a periodic force on the particle (Uhlmann and Dušek, 2014, Mazzuoli et al., 2014, Mazzuoli et

al., 2019). According to the study performed by (Hwang, 1985), the three major factors that govern the variation of effective fall velocity of particles in oscillating flows are the terminal velocity Reynolds number (Reynolds number of the settling sphere in still fluid), the velocity amplitudes of the flow and particle oscillations and the phase lag. However, (Ikeda and Yamasaka, 1989) replace the phase lag by the dimensionless frequency of the fluid oscillation and state that an increase of any parameter would increase the retardation of the particle settling. The terminal velocity Reynolds number of the particle ($Re_{p0} = \rho_f v_p d/\mu_f$) is not the same as the instantaneous particle Reynolds number (Re_p) in oscillatory conditions which can be explained as (Boyadzhiev, 1973, Schöneborn, 1975);

$$Re_p = \frac{\rho_f (v_p - v_f) d}{\mu_f}, \tag{8}$$

where, μ_f is the dynamic viscosity of the fluid medium. However, based on the simple conceptual basis provided by (Bailey, 1974) for the particle retardation in oscillatory Newtonian fluid flows, he claims that the settling velocity of the particle can be altered either positively or negatively from its value in steady flow by imposing a "well designed" oscillatory motion on it. The oscillatory motion should have its largest velocity in the direction of the preferred particle motion.

1.2 Significance for non-Newtonian fluids

The related literature mentioned above suggests that the liquid oscillation would retard settling, but the problem of a particle that is free to move in an oscillating fluid is more complicated than we expect. More importantly, when the continuous oscillating fluid is non-Newtonian, the oscillatory motion could generate different shear regions within the pipe area that make the scenario more complicated. When a relatively dense particle settles through a sheared flow in a non-Newtonian fluid, the shear rate of the background flow varies and thus the settling velocity of that particle may vary spatially and temporally due to the non-linear rheology of the fluid. Significant measures to be taken into account with this regard such as the distance that those particles can be transported before settling out, the time they take to do so and the geometry of the deposit, etc.

According to the experimental study performed by (Van den Brule and Gheissary, 1993), the settling velocity of spherical particles at stationary conditions is reduced by the elastic effects of the non-Newtonian fluid medium due to the presence of normal stress differences and high elongational viscosity. However, in the latter part of their study, they mention about a reduction of the average settling velocity in viscoelastic fluids in the presence of an orthogonal shear-flow field. In a later study (Gheissary and Van den Brule, 1996), the same authors extend their experiments to claim that an increment in the settling velocity could be observed with the increase of the shear rate of the main flow of non-Newtonian fluids. This is just because of the non-linear rheology of the fluids and thus the reduced viscosity with increased shear rate. The same conclusion has been confirmed by (Talmon and Huisman, 2005) with their experimental study on particle settling in viscoplastic fluids under shear flow conditions where the settling velocities increase with increasing shear rate.

In the oil industry, most fracturing/drilling fluids exhibit highly shear-thinning, non-Newtonian fluid characteristics. They are used to suspend drilled cuttings where they expose to different

oscillatory conditions while they are circulating through the well or during the solids control operations. They possess completely different properties under shear than when it is at rest. Even though most of the particle settling studies are undertaken in stationary fluids, in the actual drilling process the cuttings are settling while the fluid is moving and mostly oscillating within the fracture. For example, in real drilling operations, the local uneven geometries might induce flow instabilities (Time and Rabenjafimanantsoa, 2013) while the effect of eccentricity in annulus systems is significant in the case of non-Newtonian fluid flow since it may lead to a substantial variation in pressure drop. Generally, the properties of the cuttings being settled, rheology, and density of the drilling fluid, the retardation effect of the confining fracture walls determine the settling rate of cuttings (Malhotra and Sharma, 2012). However, this study proves that the settling of cuttings is governed by the properties of oscillatory motion as well and illustrates the relative importance of studying the settling of particles in non-Newtonian fluids under oscillatory conditions since it is not desirable to have deposition of particles in pipes and boreholes.

1.3 Objective

An extensive and coherent body of information is available for the calculation of drag on spheres settling in quiescent Newtonian and shear-thinning non-Newtonian fluids. However, past work on the determination of settling velocity of particles in a dynamic environment is very limited; out of which any work related to oscillatory motion is sparse.

As mentioned in section 1, low-frequency oscillations are used in several industrial applications, and despite of these practical applications, it appears to be relatively few measurements of particle behavior in non-Newtonian liquids oscillating at low frequencies. The fall velocity of the small particles is affected by the oscillation frequency, shear-thinning, and viscoelasticity of the fluid medium. The effective viscosity of the shear-thinning test liquids varies with the different shear rates results from the oscillation.

In previous publications (Amaratunga et al., 2018, Amaratunga et al., 2019a, Amaratunga et al., 2019b, Amaratunga et al., 2020), the authors clarified the rheological approach to quantify the effect of horizontal and vertical vibration on shear-thinning non-Newtonian polymers, which can be used as model drilling fluids. However, based on the present investigation of single-particle behavior in a vertically oscillating Newtonian and non-Newtonian fluid, it is aimed to bring out valuable conclusions concerning the influence of Newtonian and non-Newtonian liquid oscillations upon the average settling velocity of single particles. Furthermore, it is aimed to provide information on engineering significance in the design of engineering applications experiencing vibration/oscillation and also to understand the mechanics of particle suspension and dislodgement in wall-bounded oscillatory flows.

2. Methodology

The experiments were performed in the multiphase flow laboratory at the University of Stavanger (UiS), Norway.

2.1 Experimental setup

The effect of low-frequency oscillatory motion on particle settling in water and shear-thinning non-Newtonian fluids was investigated in a U-shaped experimental set up as shown in Fig. 1. The test section on the left limb of the U-tube has a circular cross-section with an internal

diameter of 50 mm and a total length of 1200 mm. The bottom and the right limbs of the U-tube were also circular in cross-section and 30 mm in internal diameter. The whole U-tube including the piston cylinder (with an internal diameter of 50 mm) was made of transparent acrylic for visualization purposes.

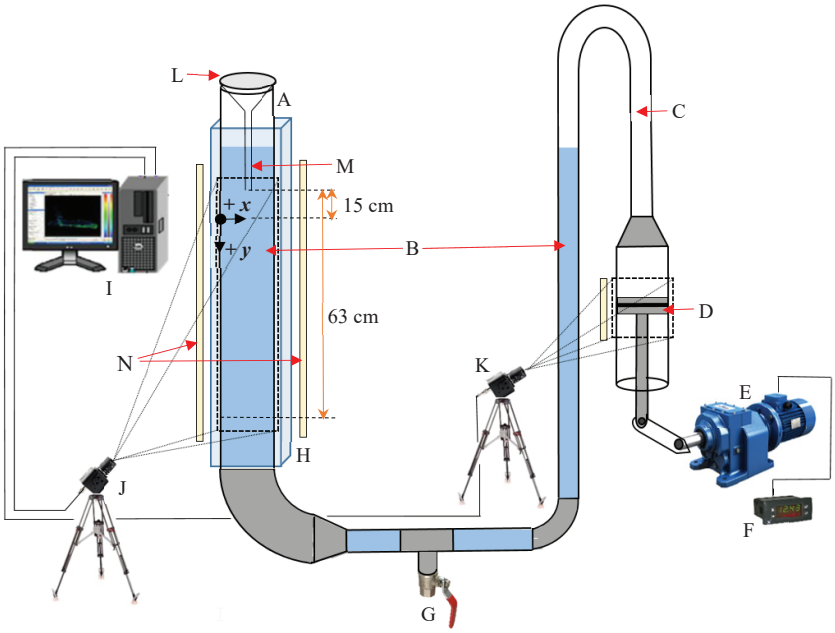

A – Acrylic pipe with ID = 50 mm
B – Test Fluids (Deionized water and non-Newtonian fluids)
C – Air
D – Piston
E – Motor and gearbox
F – Frequency controller
G – Drain valve
H – Transparent box
I – Control PC with frame grabber
J – Camera 1
K – Camera 2
L – Funnel arrangement
M – Dropping tube
N – LED lamps

Figure 1: Sketch of the experimental setup

The harmonic oscillations were provided by the piston attached to the right limb of the U-tube, which is driven by a motor-gearbox unit. The rotary motion of the gearbox is converted to a reciprocating motion of the piston by mechanically projecting it into the arm of the piston. The revolution speed of the motor (model: 3DF56-2S7032 from ABM Greiffenberger, Germany) and the gearbox from David Brown (Radicon series), UK was controlled by a frequency controller (model: Micromaster 420 from Siemens) in such a way that, the required output frequency was set to the piston. A tachometer (model: AT-6L from Clas Ohlson, Norway) was used to confirm the frequency of the piston. Experiments with three different oscillation frequencies were tested as 0.25, 0.5, and 0.75 Hz while the tests with still fluid were also performed for the comparison. The length of the rotating arm was fixed in such a way that the

resulting oscillation amplitude to be 20 mm. Out of that, the oscillation amplitude ratio (A) was determined as a/D = 0.4, where a is the displacement amplitude of the piston, and D is the pipe diameter. An acrylic transparent visualization box filled with deionized water, with dimensions of 15 x 15 x 100 cm^3 was used around the test section to minimize the optical refraction through the curved pipe walls.

2.2 Materials and fluids

2.2.1 Test fluids

Deionized water, being one of the test fluids, was used to prepare three polymeric non-Newtonian Fluids (NNF), later referred to as "Fluid 1", "Fluid 2", and "Fluid 3". They are a mixture of three water-based polymers namely Poly-anionic Cellulose (PAC) called PolyPAC-R provided by MI-Swaco, Norway, medium viscous Carboxymethyl Cellulose (MV-CMC) and high viscous Carboxymethyl Cellulose (HV-CMC) provided by Sigma-Aldrich. The polymer mixtures were mixed using an overhead mixer (Model: Silverson L4RT-A) to ensure proper mixing and allowed more than 72 hours to get rid of the trapped air bubbles. The fluid system was optically transparent. The specific details of the polymers and the mixture configuration are mentioned in Table 1.

Table 1: Specific details of the polymers and the mixture configuration

Polymer type	Viscosity at 25 ℃	Used weight [g] to dissolve in 5 L of deionized water		
		Fluid 1	Fluid 2	Fluid 3
PolyPAC	800 - 1200 mPa.s (1% H_2O)	0.5	7.5	22.5
MV-CMC	400 – 1000 mPa.s (2% H_2O)	5	5	5
HV-CMC	1500 – 3000 mPa.s (1% H_2O)	4.5	7.5	2.5

The viscosity of the NNF was measured by Anton Paar MCR 302 rotational rheometer and the rheological properties are described in section 3.1 with Fig. 5. The density values of the fluids measured using Anton Paar DMA-4500 density meter were 997.55, 999.47, 1000.25, and 1001.01 kg/m^3 for water, Fluid 1, Fluid 2, and Fluid 3 respectively. All experiments were carried out and liquid properties were measured at room temperature of 22 ± 0.5 ^{0}C and atmospheric pressure.

2.2.2 Particles

Three different sizes of glass beads were employed in the experiment series to study the settling rate under oscillatory conditions. Accurate particle diameters were measured using an Olympus SZX16 stereo-microscope and an average particle diameter was used in the calculations. The weight of the particles was measured using an analytical balance with digital precision scale and the specific details of the particles used are mentioned in Table 2.

Table 2: Specific details of the particles (approx. 50 glass beads)

Particle name	Average diameter [mm]	Average Weight [g]	Density [kg/m^3]
1 mm	1.128 ± 0.003	0.00189 ± 0.0004	2514.9
2 mm	1.986 ± 0.002	0.01111 ± 0.0003	2708.8
3 mm	2.960 ± 0.001	0.03669 ± 0.0002	2701.9

However, the particles will be called with their general sizes (as 1 mm, 2 mm, and 3 mm) for clarity. To cancel out possible effects associated with imperfections of the particle surface, different particles of the same size have been used for each test.

2.3 Experimental procedure

The experimental procedure for this study considered capturing the falling (or rising) of a single spherical particle in a vertical circular column of fluid that is oscillated in the direction of the particle motion. The primary focus was to study the effects of oscillation frequency on the settling rate without any wall effects. Therefore, the particles were released along the axis of the vertical test section; which was considered as the "Location 1" – (L1). Then, two other locations within the test section which are more closer to the pipe walls were selected (L2 and L3) as illustrated in Fig. 2 to investigate the effect of shear region on particle settling in non-Newtonian fluids. Therefore, L1 ≈ R, L2 ≈ 0.5R, and L3 ≈ 0.2R, where R is the pipe radius measured from the pipe wall.

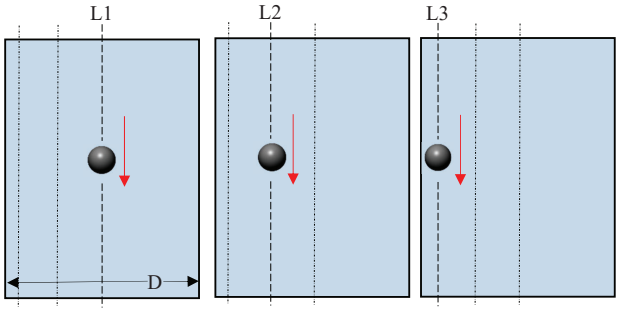

Figure 2: Particle falling in test fluids at different locations within the test section (the picture is just for the illustration purpose and not in scale)

As shown in Fig. 1, a centrally mounted small tube (represented by M in Fig. 1) that was partly immersed in the liquid surface was employed to release the spheres singly into the liquid column. After switching on the driving motor, at least 2 minutes were left for the oscillatory motion to become harmonic. Then the particles were carefully withdrawn manually into the funnel on top of the dropping tube. The funnel arrangement helped the particle to be directed at the intended dropping location within the test section and the small metal net at the bottom of the dropping tube helped the particle to reduce its initial velocity as low as possible. Therefore, based on the variables, 144 different experimental cases were tested for 4 different frequencies (including still condition), 3 different particle sizes, 4 different fluid types and at 3 different locations within the pipe. All the Newtonian and non-Newtonian fluids were assumed to be incompressible. Each experiment case was repeated three times to achieve a better averaged result and to check the repeatability.

2.3.1 The high-speed imaging system

The motion of the spherical glass beads and their trajectories between two reference points 15 cm and 63 cm below the tip of the dropping tube were captured by a high-speed camera (Camera 1). The y- axis is positive downwards. Some preliminary tests were performed to confirm that

all the particle sizes concerned in this experiment achieve their terminal settling velocity at steady conditions before entering this defined boundary. A Basler camera (Model: acA800-510um USB 3.0 camera with the ON Semiconductor) with a maximum frame rate of 500 fps at a full resolution of 800 x 616 pixel^2 was used for the acquisition of images. Basler lens of model: C125-0818-5M F1.8 f/8 mm was employed at different frame rates ranging from 25 - 200 fps depending on the speed of the particles in different experimental cases for both cameras. The images were cropped to a reduced section of 256 x 616 pixel^2 to fit the view of interest for Camera 1. The two sides of the transparent visualization box were sufficiently illuminated using two LED lamps. Another similar type of a camera (Camera 2) was employed to capture the motion of the piston so that any relation between the particle motion to the piston movement could be interpreted. The view of interest for Camera 2 was 128 x 370 pixel^2. The frame speed of Camera 2 was set identical to Camera 1 and both cameras were synchronized using a LabView program and triggered by a separate control switch. The resulting settling velocities were calculated as described in section 2.3.2. Each experiment case was performed at least three times to ensure consistency and the quality of results. All the experimental cases allocated for a single fluid type were conducted within each day to avoid any inconsistency.

2.3.2 Data treatment and analysis

The high-speed image analysis was performed using Tracker – version 4.11.0 (http://physlets.org/tracker/). The whole image was used without specifying any region of interest (ROI) since the full trajectory of the particle is preferred. Specific color adjustments were performed on each image to achieve accurate tracking. Piston movement was also tracked using the same software simultaneously for all the experimental cases incorporating oscillatory conditions.

The characteristic sinusoidal harmonic motion was identified by tracking the displacement of the piston on its vertical plane. Fig. 3 shows a typical sinusoidal movement of the piston together with its phase angle and used as a basis to introduce the notation system adopted by the authors to discuss the results in the latter part of this paper.

The phase position/angle (ωt) was normalized by the angle value ($\pi/4$), and the value for $\omega t/(\pi/4)$ has been utilized in presenting and discussing further results. From the visual observations, great care was taken to release the particle at a moment of the piston movement corresponds to $\omega t/(\pi/4)$ = 2 or 10. Once the sinusoidal phase position of the piston is identified and tracked in data analysis, the displacement of the particle is started to track from the moment that corresponds to $\omega t/(\pi/4)$ = 0 of the piston movement. Based on the preliminary investigations related to the experiment, the authors verify that both steady and periodic regimes are reached by the particles within the span of the trajectory image frame.

Since the velocity of the particle is fluctuating with the oscillatory motion, it was challenging to determine the velocity of each particle directly. However, the trajectory of any particle is a function of space and its gradient is the instantaneous velocity of it. Therefore, the obtained particle trajectory (vertical component of the displacement) is fitted to a linear curve to achieve its average settling velocity within the test section as depicted in Fig. 4.

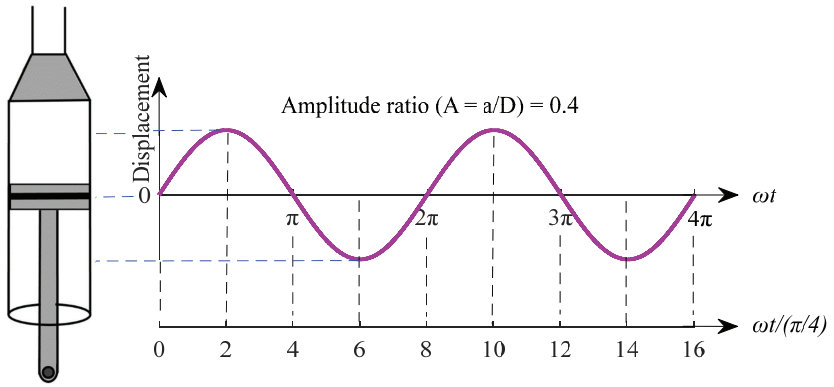

Figure 3: Introduction of the different phase positions within the oscillation period based on the displacement of the piston

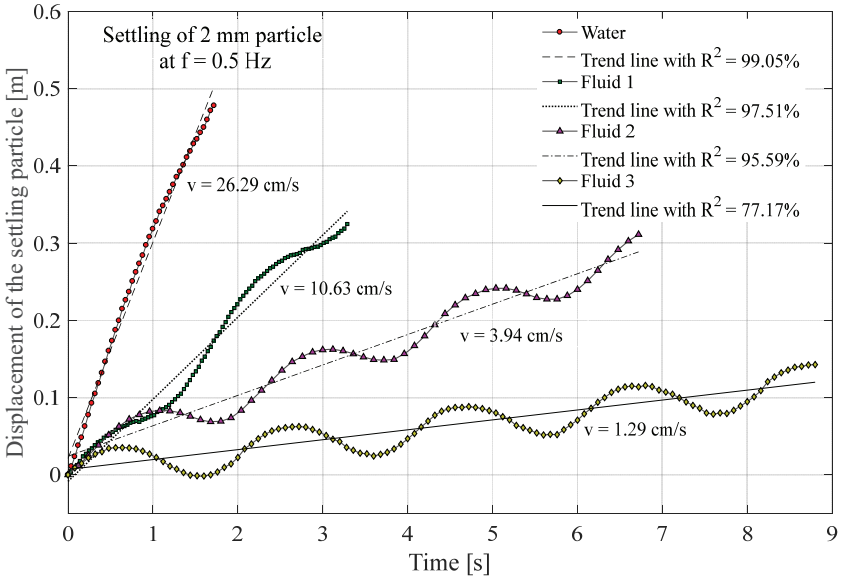

Figure 4: Illustration of the data treatment and analysis method to achieve the average settling velocity of particles (The trajectories are shown for the whole span of the image frame with time and not based on the phase positions. Number of data points are different due to the different acquisition rates and data filtering in plotting the figure. The y- axis is positive downwards.)

According to the specific test conditions depicted in Fig. 4, it can be seen that the trajectories are not 100% straight in the experimental cases associated with oscillatory motion. Therefore, the error associated with linear curve fitting of the trajectory becomes significant for some experimental cases. This will be discussed separately in section 3.6 under error analysis. The obtained average settling velocities are used to compare the effect of different oscillatory conditions on particle settling rate in Newtonian and non-Newtonian fluids.

It was observed that the particle motion was not oblique for almost 98% of the test cases, but in certain instances, some particles exhibited spiral or rocking motion on traveling down the liquid column. Even though it is interesting in themselves for other studies, such cases were neglected in the data processing. Based on the calculations on the oscillatory Reynolds number (Re_δ) for the same experimental setup and conditions (Amaratunga et al., 2020), it was found that the oscillatory boundary layer close to the pipe wall was laminar in all cases.

3. Results and Discussion

The significance of the different test fluids selected for this study in a rheological context and the effect of oscillatory motion on the settling of spherical particles in Newtonian and non-Newtonian fluids are described in the following section.

3.1 Rheology of the fluids

The rheological properties of the non-Newtonian fluids were measured by a modular compact rheometer (Anton Paar – MCR 302), using the concentric cylinder configuration (CC27). Fig. 5 shows the dynamic viscosity (μ) curves for the all the three Non-Newtonian fluids used in the experiment. The power-law rheological model was used to model the viscous and the shear-thinning behavior of the test fluids as shown in Eq. (9);

$$\mu_{PL} = K\dot{\gamma}^{n-1}. \tag{9}$$

Here, μ_{PL} is the viscosity predicted by the power-law model, K is the consistency index, n is the behavioral index and $\dot{\gamma}$ is the shear rate. It is important to mention here, that the power-law model is fitted to the experimental data in the range of shear rates encountered by the particles within all the experimental cases. Also, it does not cover the constant viscosity plateau observed in the low values of shear rate. The shear rate used is the maximum particle shear rate defined as (Shah et al., 2007, Uhlherr et al., 1976);

$$\dot{\gamma} = \frac{3v_p}{d}. \tag{10}$$

The parameters for the model are mentioned in Fig. 5 and also summarized in Table 3. The shear-thinning behavior of the test fluids can be easily distinguished from the viscosity curves where Fluid 3 is the most shear-thinning fluid with the lowest n value. The viscoelastic properties of the test fluids were also measured in small-amplitude oscillation shear (SAOS) tests as part of the rheological investigation. Strain amplitude sweeps (results are not presented in this paper) were conducted to determine the linear viscoelastic (LVE) region of the non-Newtonian test fluids at low strain amplitudes.

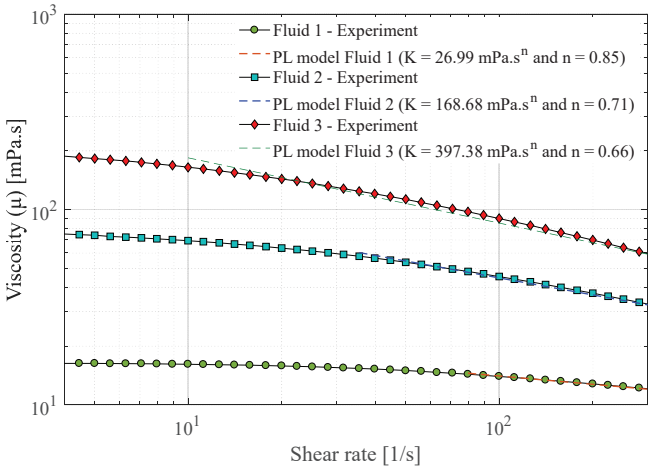

Figure 5: Viscosity curves for the test fluids at 22 °C

The viscoelastic property of the non-Newtonian test fluids in their obtained LVE range was investigated by carrying out frequency sweeps. Fig. 6 shows the results of the frequency sweep test for Fluid 3 over a given angular frequency (ω) range (ramped down logarithmically from 100 to 1 rad/s) at a constant strain 1%.

It can be seen from Fig. 6 that both the storage and the loss moduli increase when the frequency is increased. However, the storage modulus (G') increases faster than the loss modulus (G'') and the elastic behavior of the fluid becomes dominant over its viscous behavior after a certain angular frequency. This particular frequency where $G' = G''$, is termed as the crossover frequency as illustrated in Fig. 6. The inverse of this crossover frequency represents the longest characteristic relaxation time (λ) of the polymer solution (Arnipally and Kuru, 2018) which can be used to quantify the elasticity of the fluid. The corresponding λ values for the three fluids are mentioned in Table 3.

According to the values presented in Table 3, it can be observed that Fluid 1 has the highest relaxation time of the test fluids and therefore has the highest elasticity. Since the λ values after all are very small, it could be concluded that the test fluids are only slightly viscoelastic. All the aforementioned rheological properties were measured just after the corresponding experimental run.

Table 3: Rheological parameters for the test fluids

	K [mPa.s^n]	n [-]	λ [s]
Fluid 1	26.99	0.85	0.037
Fluid 2	168.68	0.71	0.019
Fluid 3	397.38	0.66	0.015

The dynamic viscosity of water was measured to be 0.9544 mPa.s at 22 °C.

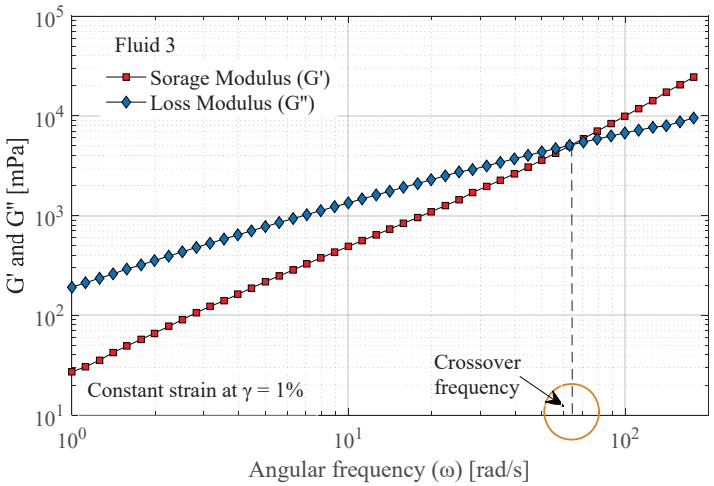

Figure 6: Frequency sweep test for Fluid 3 at a constant strain at $\gamma = 1\%$

3.2 Settling velocity at stationary conditions (in quiescent fluid) along pipe axis (Location 'L1')

As described in the experimental procedure, the settling of spherical particles was captured by a high-speed camera under stationary conditions before imposing any oscillatory motion. That helped in assessing the experimental data and results of the present analysis in comparison to the well-established knowledge on particle settling in stationary Newtonian and non-Newtonian fluids.

Fig. 7 shows the terminal settling velocities of spherical particles falling in all the test fluids without any oscillatory motion imposed. The particles were carefully released with the help of the dropping tube so that they obtain very little or negligible initial velocity at the beginning. It can be observed in Fig. 7 that the terminal settling velocity of particles within the Newtonian fluid (deionized water) is larger than that within all the other non-Newtonian fluids. This is due to the increased viscosity of non-Newtonian fluids and therefore the increased drag force exerted on the particles. The increased drag effect becomes significant when the non-Newtonian fluids become more viscous and shear-thinning which can be seen from the low terminal settling velocities achieved by the particles settled in Fluid 3 compared with other two NNFs. This reduction of terminal settling velocity could also be attributed to the negative wake that is perceived to happen only in shear-thinning viscoelastic fluids (Maalouf and Sigli, 1984).

Moreover, when the particle diameter is increased the terminal settling velocities show an increasing trend for all the test fluids. However, it can be noticed that the rate of increase in terminal settling velocity (with increasing particle size) is higher for water and low viscous NNFs compared to that with high viscous Fluid 3. This means that larger particles settle down at a slower rate than the smaller particles when the shear-thinning of the NNF is increasing (when n becomes low). From the practical point of view, increasing shear viscosity may be an effective solution to achieve suspensions of large-sized particles.

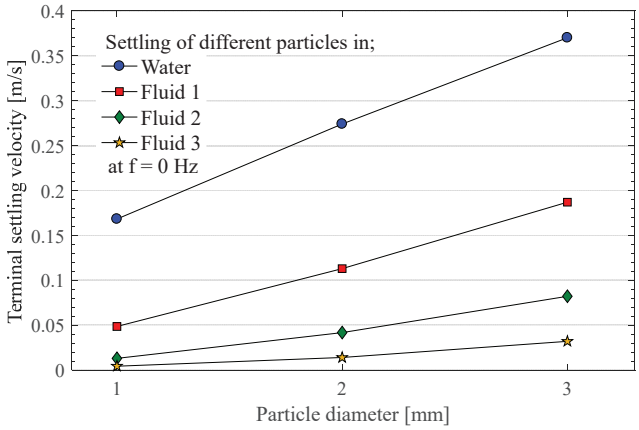

Figure 7: Terminal settling velocities of spherical particles at stationary conditions

Many theoretical (Houghton, 1963, Houghton, 1966, Houghton, 1968, Herringe and Flint, 1974, Bailey, 1974, Hwang, 1985) and experimental studies (Tunstall and Houghton, 1968, Ikeda and Yamasaka, 1989) have indicated that the proximity to a cylindrical wall can noticeably increase the drag on spheres when the ratio of the particle to the pipe diameter (d/D) exceeds 0.1. However, in the present analysis all the test results taken at Location 'L1' has a value of $d/D < 0.06$. Therefore, it is assumed that the settling velocities obtained at this specific location are free from wall effects. Furthermore, (Uhlmann and Dušek, 2014) state that when steady, vertical particle motion is concerned, four basic regimes can be defined based on the Galileo number (Ga) that can be expressed as;

$$Ga = \frac{\sqrt{\left|\frac{\rho_p}{\rho_f} - 1\right| \, g d^3}}{\nu}. \tag{11}$$

Ga is the ratio of gravity forces to the viscous forces and quantitatively it is less than 300 for all the steady-state test cases except for the settling of 2 mm and 3 mm particles in water. Despite those two outlier cases, all the test runs can be categorized as 'steady vertical' based on the classification provided by (Uhlmann and Dušek, 2014).

3.2.1 Validation of particle tracking method and the experimental results

To validate the experimental measurements captured by the high-speed imaging system, and to prove the accuracy of the particle tracking method, the terminal settling velocities (at quiescent conditions) of the three particles in water at Location 'L1' were used. Based on the terminal settling velocities for those three sizes of glass beads, the drag coefficient was calculated using Eq. (12), which is just a re-arrangement of Eq. (3);

$$C_{D0} = \frac{4}{3} \frac{g d (\rho_p - \rho_f)}{\rho_f \, v_{p0}^2}. \tag{12}$$

The terminal velocity Reynolds number of the particle ($Re_{p0} = \rho_f v_p d/\mu_f$) was then calculated as described in section 1.1. The calculated C_{D0} values were plotted upon the drag coefficient ($C_{D0-correlation}$) versus Re_{p0} correlation (Morrison, 2013, Morrison, 2016) graph as shown in Fig. 8. This correlation is shown in Eq. (13).

$$C_{D0-correlation} = \frac{24}{Re_{p0}} + \frac{2.6\left(\frac{Re_{p0}}{5.0}\right)}{1+\left(\frac{Re_{p0}}{5.0}\right)^{1.52}} + \frac{0.411\left(\frac{Re_{p0}}{263000}\right)^{-7.94}}{1+\left(\frac{Re_{p0}}{263000}\right)^{-8.00}} + \frac{0.25\left(\frac{Re_{p0}}{10^6}\right)}{1+\left(\frac{Re_{p0}}{10^6}\right)}. \quad (13)$$

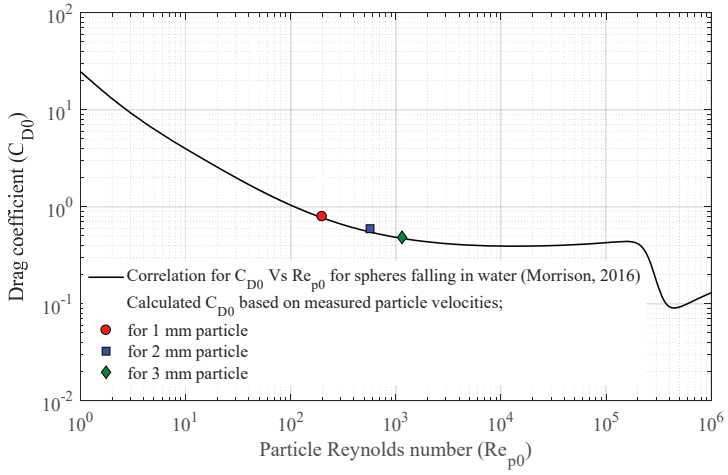

Figure 8: Drag coefficient versus particle Reynolds number

According to Fig. 8, it can be seen that all the drag coefficient values calculated from experimentally measured terminal settling velocity values (using high-speed imaging technique and the particle tracking method) are within 5% deviation from the data correlation presented by (Morrison, 2013, Morrison, 2016), which is an acceptable variance.

3.3 Particle displacement in oscillatory conditions along pipe axis (Location 'L1')

When a particle is settled in a dynamic environment, it experiences an imbalance in hydrodynamic forces, and it tries to exhibit different falling/rising patterns from that we expect at steady situations. When particles are settled in either stationary or oscillatory conditions, the deviations in their straight vertical path as well as their unsteadiness originate from the characteristics of the fluid motion in the near field around the particle and in its wake (Uhlmann and Dušek, 2014). Tracking the particle displacement is a proven technique to analyze and study the motion particles in unsteady oscillatory conditions while the observation of wake patterns provides more in-depth details regarding the hydrodynamics.

3.3.1 Variation of particle displacement with the frequency of oscillation

The oscillatory motion imposed on the fluid medium was mainly characterized by the driving frequency and the amplitude of the fluid oscillations being fixed. Therefore, it is important to

check how the particle moves downwards (or upwards) at different frequencies. Fig. 9 presents the vertical component of the displacement of the spherical particles (1, 2, and 3 mm) in water and Fluid 3 when the fluids are at rest (f = 0 Hz) while Fig. 10 presents the same results when the fluids have been oscillated. The three panels of Fig. 10 are drawn based on the notation basis illustrated in Fig. 3, which is basically for a time period of one phase cycle. Diagrams for the displacement evolution for the other two test fluids are not shown for the clarity of the figure. Note again that the y-axis is positive downwards in all Figs. 9-11.

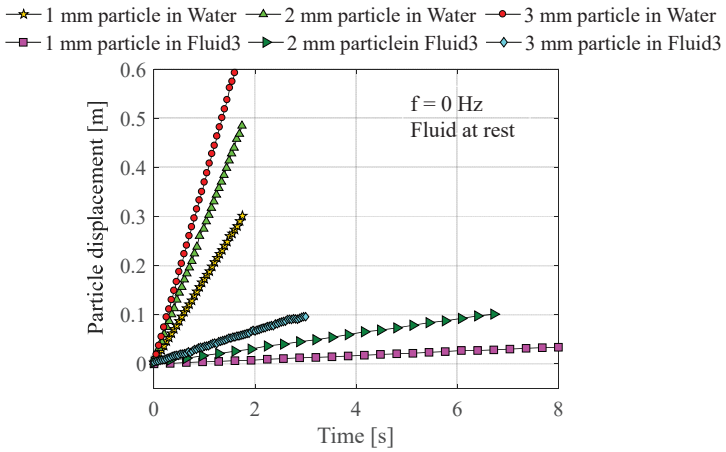

Figure 9: Vertical component of the particle displacement in water and Fluid 3 when the fluids are at rest (stationary conditions). The y- axis is positive downwards.

It can be seen that the time development plots of the particle displacement shown in Fig. 9 are pretty straight forward since they were recorded in quiescent conditions. All of them, no matter whether it is Newtonian or non-Newtonian, possess a linear displacement profile along the test section, and determination of their terminal settling velocity is easy. The typical observations for a particle that settles in a quiescent Newtonian (or non-Newtonian) fluid could be seen here. For example, larger particles travel through the image frame faster than the smaller ones indicating they settle faster. The same-sized large particles take a bit extended time to leave the image frame when it is allowed to settle non-Newtonian fluid due to the viscous resistance of the non-Newtonian fluid.

However, the displacement profile of the particle when they are allowed to settle in an oscillated fluid medium (see Fig. 10) is different than that at stationary conditions. The vertical displacement of particles in water does not show to be much affected by the oscillation at lower frequencies. When the frequency is increased the displacement curves for water tend to show some response to the oscillatory motion. However, it could be seen that the vertical component of the displacement curves of the particles in non-Newtonian fluids is significantly affected at all frequencies. It seems like particles follow the motion of the continuous non-Newtonian fluid medium than it does in a Newtonian fluid. When the oscillatory motion is present, the frictional force or the drag force together with lift force on the particle act either in the same direction as the buoyancy force or in the opposite direction. The magnitude of each force depends on the viscosity of the fluid medium and the size of the particle.

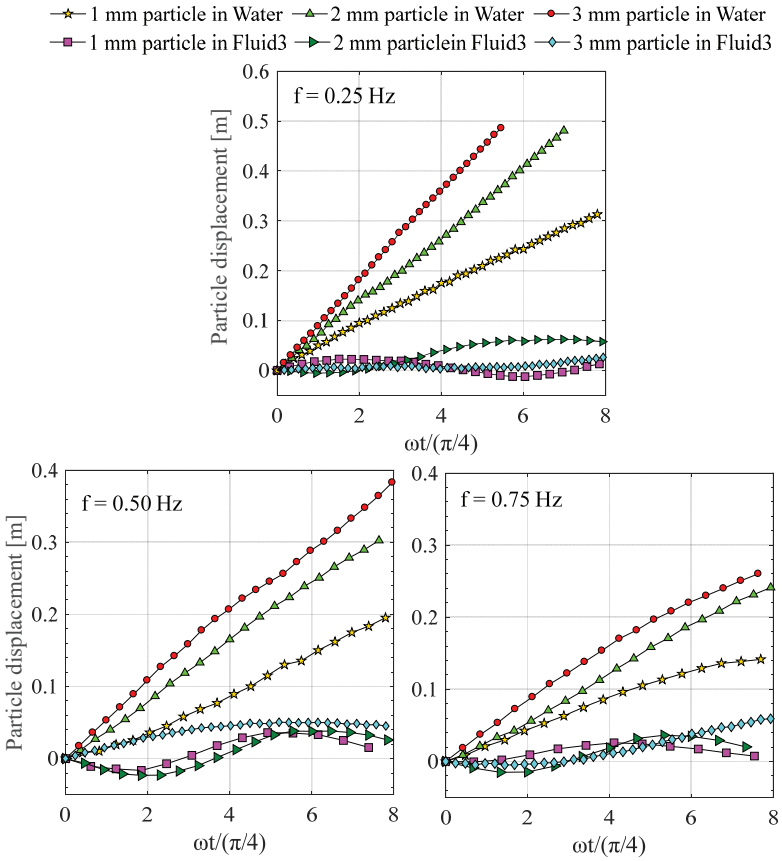

Figure 10: Vertical component of the particle displacement in water and Fluid 3 at all frequencies. The y- axis is positive downwards.

The slopes of the curves provide the settling velocity of each particle and since in some cases, more than one oscillation period is considered, it could be termed as 'average velocity'. Thus, it could be seen that large-sized particles have achieved higher settling velocities at all the oscillation frequencies and all sized particles tend to settle faster in water than in any non-Newtonian fluid even at oscillatory conditions.

3.3.2 Variation of particle displacement with different fluid types

The displacement profiles shown in Figs. 9 and 10 are only for one period of oscillation. However, it is of interest to know how the particles settle/rise in different test fluids for a bit of longer oscillation time. Therefore, Fig. 11 shows the vertical component of the particle displacement for different fluid types, all the particle sizes, and for the oscillation frequency equal to 0.75 Hz.

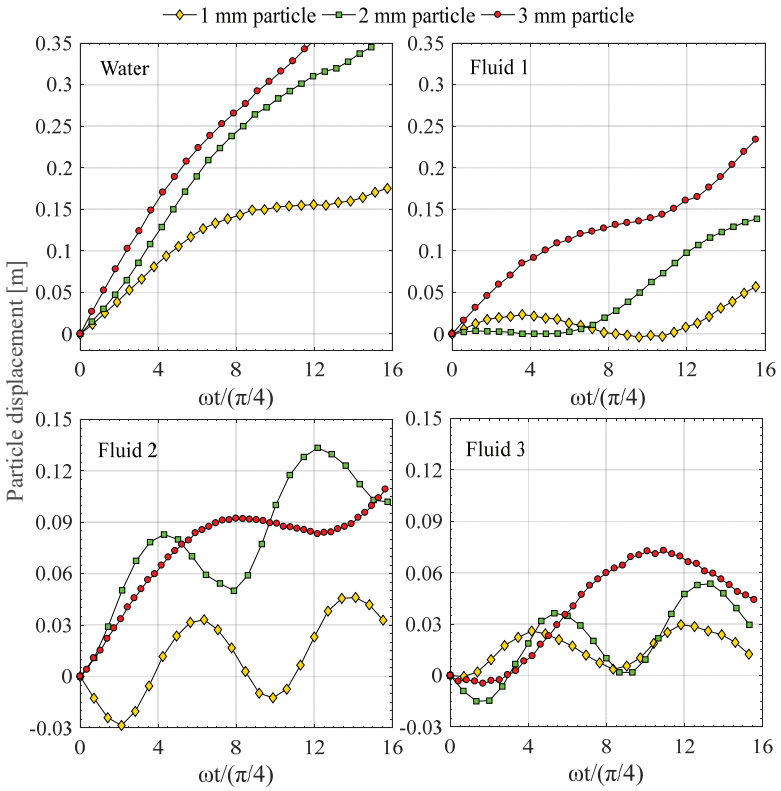

Figure 11: Vertical component of the particle displacement in all test fluids at f = 0.75 Hz. The y- axis is positive downwards.

According to Fig. 11, it can be seen that the displacement of the particles in water is not affected significantly even at higher frequencies; especially for the large-sized particles. In comparison to that, all particle sizes are greatly affected and influenced by the oscillatory motion in such a way that they alter their displacement direction (vertically as downwards and upwards) from time to time within the oscillation period in the course of settling. Fig. 10 shows that the time development of the vertical displacement is dominated by sub-harmonic oscillations and this could be caused by the phase lag between the particle dynamics and the oscillatory flow due to the particle inertia. According to the plots of displacement evolution of the particles shown in Fig. 11, a condition of partial stability (or stagnation) of the particles could be observed in some instances especially at higher fluid viscosities and also for smaller sized particles. This temporary stability is simply due to the initial relaxation of the particle to align with the action of the combined gravitational force (downwards) and the viscous drag (oscillating). If the liquid was purely oscillating in absence of gravitation the particles would follow nearly the same motion. The only difference would be the particle inertia. If the liquid flowed with constant speed in absence of gravity, the particle would follow more or less completely aligned, except

for local liquid perturbations. An alternative but fully equivalent way to depict the motion would be to take the numerical time derivative of the displacement trajectories to give the "falling speed" of the particles. However, we chose to show the displacement as these are the raw data, and the numerical derivative could be too fluctuating. Fig. 4 shows how the trend lines are used to give a steadier estimate.

Moreover, the displacement plots in Fig. 11 reveal that the disturbances to the settling velocity and consequently the possible retardation effect would become significant with increasing viscosity of the test fluids. Indeed, the larger the viscosity, the smaller the Stokes number of settling particles. The relaxation time for particles settling in Fluids 2 and 3 is small and particles follow the oscillatory flow. Contextually, the particle Reynolds number is smaller than in the cases with water, and Fluid 1 and correspondingly fluctuations of the fluid velocity around the particle are foreseeably weaker. Therefore, when the particle becomes smaller in size, it possesses a lower amount of buoyancy compared to the drag forces exerted by the continuous liquid medium, and highly viscous fluids would arrest the fall velocities at higher oscillation frequencies.

3.4 Settling velocity of particles in different oscillatory conditions along pipe axis (Location 'L1')

As explained in section 2.3.2, the average settling velocity of the particles at different oscillatory conditions was approximated by fitting the vertical component of the displacement profiles of the particles into a linear curve and considering its slope. To provide a clear idea about the changes in settling velocity of particles at each oscillating condition by comparing those with the non-oscillating condition, a velocity ratio (β) is defined as;

$$\beta = \frac{v_p}{v_{p0}}, \tag{14}$$

where, v_p is the average settling velocity of given particle size at a particular oscillation frequency settled along the pipe axis ('L1') in a particular test fluid. Then v_{p0} is selected as the terminal settling velocity (at non-oscillating conditions) of the same sized particle settled along 'L1' within the same test fluid. Fig. 12 shows how β varies with the changing of oscillation frequency for different particle sizes while Fig. 13 shows the same for different fluid types for better understanding.

According to Figs. 12 and 13, it can be observed that the settling velocity of the particles at oscillatory conditions has been reduced from that at stagnant condition except for a couple of outlier values for the combinations of 2 mm particle in Fluid 1 and 1 mm particle in water and Fluid 2. The slight variance in β that can be observed at oscillatory conditions compared to the terminal settling velocities presented in Fig. 7 could be due to the uncertainty effects related to slight variations in particle shape and the exact radial position could perhaps be masked by azimuthal movement. Moreover, it could also be attributed to a condition of adverse pressure-gradient where the wake becomes unstable and fluctuations of the drag force appear even though the flow is laminar for all the test cases based on the oscillatory Reynolds number explained in (Mazzuoli et al., 2014, Amaratunga et al., 2020).

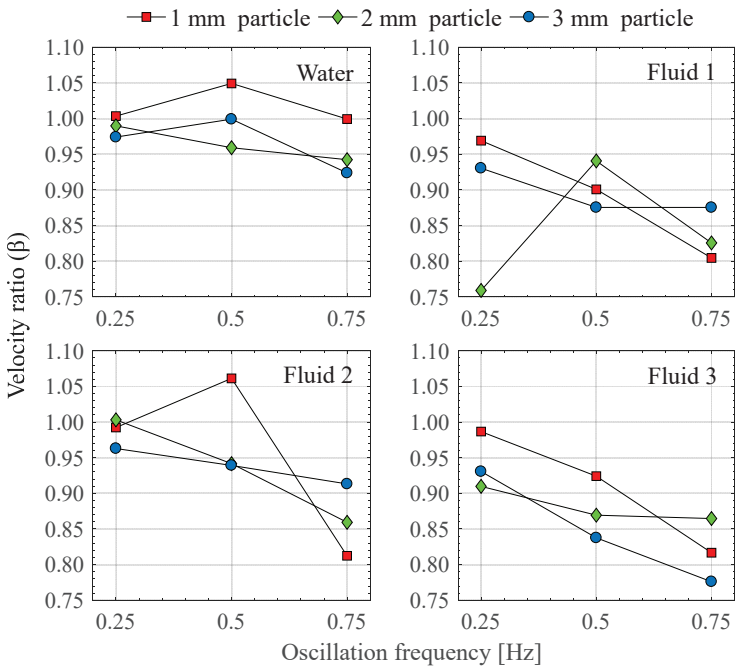

Figure 12: Variation of β at different oscillation frequencies for different particle sizes

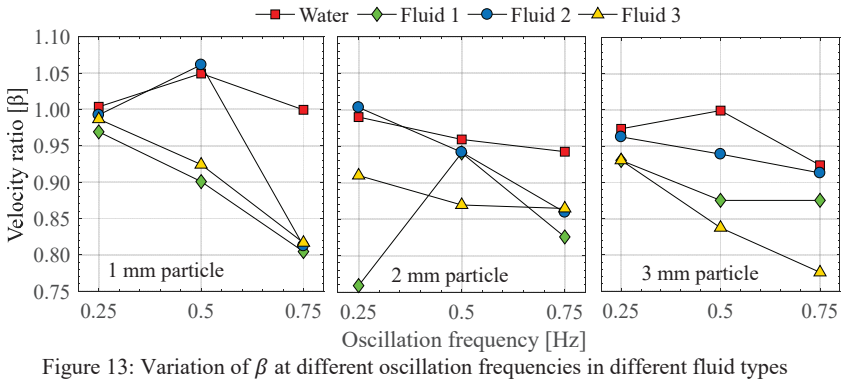

Figure 13: Variation of β at different oscillation frequencies in different fluid types

However, Figs. 12 and 13 again prove the fact that water being the Newtonian fluid shows the least affected by the oscillations in terms of the velocity reduction while the significance of retardation becomes increased when the non-Newtonian fluids become more viscous with increased shear-thinning effects.

The variation of β within water always lies close to unity, which ranges from 1.05 to 0.92 for all the particle sizes. That indicates that there has been only a slight drag enhancement on the

particles due to the oscillations when they are settled in the water. However, a reduction of β in the range from 4 – 23% could be observed in non-Newtonian fluids where the maximum reduction is achieved when the particles are settled in Fluid 3. This reduction of velocity could be attributed to the oscillation-induced increases in the drag coefficient on the particles at unbounded shear conditions and to the unstable wake due to the continuous changing of the oscillatory flow (Zeng et al., 2009). The drag force on the particles in oscillatory conditions is significantly modified by the instantaneous relative velocity between the particles and fluids (Hwang, 1985) because of the continuous flow changes within the flow.

Furthermore, (Tunstall and Houghton, 1968) state that the occurrence of any secondary effects such as phase lag, virtual mass, etc. can also not be negligible with this regard. The existence of fluid inertia and viscosity could lead to a phase lag between the fluid and the particles. The compressibility of the air pocket in between the piston and fluid system has a greater responsibility for this. (Houghton, 1966) states that, any technique that can increase the phase lag between particle motion and the motion of displaced fluid would reduce the settling velocity that will eventually increase the hold-up time in two-phase particulate systems. Furthermore, particle inertia is not negligible to that of the fluid in this scenario and the drag coefficient is most likely be affected by the unsteadiness of the wake.

3.5 Effect of the shear region on settling velocity (settling at 'L2' and 'L3')

As explained in the introduction, since the unsteady oscillatory pipe flow undergoes flow reversals continuously and thus the axial velocity is varying both in magnitude and direction, the shear rate is time-varying and effects from that become more pronounced for non-Newtonian fluids.

The same approach has been taken as described in Eq. (13) to quantify the effect of walls at stationary conditions and the effect of the shear region at oscillatory conditions. Here the instantaneous settling velocity of the particle (v_p) refers to the value either along 'L2' or 'L3'. v_{p0} is the same as that measured along 'L1' for resting fluid.

3.5.1 Wall effects at stationary conditions

When a spherical particle settles within some confined walls, it experiences a retardation effect and reduces its settling velocity. This effect is quantified in terms of a wall factor (Malhotra and Sharma, 2012) which is defined as the ratio of the settling velocity in the presence of confining walls to the unbounded settling velocity in the same fluid. The presence of walls generally creates an enhancement of the drag force (Zeng et al., 2009), and more importantly the particle experiences a lift force that is either directed toward or away from the wall. This lift force (Fischer et al., 2002) is often much smaller in magnitude than the drag force and plays a vital role in determining the solids separation or suspension capacities in many industrial applications. Authors have investigated the wall effects on particle settling at steady conditions and Fig. 13 shows the velocity ratio at different locations where β at 'L1' always reads as unity based on the definition of β in Eq. (14).

According to Fig. 14, it can be seen that the wall effects are significant when smaller sized particles settle in both Newtonian and non-Newtonian fluids. When a 1 mm particle settles in water, β shows a reduction of around 25% while it is just around 3% when a 3 mm particle settles in water.

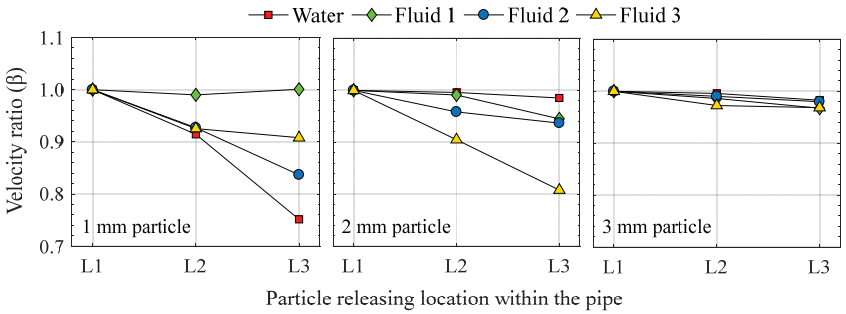

Figure 14: Wall effects on particle settling at steady conditions in different fluid types

Furthermore, it is observed that the wall retardation becomes less significant when the non-Newtonian fluids become more viscous and it becomes less severe in power-law fluids than in Newtonian fluids. The outliers in the experimental data points presented in Fig. 14 could be attributed to the transverse (lift) force that is directed away from the wall at those particular instances. According to (Zeng et al., 2005, Zeng et al., 2009), when the Re becomes higher (around 200), a more pronounced one-sided double-threaded wake could be observed between the particle and the wall. Furthermore, when the particle becomes closer and closer to the wall, the recirculation region opposite of the wall and the vorticity are significantly larger than that within the gap between the particle and the wall which will eventually increase the drag force on the particle. However, the effect of particle size on oscillation-induced retardation is more significant than that observed for the wall-effect in the absence of oscillation.

3.5.2 Effect of the shear region at oscillatory conditions

In comparison to the wall-effects at stationary conditions, a particle which moves parallel to a wall in an oscillatory flow behaves in a slightly different manner since it does not experience a transverse (lift) force at least within the Stokes region (Zeng et al., 2009). However, with the introduction of the inertial effects in oscillatory flow, the lift force has three contributions from the shear flow, from the rotation itself and from the wall where it is bounded. The relative motion of the surrounding liquid and the particle within the gap between the particle and the wall contributes to this inward or outward lift forces which can be significant when the flow becomes more inertia dominated (high Re). Fig. 15 shows how the velocity ratio (β) varies when the particle can settle closer to the pipe wall in oscillatory conditions.

It could be seen that when the particle is close to the wall in water, β tends to reduce. But, when it is allowed to settle in non-Newtonian fluids closer to the wall and at oscillating conditions, β tends to show a slight increase. This slight increase may not be sufficient to overcome the terminal settling velocity at stationary conditions, but that is considerable and interesting to study since it is expected to have an increased drag as a result of both shear flow and the wall-effect. Despite the slight anomalies shown by the 1 mm particle from the above-mentioned observation, 2 mm and 3 mm particles are in good agreement. Such slight anomalies shown by the 1 mm particle could be attributed to the irregularities of the shape and size of the particle and also the break-neck effects exerted by the mechanical oscillatory system to the fluid medium. The slight increase in β could be attributed to the increased shear effects and the

slight drag reduction within the Stokes region (Zeng et al., 2005, Zeng et al., 2009) in the presence of the oscillations, which can be elucidated as follows.

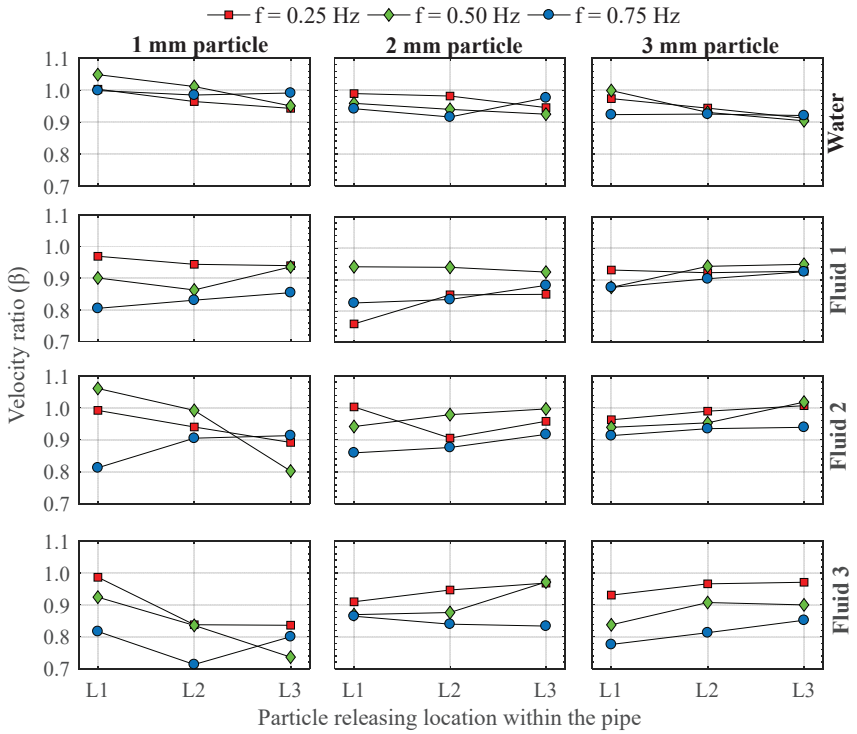

Figure 15: Effect of the shear region on particle settling at oscillatory conditions in different fluid types

The viscosity of most water-based drilling fluids is formulated by a combination of polymers similar to the test fluids in the current study. Besides, water-based drilling fluids may contain some additives to achieve desired agglomeration effects. The structural units and surface charges between those particles in polymeric liquids may get weakened by the oscillations/vibrations and that leads to a reduction of internal liquid viscosity. It is to be noted that the cyclic maximum shear rate change occurs mostly near the pipe wall, and thus the resulting viscosity reduction is more pronounced in the near-wall regions (Amaratunga et al., 2020). This explains the fact that, when the shear-thinning non-Newtonian fluids (primarily water-based polymeric liquids) are subjected to oscillatory motion, there will be a substantial reduction of viscosity of the fluid and that will result in the reduction of the drag force on the settling particles and consequently experiences faster settling. Furthermore, it is important to know that there exist some interactions of the particle with the coherent vortex structures in the near-wall region as explained by (Mazzuoli et al., 2014) and the hydrodynamic force on the sphere is characterized by such complex time development. Since the particles are released fairly close to the wall at L3, their trajectory (and thus the average velocity) is largely influenced

by the vorticity present in the vicinity of the wall. Vortices are generated in the boundary layer during some positions of the oscillation period.

Therefore, the non-linear dependence of the drag force on the relative velocity of the particle to fluid becomes apparent in the presence of oscillatory motion since the shear effects come into action and the shear rate increases closer to the walls. It can be concluded that the mean relative velocity of settling (or rising) of particles in a liquid medium is reduced if the liquid medium is made to undergo sinusoidal vertical oscillations. However, the settling particles in that oscillating fluid medium closer to the pipe wall would experience a slight reduction in drag within the shear region than that in the core region.

3.6 Error analysis

As stated previously, it is important to discuss the error associated with the current analysis since it contains some approximations in averaging the settling velocity at oscillatory conditions, which is the significant parameter in the present study. The error sources associated with this study could be two-fold; namely, (i) the experimental (or the random) error when capturing the position of the settling particle and (ii) the error associated with approximating the slope for the displacement profile of the particles when they are settling in oscillatory conditions. In a way, the latter could be considered as a 'systematic' error since it is obvious to deviate from the linear curve. On the other hand, the size of the particles is not exactly 1, 2, or 3 mm (as shown in Table 2) could also be a slight contribution to the systematic error of the experiment. However, it is of great importance to mention here that, the vertical displacement of the particles has been recorded for a time long enough to estimate the average slope with precision. The authors wanted to investigate the behavior of the falling particle throughout its whole path within the test section rather than just calculating the average velocity at the bottom of the test section as 'a specified distance divided by the time spent'.

To assess the associated error and to enhance the accuracy of results, all the experimental cases were repeated three times. Out of those trials, it could be observed that the terminal settling velocities at stationary conditions has the lowest standard deviation of 0.000437 m/s when 3 mm particle settles in Fluid 3 and the largest standard deviation of 0.0387 m/s when 1 mm particle settles in water. Even for the oscillatory cases, the random error was not significant in such a way that their standard deviations are comparably too small. This indicates that the random error which is associated with the results of this particular study would be not that significant.

Furthermore, when approximating the slope for the displacement profile of the particles under oscillatory conditions, some cases exhibited significant deviations as shown in Fig. 16. It can be seen that R^2 values are within the acceptable range (> 90%) for still fluids, and also when they oscillated at very low frequencies. Further increase in the frequency enhances the deviation especially for the smaller sized particles when they are settling in highly viscous non-Newtonian fluids. The lowest R^2 values recorded are around 17% when 1 mm particle settles in Fluid 3. As stated in section 3.3.2, the condition of partial stability or the temporary stagnation of the particles within its course of settling is the closest reason for this increased deviation (or lower R^2 value) for smaller-sized particles in high viscous non-Newtonian fluids. As earlier mentioned, it was found to have certain oscillation frequencies where the absolute downward displacement of the particle is smaller than its displacement in the opposite direction, regardless of the gravitational force. And so, the displacement profile of the particle also

showed more or less sinusoidal pattern which consequently reduces the R^2 value of the fitted linear curve. The authors understand the necessity of performing more tests for each experimental condition to achieve better convergence statistics and a comprehensive investigation would require observing the velocity field around the particle during its motion, for instance utilizing PIV measurements.

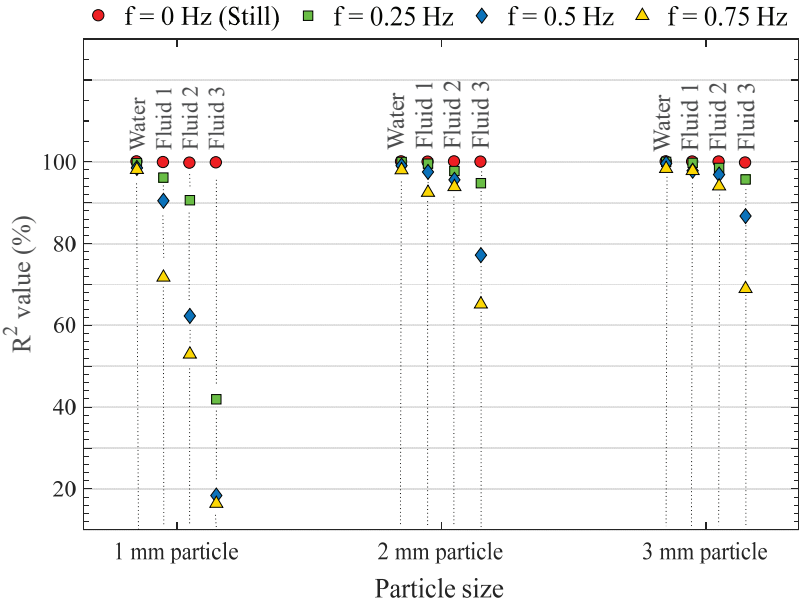

Figure 16: Resulted R^2 value in approximating the slope for the displacement profiles of particles in oscillatory conditions

However, taking the average settling velocity even with such low R^2 values were successful in quantifying the oscillation-induced reduction of settling velocity of particles in Newtonian and non-Newtonian fluids.

4 Conclusion

This experimental investigation was carried out to study the effects of oscillatory motion on the settling of spherical particles in Newtonian and slightly viscoelastic non-Newtonian fluids. 144 different experimental cases were tested for 3 different frequencies and still fluid, 3 different particle sizes, 4 different fluid types, and 3 different locations within the pipe. The study concludes that;

- Oscillations lead to increased drag force exerted on the settling particles in both Newtonian and non-Newtonian fluids.
- The increased drag effect becomes significant in stagnant conditions when the non-Newtonian fluids are more viscous and shear-thinning. This reduction of terminal settling velocity could also be attributed to the negative wake that is perceived to happen only in shear-thinning viscoelastic fluids.

- In quiescent fluids, the rate of increase in terminal settling velocity (with increasing particle size) is higher for water and low viscous NNFs compared to that in high viscous NNFs. This means that larger particles settle down at a slower rate than the smaller particles when the shear-thinning of the NNF is increasing (when n becomes low). Therefore, increasing shear viscosity may be an effective solution to achieve suspensions of large-sized particles.
- A condition of partial stability of the particles within its course of settling could be observed in some instances especially at higher fluid viscosities and also for smaller sized particles under oscillatory conditions. Such temporary stable condition could be seen only when the fluid medium moves upward in its oscillating period due to the neutralization of finite buoyancy forces by the gravitational and drag forces acting on the particle.
- The settling velocity of particles in both Newtonian a non-Newtonian fluids experiences reduction under oscillatory conditions. This reduction of settling velocity may be primarily related to increased drag forces induced by the fluid oscillations.
- Velocity retardation effect under oscillatory conditions becomes significant by reduction of the power-law index, n and with relatively large-sized particles.
- The impact of wall retardation at steady conditions becomes less significant when the non-Newtonian fluids become more viscous and it becomes less severe in power-law fluids than in Newtonian fluids.
- The effect of particle size on oscillation-induced retardation is more significant than that observed for the wall-effect in the absence of oscillation.
- When the shear-thinning non-Newtonian fluids (primarily water-based polymeric liquids) are exposed to oscillatory motion, there will be a reduction of viscosity of the fluid closer to the pipe walls where the shear region exists and that will result in the reduction of the drag force on the settling particles.
- Even though the approximation of average settling velocity from particle displacement profile (as described in section 2.3.2) seems less accurate in some instances, it is a successful way in quantifying the oscillation-induced retardation of settling velocity of particles in Newtonian and non-Newtonian fluids.

As an overall idea, the analysis presented in this manuscript reveals that an enhancement of suspension and mixing in both Newtonian and non-Newtonian fluids could occur in oscillatory flows. However, when particles are moving close to the pipe wall in oscillatory shear-thinning non-Newtonian fluid medium, they experience a slight reduction in drag compared with the Newtonian case. The shear rate at equivalent flow rate is higher in shear-thinning liquids close to the wall, thus the effective viscosity is reduced. Furthermore, the authors expect that this work will stimulate further experimentation on different aspects especially in understanding the hydrodynamics forces on the particles being settled in oscillatory non-Newtonian fluids.

Acknowledgment

Authors gratefully acknowledge the Norwegian Research Council for funding this study under the project “NFR Improved Model Support in Drilling Automation”. We appreciate the valuable support provided by Jon Arne Evjenth, from the Department of Energy & Petroleum Engineering at the University of Stavanger in preparing the data acquisition system for the experiments. The advice and encouragement provided by Roar Nybø and Knut S. Bjørkevoll from SINTEF, Bergen are also greatly appreciated.

Notations

CMC	Carboxymethyl Cellulose
CFD	Computational Fluid Dynamics
HV	High viscous
LVE	Linear viscoelastic range
MV	Medium viscous
NNF	Non-Newtonian fluid
PAC	Poly-anionic Cellulose
PIV	Particle Image Velocimetry technique
ROI	Region of interest
SAOS	Small amplitude oscillation shear
a	Displacement amplitude of the piston
a'	Displacement amplitude of the oscillation (in liquid medium)
A	Amplitude ratio based on the displacement amplitude of the piston
$B(t)$	Basset term
d	Diameter of the spherical particle
C_D	Drag coefficient at oscillatory conditions
C_{D0}	Drag coefficient at stationary conditions
$C_{D0-correlation}$	Drag coefficient of particles at stationary conditions based on the correlation presented in (Morrison, 2013, Morrison, 2016)
D	Diameter of the pipe
f	Frequency of oscillation, Hz; $\omega/2\pi$
g	Gravitational acceleration
Ga	Galileo number
G'	Elastic (or storage) modulus
G''	Viscous (or loss) modulus
K	Consistency index of the non-Newtonian fluid
n	Behavior index for the non-Newtonian fluid
R	Radius of the pipe
t	Time
v_p	Instantaneous velocity of the particle taken as positive downwards
v_{p0}	Terminal settling velocity of the particle at stationary conditions
$\overline{v_{ps}}$	Stationary velocity component within the relative velocity of the particle under oscillatory conditions
v_{pp}	Periodic velocity component within the relative velocity of the particle under oscillatory conditions
v_f	Velocity of the fluid medium taken as positive downwards
R^2	R-squared value of the linear curve fitting
Re_p	Particle Reynolds number in oscillatory conditions
Re_{p0}	Particle Reynolds number in stationary conditions
Re_δ	Oscillatory Reynolds number of the liquid medium

Greek Letters

β	Velocity ratio; v_p/v_{p0}
γ	Strain
$\dot{\gamma}$	Shear rate
ω	Angular frequency; $2\pi f$

λ	Relaxation time of the (slightly viscoelastic) non-Newtonian fluid
μ_f	Dynamic viscosity of the fluid medium
μ_{PL}	Viscosity predicted by the power-law model
ρ_p	Density of the particle
ρ_f	Density of the oscillating fluid (continuous phase)
χ	Added mass coefficient

References

ACHARYA, A. R. 1986. Particle transport in viscous and viscoelastic fracturing fluids. *SPE Production Engineering,* 1**,** 104-110.

AMARATUNGA, M., NYBØ, R. & TIME, R. W. PIV analysis of dynamic velocity profiles in non-Newtonian drilling fluids exposed to oscillatory motion. ASME 2018 37th International Conference on Ocean, Offshore and Arctic Engineering, 2018. American Society of Mechanical Engineers Digital Collection.

AMARATUNGA, M., RABENJAFIMANANTSOA, H. A. & TIME, R. W. 2019a. CFD Analysis of low frequency oscillations in Newtonian and non-Newtonian fluids in a vertical pipe. *WIT Transactions on Engineering Sciences,* 125**,** 37-48.

AMARATUNGA, M., RABENJAFIMANANTSOA, H. A. & TIME, R. W. 2019b. Comparison of oscillatory flow conditions in Newtonian and non-Newtonian fluids using PIV and high-speed image analysis. *Flow Measurement and Instrumentation,* 70**,** 101628.

AMARATUNGA, M., RABENJAFIMANANTSOA, H. A. & TIME, R. W. J. J. O. N.-N. F. M. 2020. Estimation of shear rate change in vertically oscillating non-Newtonian fluids: Predictions on particle settling. 277**,** 104236.

ARNIPALLY, S. K. & KURU, E. 2018. Settling Velocity of Particles in Viscoelastic Fluids: A Comparison of the Shear-Viscosity and Elasticity Effects. *SPE Journal*.

BAILEY, J. 1974. Particle motion in rapidly oscillating flows. *Chemical Engineering Science,* 29**,** 767-773.

BAIRD, M., SENIOR, M. & THOMPSON, R. 1967. Terminal velocities of spherical particles in a vertically oscillating liquid. *Chemical Engineering Science,* 22**,** 551-558.

BECKER, L., MCKINLEY, G., RASMUSSEN, H. K. & HASSAGER, O. 1994. The unsteady motion of a sphere in a viscoelastic fluid. *Journal of Rheology,* 38**,** 377-403.

BOYADZHIEV, L. 1973. On the movement of a spherical particle in vertically oscillating liquid. *Journal of Fluid Mechanics,* 57**,** 545-548.

BROWN, P. P. & LAWLER, D. F. 2003. Sphere drag and settling velocity revisited. *Journal of environmental engineering,* 129**,** 222-231.

CHENG, N.-S. 2009. Comparison of formulas for drag coefficient and settling velocity of spherical particles. *Powder Technology,* 189**,** 395-398.

CHERUKAT, P. & MCLAUGHLIN, J. B. J. J. O. F. M. 1994. The inertial lift on a rigid sphere in a linear shear flow field near a flat wall. 263**,** 1-18.

CHHABRA, R., AGARWAL, L. & SINHA, N. K. 1999. Drag on non-spherical particles: an evaluation of available methods. *Powder Technology,* 101**,** 288-295.

CHILDS, L., HOGG, A. & PRITCHARD, D. 2016. Dynamic settling of particles in shear flows of shear-thinning fluids. *Journal of Non-Newtonian Fluid Mechanics,* 238**,** 158-169.

CLIFT, R., GRACE, J. R. & WEBER, M. E. 1978. *Bubbles, drops, and particles*, Academic Press, 1978 - New York.

FISCHER, P. F., LEAF, G. K. & RESTREPO, J. M. J. J. O. F. M. 2002. Forces on particles in oscillatory boundary layers. 468**,** 327-347.

GHEISSARY, G. & VAN DEN BRULE, B. 1996. Unexpected phenomena observed in particle settling in non-Newtonian media. *Journal of Non-Newtonian Fluid Mechanics,* 67**,** 1-18.

HAIDER, A. & LEVENSPIEL, O. 1989. Drag coefficient and terminal velocity of spherical and nonspherical particles. *Powder technology,* 58**,** 63-70.

HARBAUM, K. & HOUGHTON, G. 1960. Effects of sonic vibrations on the rate of absorption of gases from bubble beds. *Chemical Engineering Science,* 13**,** 90-92.
HARRINGTON, L. J., HANNAH, R. R. & WILLIAMS, D. Dynamic experiments on proppant settling in crosslinked fracturing fluids. SPE Annual Technical Conference and Exhibition, 1979. Society of Petroleum Engineers.
HERRINGE, R. 1976. On the motion of small spheres in oscillating liquids. *The Chemical Engineering Journal,* 11**,** 89-99.
HERRINGE, R. & FLINT, L. Particle motion in vertically oscillated liquids. Fi□ h Australian Conference on Hydraulics and Fluid Mechanics, 1974. 103-110.
HOUGHTON, G. 1963. The behaviour of particles in a sinusoidal velocity field. *Proceedings of the Royal Society of London. Series A. Mathematical and Physical Sciences,* 272**,** 33-43.
HOUGHTON, G. 1966. Particle trajectories and terminal velocities in vertically oscillating fluids. *The Canadian Journal of Chemical Engineering,* 44**,** 90-95.
HOUGHTON, G. 1968. Particle retardation in vertically oscillating fluids. *The Canadian Journal of Chemical Engineering,* 46**,** 79-81.
HWANG, P. A. 1985. Fall velocity of particles in oscillating flow. *Journal of Hydraulic Engineering,* 111**,** 485-502.
IKEDA, S. & YAMASAKA, M. 1989. Fall velocity of single spheres in vertically oscillating fluids. *Fluid dynamics research,* 5**,** 203.
JIN, L. & PENNY, G. S. 1995. Dimensionless methods for the study of particle settling in non-Newtonian fluids. *Journal of Petroleum Technology,* 47**,** 223-228.
KEHLENBECK, R. & FELICE, R. D. 1999. Empirical relationships for the terminal settling velocity of spheres in cylindrical columns. *Chemical Engineering & Technology: Industrial Chemistry-Plant Equipment-Process Engineering-Biotechnology,* 22**,** 303-308.
KELESSIDIS, V. C. 2004. An explicit equation for the terminal velocity of solid spheres falling in pseudoplastic liquids. *Chemical engineering science,* 59**,** 4437-4447.
KHAN, A. & RICHARDSON, J. 1987. The resistance to motion of a solid sphere in a fluid. *Chemical Engineering Communications,* 62**,** 135-150.
LEE, H. & BALACHANDAR, S. J. J. O. F. M. 2010. Drag and lift forces on a spherical particle moving on a wall in a shear flow at finite Re. 657**,** 89-125.
MAALOUF, A. & SIGLI, D. 1984. Effects of body shape and viscoelasticity on the slow flow around an obstacle. *Rheologica acta,* 23**,** 497-507.
MALHOTRA, S. & SHARMA, M. M. 2012. Settling of spherical particles in unbounded and confined surfactant-based shear thinning viscoelastic fluids: An experimental study. *Chemical Engineering Science,* 84**,** 646-655.
MAZZUOLI, M., KIDANEMARIAM, A. G. & UHLMANN, M. J. J. O. F. M. 2019. Direct numerical simulations of ripples in an oscillatory flow. 863**,** 572-600.
MAZZUOLI, M., SEMINARA, G. & VITTORI, G. J. A. I. W. R. 2014. Settling of heavy particles in a turbulent Stokes layer: Numerical simulations. 72**,** 2-14.
MORRISON, F. A. 2013. *An introduction to fluid mechanics*, Cambridge University Press.
MORRISON, F. A. 2016. Data correlation for drag coefficient for sphere. Available: https://pages.mtu.edu/~fmorriso/DataCorrelationForSphereDrag2016.pdf.
SCHÖNEBORN, P.-R. 1975. The interaction between a single particle and an oscillating fluid. *International Journal of Multiphase Flow,* 2**,** 307-317.
SHAH, S. N. 1982. Proppant settling correlations for non-Newtonian fluids under static and dynamic conditions. *Society of Petroleum Engineers Journal,* 22**,** 164-170.
SHAH, S. N. 1986. Proppant-settling correlations for non-Newtonian Fluids. *SPE Production Engineering,* 1**,** 446-448.
SHAH, S. N., EL FADILI, Y. & CHHABRA, R. 2007. New model for single spherical particle settling velocity in power law (visco-inelastic) fluids. *International journal of multiphase flow,* 33**,** 51-66.
SHARMA, H. 1979. Creeping Motion of a Non-Newtonian Fluid Past a Sphere. *Ind. J. Pure Appl. Math,* 10**,** 1565.
SINGH, S. P., SRIVASTAVA, A. K. & STEFFE, J. F. 1991. Vibration induced settling of a sphere in a Herschel-Bulkley fluid. *Journal of food engineering,* 13**,** 181-197.
STILL, A. 2012. *Multiphase phenomena in a vibrating column reactor.* Oklahoma State University.

TALMON, A. & HUISMAN, M. 2005. Fall velocity of particles in shear flow of drilling fluids. *Tunnelling and underground space technology,* 20**,** 193-201.
TIME, R. W. & RABENJAFIMANANTSOA, A. 2013. On the Relevance of Laboratory Scale Rheometric Measurements for Calculation of Complex Large Scale Flows in Well Drilling and Pipe Flows. *Annual Transactions of the Nordic Rheology Society,* 22.
TUNSTALL, E. & HOUGHTON, G. 1968. Retardation of falling spheres by hydrodynamic oscillations. *Chemical Engineering Science,* 23**,** 1067-1081.
UHLHERR, P., LE, T. & TIU, C. J. T. C. J. O. C. E. 1976. Characterisation of inelastic poweriaw fluids using falling sphere data. 54**,** 497-502.
UHLMANN, M. & DUŠEK, J. J. I. J. O. M. F. 2014. The motion of a single heavy sphere in ambient fluid: a benchmark for interface-resolved particulate flow simulations with significant relative velocities. 59**,** 221-243.
VAN DEN BRULE, B. & GHEISSARY, G. 1993. Effects of fluid elasticity on the static and dynamic settling of a spherical particle. *Journal of non-newtonian fluid mechanics,* 49**,** 123-132.
ZENG, L., BALACHANDAR, S. & FISCHER, P. J. J. O. F. M. 2005. Wall-induced forces on a rigid sphere at finite Reynolds number. 536**,** 1-25.
ZENG, L., NAJJAR, F., BALACHANDAR, S. & FISCHER, P. J. P. O. F. 2009. Forces on a finite-sized particle located close to a wall in a linear shear flow. 21**,** 033302.
ZHIYAO, S., TINGTING, W., FUMIN, X. & RUIJIE, L. 2008. A simple formula for predicting settling velocity of sediment particles. *Water Science and Engineering,* 1**,** 37-43.

---- 000 ----